

The Preparation of Organosulfur Derived Electron Transfer Salts

Andrew C. Brooks

A thesis submitted in partial fulfilment of the
Requirements of Nottingham Trent University
For the degree of Doctor of Philosophy

July 2009

School of Science and Technology
Nottingham Trent University
Clifton Lane
Nottingham
NG11 8NS

Davy-Faraday Research Laboratory
Kathleen Lonsdale Building
University College London
Gower Street
London
WC1E 6BT

This work is the intellectual property of the author, and may also be owned by the research sponsor(s) and/ or Nottingham Trent University. You may copy up to 5 % of this work for private study, or personal, non-commercial research. Any re-use of the information contained within this document should be fully referenced, quoting the author, title, university, degree level and pagination. Queries or requests for any other use, or if a more substantial copy is required, should be directed in the first instance to the author.

Abstract

The concept of this thesis is to effect greater control over the crystalline state of radical cation salts in order to enhance electron transport, and to allow for the incorporation of additional functionality such as optical activity or magnetism. The salts formed are based on the bis(ethylenedithio)tetrathiafulvalene (BEDT-TTF or ET) framework, and are produced using the technique of electrocrystallisation. In attempts to control the crystal packing arrangements observed, a number of approaches have been explored including the incorporation of chirality, hydrogen bonding interactions and coordinate bonding interactions. These properties have been installed on the electron donor molecule and/ or the charge stabilising anion component.

This thesis presents a novel radical cation salt that has been prepared from ET and the sulfamate anion, and which exhibits ordered channels of hydrogen bonded anions and water molecules extending in one crystallographic dimension. This research has also discovered an unusual chiral crystallographic packing observed in a novel semiconducting radical cation salt formed from ET and the bromide anion. Also presented are the synthesis of a family of metal-binding electron donors and the first radical cation salts formed from these, including a perrhenate salt which is both *N*-protonated and oxidised, giving an overall charge of +2 on the electron donor molecule. A group of novel aldehyde-functionalised donors are discussed, one of which could lead to a Little-type superconductor, and the syntheses towards a bis(donor) molecule containing a spiro centre, and separately a porphyrin appended electron donor are presented.

Acknowledgements

First and foremost I have to thank Professor John D. Wallis and Professor Peter Day FRS, for providing me with the opportunity to undertake research into this most fascinating field of interdisciplinary science. Your encouragement, enthusiasm and advice have inspired me throughout the past few years.

Thank you also to Dr Lee Martin for your help with measurements and training, and for your friendship over the past couple of years, and to Dr Gary Hix for your advice and support. I also want to thank Dr Rob Smith, Dr Qiang Wang, Dr Songjie Yang and Dr Sara Krivikas for their advice and friendship over the past few years.

Thank you to Dr Ian Watts (UCL) for assistance with conductivity measurements, and Dr Steve Firth (UCL) for the use of the Raman microscope. A big thank you to Dr David Chambers-Asman, Mr Mark Sladen, Mrs Marilyn Johnson, Mr Mark Cosgrove and Ms Barbara Stevenson for assistance with training on equipment and providing valuable technical support.

Thank you to Gary Baker and Muriel Funck for providing the entertainment in the lab, the numerous food challenges, and the endless river of tea and coffee. Thank you to Vicky Mundell, Daniel Paul-Guest and Laura Neeves for the laughs, stories and experiences shared over the past few years, and to the many other students who have made the labs enjoyable places in which to conduct research.

Thank you to Dr Bob Baker, Dr Gareth Cave, Dr Chris Garner, Dr Patrick Huddleston, Dr Michael Stockenhuber, Professor Richard Joyner, Professor Vernon Richardson and Professor Carole Perry for their advice during my studies. A special thank you to Mr Jim Bottrill, who introduced Nottingham Trent University to me, and whose encouragement and positive outlook always helped when the situation seemed grim.

Thanks to John Spray for preparing the electrocrystallisation cells and electrodes, Brian O'Neill and Peter Moore for preparing the constant current sources, the EPSRC National X-ray service at Southampton for the X-ray data sets, the EPSRC National Mass Spectrometry Service for the mass spectrometry data, and Mr Stephen Boyer (London Metropolitan University) for providing the elemental analysis data.

A special thank you to Neil Bowley whose friendship, support, and singing has constantly encouraged me to succeed over the last eight years, amused me, and ruined my hearing. Thanks mate...

Many thanks go to Luke Headland and Laura Vahter for being great friends, and helping me to leave work at work when I needed to relax.

Lastly, my biggest thanks go to my fiancée Laura, for supporting me, and to Mum, Dad, Elaine, Aivars, Matthew, Jessica, Andrew, Katherine, Richard, Annette, Antony, Danielle, Winston and every other member of the family who have in one way or another helped me achieve this thesis. Without all of your support, this couldn't have been done.

*This thesis is dedicated to Laura and my family,
without whom this thesis could never have been completed.*

Contents

1	Introduction	1
1.1	Types of conductivity	2
1.1.1	Band theory	2
1.1.2	Insulator	3
1.1.3	Semiconductor	4
1.1.4	Metal	6
1.1.5	Superconductor	7
1.2	Superconductivity	7
1.3	B. C. S. theory	8
1.4	Superconducting metal alloys	10
1.5	Conductivity in non-metallic materials	12
1.6	Non-metallic superconductors	13
1.7	Tetrathiafulvalene	17
1.8	Bis(ethylenedithio)tetrathiafulvalene	20
1.9	First organosulfur superconductor	25
1.10	First ambient pressure organosulfur superconductor	26
1.10.1	α - Phase packing of ET	29
1.10.2	β - Phase packing of ET	30
1.10.3	γ - Phase packing of ET	31
1.10.4	δ - Phase packing of ET	32
1.10.5	ϵ - Phase packing of ET	32
1.10.6	κ - Phase packing of ET	32
1.10.7	Unusual ligating behaviour of ET	36
1.10.8	ET halide salts	38
1.11	Temperature effects on the crystal conductivity	40
1.12	Functionalisation of the ET donor	41
1.13	Bis(vinylenedithio)tetrathiafulvalene	44
1.14	Techniques for the characterisation of electron-transfer salts	45
1.14.1	Raman spectroscopy	45
1.14.2	Elemental analysis	47
1.14.3	Thermal gravimetric analysis	48
1.14.4	Infrared spectroscopy	48
1.14.5	Single crystal X-ray crystallography	49
1.14.6	EPR spectroscopy	50
1.14.7	X-ray electron microprobe analysis	51
1.14.8	Superconducting quantum interference device	51
1.14.9	RF measurements	52
1.15	The magnetic properties of electron-transfer salts	52
1.15.1	Types of magnetism	54
1.15.2	Magnetic susceptibility	56
1.16	Electrocrystallisation	58
1.17	Other types of conducting materials	61
1.17.1	Polymers	61
1.17.2	Inorganic and ceramic superconductors	62

1.18	Applications of electron-transfer materials	64
1.19	References	66
2	Chiral organosulfur-derived electron donors	74
2.1	Introduction	75
2.2	Results and discussion	80
2.3	Materials made by electrocrystallisation	90
2.4	Experimental	95
2.5	Electrocrystallisation experimental	105
2.6	References	111
3	Metal-binding electron donors	113
3.1	Introduction	114
3.2	Results and discussion	119
3.3	Materials made by chemical oxidation or electrocrystallisation	137
3.3.1	(70)(CuCl ₂) ₃ (CH ₃ CN) _{0.75} (H ₂ O) _{1.5}	137
3.3.2	(70) _x (CoCl ₄) _y	138
3.3.3	(70-H) ⁺ (ReO ₄) ₂ ·0.5(CH ₂ Cl ₂)	139
3.3.4	Experimental	144
3.3.5	Electrocrystallisation experimental section	156
3.4	References	158
4	Novel radical cation salts formed from ET	159
4.1	Synthesis of new radical cation salts of ET with the sulfamate anion	160
4.1.1	Introduction	160
4.1.2	Results and discussion	163
4.1.3	(ET) ₃ (H ₂ NSO ₃) ₂ ·2H ₂ O	163
4.1.4	Electron transfer properties of (ET) ₃ (H ₂ NSO ₃) ₂ ·2H ₂ O	173
4.1.5	Charge state of the donor species	175
4.1.6	Experimental	176
4.2	Electrochemical synthesis of a new solvated structure of ET chromium hexathiocyanate, (ET) ₄ [Cr(NCS) ₆]·C ₆ H ₅ NO ₂	180
4.2.1	Introduction	180
4.2.2	Results and discussion	185
4.2.3	Experimental	199
4.2.4	Electrocrystallisation experimental	202
4.3	Chiral packing of achiral components	203
4.3.1	Introduction	203
4.3.2	Results and discussion	204
4.3.3	Experimental	219
4.3.4	Electrocrystallisation experimental	221
4.4	(ET) ₃ (CoCl ₄) ₂	223
4.4.1	Introduction	223

4.4.2	Results and discussion	223
4.4.3	Experimental	226
4.5	References	228
5	Chiral metal anion complexes	231
5.1	Introduction	232
5.2	Results and discussion	233
5.3	Experimental	237
5.4	Electrocrystallisation experiments	244
5.5	References	247
6	Aldehyde functionalised organosulfur electron donors	248
6.1	Introduction	249
6.2	Results and discussion	252
6.3	Experimental	269
6.4	References	278
7	A Porphyrin based electron donor	279
7.1	Introduction	280
7.2	Results and discussion	281
7.3	Experimental	284
7.4	References	289
8	A spiro organosulfur compound	290
8.1	Introduction	291
8.2	Results and discussion	292
8.3	Experimental	294
8.4	References	296
9	Recommendations for further work	297
Appendix 1	GC-MS method	300
CD-ROM	X-ray crystal structure .cif files	

Table of Figures

Figure 1: Possible band structures of a solid.	3
Figure 2: Representative resistivity data for a solid as a function of temperature.	5
Figure 3: Plot of the logarithm of the resistance against inverse temperature showing a linear dependency for a semiconducting material.	6
Figure 4: Primitive cubic cell exhibited by A-15 superconductors.	10
Figure 5: Crystal structure of (TMTSF) ₂ PF ₆ , showing stacking of the donor molecules.	13
Figure 6: ET interstack packing motifs.	21
Figure 7: ET intrastack packing motifs.	23
Figure 8: Packing of donor molecules in β -(ET) ₂ I ₃ .	27
Figure 9: Packing motif of α -(ET) ₂ I ₃ , as viewed along the a' diagonal.	29
Figure 10: The γ -(ET) ₃ (I ₃) _{2.5} packing motif, viewed along the a axis.	31
Figure 11: δ -(ET)I ₃ , viewed along the a axis.	33
Figure 12: ϵ -(ET) ₂ I ₃ (I ₈) _{0.5} , viewed along the a axis.	35
Figure 13: κ -(ET) ₂ I ₃ , 3-D view.	36
Figure 14: κ -(ET) ₂ I ₃ , viewed along the length of the donor molecules. Numbers shown correspond to S...S contacts (Å).	37
Figure 15: Proposed mechanistic formation of the zinc bis(dithiolate) salt 19.	44
Figure 16: Example Raman spectrum indicating the presence of ET ⁰ and ET ¹⁺ donor molecules.	47
Figure 17: Bond lengths required for calculation of charge on ET.	49
Figure 18: Responses of superconductors to magnetic fields.	53
Figure 19: Electrochemical cell used for experiments conducted in this thesis.	59
Figure 20: YBa ₂ Cu ₃ O ₇ .	64
Figure 21: Carbon numbering in compound 31.	80
Figure 22: Two stereoisomers formed by the Diels-Alder reaction of the trithione species and an alkene.	82
Figure 23: Proposed mechanism for sulfur-oxygen exchange.	84
Figure 24: Proposed mechanism for triethyl phosphite coupling reaction to form ET.	85
Figure 25: Resistivity as a function of temperature for (37) ₂ Cl.	91
Figure 26: Linear relationship of (37) ₂ Cl indicating semiconducting behaviour.	92
Figure 27: Temperature profile over the period of resistivity data collection for (37) ₂ Cl.	93
Figure 28: Asymmetric unit showing slightly bent structure. Hydrogen atoms and alternative ethylene carbon positions have been removed for clarity. Thermal ellipsoids are drawn at the 50 % probability level.	131
Figure 29: Asymmetric unit. Hydrogen atoms and alternative ethylene carbon positions have been removed for clarity. Thermal ellipsoids are drawn at the 50 % probability level.	132
Figure 30: Lattice as viewed down the crystallographic a axis. Hydrogen atoms have been removed for clarity. Thermal ellipsoids are drawn at the 50 % probability level.	133

Figure 31: Lattice as viewed down the crystallographic <i>b</i> axis. Hydrogen atoms have been removed for clarity. Thermal ellipsoids are drawn at the 50 % probability level.	133
Figure 32: π -electron delocalisation in pyridylethyne analogues.	136
Figure 33: Normalised resistance profile for (70)CoCl ₄ .	139
Figure 34: Asymmetric unit of (70-H) ⁺ (ReO ₄) ₂ ·0.5(CH ₂ Cl ₂). Hydrogen atoms have been removed for clarity. Thermal ellipsoids are shown at the 50 % probability level. Dichloromethane is disordered about a centre of symmetry.	140
Figure 35: Lattice as viewed down the crystallographic <i>a</i> axis, showing dimerisation of the donor molecules. Hydrogen atoms have been removed for clarity. Thermal ellipsoids are shown at the 50 % probability level.	141
Figure 36: Short S···S contacts (red dashed lines) extending in the crystallographic <i>a</i> direction. Hydrogen atoms have been removed for clarity. Thermal ellipsoids are shown at the 50 % probability level.	142
Figure 37: Lattice as viewed down the crystallographic <i>b</i> axis. Hydrogen atoms have been removed for clarity. Thermal ellipsoids are shown at the 50 % probability level.	143
Figure 38: Slice of lattice structure, illustrating the sandwich of perrhenate anions between organosulfur donor molecules. Hydrogen atoms have been removed for clarity. Thermal ellipsoids are shown at the 50 % probability level.	144
Figure 39: Representative diagram of the expanded unit cell of (ET) ₃ (H ₂ NSO ₃) ₂ ·2H ₂ O.	164
Figure 40: Crystal structure as viewed down the crystallographic <i>a</i> axis. Thermal ellipsoids are shown at the 50 % probability level.	164
Figure 41: Organosulfur donors form stacks along the crystallographic <i>b</i> axis, as viewed down the <i>b</i> axis. Hydrogen atoms have been removed for clarity. Thermal ellipsoids are shown at the 50 % probability level.	165
Figure 42: Crystal structure as viewed down the crystallographic <i>c</i> axis. Hydrogen atoms have been removed for clarity. Thermal ellipsoids are shown at the 50 % probability level.	166
Figure 43: Twisted arrangement of the donor stacks, as viewed down the crystallographic <i>b</i> axis.	167
Figure 44: Twisted arrangement of the donor stacks, as viewed down the crystallographic <i>c</i> axis.	167
Figure 45: Interstack S···S close contacts in type I donor in the salt (ET) ₃ (H ₂ NSO ₃) ₂ ·2H ₂ O. Thermal ellipsoids are shown at the 50 % probability level.	168
Figure 46: Interstack S···S close contacts in type II donor in the salt (ET) ₃ (H ₂ NSO ₃) ₂ ·2H ₂ O. Thermal ellipsoids are shown at the 50 % probability level.	169
Figure 47: Overlapping of types I and II of donor molecule, with S···S short contacts shown.	170
Figure 48: Supramolecular anion ribbons (left to right) of H ₂ NSO ₃ ⁻ and H ₂ O, as viewed down the crystallographic <i>c</i> axis. Thermal ellipsoids are shown at the 50 % probability level.	171

- Figure 49:** Numbering scheme and hydrogen bonding interactions within two anion channels (channels run top to bottom), as viewed down the crystallographic *c* axis. Thermal ellipsoids are shown at the 50 % probability level. 172
- Figure 50:** Encapsulation of the channel of hydrated dimeric H_2NSO_3^- anions by the ethylene functions. As viewed just off the crystallographic *a* axis. 173
- Figure 51:** Resistivity data for $(\text{ET})_3(\text{H}_2\text{NSO}_3)_2 \cdot 2\text{H}_2\text{O}$ as a function of temperature. 174
- Figure 52:** Resistivity against temperature for a further sample of $(\text{ET})_3(\text{H}_2\text{NSO}_3)_2 \cdot 2\text{H}_2\text{O}$. 175
- Figure 53:** β'' - $(\text{ET})_4[(\text{H}_3\text{O})\text{M}^{3+}(\text{C}_2\text{O}_4)_3]$ ($\text{M} = \text{Cr}, \text{Fe}$), showing isolated channels of D- and L- enantiomers of the trisoxalate, thus overall the material is racemic. 185
- Figure 54:** $(\text{ET})_4[\text{Cr}(\text{NCS})_6] \cdot \text{C}_6\text{H}_5\text{NO}_2$ as viewed down the crystallographic *a* axis. Thermal ellipsoids are shown at the 50 % probability level. Hydrogen atoms have been removed for clarity. 189
- Figure 55:** $(\text{ET})_4[\text{Cr}(\text{NCS})_6] \cdot \text{C}_6\text{H}_5\text{NO}_2$ as viewed down the crystallographic *b* axis. Thermal ellipsoids are shown at the 50 % probability level. Hydrogen atoms have been removed for clarity. 190
- Figure 56:** $(\text{ET})_4[\text{Cr}(\text{NCS})_6] \cdot \text{C}_6\text{H}_5\text{NO}_2$ as viewed down the crystallographic *c* axis. Thermal ellipsoids are shown at the 50% probability level. Hydrogen atoms have been removed for clarity. 191
- Figure 57:** S...S short contacts, as viewed down the *c* axis. Thermal ellipsoids are shown at the 50 % probability level. Hydrogen atoms have been removed for clarity. 191
- Figure 58:** S...S short contacts, as viewed down the *a* axis. Thermal ellipsoids are shown at the 50 % probability level. Hydrogen atoms have been removed for clarity. 192
- Figure 59:** Anion and solvent sheet. Thermal ellipsoids are shown at the 50% probability level. Hydrogen atoms have been removed for clarity. 193
- Figure 60:** Nitrobenzene molecule (spacefill representation) within the ET pocket. Thermal ellipsoids (donors and anions) are shown at the 50 % probability level. Hydrogen atoms have been removed for clarity. 194
- Figure 61:** Resistivity data for $(\text{ET})_4[\text{Cr}(\text{NCS})_6] \cdot \text{C}_6\text{H}_5\text{NO}_2$ as a function of temperature. 195
- Figure 62:** ET box-like tube structure. Thermal ellipsoids are shown at the 50% probability level. Hydrogen atoms have been removed for clarity. 197
- Figure 63:** ET tube, end-on view. Thermal ellipsoids are shown at the 50% probability level. Hydrogen atoms have been removed for clarity. 197
- Figure 64:** Crystalline packing of ET tube, end-on view. Thermal ellipsoids are shown at the 50% probability level. Hydrogen atoms have been removed for clarity. 198
- Figure 65:** Crystalline packing of ET tube, side-on view. Thermal ellipsoids are shown at the 50% probability level. Hydrogen atoms have been removed for clarity. 199
- Figure 66:** Filled unit cell, showing the arrangement of ET molecules and bromide ions. 206

Figure 67: (ET)Br as viewed along the crystallographic <i>a</i> axis. Thermal ellipsoids are shown at the 50 % probability level. Hydrogen atoms have been removed for clarity.	207
Figure 68: (ET)Br as viewed along the crystallographic <i>b</i> axis. Thermal ellipsoids are shown at the 50 % probability level. Hydrogen atoms have been removed for clarity.	208
Figure 69: (ET)Br as viewed along the crystallographic <i>c</i> axis. Thermal ellipsoids are shown at the 50% probability level. Hydrogen atoms have been removed for clarity.	208
Figure 70: (ET)Br as viewed along the length of the ET molecule.	209
Figure 71: The ethylene groups on the ET molecules are displaced to accommodate the bromide ion.	209
Figure 72: Normalised resistivity data for (ET)Br as a function of temperature.	210
Figure 73: Expanded data section illustrating large increment in resistance at 192 K.	211
Figure 74: Temperature profile (as a function of time) in the region of the increment of resistance at 192 K, showing the absence of a deviation in the cooling/ warming rate.	212
Figure 75: Electron microprobe analysis using X-ray diffuse scattering, on the scanning electron microscope indicating the presence of bromine.	212
Figure 76: Electron microprobe analysis using X-ray diffuse scattering, on the scanning electron microscope indicating the presence of sulfur.	213
Figure 77: Resistivity data for (ET)Br grown in acetonitrile, as a function of temperature.	214
Figure 78: Temperature profile of the resistivity measurements for (ET)Br grown in acetonitrile.	214
Figure 79: Hydrated ET bromide salt, as viewed down the crystallographic <i>a</i> axis.	216
Figure 80: Hydrated ET bromide salt, as viewed down the crystallographic <i>b</i> axis.	217
Figure 81: Hydrated ET bromide salt, as viewed down the crystallographic <i>c</i> axis.	218
Figure 82: Cluster of bromides (deep red) and waters with short contacts shown as red lines.	218
Figure 83: Resistivity profile for (ET) ₃ (CoCl ₄) ₂ .	224
Figure 84: (ET) ₃ (CoCl ₄) ₂ as viewed down the crystallographic <i>a</i> axis.	225
Figure 85: (ET) ₃ (CoCl ₄) ₂ as viewed down the crystallographic <i>b</i> axis.	225
Figure 86: Versatility of the aldehyde function as a reaction centre.	250
Figure 87: Crystallographic image of 122, showing the bent structure. Thermal ellipsoids are shown at the 50 % probability level.	255
Figure 88: X-ray crystallographic image of 122 as viewed down the crystallographic <i>a</i> axis. Thermal ellipsoids are shown at the 50 % probability level.	256
Figure 89: Asymmetric unit for 124, showing atom numbering scheme. Hydrogen atoms have been removed for clarity. Thermal ellipsoids are shown at the 50 % probability level. The ethylene function C1/C1A and C2/C2A exhibits positional disorder as shown (isolated carbon atoms).	258

- Figure 90:** Asymmetric unit for 124, showing the bent structure with displacement of exterior sulfur atoms to the same side of the central mean plane. Hydrogen atoms have been removed for clarity. Thermal ellipsoids are shown at the 50 % probability level. 258
- Figure 91:** Packing of donor 124 as viewed down the crystallographic *a* axis. Hydrogen atoms have been removed for clarity. Thermal ellipsoids are shown at the 50 % probability level. The ethylene function C1/C1A and C2/C2A exhibits positional disorder as shown (isolated carbon atoms). 259
- Figure 92:** Extended hydrocarbon donors attached to polyamine backbone. 261
- Figure 93:** Chemical structure indicating the α - and β - positions. 266

List of acronyms, abbreviations and symbols

A	Electron Acceptor <i>or</i> Charge Stabilising Anion
B. C. S. Theory	Bardeen, Cooper and Schrieffer Theory
ATR	Attenuated Total Reflectance
BDH	2,5-bis(1,3-dithiolan-2-ylidene)-1,3,4,6-tetrathiapentalene
BEDT-TTF	Bis(ethylenedithio)tetrathiafulvalene
BETS	Bis(ethylenedithio)tetraselenafulvalene
D	Electron Donor
DDQ	Dichlorodicyanoquinine
ddd	5,6-dihydro-1,4-dithiin-2,3-dithiolate
DTDH-TTP	2-(1,3-dithiolan-2-ylidene)-5-(1,3-dithiole-2-ylidene)-1,3,4,6-tetrathiapentalene
E_a	Activation Energy
E_g	Energy Gap
EDDH-TTP	2-(4,5-ethylenedithio-1,3-dithiol-2-ylidene)-5-(1,3-dithiolan-2-ylidene)-1,3,4,6-tetrathiapentalene
EPR	Electron Paramagnetic Resonance
ET	Bis(ethylenedithio)tetrathiafulvalene
eV	Electron Volts
GC-MS	Gas Chromatography-Mass Spectrometry
IR	Infrared
k	Boltzmann Constant
MEM	Methoxyethoxymethoxymethyl
Mp	Melting Point
MS	Mass spectrometry
MW	Microwave
NMR	Nuclear Magnetic Resonance
<i>p</i> TSA	<i>p</i> -Toluenesulfonic acid
R_f	Retention Factor
SQUID	Superconducting Quantum Interference Device
T_A	Superconducting Temperature of Pure component A
T_C	Superconducting Transition Temperature
TCNQ	Tetracyanoquinodimethane
TEMPO	Tetramethylpiperidine- <i>N</i> -oxide
TGA	Thermal Gravimetric Analysis
TLC	Thin Layer Chromatography
T_{M-I}	Metal-insulator Transition Temperature
TMTSF	Tetramethyltetraselenafulvalene
TMTTF	Tetramethyltetrathiafulvalene
TTF	Tetrathiafulvalene
V_A	Geometric Volume of Anion
V_C	Geometric Volume of Crystallographic Unit Cell
VT	Bis(vinylenedithio)tetrathiafulvalene
Z	Electrical Charge on Electron Donor (positive)

Chapter 1

Introduction

1 Introduction

The relationships between the structure of a molecule, material or crystal and the properties it exhibits have undergone extensive studies by biologists, chemists, physicists and all combinations of interdisciplinary researchers. Understanding how devices and processes work on the molecular scale provides crucial information on everyday occurrences and phenomena. Whereas some properties have well-established theories and are ‘understood’, the phenomenon of superconductivity observed in such diverse structures as ceramics ($\text{Bi}_2\text{Sr}_2\text{Ca}_{n-1}\text{Cu}_n\text{O}_{2n+4}$ T_C 's = 10 – 110 K),^{1, 2} metals (Hg at 4 K)^{3,4} and low temperature one-dimensional superconductors ($\kappa\text{-ET}_2\text{I}_3$ at 3.6 K)⁵ poses many questions. In order to answer these questions, different theories have been developed which are able to account for different types of superconductivity. As such, the field is sub-categorised according to the structural aspects exhibited, with researchers constantly observing novel features and adapting theories to account for them.

1.1 Types of conductivity

Electrical conducting materials may be broadly described as falling into one of four categories: Insulating, Semi-conducting, Metallic or Superconducting. These groupings are defined by the observation of the energy of their conducting and valence bands of electrons, and the difference between these two states, as according to the band theory and illustrated in Figure 1.

1.1.1 Band theory

In an isolated atom, a^0 , the energy levels do not experience any external influence, and are therefore quantised as having a specific energy, $E(a)$. As another chemically and energetically identical atom, a^1 of energy $E(a)$, is brought closer to a^0 , the energy levels associated with each atom are perturbed by the influence of its neighbour. As a result, the energy levels each split into n levels ($n = 2$ in this case) where n is the number of atoms present, i.e.

$$E(a) \rightarrow E(a)^{*1} + E(a)^{*2}$$

In a lattice structure, n is of the order of 10^{23} , and the discretely spaced energy levels can be viewed as a band. The lower energy bands are filled with electrons bound to the atoms present. Conduction electrons thus occupy the higher energy bands, termed the valence bands. Incomplete filling of the valence bands leave empty energy states that are available to the conduction electrons to occupy when excited. The lowest band that

contains vacant energy states is termed the conduction band, and the difference in energy between the valence and conduction bands is termed the band gap (E_g).

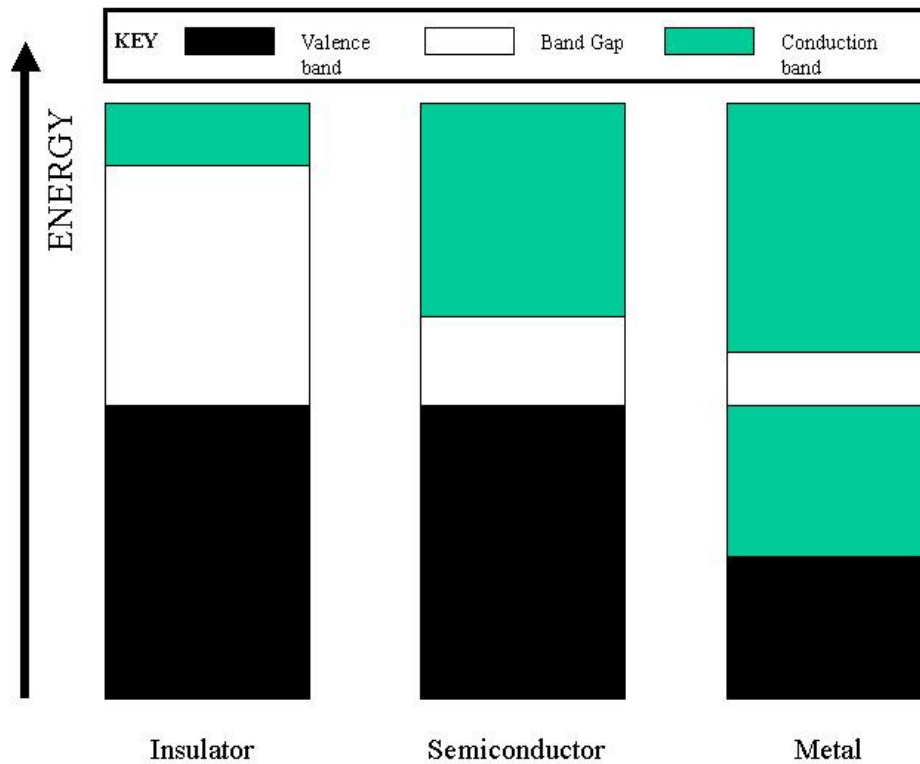


Figure 1: Possible band structures of a solid.

1.1.2 Insulator

An electrically insulating material is one in which the current is impeded, and thus the material exhibits high resistance. This is ascribed to a large energy separation between the conducting and valence electron bands of the material. Valence electrons, with their

defined thermal energy are unable to be promoted into the conduction band, resulting in a conduction band that is essentially empty, and the material having little conductivity.

Experimentally, the material shows resistance at the upper-limit of detection, as portrayed (Figure 2, green line). Insulating behaviour is observed for materials such as rubber and wood.

1.1.3 Semiconductor

Semiconducting materials exhibit increased resistance as the temperature is lowered. At higher temperatures the valence band electrons have sufficient thermal energy to be promoted out of the valence band into vacancies in the conduction band. As the temperature of the material is decreased there are fewer electrons with sufficient thermal energy to overcome the energy gap and occupy the excited state. As a result the conductivity decreases, with the valence band becoming increasingly full, and the material enters an insulating state.

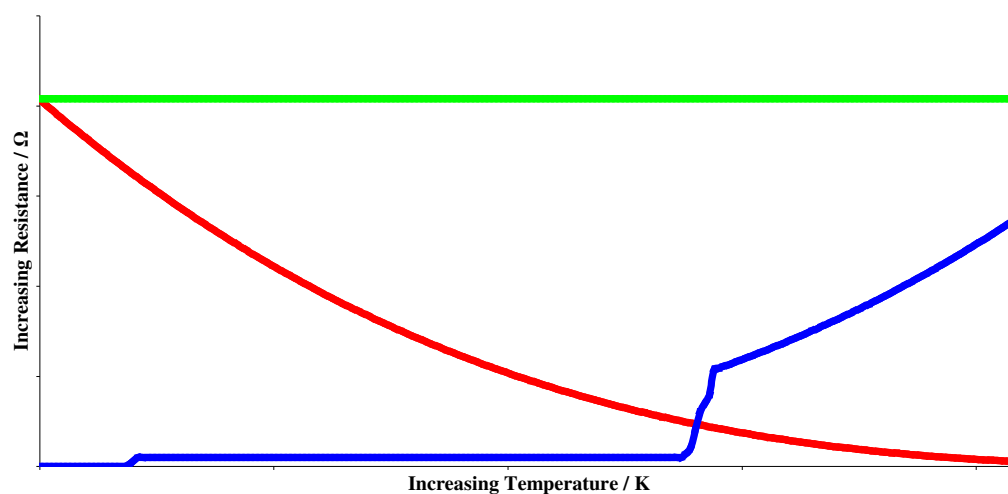


Figure 2: Representative resistivity data for a solid as a function of temperature: Insulator (green line), Semiconductor (red line), Metal (blue line), Superconductor (blue line, near the origin).

Experimental data shows a curve for a plot of the resistance (Ω) against temperature (K). The slope of the curve increases in an exponential fashion with decreasing temperature (Figure 2, red line). Application of an Arrhenius-type equation allows the activation energy (E_a) of the material to be determined from a plot of the natural log of the resistance against one thousand over the temperature (Figure 3). The slope of the straight line is equal to the activation energy divided by the Boltzmann constant (E_a/k). The activation energy is normally quoted in electron volts (eV) and has a typical value of the order of 100 meV for a bis(ethylenedithio)tetrathiafulvalene (BEDT-TTF, or known hereafter in this thesis as ET) semiconductor.⁶

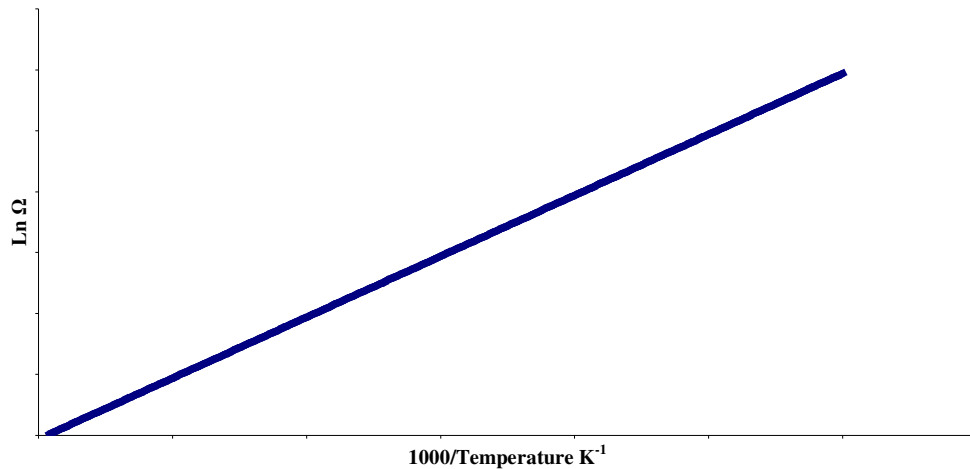


Figure 3: Plot of the logarithm of the resistance against inverse temperature showing a linear dependency for a semiconducting material.

1.1.4 Metal

Metallic or metal-like materials are those that exhibit the conductive properties of a true metal, but that do not necessarily contain any metallic elements. The conductivity of this type of material decreases with increasing temperature, due to the increased thermal energy of the atoms in the crystal lattice. Upon heating the material the lattice vibrations (phonons) distort the crystal structure, causing migrating electrons to be scattered by the imperfect structure. In addition to the phonon interaction, slight impurities may also alter the conductivity.

Metallic behaviour is illustrated on the almost horizontal section of the resistance plot (Figure 2, blue line).

1.1.5 Superconductor

A superconducting material is one that, below a critical temperature (T_C) conducts electricity with no or negligible resistance. Above this critical temperature, the material may exhibit metallic behaviour. The occurrence of such a state of matter is understood by use of the Bardeen-Cooper-Schrieffer (B. C. S.) theory. Superconductivity is illustrated in the resistance plot in the section where resistance drops to (and follows) the baseline (Figure 2, blue line near origin).

1.2 Superconductivity

The ability of a material to exhibit no resistance to electrical conductivity was first observed in 1911.^{3,4} In the investigation of properties of materials at liquid helium temperatures, Onnes described that the electrical resistance of pure gold was ‘inappreciable’ at the boiling point of liquid helium. Further work revealed that the resistance of mercury was, below 3 K, lower than $3 \times 10^{-6} \Omega$, *i.e.* essentially non-existent. As the author confesses, the error in the experiment led to difficulties reproducing results accurately, and upon further electrical resistance studies of mercury at low temperatures, it was observed that the resistance was only just measurable above 4.2 K, having a value of $2.3 \times 10^{-4} \Omega$ upon warming the sample. A new physical concept had been observed, which was to stimulate materials research, leading to further properties, such as the Quantum Hall effect,^{7,8} and a vast array of applications.

In the same year another important discovery was announced. Researchers in America reported that using electrochemical methods, they had prepared tetramethylammonium-mercury amalgam and that it exhibited metal-like properties.⁹ Prior to this, it was generally accepted that binary alloys were only formed from components that were both true metals, and as such the authors proposed that the organic radicals present in their amalgam were in a metallic state. As a closing remark to their paper, McCoy and Moore stated, “It is possible to prepare composite metallic substances from non-metallic constituent elements”. This initial hybrid metal-like material paved the way for extensive studies into binary metal alloys, and tetraalkylammonium salts are still used today in the preparation of electron-transport radical cation salts.

As the research into materials developed, so too did the theories attempting to account for the superconducting state. Explanations proposed by London in 1935,¹⁰ and Fröhlich in the 1950s,¹¹ were later incorporated into a theory that has been used to describe superconducting behaviour for over 50 years. The theory, published in December 1957, was rapidly accepted by the scientific community. Known by reference to the authors’ initials, Bardeen, Cooper and Schrieffer, the B. C. S. theory attempted to account for the observation of low temperature superconductivity in metals and their alloys.¹²

1.3 B. C. S. theory

The theory places much emphasis on the observation by Meissner in 1933,¹³ that a material in its superconducting state exhibits perfect diamagnetic behaviour. The

reasoning follows similar lines to that proposed by London in which the wave functions are not altered significantly by application of an external magnetic field due to a coherence effect in the superconducting state. There is also inclusion of Fröhlich's suggestions that the primary reason for superconductivity may be attributed to electron – phonon interactions, and that the property itself may be described as the movement of a single entity through the lattice structure.

Bardeen *et al.* propose that the mobile electrons present in a superconducting material at low temperatures, exist in pairs. These Cooper pairs can be treated as a single entity, consisting of two electrons possessing equal but opposite spin. The formation of the Cooper pair occurs as an individual electron interacts with the lattice structure of the crystal, causing the lattice to be disturbed slightly. The disturbed lattice subsequently interacts with another electron, causing an attraction between the two electrons that is of greater magnitude than the Coulombic repulsion between them. The Cooper pairs do not obey the Pauli exclusion principle, and as such many may exist in the same quantum state with the same energy. As a material passes from the ground state to the superconducting state, the Cooper pairs act as one body moving together without resistance until at a T_C there is sufficient thermal energy to overcome the energy gap (E_g) and the paired electrons break apart allowing collisions into the lattice.¹⁴

$$E_g = 3.5 \cdot k \cdot T_C$$

Where k is the Boltzmann constant (8.617343×10^{-5} eV/K).

1.4 Superconducting metal alloys

By the mid 1970s, the highest critical temperature achieved for the onset of superconducting behaviour was 23 K. The material, an alloy of Niobium and Germanium (Nb_3Ge), was prepared as a film by a sputtering technique.¹⁵ Gavalier *et al.* highlighted correlations between the superconducting transition temperature and the mechanical methods of preparing the films, namely the sputtering voltage, gas pressure, and substrate temperature. The optimum conditions determined were a low voltage of less than one thousand volts, a high gas pressure of greater than 0.1 Torr and a substrate temperature of between 700 and 950 °C. This was perhaps the first indication that how a sample is mechanically prepared is equally as important as the components (and the purity) of the material.

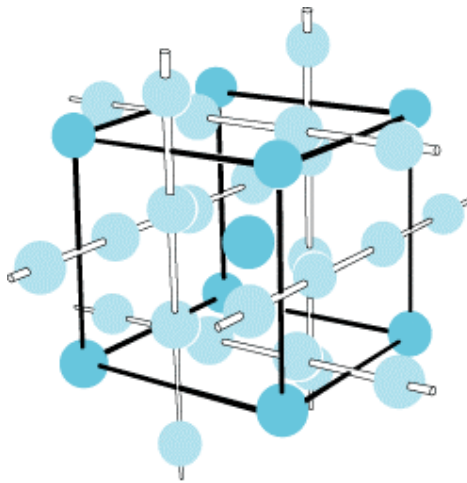


Figure 4: Primitive cubic cell exhibited by A-15 superconductors.¹⁶

The structure of the material was determined to be a primitive cubic cell at the low temperatures of superconductivity (O_h^3 , $Pm3m$), in which the Ge ions occupy the corner positions with orthogonal chains of Nb ions occupying facial positions (Figure 4). This structure has the generic formula (and is referred to as type) A_3B , and forms part of the A-15 superconductors as determined by Dew-Hughes and Rivlin.¹⁷

There is a structural relationship in alloys of this type, in which the minor component (B component) is from group IVB (Si, Ge, Sn) and the major component (the A component) is from group VA (Nb, V, Ta). For these materials there is a linear dependency of the superconducting transition temperature of the alloy when correlated against a function of the atomic mass of the minor component. The gradient of the slope varies as the A component is changed showing the importance of the major component, and the plot extrapolates accurately to zero suggesting there are no unaccounted variables involved in the model. The T_C for the A-15 superconductors can be calculated from the equation:

$$T_C = 27.5 \cdot (T_A - 2) \cdot M_B^{-0.5}$$

Where T_A is the superconducting transition temperature for the pure A component, and M_B is the atomic mass of the B component.

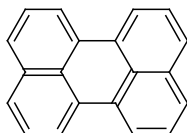
This was rationalised by assuming that the only phonon modes involved in the B. C. S. theory are those that are close to the zone boundary, where the relationship for each

branch of the dispersion relationship in the polyatomic crystal reduces to a form that is inversely proportional to only one of the masses.

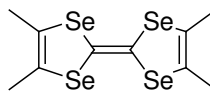
The upper limit of the superconducting transition temperature, determined by the maximum phonon frequency (Debye frequency), led Little to propose that high temperature transitions into the superconducting phase may be achieved in molecular metals, since the frequency of their internal vibrations could play a role similar to that of phonons in metal-based superconductors.¹⁸ The possibility of creating an organic-based superconductor led to intensive research, and was eventually realised in the early 1980s.

1.5 Conductivity in non-metallic materials

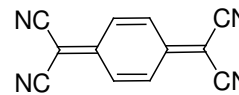
A report in 1954 from Japanese researchers indicated that they had observed high electrical conductivity in a complex formed from non-metallic elements, and in which the principal reagent had a resistivity much higher than that of the product.¹⁹ The black complexes formed upon chemical oxidation of perylene (**1**) by bromine indicated a structure of $C_{20}H_{12}.Br_{3-4}$ and exhibited semiconductor behaviour, as illustrated by the linear relationship of the logarithm of the resistance against reciprocal temperature (e.g. Figure 3)



1



2



3

1.6 Non-metallic superconductors

The synthesis of tetramethyltetraselenafulvalene (TMTSF, **2**) was first reported in 1974.²⁰ Bechgaard reported the first charge transfer salt of this organoselenium donor with tetracyanoquinodimethane (TCNQ, **3**) to have a room temperature conductivity of around $800 \Omega^{-1}\text{cm}^{-1}$. It was six years later though, before the first organic superconductor was reported in 1980.²¹ TMTSF was electrochemically oxidised in the presence of the hexafluorophosphate anion, affording elongated crystals of $(\text{TMTSF})_2\text{PF}_6$ (Figure 5).

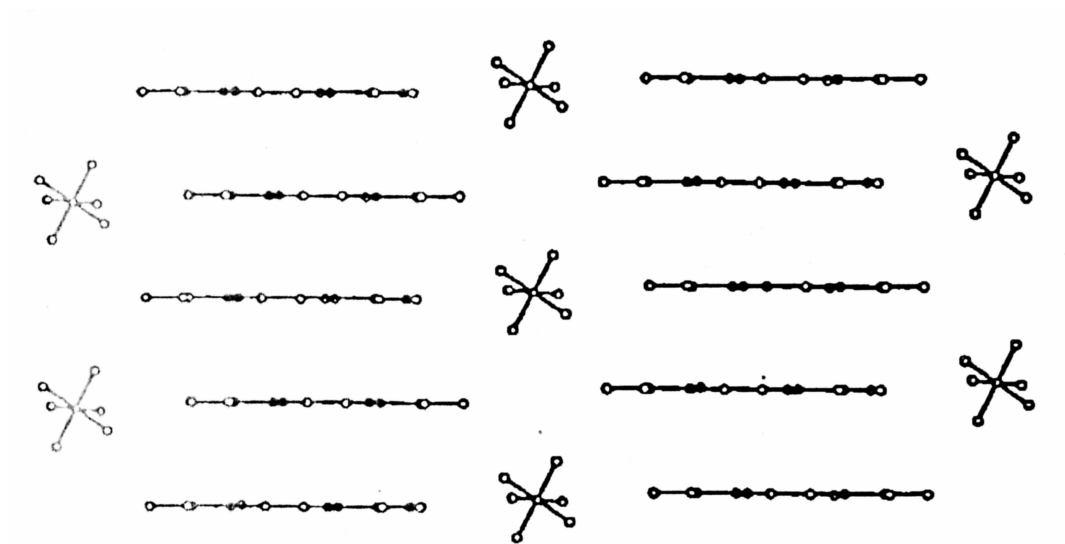


Figure 5: Crystal structure of $(\text{TMTSF})_2\text{PF}_6$, showing stacking of the donor molecules.²¹

The resistivity was measured as a function of temperature down to almost absolute zero. At atmospheric pressure the material showed a one-dimensional conductivity in excess of $10^5 (\Omega\cdot\text{cm})^{-1}$ arising from the orbital overlapping in the stacks of the donor molecules,²² and a sharp metal-insulator transition at $T_{\text{M-I}} = 15 \text{ K}$. However, under an

applied hydrostatic pressure of 12 kbar, the transition was suppressed and a superconducting state was observed at 0.9 K. Further evidence of the superconducting state was provided by application of an external magnetic field perpendicular to the stacks of donors, resulting in a shift of the resistivity curves. A systematic study of 13 different anion components (PF_6^- , AsF_6^- , TaF_6^- , NbF_6^- , ClO_4^- , ReO_4^- , BF_4^- , BrO_4^- , IO_4^- , NO_3^- , FSO_3^- , CF_3SO_3^- , TeF_5^-) allowed the properties of the acceptor species to be identified and removed in order to focus on the electron donor itself. These salts, of general form D_2A , where D is the electron donor TMTSF, and A is the anion/electron acceptor species, became known as the Bechgaard salts. At room temperature they exhibit a crystalline structure (crystallographic space group P-1) in which the molecules are centrosymmetrically related. From the study, some key concepts were highlighted, including structural disorder effects, pressure-suppressed metal-insulator transitions and the steric demands of the anion species in the salts.

The requirement for the application of pressure in order to induce a superconducting state in the system identified that closer packing was required in order to achieve zero resistance materials. As such, Bechgaard employed the less sterically demanding tetrahedral anions.²³ Salts of perchlorate, tetrafluoroborate and perrhenate anions were synthesised with TMTSF, and for the first time ambient pressure superconductivity was demonstrated. Upon cooling from a metallic state, the ClO_4^- salt underwent a superconducting transition between 1.3-1.5 K. In the other two systems an insulating transition occurred at $T_{\text{M-I}} = 41$ K (BF_4^-) and $T_{\text{M-I}} = 182$ K (ReO_4^-). The onset of bulk superconductivity in the perchlorate salt was confirmed independently by radio-

frequency penetration depth measurements (rf measurements) and determined to be $T_C = 1.21$ K for slow cooled samples.²⁴

In the TMTSF salt formed when A is ReO_4^- , the metallic phase observed upon cooling from room temperature to around 180 K, is destroyed by a transition to an ordered structure, leading to an electron – phonon instability and the material becoming insulating. The transition can be suppressed by the application of positive pressure.

Under moderate pressure (1.2 GPa), the salts containing the symmetrical (and crystallographically ordered) octahedral anions were found to exhibit a superconducting phase with $T_C = 1.5$ K. In similar fashion to the PF_6^- salt, at ambient pressure they all exhibited a metal-insulator transition, with $T_{M-I} < 20$ K.

In the room temperature crystal structure of the BF_4^- salt (crystallographic space group P-1), the donors exist in a planar conformation as stacks.²⁵ Short intrastack distances between neighbouring Se atoms give the salt a 2-D structure, and the material exhibits metallic behaviour from room temperature until an insulating transition occurs at $T_{M-I} = 40$ K. The structures of the PF_6^- , ClO_4^- , BrO_4^- and FSO_3^- salts are isomorphic but the physical properties differ in each case.

Similar studies of a compound that is isostructural to TMTSF in terms of its chemical and crystallographic properties is tetramethyltetrafulvalene (TMTTF, **4**). Parkin found that it too formed D_2A structures, however it exhibited different electrical properties at ambient pressure.²⁶ The room temperature conductivities of the

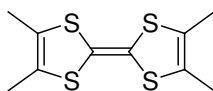
(TMTTF)₂X salts typically have conductivities in the range 300-500 (Ω·cm)⁻¹ whereas the (TMTSF)₂X salts exhibit 50-300 (Ω·cm)⁻¹. However, for these salts the T_{M-I}'s are considerably higher, and the conductivities of the salts decrease with applied pressure.

In general for TMTSF and TMTTF systems, the interactions between either the Se...Se or S...S are more significant in the intrastack direction as opposed to the interstack direction.

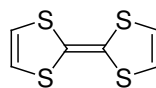
The observation of the importance of the anion size as a determinant of the physical properties exhibited, paralleled the discovery of the minor component dependency in the A-15 superconductors. Identification of a linear correlation between the unit cell volume (V_C) and the anion volume (V_A) is observed both at room temperature and 120 K, for the D₂A salts. As such, with the consideration of lattice order and intermolecular interactions in mind, it is plausible to expect that anions of volumes similar to that of the perchlorate should lead to superconducting phases being observed.^{27, 28}

$$V_C = 0.65 V_A + 645 \quad (\text{when } T = 298 \text{ K})$$

$$V_C = 0.42 V_A + 642 \quad (\text{when } T = 125 \text{ K})$$



4

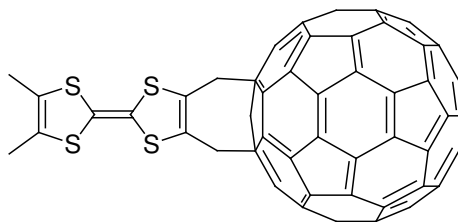


5

1.7 Tetrathiafulvalene

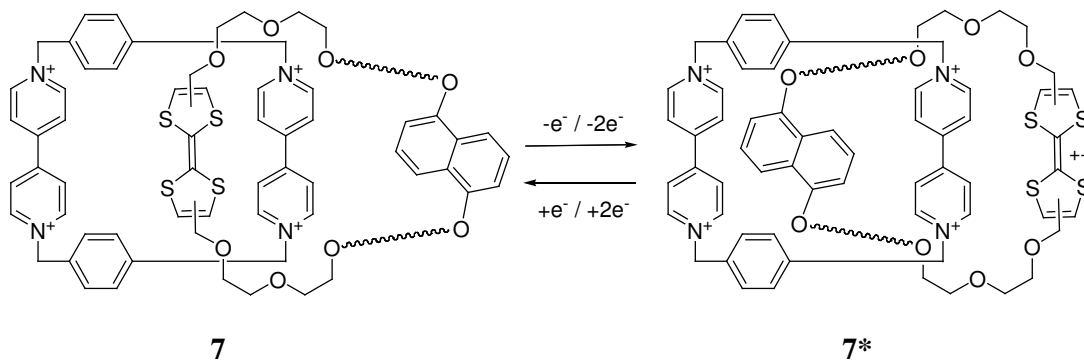
The first organosulfur donor was synthesised over 30 years ago. Tetrathiafulvalene (TTF, **5**) has been widely studied since its discovery, and is still under investigation today. The small electron-dense molecule exists in the neutral oxidation state as several polymorphs in the crystalline state.²⁹ TTF has since been functionalised exhaustively, including (not exclusively) derivatives containing amides,³⁰ thioamides,³⁰ thioesters,³⁰ cyanides,³¹ and acids,³¹ and has been extensively reviewed.^{32,33,34}

Investigation of the electrical properties of TTF originated with the preparation of a 1:1 charge transfer salt produced by partial chemical oxidation of TTF by TCNQ. The salt is metallic over a large temperature range, and exhibits a semiconductor-metal transition at 66 K.³⁵ The chloride salt of TTF has also been shown to exhibit high electrical conductivity.³⁶ More recently, the electrical properties have been investigated for the tetramethyl-TTF species appended to buckminsterfullerene (**6**).^{37,38,39,40}

**6**

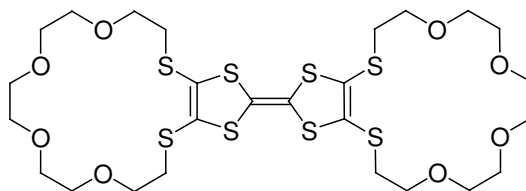
With materials science applications in mind, research groups have prepared numerous peripheries for the TTF core structure leading to molecules in which the electron donor has been substituted with cyanobiphenyl groups.⁴¹ The material is a liquid crystalline derivative, and undergoes a change from the Isotropic liquid into a Nematic phase, and then into a Smectic A phase. A compound such as this could find application in lightweight, low energy consumption display devices.

More exotic functional structures have also been synthesised, such as TTFs linked by polyether chains incorporating a naphthyl group in a ring system. The combination of this with a bis(4,4-bipyridinium) ring system leads to the formation of a catenane. The compound is able to act as a molecular switch, in which a colour change reflects a change in the position of the TTF moiety with respect to the location of the bipyridinium cycle, being inside or outside the loop (**7-7***).⁴²

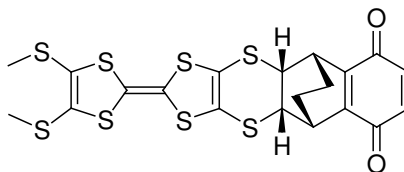


Other examples include a derivative with a phthalocyanine moiety attached to the TTF compound,⁴³ which shows liquid crystalline behaviour. Compounds showing an application in the sensing of cations have also been developed, with the TTF core being appended with crown-ether type systems (**8**).^{44,45,46,47}

There has also been significant effort in the preparation of materials which can exhibit intramolecular charge transfer interactions, such as TTFs linked to TCNQ derivatives via ester groups,⁴⁸ and TTF molecules which have undergone Diels-Alder reactions with substituted *p*-benzoquinones (**9**) linked *via* a rigid bicyclic cage,⁴⁹ which has been shown to exhibit such an interaction.

**8**

Poly-TTF species, and dendritic-type molecules have also been prepared by palladium cross coupling reactions, and charge transfer salts prepared with TCNQ show room temperature conductivities of around $30 \text{ S}\cdot\text{cm}^{-1}$.⁵⁰ Incorporation of chirality in the donor species, led to the preparation of racemic mixtures of a chiral bis-TTF, functionalised with a chiral alcohol fragment bridging the two TTF molecules. The charge transfer salt with TCNQ showed a structure based on centrosymmetrically related dimers.⁵¹

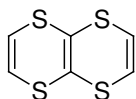
**9**

A structural isomer of TTF (in which the central double bond is rotated 90° in order to create a fused bicyclic system ($\text{C}_6\text{S}_4\text{H}_4$, **10**)) was prepared by the hydrolysis of a thione

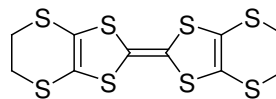
compound, which was subsequently trapped by 1,2-dibromoethane, and oxidised.⁵² NMR experiments indicated a non-planar structure, suggesting that the material was not exhibiting the 14- π aromatic system possible. The isomer was hard to oxidise with $E_{1/2}^1$ 0.561 V and $E_{1/2}^2$ 0.965 V (irreversible 2nd step) compared to 0.006 and 0.385 V for TTF.*

1.8 Bis(ethylenedithio)tetrathiafulvalene

Bis(ethylenedithio)tetrathiafulvalene, **11**, also known as BEDT-TTF or ET, was first synthesised by Mizuno *et al.*,⁵³ using methodology devised for the synthesis of the TTF isomer **10**.⁵² The first charge transfer salt with TCNQ exhibited 1:1 stoichiometry, and showed room temperature conductivity two and a half times that of the TTF complex, being $50 (\Omega\cdot\text{cm})^{-1}$ and $20 (\Omega\cdot\text{cm})^{-1}$ respectively.



10



11

Since its discovery, ET has become the dominant structure employed in the preparation of radical cation salts. This can be attributable to three key factors:

* Conditions: Acetonitrile, TEA[ClO₄] 0.05 M, Ag/Ag⁺ 0.1 M in acetonitrile, with glassy carbon electrode as working electrode.

- (1) ET forms salts with a large array of electron acceptors/anions due to its increased core π -delocalised structure;
- (2) A variety of stoichiometries of the salts formed may be observed for each particular electron acceptor/anion;
- (3) The salts that are formed from the same component species may exhibit a range of crystalline structures (phases).

In ET salts the ratio of electron donor to anion varies greatly, as do the crystallographic space groups that are exhibited. However, the ways in which the ET molecules pack generally follow two types of packing when one layer is viewed face-on (interstack interactions): (1) Zigzag (Figure 6, Left-hand diagram); (2) Linear (Figure 6, Right-hand diagram).⁵⁴

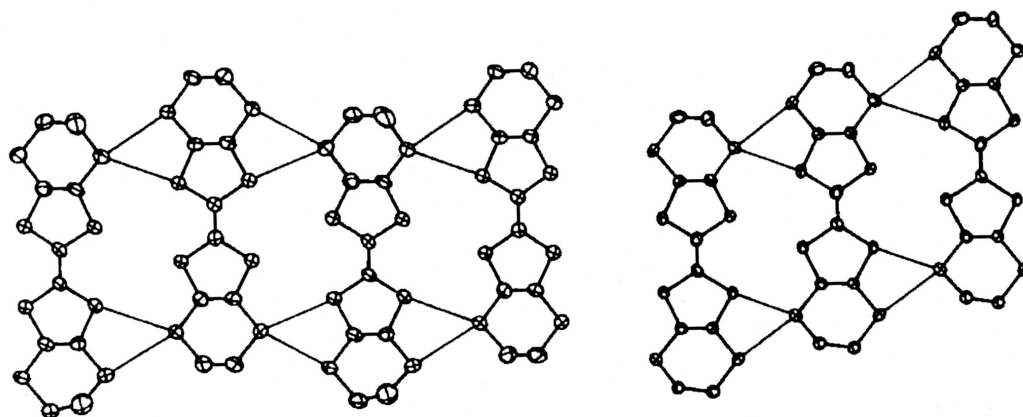


Figure 6: ET interstack packing motifs.⁵⁴

When viewing several layers, the stacks observed (intrastack) generally adopt one of three motifs:

- (1) Longitudinal overlap distortion (Figure 7, Top diagram);
- (2) Latitudinal overlap distortion (Figure 7, Middle diagram), and;
- (3) Twisted overlap distortion (Figure 7, Bottom diagram).

Within five years of the synthesis of ET, metallic conductivity was observed from room temperature to 1.4 K in the material $(\text{ET})_2\text{ClO}_4(\text{TCE})_{0.5}$.⁵⁵ Thin black leaf-like crystals with a metallic lustre were prepared by electrochemical oxidation in trichloroethane. The triclinic crystal structure was shown to consist of non-planar donor molecules, stacked along a crystallographic axis. The deviation from planarity is thought to be due to the thermal motion of the exterior carbon atoms. Along another axis, the donor molecules are separated by sheets of ClO_4^- anions and solvent molecules.

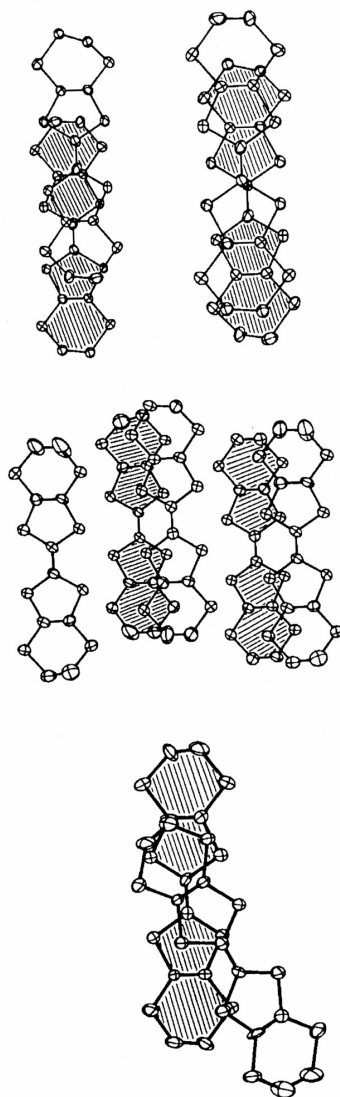


Figure 7: ET intrastack packing motifs.⁵⁴

Further perchlorate salts were reported in which the trichloroethane molecule had been replaced in the crystal structure by a dioxane molecule, prepared from a mixed solution system of dioxane and trichloroethane.⁵⁶ The structure $(\text{ET})_2\text{ClO}_4(\text{C}_4\text{H}_8\text{O}_2)$ crystallised in the space group $P2/c$. Although the donor molecules form stacks, short $\text{S}\cdots\text{S}$ contacts are only observed in the interstack direction, compared with short intrastack contacts in

the TMTSF and TMTTF perchlorate salts. The salt showed semiconductor behaviour, with $E_g = 0.3$ eV. The structure showed linear chains of ET molecules. Investigation of the properties of the donor and anion in the salt was complex, as it included the solvent too. However electrocrystallisation in dichloromethane afforded a salt that did not contain solvent molecules. The salt $(\text{ET})_3(\text{ClO}_4)_2$ crystallised in the triclinic space group P-1. Short interstack S...S contacts were observed, and a zigzag packing behaviour exhibited. The resistivity profile of the compound indicated metallic behaviour from room temperature to $T_{M-I} = 170$ K at ambient pressure, which may be suppressed to around $T_{M-I} = 95$ K under a pressure of 10 kbar.⁵⁷ The low temperature β'' - $(\text{ET})_3(\text{ClO}_4)_2$ structure in the charge ordered state is shown to consist of two donor molecules which are slightly dimerised, with the remaining donor molecule appended to the dimer.⁵⁸

In the case of the isostructural hydrogensulfonate anion, the γ - $(\text{ET})_3(\text{HSO}_4)_2$ structure undergoes a structural change causing the metallic character to be lost at $T_{M-I} = 125$ K.⁵⁹ Interestingly, deuteration of the anion increases the length of the O...O distances of intermolecular hydrogen bonds, but the T_{M-I} is not appreciably affected. In specific heat measurements, an anomaly is observed at 125.8 K (undeuterated case) and around 127 K (deuterated case). Again, low temperature Raman studies indicated a slight dimerisation of two of the donor molecules with an additional donor molecule appended to the dimer. Crystallographically analogous structures consisting of $[\text{Ni}(\text{dddtd})_2]_3(\text{HSO}_4)_2$ show metal-semimetal phase transitions occur at around 25 K.⁶⁰ Drastic differences exist in the thermopower properties of the two materials, and these have been attributed to the complexity of their band structures.

1.9 First organosulfur superconductor

The first sulfur based organic superconductor, $(\text{ET})_4(\text{ReO}_4)_2$, exhibited superconducting behaviour with $T_C = 2$ K (broad transition), when a pressure of 4-6 kbar was applied.⁶¹ At 7 kbar pressure, $T_C = 1.4$ K, and at ambient pressure no superconductivity is observed, and an insulating phase is demonstrated at $T_{M-I} = 81$ K. The material did not experience dielectric instability at pressures greater than 6 kbar.⁶² The centrosymmetrically related structure crystallised in the space group P-1, with the non-planar ET molecules exhibiting a zigzag arrangement, and loosely stacked. The stacks were shown to be separated by sheets of anions that are situated in voids/cages created by the surrounding donor molecules. At room temperature these anions showed ordering. This phase grew from a tetrahydrofuran solution which also afforded crystals determined to be $(\text{ET})_4(\text{ReO}_4)_2(\text{THF})$ and $(\text{ET})_6(\text{ReO}_4)_4$. Their easily distinguished morphologies allowed easy separation, and upon investigation each behaved differently under applied pressure.

Variable temperature crystallography ($T = 198$ and 125 K) performed on the superconducting $(\text{ET})_2\text{ReO}_4$ phase grown from trichloroethane, highlighted the lack of close intrastack S...S contacts, but the existence of interstack contacts, giving a corrugated sheet network within the $(\text{ET})_2\text{ReO}_4$ system.⁶³

The 2-D structure of $\alpha\text{-(ET)}_3(\text{ReO}_4)_2$ is similar to that of the 3:2 perchlorate salt, however the 3-D structure is considerably different.⁶⁴ The perrhenate salt exhibited metallic conductivity until an insulating transition occurred at $T_{M-I} = 88$ K, whereas the

perchlorate salt exhibited this transition at $T_{M-I} = 170$ K. The structure adopts a $P2_1/n$ packing arrangement, with no short $S\cdots S$ intrastack contacts, but some short interstack contacts. There also exists a network of $S\cdots O$ close contacts ($2.82 - 3.04$ Å) that serve to stabilise the conductivity in the perrhenate salt.

In contrast to the perchlorate and perrhenate structures, an unsolvated 2:1 salt prepared containing the perbromate anion showed metallic behaviour from room temperature down to 6 K. Below this temperature a magnetic phase transition was observed. Three different morphologies were identified from the electrocrystallisation, $(ET)_2BrO_4$ as needles, $(ET)_2BrO_4(TCE)_{0.5}$ as thick plates, and $(ET)_3(BrO_4)_2$ as thin plates. The ET_2BrO_4 phase showed complete ordering in the crystal structure at both 298 and 125 K.⁶³

1.10 First ambient pressure organosulfur superconductor

In 1984, the first ambient pressure sulfur based organic superconductor was discovered. The structure, now termed β - $(ET)_2I_3$, (Figure 8) was observed to undergo a transition into a superconducting phase at $T_C = 1.4$ K.^{65,66,67} Despite undergoing a structural phase transition at 195 K, the electron transport properties were not significantly altered within the salt to destroy the zero-resistance phase. The high temperature transition is observed in the thermoelectric power of the material as an anomaly at 195 K.⁶⁸ Below 200 K, satellite reflections identified by X-ray and neutron diffraction data illustrate a structural modification suggesting long-range structural ordering, a prerequisite for superconducting behaviour.⁶⁹ The structural modification at 195 K is persistent to

11 K.⁷⁰ The room temperature crystal structure, portrays ribbons of I_3^- anions with loosely stacked molecules of ET, having an intrastack distance greater than the sum of the van der Waals radii. Between the stacks, short S...S contacts are present, giving a sheet structure with a high conductivity parallel to the sheets. Observation of the crystal structures collected at 298 K and 125 K showed a 2% contraction of the S...S close contacts upon cooling. The modulation of the structure is ascribed to the anion-cation interactions.⁷¹ Confirmation of the superconducting phase was achieved by rf measurements $T_C = 1.4$ K,⁷² for both hexagonal and needle crystal morphologies produced.

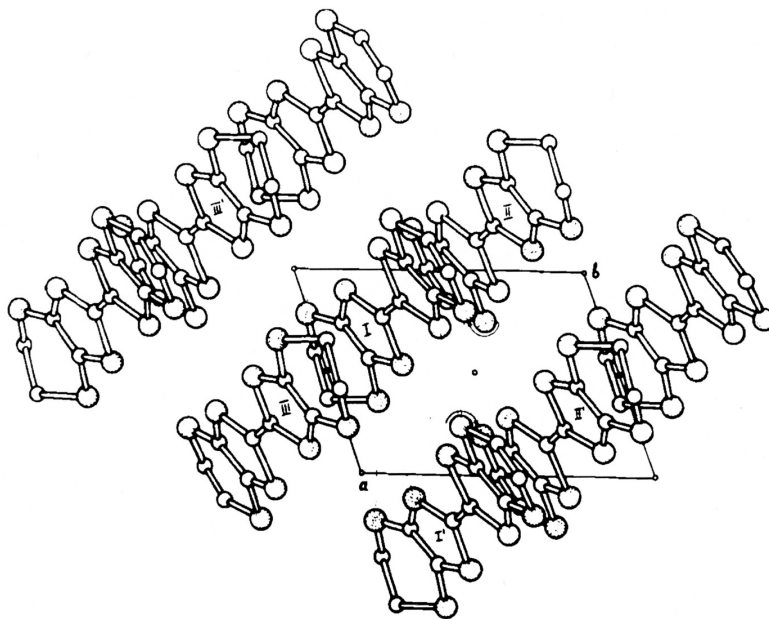


Figure 8: Packing of donor molecules in β -(ET) $_2$ I $_3$.⁶²

The 2-D metallic nature of the material was identified by thermopower measurements across two different axis of a crystal. The measurements showed parallel traces when

measured as a function of temperature. By comparison, similar measurements on TMTSF salts showed that they only exhibited 2-D behaviour below 100 K.⁷³ Measurements indicated that in the temperature range 30-120 K, small sample regions may have existed in which semi-metal behaviour occurred. In addition, the microwave and d.c. conductivity measurements were similar at room temperature. The 2-D network was apparent by the observation that the conductivity in the interstack direction is higher than in the intrastack direction. Above 135 K there existed a metallic region, observed in both the microwave and d.c. conductivities. However, below 120 K the two techniques started to give different results. The microwave conductivity remained constant to 40 K, at which point a dramatic drop was observed between 20-30 K. The d.c. resistivity measurements increase suddenly in the range 120-140 K but exhibit a reduced negative gradient below 120 K. The observed difference in results may be due to isolated semi-metal regions, which can only be observed by the microwave conductivity, which measures the bulk conductivity of the sample rather than a single crystal.⁷⁴

The various phases of $ET_x(I_y)_z$ that are formed in one cycle of electrocrystallisation, have very different electrical conductivity properties associated with them, and the materials vary from insulator through to superconductor. The different polymorphs are separable by the careful observation of the crystal habit.

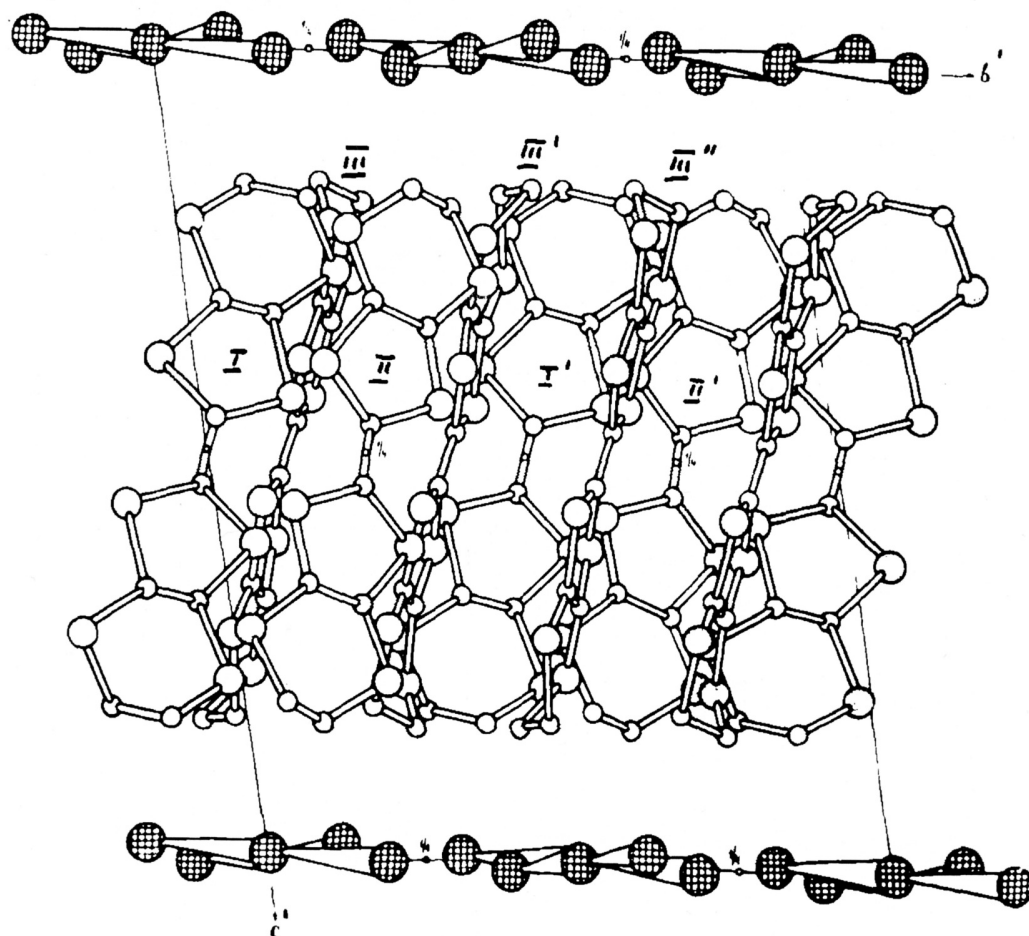


Figure 9: Packing motif of α -(ET)₂I₃, as viewed along the a' diagonal.⁶²

1.10.1 α - Phase packing of ET

The α - form of the (ET)₂I₃ crystals exhibit two types of habit, either elongated plates or square plates. There are two types of ET molecules present in the crystallographic unit cell (Figure 9). The α -phase has S...S interstack distances shorter than that of the S...S intrastack distances. It behaves as a 2-D metal upon cooling from room temperature down to a point at which a sharp insulating transition occurred at $T_{M-I} = 135$ K.⁷⁴ Microwave conductivity (10 GHz) over the temperature range 30-120 K shows a

frequency dependence, which could be due to the presence of small pockets of semi-metal material, increasing the overall bulk conductivity.

1.10.2 β - Phase packing of ET

The β - forms of ET_2I_3 are 2-D organic metals. The crystal habits observed for this phase are distorted hexagons and needles (initially observed from trichloroethane). When the solvent employed is benzonitrile, in addition to the needles, thin flakes are also observed. The structure consists of both short S...S intrastack contacts and short S...S interstack contacts (Figure 8). The increased dimensionality in the electrical conducting system stabilises the occurrence of the metallic state, and is illustrated by a corrugated sheet network of donor molecules. A superconducting phase is observed with $T_C = 1.4\text{-}1.5$ K as determined by resistivity measurements.

It is possible to distinguish between the α - and β - phases of the ET salts by observation of the room temperature Electron Paramagnetic Resonance (EPR) linewidth.⁷⁵ For the α - phase $\Delta H_{pp} = 95$ G, whereas for the β - phase $\Delta H_{pp} = 20$ G.

The α - and β - phases of $(\text{ET})_2\text{I}_3$ are formed not only by electrocrystallisation techniques, but also by the chemical oxidation of ET with either $(\text{TBA})\text{I}_3$ in trichloroethane or I_2 in benzonitrile.

1.10.3 γ - Phase packing of ET

The γ - phase, $(\text{ET})_3(\text{I}_3)_{2.5}$, is found to exhibit superconductivity at ambient pressure with $T_C = 2.5$ K (Figure 10).

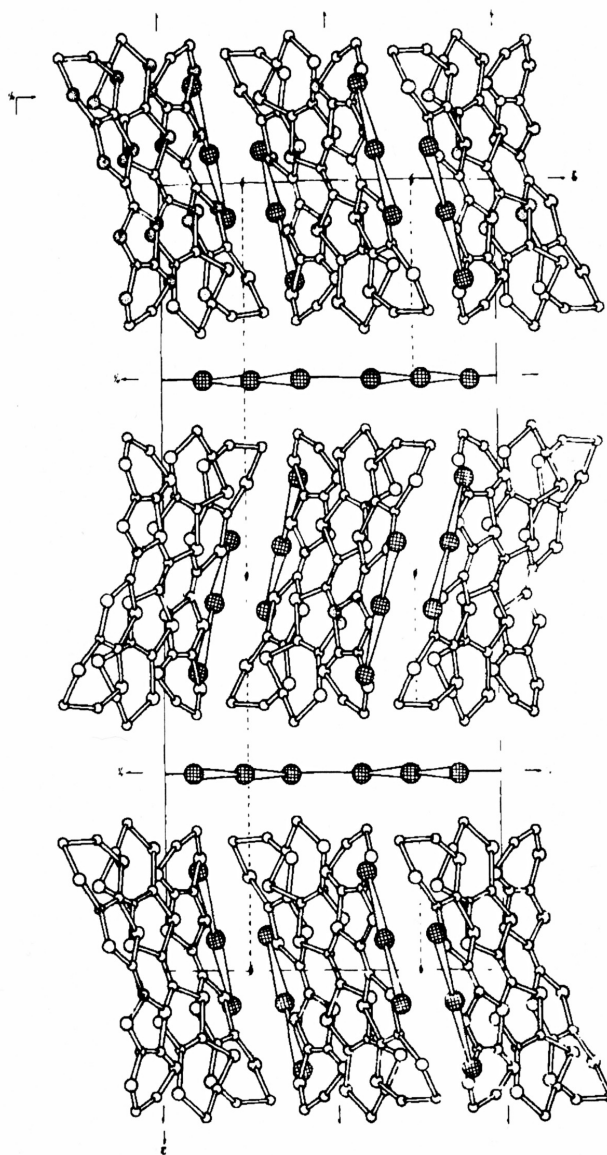


Figure 10: The γ - $(\text{ET})_3(\text{I}_3)_{2.5}$ packing motif, viewed along the a axis.⁶²

1.10.4 δ - Phase packing of ET

The δ - phase, $(\text{ET})\text{I}_3$, is obtained when employing high current densities in electrocrystallisation experiments of ET with the triiodide anion in trichloroethane. This phase exhibits metallic conductivity upon cooling from room temperature until an insulating phase is observed at $T_{\text{M-I}} = 130$ K. The structure consists of mixed stacks of the donor and the anion layers, parallel to the ab plane (Figure 11).

1.10.5 ε - Phase packing of ET

The ε - phase, $\varepsilon\text{-(ET)}_2\text{I}_3(\text{I}_8)_{0.5}$, exhibits a superconducting phase with $T_{\text{C}} = 2.5$ K. This phase can be prepared by the chemical oxidation of ET with I_2 (Figure 12).

1.10.6 κ - Phase packing of ET

The κ - phase, $(\text{ET})_2\text{I}_3$, exhibits dimers of ET molecules. The dimers pack in the space group $\text{P2}_1/\text{c}$, and exhibit a superconducting phase at $T_{\text{C}} = 3.6$ K (Figure 13 and Figure 14).⁵ Studies of the crystal structure at 295, 150 and 10 K, indicated that a structural phase transition occurred as the c -glide symmetry is broken and the space group becomes P2_1 at lower temperatures. This causes significant alteration to the conformation of the ethylene groups.⁷⁶ The resistivity measurements indicated an anomaly at 170 K, and it is proposed that this is associated with the crystallographic transformation.

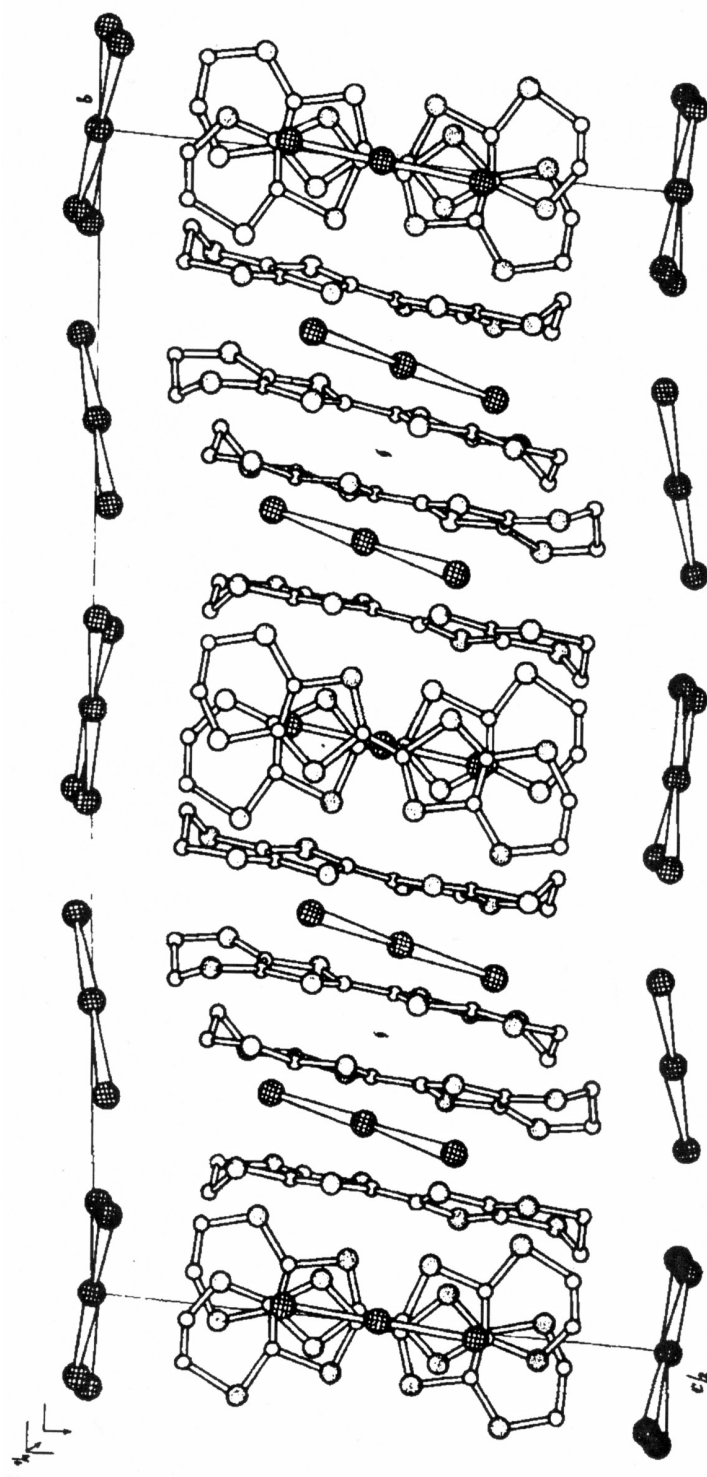


Figure 11: δ -(ET) I_3 , viewed along the a axis.⁶²

In order to understand the effect of anion disorder in the crystal lattice on the electron transport properties, Williams *et al.* prepared the non-symmetrical linear anion I_2Br^- . Distorted hexagonal crystals of the radical cation salts prepared from ET were grown, and shown to exhibit the β - phase structure. The salt composition was determined to be $(ET)_2[I-I-Br]$.⁷⁷ The material showed metallic behaviour over the temperature range 1.1-298 K, but never indicated superconducting phases, even under an applied pressure of 5 kbar. This was attributed to the random electrostatic potential generated by the asymmetry of the anion created in the lattice, which is able to influence the conducting S...S network. By comparison, the symmetrical anion salt β -(ET)₂[Br-I-Br] exhibited a completely ordered structure at 125 K, and due to the decreased length of the anion (with respect to the I_3^- anion length), the S...S short contacts are shortened.⁷⁸ Two phases were generated by the electrocrystallisation, the α - and β - phases. Both crystal types exhibited P-1 structures, with the unit cell of the α - phase being roughly twice that of the volume of that of the β - phase. The β -(ET)₂[Br-I-Br] and β -(ET)₂ I_3 structures are isostructural, the unit cell being slightly more condensed due to the reduced bond lengths for the former anion. β -(ET)₂[Br-I-Br] exhibits a superconducting phase with $T_C = 2.3$ - 2.8 K. On the belief that the length of the linear symmetric anions would provide materials in which the transition temperature into a superconducting phase would be higher, Williams *et al.* prepared the AuI_2^- of intermediate length to I_3^- and [Br-I-Br]⁻. The radical cation salt produced from tetrahydrofuran was determined to be β -(ET)₂ AuI_2 ,⁷⁹ from observation of the crystal morphology (distorted hexagons), the EPR linewidth of $\Delta H_{pp} = 20$ G, and by X-ray crystallography (P-1 at 198 K). It was found to have an ambient pressure bulk superconductivity, with $T_C = 5$ K, measured by rf measurements. The material is isostructural with the I_3 and [Br-I-Br] salts of ET. There

exist layers of AuI_2^- anions with a sheet network of ET molecules between the layers. Interstack distances are less than the sum of the van der Waals radii for the sulphur atoms, however intrastack distances are greater than 3.6 Å.

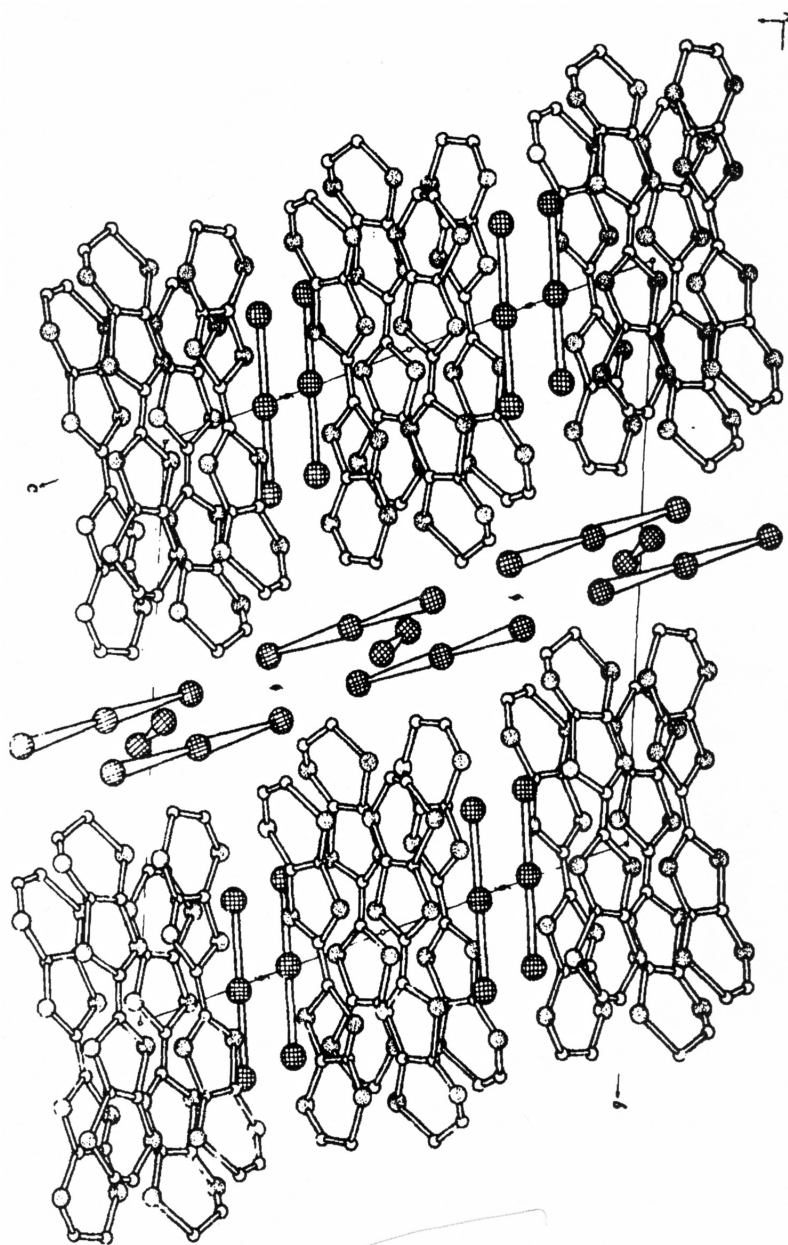


Figure 12: $\epsilon\text{-(ET)}_2\text{I}_3(\text{I}_8)_{0.5}$, viewed along the a axis.⁶²

Further salts of ET have been prepared in which the anion employed was AsF_6^- . This salt was found to exhibit a 2-D sheet network of donor molecules with short S...S contacts, and displayed semiconducting properties with a low temperature phase transition at 125 K.⁸⁰ $(\text{ET})_2\text{InBr}_4$ also exhibits semiconducting behaviour with $E_a = 0.15$ eV. The structure is composed of stacks of dimerised donor molecules with sheets of anions separating the stacks.⁸¹

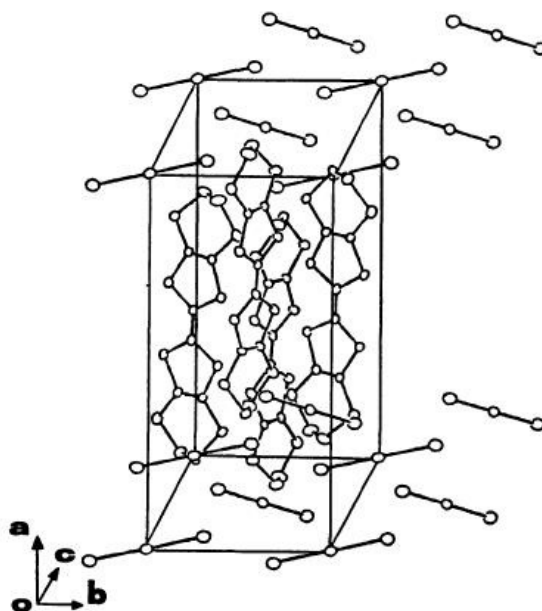


Figure 13: κ -(ET) $_2\text{I}_3$, 3-D view.⁵

1.10.7 Unusual ligating behaviour of ET

An interesting structure is that of $(\text{ET})(\text{Cu}_3\text{I}_4)$.⁸² Black parallelepiped crystals of the salt were grown from a nitrobenzene solution containing ET, I_3^- and CuI_2^- in a molar ratio of 1:5:5. The crystal structure illustrates ET molecules acting as bidentate bridging

1.10.8 ET halide salts

The formation of ET radical cation salts incorporating halide anions is well established. $(\text{ET})_2\text{Br} \cdot (\text{C}_2\text{H}_6\text{O}_2)$ shows metallic conductivity upon cooling from room temperature until a sharp metal-insulator transition occurs at $T_{\text{M-I}} = 200 \text{ K}$.⁸³ The presence of a weak hydrogen-bonding network from the included ethylene glycol solvent molecule to the bromide ion is detected in the X-ray crystal structure, and helps form the alternating layered structure. The solvent molecule is however, disordered over two equally populated sites in the $\text{P2}_1/c$ crystal structure. The ET stacks contained in the structure show the absence of short S...S intrastack contacts, however in the plane of the donor, interstack S...S distances are of the order 3.446-3.514 Å, which are less than the sum of their van der Waals radii. From crystal structure bond length calculations, the charge on the donor is identified as being $Z = +0.5$. Crystals grown from a mix of tetrahydrofuran doped with 5 % ethylene glycol showed a layered structure of alternating bromide and solvent molecules.

Lobkovskaya *et al.* unexpectedly obtained the salt $(\text{ET})_3\text{Cl}_2 \cdot 2\text{H}_2\text{O}$ from experiments that were envisaged to obtain ET salts containing anions of higher aliphatic acids.⁸⁴ The source of the chloride ion was determined to be the trichloroethane solvent employed in the electrocrystallisation. In the P-1 structure, stacks of donor molecules were shown to have no short S...S intrastack contacts. In between the stacks, layers of chloride ions with water molecules serve to create hydrogen-bonded centrosymmetric dimers of $\text{Cl}_2 \cdot 2\text{H}_2\text{O}$. The structure contains some short interstack S...S contacts, however the material is not isostructural to that of $(\text{ET})_3\text{Br}_2 \cdot 2\text{H}_2\text{O}$. The quasi- 2-D organic metal was

found to undergo a metal-insulator transition at $T_{M-I} = 100$ K, which was suppressible under a pressure of 16 kbar. A superconducting phase was observed under these conditions at $T_C = 2$ K.

The dichloride dihydrate salt was again prepared unexpectedly by Japanese workers attempting the preparation of ET salts of cobalt (II) tetrachloride.⁸⁵ Black plate crystals formed from a benzonitrile solution, and were investigated by resistivity measurements and X-ray single crystal analysis. An identical metal-insulator transition occurred at $T_{M-I} = 100$ K, and the identical crystal structure showed stacks of ET present, with all donors carrying a charge of $Z = + 0.67$. The three crystallographically independent ET molecules exhibited a twisted arrangement along the stack, with identical dimeric hydrated chloride pockets. In comparing the $(ET)_3Br_2 \cdot 2H_2O$ salt to the chloride analogue, it is noted that the chloride crystallographic unit cell is twice the size of the bromide unit cell, attributable to the presence of additional hydrogen bonding networks. The conductivity of the chloride salt at room temperature is around $500 \text{ S}\cdot\text{cm}^{-1}$, and the material exhibits semi-metallic behaviour.

Determination of the crystal structure at 10, 130 and 190 K,⁸⁶ indicated from the observed cell parameters, that the broad metal-insulator transition at ambient pressure was not due to a structural change on the ET molecules. Minor differences in bond lengths, and an ordering of the ethylene groups were observed upon cooling, as was a redistribution of charge. Across the temperature range studied, the cell volume decreased from 2304 \AA^3 (295 K), through 2267 \AA^3 (190 K), 2256 \AA^3 (130 K) to 2240 \AA^3 (10 K) due to the compression of the a and b axis and the lengthening of the c axis

(as a result α and β angles increase and γ decreases). Concurrently, the charge varied on the three individual ET molecules as the sample was cooled, increasing by 13 % on one ET ($Z_{295} = +0.85$), 21 % on another ($Z_{295} = +0.73$), and decreasing by 18 % on the third ($Z_{295} = +0.66$). The localisation of charges at low temperatures leading to the insulating phase is suppressed by the application of pressure (1.2 GPa) and a $T_C = 5$ K is observed. The other chloride salts observed, $(\text{ET})_4(\text{Cl})_2 \cdot 6\text{H}_2\text{O}$, $(\text{ET})_4(\text{Cl})_2 \cdot 4\text{H}_2\text{O}$, $(\text{ET})_3(\text{Cl})_{2.5} \cdot \text{H}_5\text{O}_2$ are metallic in behaviour, with $(\text{ET})_3(\text{Cl})_{2.5} \cdot \text{H}_2\text{O}$ showing semiconducting properties.

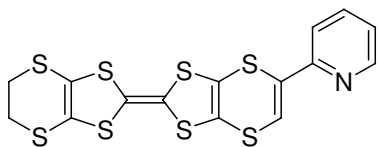
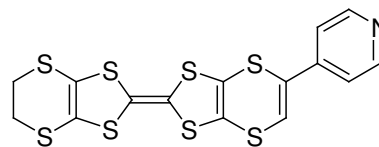
1.11 Temperature effects on the crystal conductivity

The effect of temperature on the conductivity of electron-transport salt crystals was first demonstrated in the early 1980s.⁸⁷ Takahashi showed that the process of measuring the property was as sensitive as the procedure used in the preparation of the material. In measuring the resistivity of TMTSF salts, the rate at which the sample was cooled was shown to influence the electron-transport capability. In studying $(\text{TMTSF})_2\text{ClO}_4$ two different superconducting states were observed by either fast cooling ($T_C = 0.9$ K) or slow cooling ($T_C = 1.2$ K) below 40 K. The explanation for this was proposed in terms of lattice disorder. In the P-1 structure, the perchlorate anion statistically occupied two equivalent positions at high temperatures, and is suggested to show ferroelectric type ordering at low temperatures.⁸⁸ The perchlorate was shown to not be ordered down to 15 K (in comparison to the perrhenate anion which was shown to undergo an ordering transition at 180 K), thus fast cooling would be likely to 'freeze in' some disorder and suppress the superconductivity, as proposed by Larkin.⁸⁹ In contrast the structure of the

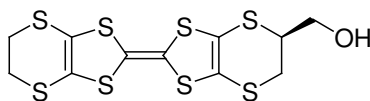
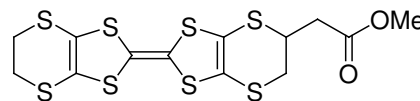
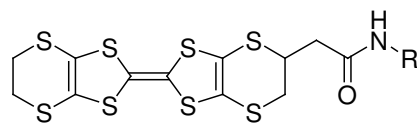
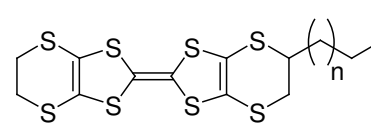
hexafluorophosphate anion has a centre of inversion symmetry and as such does not create orientational disorder in the crystal lattice.

1.12 Functionalisation of the ET donor

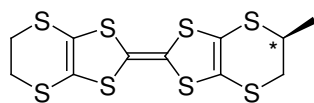
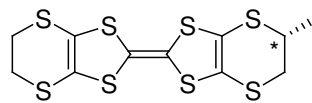
The range of different groups incorporated on the skeleton of the donor molecule has been extensively reviewed.⁹⁰ These structures include (not exclusively) modifications such as a metal ligating pyridyl group (12, 13),⁹¹

**12****13**

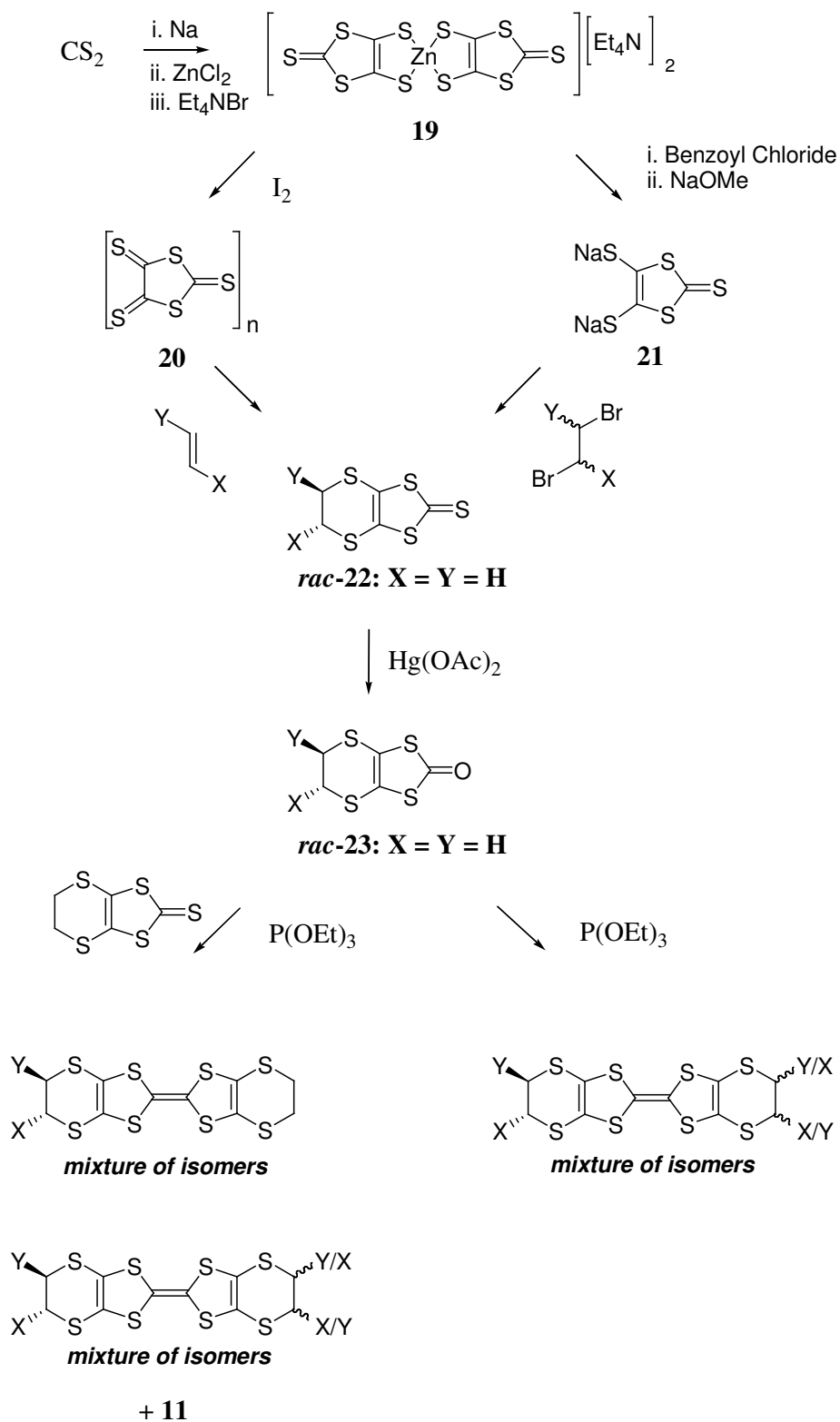
hydrogen bonding alcohol groups (14),⁹² carboxylic esters and amides (15, 16),⁹³ aldehyde functions,⁹⁴ hydroxymethyl groups,⁹⁵ aliphatic chains (17),^{96,97} and fused aromatic rings.⁹⁸

**14****15****16****17**

Functionalisation of the ET donor structure at any of the sp^3 hybridised carbon atoms creates a stereogenic centre (**18a**, **18b**). Control of the stereochemistry at this carbon is an important consideration when employing substituted ET molecules in electrocrystallisation experiments, as enantiopure species are expected to give more ordered crystalline structures over racemic species.

**18a****18b**

Enantiopure electron donors present a synthetic challenge, however advances in the methodology of preparation of these species has allowed interesting materials to be obtained. Such examples include the chiral hydroxymethyl-,⁹⁹ the 2-fluoro-1-hydroxyethyl-,¹⁰⁰ and the tetramethyl-ET derivatives,¹⁰¹ which were all accessible via the cyclic sulfate chemistry developed for the synthesis of the tetramethyl derivative. The synthetic approaches to functionalised ET compounds are shown in Scheme 1,¹⁰² with the mechanistic formation of the zinc bis(dithiolate) salt **19** shown in Figure 15.¹⁰³



Scheme 1: General synthetic route to electron donor molecules.

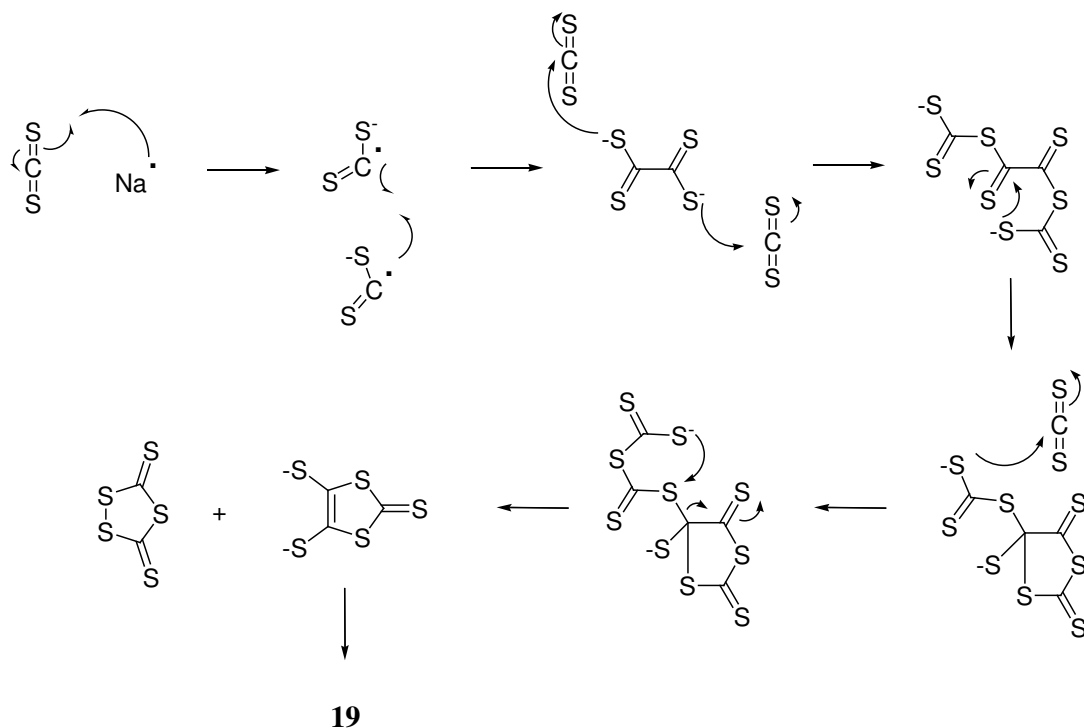
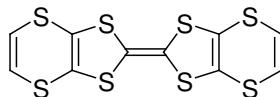


Figure 15: Proposed mechanistic formation of **19**.¹⁰³

1.13 Bis(vinylenedithio)tetrathiafulvalene, VT

In radical cation salts of ET there is often a slight disorder of the ethylene carbons, each occupying two positions approximately equally, giving an envelope conformation. This disorder, coupled with the belief that planarity of the electroactive molecule was a prerequisite for conductivity to occur led to the synthesis of VT (**24**). By preparing the donor in which the sp^3 carbon atoms are replaced by sp^2 carbon atoms, the problem of occupational disorder could be circumvented. However, this slight modification altered the conformation of the six-membered ring, and crystals of the donor were found to be stacks, with the donor molecule (viewed from the plane of central C=C bond) as a tilde (~) shape.¹⁰⁴ Despite the deviation from planarity in the neutral donor, the PF_6^- radical

cation salt displayed metallic behaviour from room temperature until an insulating phase dominated at $T_{M-I} = 180$ K. Analysis of the crystal structure of the oxidised species indicated that the two vinylenedithio moieties had displaced to the same side of the plane of sulphur atoms, forming a shallow bowl shape.



24

1.14 Techniques for the characterisation of electron-transfer salts

A variety of techniques are available to characterise the electron-transfer salts prepared by electrocrystallisation or chemical oxidation. The main techniques are discussed below.

1.14.1 Raman spectroscopy

Raman spectroscopy is a vibrational technique similar in some ways to infrared spectroscopy, however its fundamental difference lies in its ability to observe vibrations of symmetrically substituted bonds. This lends itself to the analysis of charge transfer salts, as the central (symmetrical) C=C bond in ET is extremely sensitive to the charge state of the electron donor. Thus Raman spectroscopy can be used indirectly to determine Z on the donor molecules, and in turn indicate the stoichiometry of the salt, as according to the method of Wang *et al.*¹⁰⁵ The sensitivity of the central C=C bond to the charge state lies in the large electron-phonon coupling constants of the two totally

symmetrical Raman stretching modes, ν_3 and ν_4 , between 1400-1550 cm^{-1} . The positive electrical charge associated with the C=C bonds (central and ring fusion) of the donor decreases the population of the corresponding Highest Occupied Molecular Orbital (HOMO). The weakened bonds are indicated by a shift of the ν_3 and ν_4 stretches to lower vibrational frequencies in the Raman spectrum. As such, the highest frequencies are observed for neutral ($Z=0$) ET, being 1546 and 1489 cm^{-1} (ν_3 and ν_4 respectively), decreasing to 1485-1495 and 1460-1470 cm^{-1} for 2:1 salts ($Z=0.5$), 1475-1485 and 1460-1470 cm^{-1} for 3:2 salts ($Z=0.67$), and 1445-1465 and 1405-1415 cm^{-1} for 1:1 salts ($Z=1$), (Figure 16). The correlation of the ν_3 and ν_4 vibrations with Z obey:

$$\nu_3 = -Z(86) + 1539$$

$$\nu_4 = -Z(88.4) + 1508$$

Using the frequencies from the Raman data, Z may be determined by:

$$Z = w_3[(1539-\nu_3)/86] + w_4[(1508-\nu_4)/88.4]$$

Where w_3 and w_4 are suitably related weighting factors.

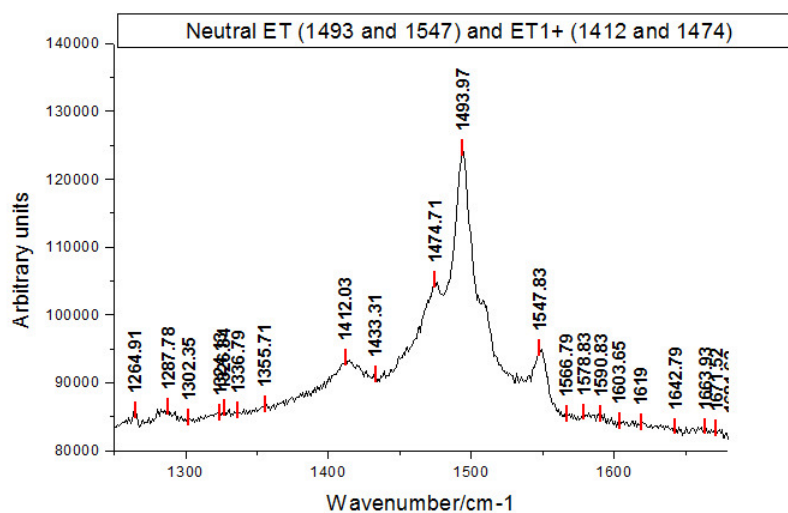


Figure 16: Example Raman spectrum indicating the presence of ET⁰ and ET⁺¹ donor molecules.

Reproduced with permission of Dr L. Martin.¹⁰⁶

1.14.2 Elemental analysis

Often, amorphous solids are produced by the electrocrystallisation technique. These solids do not lend themselves to analysis by single crystal X-ray diffraction, and so other methods of analysis are utilised. Elemental analysis is the most informative tool, as it provides accurate composition data for the charge transfer material, allowing the stoichiometry to be determined. However, complexities arise when the material has included solvent, and as such the technique is coupled with spectroscopic data such as Raman spectroscopy to determine the correct stoichiometry.

1.14.3 Thermal Gravimetric Analysis (TGA)

TGA can be used to determine the presence of solvent in the material. Coupled with elemental analysis, the data obtained allows the correct structural identification of the salt.

The technique measures the mass of a compound as a function of temperature, thus structurally mobile volatile components are eliminated from the compound at around their boiling point. The mass of the compound decreases at this point, allowing for correct identification of the solvent from the temperature at which the change occurs, and quantification of the solvent by the change in mass.

1.14.4 Infra-red spectroscopy

Infra-red spectroscopy can not only be used to confirm the presence of species in the material synthesised by observation of characteristic bands, but also to determine charges residing on donor molecules for some types of electron-transfer salts. Chappell *et al.* have shown that for TCNQ complexes, the nitrile stretching frequency has been shown to vary linearly dependant upon the charge state of the system.¹⁰⁷ The relationship is such that:

$$Z = - \frac{(\nu_{\text{CN}}^* - \nu_{\text{CN}}^0)}{}$$

Where Z is the charge residing on the cation (donor or atom), ν_{CN}^* is the infrared stretching frequency for the nitrile group in the TCNQ salt, and ν_{CN}^0 is the nitrile stretching frequency in neutral TCNQ ($\nu = 2227 \text{ cm}^{-1}$).

1.14.5 Single crystal X-ray crystallography

Providing the most structural and compositional information, X-ray crystallography is an invaluable tool in understanding the key contributing factors to a material's conductivity. The 3-D image of the crystal on the atomic scale allows for interactions between neighbouring molecules and atoms to be observed, by the relationship of the distances between them. The packing modes exhibited by the component molecules are readily accessible, and the charge state of the donor molecule(s) can be calculated from the bond lengths of well-defined structures.¹⁰⁸

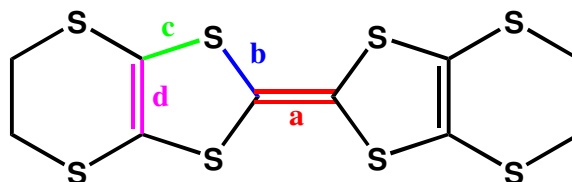


Figure 17: Bond lengths required for calculation of charge on ET.

The charge (Z) residing on the ET donor can be calculated using the equation:

$$Z = 6.347 - \{7.463 [(b+c)-(a+d)]\}$$

Where a , b , c , and d are the bond lengths (\AA) of the coloured bonds in Figure 17 labelled accordingly.

1.14.6 EPR spectroscopy

EPR spectroscopy can be used to quickly establish the type of phase packing exhibited in the crystal, from the linewidth measurements.²⁴ The values obtained for the linewidth at room temperature are shown in Table 1.

Packing phase	General linewidth $\Delta H_{pp}^{300} / G$	Example (and references)
α	70-110	70-110 <i>(ET)₂I₃ ref.^{109, 110, 111}</i>
β	15-32	18-24 <i>(ET)₂I₃ ref.^{109, 110, 112}</i>
γ	35-65	35-65 <i>(ET)₄[Pt(CN)₄] ref.¹¹³</i>
δ	25-40	25-40 <i>(ET)₄[Pt(CN)₄] ref.¹¹³</i>
κ	55-85 typically	58-68 <i>(ET)₂Cu(NCS)₂ ref.^{114, 115}</i> 80-110 <i>(ET)₄Hg₃Cl₈ ref.^{116, 117}</i>

Table 1: EPR linewidth for ET phases at 300 K

1.14.7 X-ray electron microprobe analysis

X-ray excitation techniques can be used to determine the presence of different elements due to their characteristic emission energies. In samples where there is insufficient material for traditional characterisation techniques (such as elemental analysis) to be employed, electron microprobe analysis by X-ray diffuse scattering provides composition information on the material. The surface technique probes a depth of between 0.1-1.0 nm, identifying inner-shell binding energies characteristic of each element.¹¹⁸

1.14.8 Superconducting quantum interference device (SQUID)

The SQUID, is the most sensitive detector known to science, able to detect minute changes in magnetic fields. The assembly consists of a superconducting loop disrupted in two places by non-superconducting materials, known as Josephson junctions.[†] The current present in the loop is dependent upon a difference in the phase of the wave functions that describe the Cooper pairs. When sufficient electrical current is created across the SQUID circuit, the voltage generated is proportional to the strength of any local magnetic field.

[†] The Josephson junction is named after Brian Josephson who, in 1962, predicted that Cooper pairs could tunnel from a superconducting material across a layer of non-superconducting material without resistance.

The SQUID can be used to measure the magnetism of a material as a function of temperature and applied field strength, and can also be used to detect the onset of a superconducting state due to the Meissner effect.

1.14.9 RF measurements

The onset of the Meissner effect in a material, which is indicative of a superconducting state present in the material, will serve to exclude an applied rf field. This is detected as an increase in the rf resonant frequency of an LC circuit (a circuit comprised of an inductor L and a capacitor C). The method measures the bulk sample and thus can detect the onset of bulk superconductivity, and also the presence of minor superconducting environments within the bulk sample.

1.15 The magnetic properties of electron-transfer salts

A material in its superconducting state will exhibit perfect diamagnetism. This factor itself can be used to identify superconducting phases using a SQUID as described previously.

The exposure of a material in a superconducting phase to an external magnetic field may cause the material to respond in one of two ways. As such it is important to sub-categorise superconductors. Magnetic fields are considered to destroy the superconducting state by increasing the difference in energy between the electrons in a Cooper pair. In a pair of mutually orbiting electrons that have opposing spins (s-wave

spin), the application of an external magnetic field serves to increase the energy of one electron, whilst decrease the energy of the other. This causes the pair to split, destroying the superconducting state. Type I superconductors, when exposed to an external magnetic field, behave as perfect diamagnetic materials up to a critical field strength (H_C), at which point the Cooper pairs become uncoupled and the superconducting state is destroyed (Figure 18, type I).

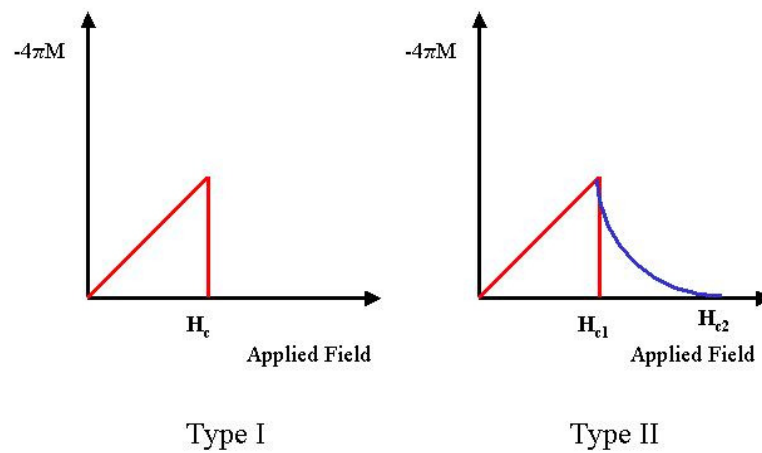


Figure 18: Responses of superconductors to magnetic fields.

In type II superconductors, an external magnetic field is expelled by the material up to a field strength (H_{C1}), at which point vortices are formed within the material. The bulk material is in a varied superconducting / non-superconducting state. Further increase in the field strength completely destroys the superconductivity at a critical limit (H_{C2}), as illustrated (Figure 18, type II).

In contrast to the observation that superconductivity is eventually destroyed by a magnetic field, research by Naughton has suggested that 're-entrant superconductivity', originally proposed in 1986 is a real possibility.¹¹⁹ By perfectly orientating the molecular superconductor (TMTSF)₂PF₆ in line with a high magnetic field of six Tesla, superconductivity was observed unhindered. Slight deviations from this perfect orientation destroyed the superconducting state. It is thought that this behaviour is due to p-wave spin on the Cooper pairs. P-wave spin is a rare phenomenon in which both electrons in the pair spin in the same direction, and as such a magnetic field only serves to increase the total energy of the electrons rather than giving a charge separation which subsequently leads to the dissociation of the Cooper pair and loss of the superconducting state.^{120, 121}

It is important to note, that a superconducting material will eventually destroy its superconducting state, as the magnetic field generated within the material by the current will overcome the binding of the Cooper pairs.

1.15.1 Types of magnetism

Materials may be classified as paramagnetic, ferromagnetic, antiferromagnetic and diamagnetic. A paramagnet is a material in which the electron spins are aligned in a random fashion in the absence of a magnetic field. As a magnetic field is applied to the material, some of the electron spins respond in a positive effect, increasing the applied field. The partial alignment is affected by thermal motion, and thus paramagnetic materials exhibit field and temperature dependency. Induced currents in the molecule

occur within the orbitals that are occupied in the ground state. In the few cases where paramagnetism is observed despite having no unpaired electrons, the induced currents flow in the opposite direction because they can utilise the unoccupied orbitals that lie close to the HOMO in energy. The orbital paramagnetism can be distinguished from spin paramagnetism by the fact that it is temperature independent.

At low temperatures, paramagnetic materials may undergo a phase transition into a state in which large domains have their spins aligned with parallel orientations, and the phase is known as a ferromagnetic phase. The temperature at which this occurs is known as the Curie temperature. The cooperative effect of the combined electronic spins creates a very strong magnetisation. In the absence of a magnetic field the electronic spins do not cancel due to their random alignments, thus the material has a non-zero magnetisation state. This can be observed by measuring the magnetic susceptibility as a function temperature and at the Curie temperature there will be a sharp rise in the susceptibility. At temperatures above the Curie temperature the magnetic susceptibility will obey the Curie-Weiss law and exhibit a positive Weiss constant.

In an antiferromagnetic material the electron spins are locked into an antiparallel alignment, giving a material of low magnetisation. In the absence of a magnetic phase, the electron spins cancel each other. The transition into an antiferromagnetic state occurs at the Néel temperature, and can be observed by a decrease in the magnetic susceptibility when measuring susceptibility as a function of temperature. At temperatures higher than the Néel temperature, the Curie-Weiss law is obeyed and has a negative Weiss constant.

Diamagnetic materials repel magnetic fields, due to the closed electronic shells existing at a lower energy than the Fermi level. Faraday first determined diamagnetism in 1845, when he observed that a piece of Bismuth was repelled by both poles of a magnet. The ability of a material to repel an external magnetic field leads to such properties as levitation, with uses in transport and industrial applications. As diamagnetism is a property of all matter, all magnetic measurements must be corrected for its existence, by the subtraction of the calculated component diamagnetic factors, known as Pascal Constants.

1.15.2 Magnetic susceptibility

The magnetic susceptibility of a simple paramagnet is given by:

$$\chi_m = C/(T-\theta)$$

Where χ_m is the molar susceptibility, C is the Curie constant, T is the temperature and θ is the Weiss constant. A plot of $1/\chi_m$ as a function of temperature gives a straight line with a slope equal to the reciprocal of the Curie constant, and the x -intercept being the Weiss constant. The Curie constant is related to the average molar spin value and to the spin only magnetic moment (Table 2). The sign of the Weiss constant indicates the type of magnetic interaction exhibited in the material, with short range ferromagnetic interactions portrayed by a positive value, and antiferromagnetic interactions portrayed by a negative value.

Spin value (S)	Curie constant (C) / $\text{emu}\cdot\text{K}\cdot\text{mol}^{-1}$	Magnetic moment (μ) / BM
1	0.375	1.73
2	1	2.83
3	1.875	3.87
4	3	4.90
5	4.375	5.92

Table 2: Values of Curie constant for various spin values and magnetic moments.

The magnetisation (M) of a material is a bulk magnetic quantity. Derived from the average molecular magnetic dipole moment, the magnetisation induced by a field of strength H is proportional to H, such that:

$$M = \chi_v \cdot H$$

Where χ_v is the volume magnetic susceptibility, and is dimensionless. The molar magnetisation susceptibility may therefore be calculated:

$$\chi_m = \chi_v \cdot V_m$$

Where V_m is the molar volume of a substance.

1.16 Electrocrystallisation

Since the 1970s, the technique of electrocrystallisation has been used to prepare highly ordered single crystals of molecular conductors. The first experiments involved the galvanostatic oxidation of perylene with tetrabutylammonium perchlorate, which afforded black single crystals that were shown to be conducting and were characterised by X-ray crystallography.¹²² A significant milestone was achieved using this technique at the beginning of the 1980s, when Bechgaard prepared the perchlorate and hexafluorophosphate salts of TMTSF, and found that they exhibited superconducting properties at ambient pressure, and under 12 kbar pressure respectively.^{21, 22, 23} More recently, the technique has flourished with the identification of ET, and has led to numerous superconducting materials.

The method of electrocrystallisation requires a moiety that is able to lose an electron (the electron donor), to form a radical cation, and the presence of an anionic species to trap the radical cation as a salt. By modifying the solvent employed, the concentration of the reagents, the temperature and the current applied, the formation of single crystals may be achieved, either on the anode, or on the glass wall of the cell.^{123, 124} By employing a constant, low current, the number of electrons taken from the electron donor is controlled, and thus so is the number of radical cations formed. This in turn affects the rate of crystal growth, with slower growth typically affording better ordered (less flawed) crystals.¹²⁵ The solubility of the crystals formed in the electrocrystallisation experiment are determined by the solvent employed, the reagent

concentrations and the temperature of the electrocrystallisation cell, which is shown diagrammatically in Figure 19.

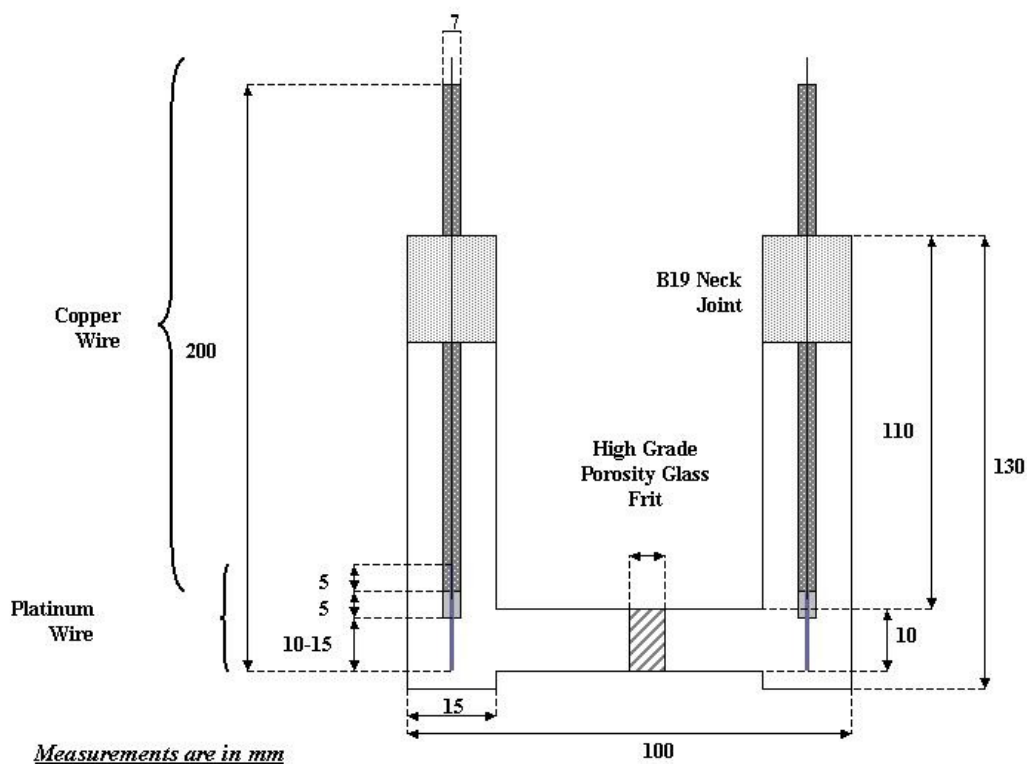


Figure 19: Electrochemical cell used for experiments conducted in this thesis.

The technique is still very much a form of art, despite extensive research having been carried out both on and with it. For when two electrocrystallisation experiments are prepared identically, and conducted in exactly the same manner, one may produce a crystalline material and the other may produce an amorphous solid, or indeed nothing. The complexity of the situation worsens, as within one cycle of electrocrystallisation, many different products may form, differing by their composition, or by the atom positions in the crystal structure. Despite the downside to the technique, it remains the

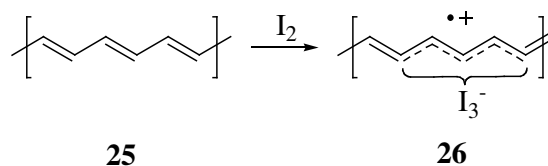
most invaluable tool for the investigation of structure-property relationships, and will remain so for many years to come.

The technique involves placing an amount (usually of the order of 10 mg) of an electron donor molecule in one arm of an electrochemical cell (Figure 19), separated from the other arm by a porous glass frit (which serves to control material movement into the active arm of the cell). Separately, a solution of a molar excess of the tetraalkylammonium salt of the anion required is prepared, using freshly dried and distilled solvent. The solvent employed should be chosen for in which the electron donor has limited solubility (at this point care is to be taken, as salts formed from abstraction of ions from solvent molecules can form, such as chloride salts from dichloromethane, as discussed previously). The solution is poured into the cell arm not containing the electron donor, and is allowed to flow slowly through the glass frit. When the sides equilibrate, the system may be placed under an inert atmosphere if required, and platinum tipped electrodes are introduced to both arms. A constant current is applied from a current source, and is typically of the order of 0.1 μA . The cell is left in the dark, on a vibration proof stand, at constant temperature, and is periodically checked for crystal growth. If after a reasonable period of time (up to a couple of months) there appears to be no crystal growth, then the current may be increased carefully and again left. The isolation of crystals from the anode involves careful removal of the anode, and transferral of the crystals to a filter paper, upon which they can be washed with acetone and dried before being measured and determined.

1.17 Other types of conducting materials

1.17.1 Polymers

The relative ease with which polymers can be synthesised and manipulated has led to a drive in research for conducting polymer systems. The mechanical properties exhibited by such systems allows for a great range of potential applications, ranging from Light Emitting Diodes (LEDs), camouflage, and viewing screens to corrosion protection for metal work.¹²⁶

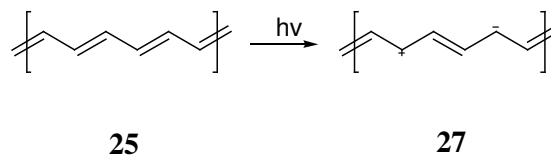


Scheme 2: Chemical oxidation of 25 with iodine to give 26.

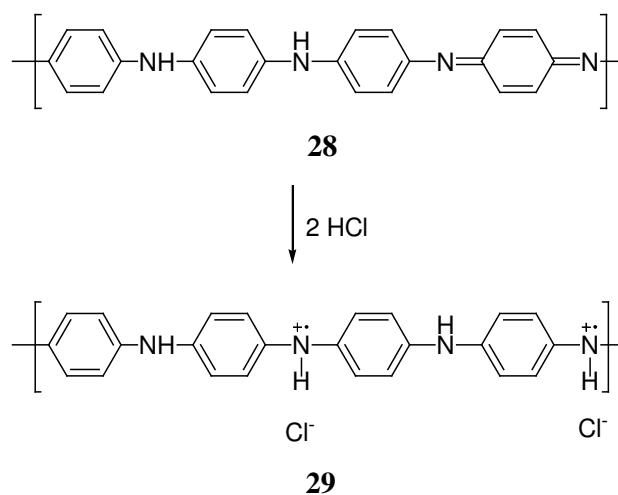
The activation of polymers to allow electron transport can be achieved by a variety of ‘doping’ methods,¹²⁷ including:

- Chemical doping by charge transfer, in which the polymer **25** is either oxidised (e. g. with iodine vapour) to give a p-type conductor **26**, or reduced (e. g. with sodium naphthalide) to give an n-type conductor (Scheme 2);
- Electrochemical doping, where the electrode supplies charge to the polymer and the electrolyte solution stabilises charge by ion uptake into the polymer;
- Photo-doping, in which localised oxidation occurs on the polymer **25**, and adjacent to this photo-absorption affords a reduced site (Scheme 3);

- Acid-base chemistry, such as that achieved on polyaniline **28**, which induced an internal redox reaction, and migration of an unpaired spin to each repeating unit **29** (Scheme 4), and;
- Charge injection, by either the addition of electrons or holes into the polymer.



Scheme 3: Photosynthetic charge separation on **25** to give **27**.



Scheme 4: Internal redox reaction promoted by acidification of **28** to give **29**.

1.17.2 Inorganic and ceramic superconductors

Superconducting inorganic species have received increasing research interest due to the high T_C values observed. The macro-structures exhibited by these compounds are in stark contrast to the aforementioned molecular conductors. The mixed barium and

copper oxides are a rich class of compounds, giving rise to many high temperature superconductors. In 1986, Bednorz and Muller published an article in which they described a material which exhibited an onset of superconductivity close to 30 K.¹²⁸ The composite material of $\text{Ba}_x\text{La}_{5-x}\text{Cu}_5\text{O}_{5(3-y)}$ showed the bulk superconducting phase when $x = 0.75$, and a metallic phase when $x = 1.0$. The dramatic improvement in T_C from the then-leading metal oxide (Li-Ti-O, with T_C 13.7 K),¹²⁹ created an increased drive for obtaining higher temperature oxide superconductors. In 1987, Chu *et al.* announced the synthesis of a material containing Yttrium, $\text{YBa}_2\text{Cu}_3\text{O}_7$, having T_C 93 K (Figure 20).¹³⁰ This truly remarkable achievement was followed up by $\text{Tl}_2\text{Ba}_2\text{Ca}_2\text{Cu}_3\text{O}_{10}$ having T_C 125 K,¹³¹ only six years later. In the same year, an oxide was synthesised that demonstrated an onset of superconductivity at 150 K,¹³² albeit under a pressure of 150 kbar. The pressure dependency of the T_C for the material, $\text{HgBa}_2\text{Ca}_2\text{Cu}_3\text{O}_{8+\delta}$, suggested that ambient pressure superconductivity on this temperature scale could be possible if the correct chemical substitution is determined. The doping of the material was key, and much research has been undertaken into the levels at which optimum results are obtained. For example La_2CuO_4 was doped by replacing some of the La^{3+} by Sr^{2+} yielding $\text{La}_{2-x}\text{Sr}_x\text{CuO}_4$. The result is that x electrons per copper atom are removed from the copper oxide plane. When x was between 0.05 and 0.25 the material was found to be superconducting, with the highest T_C around $x=0.15$.¹³³ Interestingly, the parent oxide is an insulator. In May 2009, a new record for the highest T_C was reported as 242 K for $(\text{Tl}_4\text{Ba})\text{Ba}_4\text{Ca}_2\text{Cu}_{10}\text{O}_y$.

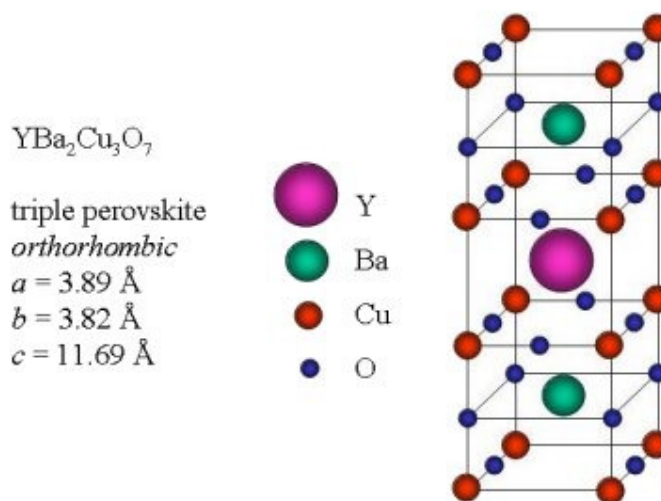


Figure 20: $\text{YBa}_2\text{Cu}_3\text{O}_7$.¹³⁴

1.18 Applications of electron-transfer materials

The potential range of applications for electron-transfer salts is as diverse as the properties that they exhibit, and will probably expand as much as the field of research broadens.¹³⁵ The coupling of electron conductivity with magnetic properties in some materials, producing bifunctional materials, lends itself directly to applications such as memory devices in computing technology and molecular switches. The optical properties of related conducting polymer compounds have found use in display devices due to their low weight and flexibility. Other uses include the sensing of cations with applications in environment and medical monitoring.^{43, 44, 45, 46, 47} The improved efficiency in the transport of electrical current possible in these low dimensionality devices opens applications in areas such as highly efficient power transfer, which will influence global environmental effects. The 1-D conducting species would create a reduction in energy-loss whilst in transfer, and this could in turn influence the

generation of power, reducing the consumption of fuel reserves. The perfect diamagnetic behaviour exhibited by superconducting materials offers the possibility of object levitation, with particular applications in transport. More controversial applications exist in the field of advanced weaponry, with electromagnetic pulse devices now accessible.¹³⁶

1.19 References

-
- ¹ M. Tarascon, W. R. Mckinnon, P. Barboux, D. M. Hwang, B. G. Bagley, L. H. Greene, B. W. Hull, Y. Lepage, *Phys. Rev. B*, **1988**, 38, 8885.
- ² W. Zandbergen, W. A. Broen, F. C. Mijhoff, G. van Tendeloo, S. Amelinckx, *Physica C*, **1988**, 156, 325.
- ³ K. Onnes, *Proc., K. Ned. Akad. Wet.*, **1912**, 13, 1274.
- ⁴ K. Onnes, *Electrician*, **1911**, 67, 657.
- ⁵ A. Kobayashi, R. Kato, H. Kobayashi, S. Moriyama, Y. Nishio, K. Kajita and W. Sasaki, *Chem. Lett.*, **1987**, 459.
- ⁶ J. M. Williams, J. R. Ferraro, R. J. Thorn, K. D. Carlson, U. Geiser, H. H. Wang, A. M. Kini and M.-H. Whangbo, *Organic Superconductors (Including Fullerenes) Synthesis, Structure, Properties and Theory*: Prentice Hall, **1992**.
- ⁷ D. C. Tsui, H. L. Störmer and A. C. Gossard, *Phys. Rev. Lett.*, **1982**, 1559, 48.
- ⁸ R. B. Laughlin, *Phys. Rev. Lett.*, **1983**, 50, 1395.
- ⁹ H. N. McCoy and W. C. Moore, *J. Am. Chem. Soc.*, **1911**, 273.
- ¹⁰ F. London, *Proc. Roy. Soc. (London)*, **1935**, A152, 24.
- ¹¹ H. Fröhlich, *Proc. Roy. Soc. (London)*, **1954**, A223, 296.
- ¹² J. Bardeen, L. N. Cooper and J. R. Schrieffer, *Phys. Rev.*, **1957**, 108, 5, 1175.
- ¹³ W. Meissner and R. Ochsenfeld, *Naturwiss*, **1933**, 21, 787.
- ¹⁴ Explanation adapted from P. A. Tipler and G. Mosca, in *Physics for Scientists and Engineers*, ed. C. Marshall, W. H. Freeman and Company, New York (USA), 6th edn., 2008, ch. 38, pp 1307.
- ¹⁵ J. R. Gavaler, M. A. Janocko and C. K. Jones, *J. Appl. Phys.*, **1974**, 45, 7, 3009.
- ¹⁶ "A15 phases." McGraw-Hill Encyclopaedia of Science and Technology. The McGraw-Hill Companies, Inc., 2005. Answers.com 07 Dec. 2008. <http://www.answers.com/topic/a15-phases>
- ¹⁷ D. Dew-Hughes and V. G. Rivlin, *Nature*, **1974**, 250, 723.
- ¹⁸ W. A. Little, *Phys. Rev.*, **1964**, 134, 6A, 1416.
- ¹⁹ H. Akamatu, H. Inokuchi and Y. Matsunaga, *Nature*, **1954**, 173, 168.
- ²⁰ K. Bechgaard, D. O. Cowan and A. N. Bloch, *J. Chem. Soc. Chem. Comm.*, **1974**, 938.

- ²¹ D. Jérôme, A. Mazaud, M. Ribault and K. Bechgaard, *J. Phys. Lett. (Paris)*, **1980**, 41, L95.
- ²² K. Bechgaard, C. S. Jacobsen, K. Mortenson, H. J. Pederson and N. Thorup, *Solid State Communications*, **1980**, 33, 1119.
- ²³ K. Bechgaard, K. Carneiro, F. B. Rasmussen, M. Olsen, G. Rindorf, C. S. Jacobsen, H. J. Pedersen and J. C. Scott, *J. Am. Chem. Soc.*, **1981**, 103, 2440.
- ²⁴ K. D. Carlson, G. W. Crabtree, L. N. Hall, P. T. Copps, H. H. Wang, T. J. Emge, M. A. Beno and J. M. Williams, *Mol. Cryst. Liq. Cryst.*, **1985**, 119, 357.
- ²⁵ H. Kobayashi, A. Kobayashi, G. Saito and H. Inokuchi, *Chem. Lett.*, **1982**, 245.
- ²⁶ S. S. P. Parkin, F. Creuzet, M. Ribault, D. Jerome, K. Bechgaard and J. M. Fabre, *Mol. Cryst. Liq. Cryst.*, **1982**, 79, 249.
- ²⁷ J. M. Williams and K. Carneiro, *Adv. Inorg. Chem. Radiochem.*, **1985**, 29, 249.
- ²⁸ J. M. Williams, *J. Phys (Paris) Colloq.*, **1983**, 44, C3-941.
- ²⁹ A. Ellern, J. Bernstein, J. Y. Becker, S. Zamir, L. Shahal and S. Cohen, *Chem. Mater.*, **1994**, 6, 1378.
- ³⁰ A. S. Batsanov, M. R. Bryce, G. Cooke, A. S. Dhindsa, J. N. Heaton, J. A. K. Howard, A. J. Moore and M. C. Petty, *Chem. Mater.*, **1994**, 6, 1419.
- ³¹ S. Yoneda, T. Kawase, M. Inaba and Z. Yoshida, *J. Org. Chem.*, **1978**, 43, 4, 595.
- ³² M. R. Bryce, *J. Mater. Chem.*, **2000**, 10, 589.
- ³³ J. L. Segura and N. Martín, *Angew. Chem. Int. Ed.*, **2001**, 40, 1372.
- ³⁴ M. R. Bryce, *J. Mater. Chem.*, **1995**, 5, 10, 1481.
- ³⁵ J. Ferraris, D. O. Cowan, V. Walatka and J. H. Perlstein, *J. Am. Chem. Soc.*, **1973**, 95, 3, 948.
- ³⁶ F. Wudl, D. Wobschall and E. J. Hufnagel, *J. Am. Chem. Soc.*, **1972**, 94, 671.
- ³⁷ N. Martin, L. Sánchez. B. Illescas and I. Perez, *Chem. Rev.*, **1998**, 98, 2527.
- ³⁸ M. Prato, M. Maggini, C. Giacometti, G. Scorrano, G. Sandona and G. Farnia, *Tetrahedron*, **1996**, 52, 5221.
- ³⁹ N. Martin, L. Sánchez, C. Seoane, R. Andreu, J. Garín and J. Orduna, *Tetrahedron Lett.*, **1996**, 37, 5979.
- ⁴⁰ J. Llacay, J. Veciana, J. Vidal-Gancedo, J. L. Bourdelande, R. González-Moreno and C. Rovira, *J. Org. Chem.*, **1998**, 121, 3951.

- ⁴¹ R. Andreu, J. Barberá, J. Garín, J. Orduna, J. L. Serrano, T. Sierra, P. Leriche, M. Sallé, A. Riou, M. Jubault and A. Gorgues, *J. Mater. Chem.*, **1998**, 8, 4, 881.
- ⁴² M. Asakawa, P. R. Ashton, V. Balzani, A. Credi, C. Hamers, G. Mattersteig, M. Montalti, A. N. Shipway, N. Spencer, J. F. Stoddart, M. S. Tolley, M. Venturi, A. J. P. White and D. J. Williams, *Angew. Chem. Int. Ed.*, **1998**, 37, 333.
- ⁴³ M. J. Cook, G. Cooke and A. Jafari-Fini, *Chem. Commun.*, **1996**, 1925.
- ⁴⁴ T. K. Hansen, T. Jørgensen, P. C. Stein and J. Becher, *J. Org. Chem.*, **1992**, 57, 6403.
- ⁴⁵ R. Gasiorowski, T. Jørgensen, J. Møller, T. K. Hansen, M. Pietraszkiewicz and J. Becher, *Adv. Mater.*, **1992**, 4, 568.
- ⁴⁶ A. J. Moore, L. M. Goldenberg, M. R. Bryce, M. C. Petty, A. P. Monkman, C. Marengo, J. Yarwood, M. J. Joyce and S. N. Port, *Adv. Mater.*, **1998**, 10, 5, 395.
- ⁴⁷ T. Otsubo and F. Ogura, *Bull. Chem. Soc. Jpn.*, **1985**, 58, 1343.
- ⁴⁸ P. Miguel, M. R. Bryce, L. M. Goldenberg, A. Beeby, V. Khodorkovsky, L. Shapiro, A. Niemz, A. O. Cuello and V. Rotello, *J. Mater. Chem.*, **1998**, 8, 1, 71.
- ⁴⁹ E. Tsiperman, T. Regev, J. Y. Becker, J. Bernstein, A. Ellern, V. Khodorkovsky, A. Shames and L. Shapiro, *Chem. Commun.*, **1999**, 1125.
- ⁵⁰ M. Iyoda, M. Fukuda, M. Yoshida and S. Sasaki, *Chem. Lett.*, **1994**, 2369.
- ⁵¹ A. Dolbecq, M. Fourmigué, P. Batail and C. Coulon, *Chem. Mater.*, **1994**, 6, 1413.
- ⁵² M. Mizuno, M. P. Cava and A. F. Garito, *J. Org. Chem.*, **1976**, 41, 8, 1484.
- ⁵³ M. Mizuno, A. F. Garito and M. P. Cava, *J. Chem. Soc. Chem. Commun.*, **1978**, 18.
- ⁵⁴ P. C. W. Leung, M. A. Beno, T. J. Emge, H. H. Wang, M. K. Bowman, M. A. Firestone, L. M. Sowa and J. M. Williams, *Mol. Cryst. Liq. Cryst.*, **1985**, 125, 113.
- ⁵⁵ G. Saito, T. Enoki, K. Toriumi and H. Inokuchi, *Solid State Communications*, **1982**, 42, 8, 557.
- ⁵⁶ H. Kobayashi, R. Kato, T. Mori, A. Kobayashi, Y. Sasaki, G. Saito, T. Enoki and H. Inokuchi, *Chem. Lett.*, **1984**, 179.
- ⁵⁷ K. Imaeda, T. Enoki, G. Saito and H. Inokuchi, *Bull. Chem. Soc. Jpn.*, **1988**, 61, 9, 3332.
- ⁵⁸ T. Yamamoto, M. Uruichi, K. Yamamoto, K. Yakushi and A. Kawamoto, *Synth. Met.*, **2005**, 155, 628.
- ⁵⁹ A. Miyazaki, T. Enoki and G. Saito, *Synth. Met.*, **1995**, 70, 793.

- ⁶⁰ V. A. Merzhanov, D. A. Hits, E. B. Yagubskii, M. –L. Doublet and E. Canadell, *Synth. Met.*, **1995**, 71, 1867.
- ⁶¹ S. S. P. Parkin, E. M. Engler, R. R. Schumaker, R. Lagier, V. Y. Lee, J. C. Scott and R. L. Greene, *Phys. Rev. Lett.*, **1983**, 50, 4, 270.
- ⁶² R. P. Shibaeva, V. F. Kaminskii and E. B. Yagubskii, *Mol. Cryst. Liq. Cryst.*, **1985**, 119, 361.
- ⁶³ J. M. Williams, M. A. Beno, H. H. Wang, P. E. Reed, L. J. Azevedo and J. E. Schirber, *Inorg. Chem.*, **1984**, 23, 13, 1790.
- ⁶⁴ H. Kanbara, H. Tajima, S. Aratani, K. Yakushi, H. Kuroda, G. Saito, A. Kawamoto and J. Tanaka, *Chem. Lett.*, **1986**, 437.
- ⁶⁵ E. B. Yagubskii, I. F. Schegolev, V. N. Laukhin, P. A. Kananovitj, M. V. Karljounik, A. V. Zvarykina and L. I. Buravov, *Pisma B JETP*, **1984**, 39, 12.
- ⁶⁶ J. M. Williams, T. J. Emge, H. H. Wang, M. A. Beno, P. T. Copps, L. N. Hall, K. D. Carlson and G. W. Crabtree, *Inorg. Chem.*, **1984**, 23, 2558.
- ⁶⁷ J. M. Williams, T. J. Emge, H. H. Wang, M. A. Beno, P. T. Copps, L. N. Hall, K. D. Carlson and G. W. Crabtree, *Inorg. Chem.*, **1984**, 23, 2560.
- ⁶⁸ K. Mortensen, C. S. Jacobsen, K. Bechgaard, K. Carneiro and J. M. Williams, *Mol. Cryst. Liq. Cryst.*, **1985**, 119, 401.
- ⁶⁹ J. P. Pouget, G. Shirane, K. Bechgaard and J. M. Fabre, *Phys. Rev.*, **1983**, 27, B5203.
- ⁷⁰ P. C. W. Leung, T. J. Emge, M. A. Beno, H. H. Wang and J. M. Williams, *J. Am. Chem. Soc.*, **1984**, 106, 7644.
- ⁷¹ P. C. W. Leung, T. J. Emge, M. A. Beno, H. H. Wang, J. M. Williams, V. Petricek and P. Coppens, *J. Am. Chem. Soc.*, **1985**, 107, 6184.
- ⁷² K. D. Carlson, G. W. Crabtree, L. N. Hall, P. T. Copps, H. H. Wang, T. J. Emge, M. A. Beno and J. M. Williams, *Mol. Cryst. Liq. Cryst.*, **1985**, 119, 357.
- ⁷³ K. Mortensen, *Solid State Commun.*, **1982**, 44, 643.
- ⁷⁴ K. Bender, K. Dietz, H. Endres, H. W. Helberg, I. Hennig, H. J. Keller, H. W. Schäfer and D. Schweitzer, *Mol. Cryst. Liq. Cryst.*, **1984**, 107, 45.
- ⁷⁵ P. C. W. Leung, M. A. Beno, T. J. Emge, H. H. Wang, M. K. Bowman, M. A. Firestone, L. M. Sowa and J. M. Williams, *Mol. Cryst. Liq. Cryst.*, **1985**, 125, 113.

- ⁷⁶ H. Kobayashi, K. Kawano, T. Naito and A Kobayashi, *J. Mater. Chem.*, **1995**, 5, 10, 1681.
- ⁷⁷ T. J. Emge, H. H. Wang, M. A. Beno, P. C. W. Leung, M. A. Firestone, H. C. Jenkins, J. D. Cook, J. M. Williams, E. L. Venturini, L. J. Azevedo and J. E. Schirber, *Inorg. Chem.*, **1985**, 24, 1736.
- ⁷⁸ J. M. Williams, H. H. Wang, M. A. Beno, T. J. Emge, L. M. Sowa, P. T. Copps, F. Behroozi, L. N. Hall, K. D. Carlson and G. W. Crabtree, *Inorg. Chem.*, **1984**, 23, 3839.
- ⁷⁹ H. H. Wang, M. A. Beno, U. Geiser, M. A. Firestone, K. S. Webb, L. Nuñez, G. W. Crabtree, K. D. Carlson, J. M. Williams, L. J. Azevedo, J. F. Kwak and J. E. Schirber, *Inorg. Chem.*, **1985**, 24, 16, 2465.
- ⁸⁰ P. C. W. Leung, M. A. Beno, G. S. Blackman, B. R. Coughlin, C. A. Miderski, W. Joss, G. W. Crabtree and J. M. Williams, *Acta Cryst.*, **1984**, C40, 1331.
- ⁸¹ M. A. Beno, D. D. Cox and J. M. Williams, *Acta Cryst.*, **1984**, C40, 1334.
- ⁸² S. V. Konovalikhin, O. A. D'yachenko, A. B. Zolotoi, V. V. Gritsenko, Lo.O. Atovmyan and E. É. Laukhina, *Izv. Akad. Nauk SSSR, Ser. Khim.*, **1991**, 4, 811.
- ⁸³ E. I. Zhilyaeva, R. N. Lyubovskaya, N. P. Onishchuk, S. V. Konovalikhin and O. A. D'yachenko, *Izv. Akad. Nauk SSSR, Ser. Khim.*, **1990**, 6, 1438.
- ⁸⁴ R. M. Lobkovskaya, R. P. Shibaeva, E. É. Laukhina and A. V. Zvarykina, *Zh. Strukt. Khim.*, **1990**, 31, 5, 3.
- ⁸⁵ T. Mori and H. Inokuchi, *Chem. Lett.*, **1987**, 1657.
- ⁸⁶ J. Gaultier, S. Hébrard-Bracchetti, P. Guionneau, C. J. Kepert, D. Chasseau, L. Ducasse, Y. Barrans, M. Kurmoo, P. Day, *Journal of Solid State Chemistry*, **1999**, 145, 496.
- ⁸⁷ T. Takahashi, D. Jérôme and K. Bechgaard, *J. Physique Lettres*, **1982**, 43, L565.
- ⁸⁸ S. Tomić, D. Jérôme, P. Monod and K. Bechgaard, *J. Physique Lettres*, **1982**, 43, L839.
- ⁸⁹ A. I. Larkin and V. I. Mel'nikov, *Sov. Phys. JETP*, **1976**, 44, 1159.
- ⁹⁰ J. D. Wallis and J. -P. Griffiths, *J. Mater. Chem.*, **2005**, 15, 347.
- ⁹¹ W. Xu, D. Zhang, H. Li and D. Zhu, *J. Mater. Chem.*, **1999**, 9, 1245.
- ⁹² N. Saygili, R. J. Brown, P. Day, R. Hoelzl, P. Kathirgamanathan, E. R. Mageean, T. Ozturk, M. Pilkington, M. M. B. Qayyum, S. S. Turner, L. Vorwerg and J. D. Wallis, *Tetrahedron*, **2001**, 57, 5015.
- ⁹³ R. J. Brown, G. Camarasa, J. -P. Griffiths, P. Day and J. D. Wallis, *Tetrahedron Letters*, **2004**, 45, 5103.

- ⁹⁴ Y. Ishikawa, T. Miyamoto, A. Yoshida, Y. Kawada, J. Nakazaki, A. Izuoka and T. Sugawara, *Tetrahedron Letters*, **1999**, 40, 8819.
- ⁹⁵ H. Li, D. Zhang, B. Zhang, Y. Yao, W. Xu, D. Zhu and Z. Wang, *J. Mater. Chem.*, **2000**, 10, 2063.
- ⁹⁶ V. Y. Khodorovskii, G. G. Pukitis, A. Y. Puplovskii, A. S. Édzhinya and O. Y. Neiland, *Khim. Geterotsikl. Soedin.*, **1990**, 1, 131.
- ⁹⁷ L. M. Goldenberg, V. Y. Khodorkovsky, J. Y. Becker, P. J. Lukes, M. R. Bryce, M. C. Petty and J. Yarwood, *Chem. Mater.*, **1994**, 6, 1426.
- ⁹⁸ J. P. Parakka, A. M. Kini and J. M. Williams, *Tetrahedron Letters*, **1996**, 37, 45, 8085.
- ⁹⁹ F. Leurquin, T. Ozturk, M. Pilkington and J. D. Wallis, *J. Chem. Soc., Perkin Trans. 1*, **1997**, 3173.
- ¹⁰⁰ T. Ozturk, C. R. Rice and J. D. Wallis, *J. Mater. Chem.*, **1995**, 5, 1553.
- ¹⁰¹ A. Karrer, J. D. Wallis, J. D. Dunitz, B. Hilti, C. W. Mayer, M. Bürkle, and J. Pfeiffer, *Helv. Chim. Acta.*, **1987**, 70, 942.
- ¹⁰² G. G. Abashev and E. V. Shklyeva, *Chem. Heterocycl. Compd.*, **2006**, 42, 4, 423.
- ¹⁰³ C. S. Wang, A. S. Batsanov, M. R. Bryce, J. A. K. Howard, *Synthesis*, **1998**, 11, 1615.
- ¹⁰⁴ H. Kobayashi, A. Kobayashi, T. Nakamura, T. Nogami and Y. Shirota, *Chem. Lett.*, **1987**, 559.
- ¹⁰⁵ H. H. Wang, J. R. Ferraro, J. M. Williams, U. Geiser and J. A. Schlueter, *J. Chem. Soc., Chem. Commun.*, **1994**, 1893.
- ¹⁰⁶ L. Martin, *Structures and Properties of Magnetic Molecular Charge Transfer Salts*, Ph. D. Thesis, Royal Institution of Great Britain and University College London, May 1999.
- ¹⁰⁷ J. S. Chappell, A. N. Bloch, W. A. Bryden, M. Maxfield, T. O. Poehler and D. O. Cowan, *J. Am. Chem. Soc.*, **1981**, 103, 2442.
- ¹⁰⁸ P. Guionneau, C. J. Kepert, G. Bravic, D. Chasseau, M. R. Truter, M. Kurmoo and P. Day, *Synthetic Metals*, **1997**, 86, 1973.
- ¹⁰⁹ T. Sugano, G. Saito and M. Kinoshita, *Phys. Rev. B: Condens. Matter*, **1986**, 34, 117.
- ¹¹⁰ E. L. Venturini, L. J. Azevedo, J. E. Schirber, J. M. Williams and H. H. Wang, *Phys. Rev. B: Condens. Matter*, **1985**, 32, 2819.
- ¹¹¹ S. Klotz, J. S. Schilling, S. Gärtner and D. Schweitzer, *Solid State Commun*, **1988**, 67, 981.
- ¹¹² E. L. Venturini, J. E. Schirber, H. H. Wang and J. M. Williams, *Synth. Met.*, **1988**, 27, A243.

- ¹¹³ S. Gärtner, I. Heinen, D. Schweitzer, H. J. Keller, R. Niebl and B. Z. Nuber, *Naturforsch*, **1990**, 45, 763.
- ¹¹⁴ H. Urayama, H. Yamochi, G. Saito, S. Sato, T. Sugano, M. Kinoshita, A. Kawamoto, J. Tanaka, T. Inabe, T. Mori, Y. Maruyama, H. Inokuchi and K. Oshima, *Synth. Met.*, **1988**, 27, A393.
- ¹¹⁵ H. H. Wang, L. K. Montgomery, A. M. Kini, K. D. Carlson, M. A. Beno, U. Geiser, C. S. Cariss, J. M. Williams and E. L. Venturini, *Physica C*, **1988**, 156, 173.
- ¹¹⁶ G. Sekretarczyk and A. Graja, *Synth. Met.*, **1988**, 24, 161.
- ¹¹⁷ G. Sekretarczyk, A. Graja, J. Pichet, R. N. Lyubovskaya and R. B. Lyubovskii, *J. Phys., France*, **1988**, 49, 653.
- ¹¹⁸ P. Atkins and J. de Paula, in *Atkins' Physical Chemistry*, Oxford University Press, Trento (Italy), 7th edn., 2002, ch. 28, pp 980.
- ¹¹⁹ E. I. Chashechkina, I. J. Lee, S. E. Brown, D. S. Chow, W. G. Clark, M. J. Naughton and P. M. Chaikin, *Synth. Metals*, **2001**, 119, 13.
- ¹²⁰ D. D. Osheroff, R. C. Richardson and D. M. Lee, *Phys. Rev. Lett.*, **1972**, 28, 885.
- ¹²¹ D. D. Osheroff, W. J. Gully, R. C. Richardson and D. M. Lee, *Phys. Rev. Lett.*, **1972**, 29, 920.
- ¹²² T. C. Chiang, A. H. Reddoch and D. F. Williams, *J. Chem. Phys.*, **1971**, 54, 2051.
- ¹²³ H. Anzai, M. Tokumoto and G. Saito, *Mol. Cryst. Liq. Cryst.*, **1985**, 125, 385.
- ¹²⁴ D. R. Rosseinsky and P. Kathirgamanathan, *Mol. Cryst. Liq. Cryst.*, **1982**, 86, 43.
- ¹²⁵ P. Batail, K. Boubekeur, M. Fourmigué and J. -C. P. Gabriel, *Chem. Mater.*, **1998**, 10, 3005.
- ¹²⁶ C. B. Breslin, A. M. Felon and K. G. Conroy, *Materials and Design*, **2005**, 26, 233.
- ¹²⁷ A. J. Heeger, Nobel Prize Lecture "Semiconducting and Metallic Polymers: The Fourth Generation of Polymeric Materials", 8th December 2000.
- ¹²⁸ J. G. Bednorz and K. A. Muller, *Z. Phys. B Condensed Matter*, **1986**, 64, 189.
- ¹²⁹ D. C. Johnston, H. Prakash, W. H. Zachariasen and R. Viswanathan, *Mat. Res. Bull.*, **1973**, 8, 777.
- ¹³⁰ C. W. Chu, P. H. Hor, R. L. Meng, L. Gao, Z. J. Huang and Y. Q. Wang, *Phys. Rev. Lett.*, **1987**, 58, 405.
- ¹³¹ A. M. Hermann and J. V. Yakhmi, *Thallium Based High Temperature Superconductors*, Dekker, Besel, **1993**.
- ¹³² C. W. Chu, L. Gao, F. Chen, Z. J. Huang, R. L. Meng and Y. Y. Xue, *Nature*, **1993**, 365, 323.

¹³³ P. A. Lee, *Nature*, **2000**, 406, 467 and references cited therein.

¹³⁴ Condensed Matter Physics at the University of Birmingham, "Thin Film HTS Deposition", www.cm.ph.bham.ac.uk/~thinfilms.html, Accessed: 7th December 2008.

¹³⁵ H. Klauk, *Organic Electronics: Materials, Manufacturing and Applications*, Wiley-VCH, Mörlenbach (Germany), 2008.

¹³⁶ J. Roberts, News article on CBS, "U.S. Drops 'E-Bomb' on Iraqi TV", Article reported: 25th March 2003, Accessed: 7th December 2008.

Chapter 2

Chiral organosulfur-derived electron donors

2 Chiral organosulfur-derived electron donors

2.1 Introduction

The preparation of radical cation salts of ET often leads to multiple donor packing motifs in the crystal phases observed from a single electrocrystallisation cycle. Each packing phase exhibits different electron conductivity properties, due to the orientation of the molecules in the crystal. The apparent absence of control over which crystalline phases are formed, has led researchers to try to introduce intermolecular interactions that could serve to dictate the supramolecular structure.

Organosulfur electron donor molecules and the anionic species encapsulated in the radical cation salts have been functionalised to incorporate hydrogen bonding capabilities,^{1, 2} and increased van der Waals attractions.^{3, 4}

In determining how the intermolecular interactions affect the crystalline structure and thus the electron transfer properties, better reagents can be designed for use in preparing electro-active materials. The evolution of ET, with its extended conjugated structure, and increased van der Waals interactions over TTF is such an example.⁵

The S...S network of close contacts is paramount to the existence of increased conductivity in derivatives of TTF and its offspring, ET. The distance between sulfur atoms of a donor and its neighbouring donor molecules range from greater than the sum of the corresponding van der Waals radii (>3.6 Å) in an insulating – low conducting

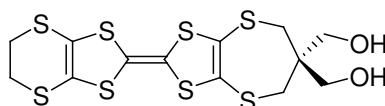
salt, through to much less than the sum of their radii, e.g. 3.51 Å in the superconducting salt κ -(ET)₂Cu[N(CN)₂]Br.⁶ Associated with the positively electrically charged donor molecules are the anionic counterparts/electron acceptors, which serve to trap and stabilise the material.

Incorporating hydrogen bonding capability on both the donor and the anion components of the salt could lead to a closer packing of the crystallographic unit cell, shown to be important by Williams *et al.* and separately by Bechgaard *et al.*, who observed that the superconducting transition temperature was elevated by the contraction of the unit cell.^{7, 8, 9, 10, 11} Significant control over the formation of electron donor stacks and sheets could be expected, giving greater order at atomic sites and thus reduced phonon interactions, leading to an increase in the observed superconducting transition temperature.

In the radical cation salts formed from ET in which the anion employed is Cu(NCS)₂⁻, the distance between the conducting planes is 5.32 Å.¹² When a larger anion is employed such as [KHg(SCN)₄]⁻ the distance between conducting planes is much greater at 7.42 Å.¹³ In these salts the transition to a superconducting phase is observed at 10.4 K and 1.1 K respectively, suggesting that more closely packed systems exhibit higher T_C values. However, Day refers to this interesting aspect when presenting (ET)₄(H₂O)Fe(C₂O₄)₃·C₆H₅CN (T_C = 7.0 K) which has a distance between the superconducting planes of 4.86 or 6.08 Å (dependant on the charge of the donor molecule in the crystal structure),¹⁴ stating that such a simple parameter cannot predict

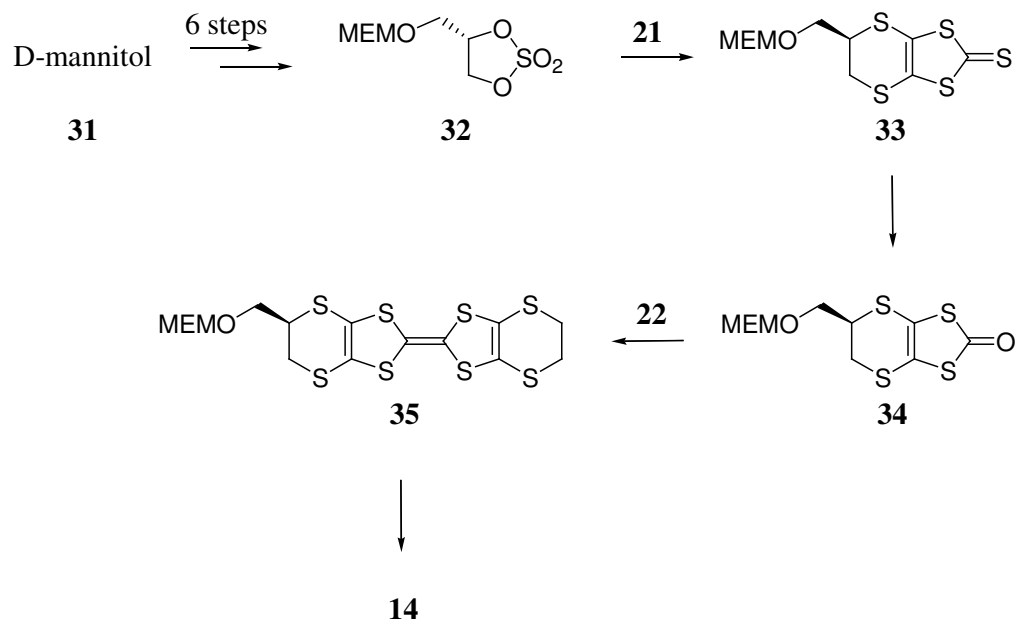
whether a given phase will be superconducting or not, or the T_C at which the superconducting phase will be observed.

Decurtins prepared the ET derivative **30** in which one of the exterior ethylene functions had been replaced by a propylene function bearing a *gem*-di(hydroxymethyl) fragment on the middle carbon.¹⁵ A radical cation salt was prepared with the linear triiodide anion and was shown to have a ratio of donor to anion of 2:1. This salt crystallised in the space group $P2_1/c$ with both donor molecules adopting a coplanar orientation, and the donor molecules being dimerised with the hydroxyl functionalities on adjacent donor pairs hydrogen bonding to give a head-to-tail arrangement. At room temperature the salt showed a relatively high conductivity ($\sigma = 2.95 \text{ S cm}^{-1}$), and exhibited semiconductor behaviour below 240 K.



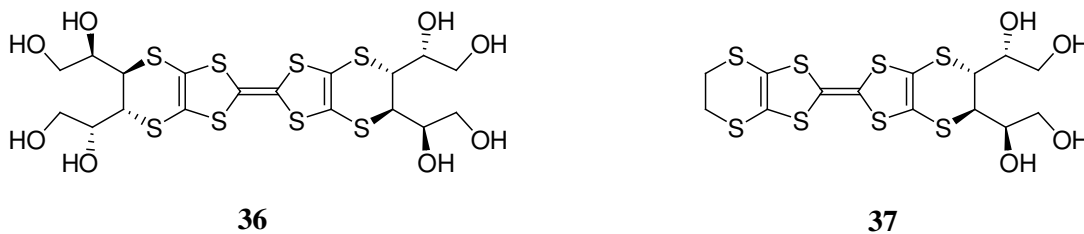
30

Li *et al.* have achieved the functionalisation of the ET skeletal structure with hydroxymethyl groups.¹⁶ However it is expected that the increase in the control of the lattice structure through the potential hydrogen bonding facilities incorporated, will be counteracted by the presence of chiral disorder at the carbon bearing the hydroxymethyl substituent. The preparation of the single enantiomer of the hydroxymethyl derivative was achieved *via* cyclic sulfate ester chemistry (Scheme 5).¹⁷ The racemic hydroxymethyl group was prepared by Saygili *et al.*¹



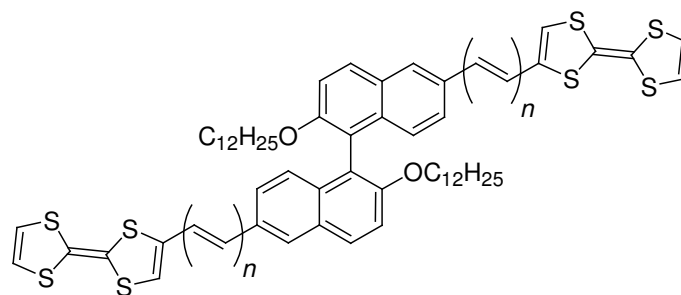
Scheme 5: Preparation of hydroxymethyl-ET (14) via cyclic sulfate ester chemistry.

Building on this work, it was decided to prepare chirally pure hydroxyl-bearing electron donors, derived from *D*-mannitol (31). This approach afforded the electron donor species bearing eight (36) or four (37) hydroxyl groups, with controlled stereochemistry at each carbon atom.



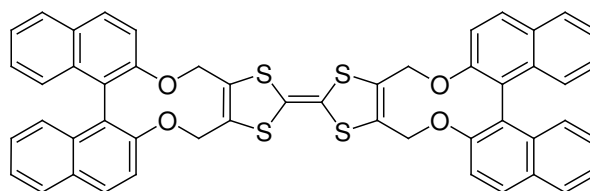
Another area of interest was the incorporation of chirality by employment of 2,2'-binaphthol systems into molecular conductors. This has been little investigated despite the great versatility of the aromatic substituent, and extensive use in the preparation of

chiral catalysts.^{18, 19, 20} The bulky aromatic moiety infers a great steric influence, with the delocalised π -electrons allowing weak intermolecular bonding interactions to occur.



38

Both enantiomeric forms of the binaphthol unit are available commercially, however chiral resolution of racemic material has been achieved by Wang *et al.* using *N*-benzylcinchonium chloride.²¹ Gómez *et al.* incorporated the binaphthol unit into their TTF derivative **38**, and found that charge transfer complexes were readily formed with DDQ.²² Building on this, it was decided to undertake the preparation of electron donor **39** in enantiopure form.



39

2.2 Results and discussion

The synthetic route to target materials **36** and **37** proceeded as in Schemes 6 and 7. The initial protection of the exterior hydroxyl functions residing on C¹, C², C⁵ and C⁶ of **31** (Figure 21) as ketals. This was achieved using zinc chloride in acetone, as described in the literature to give **40**.^{23, 24}

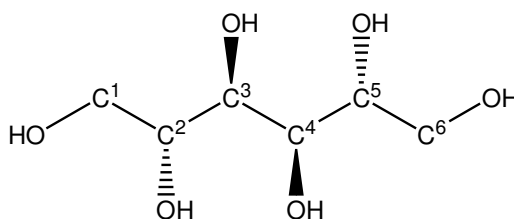
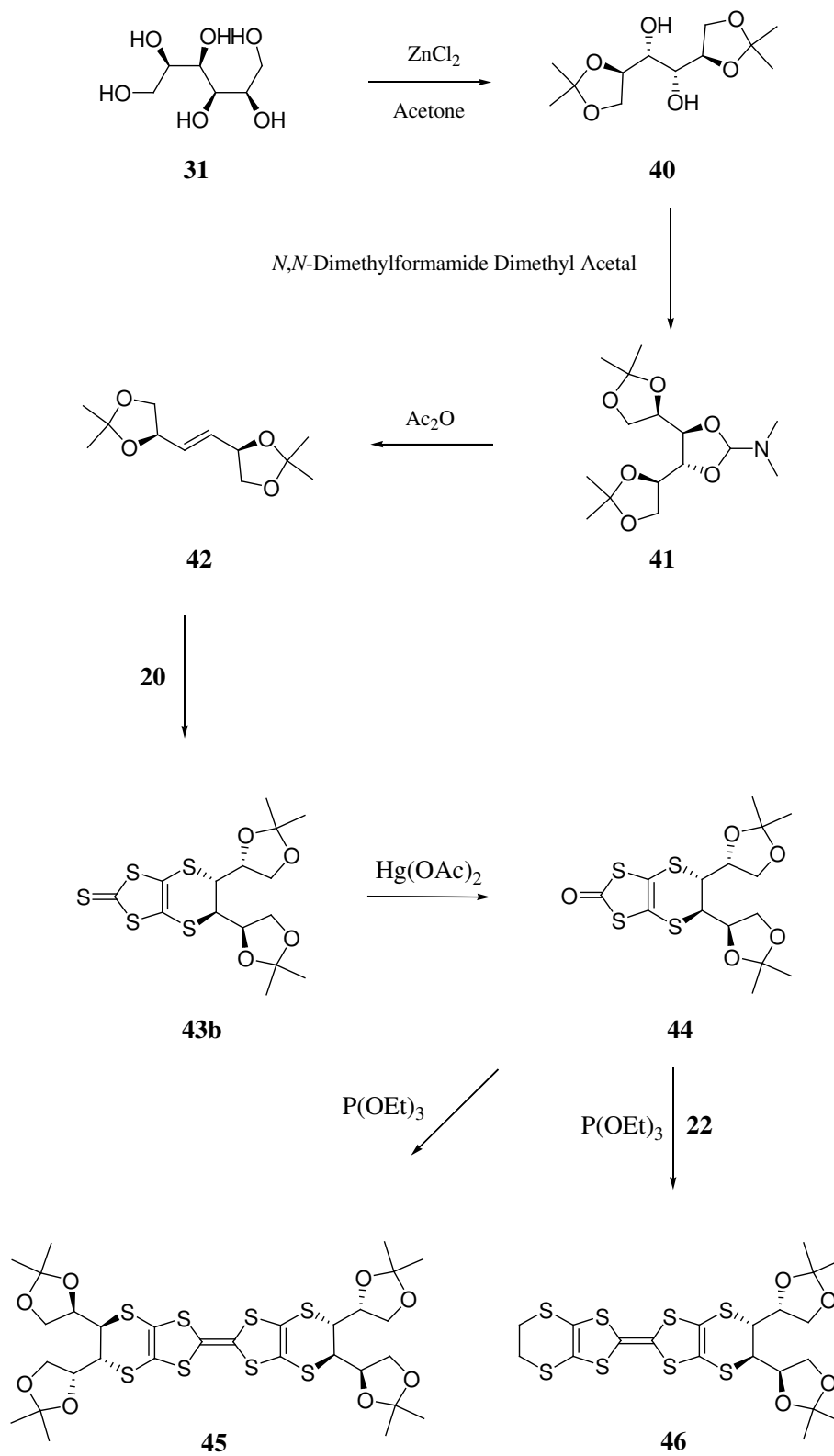


Figure 21: Carbon numbering in 31.

Simple work-up allowed the isolation of the required species as a pure white solid. Subsequently, the interior hydroxyl functions residing on C³ and C⁴ (Figure 21) were derivatised as the *N, N*-dimethyl formamide cyclic acetal, **41**. The elimination of the acetal function in neat acetic anhydride afforded, after chromatographic purification, the *trans*- alkene **42**, as a colourless crystalline compound with the stereochemistry locked at C² and C⁵, having the *R*- arrangement.



Scheme 6: Synthetic route to protected donors 45 and 46.

The 1,3-cycloaddition heteroatom Diels-Alder type reaction was employed between the *trans*- alkene **42** and the oligomeric trithione species **20** in refluxing toluene. The trithione species **20** rapidly depolymerises at *ca.* 112 °C forming the dithione, and is trapped by the dienophile affording the cyclic target material. Upon completion of the reaction, two products were isolated by chromatography. These products were assigned as the two stereoisomers **43a** and **43b** (Figure 22) possible from the reaction, and their stereochemistry has been assigned based upon the X-ray crystal structure of the minor *R*-, *S*-, *S*-, *R*- adduct **43a**.

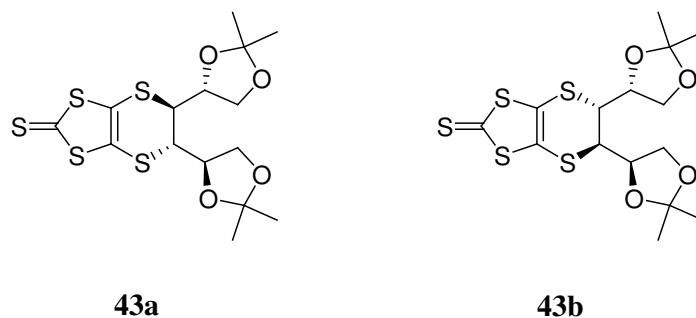


Figure 22: Two stereoisomers formed by the Diels-Alder reaction.

The required stereoisomer, **43b** was isolated in *ca.* 20 % yield, and characterised by its ¹H NMR spectrum displaying two singlet resonances due to the hydrogen atoms of the four methyl groups at δ 1.41 and 1.33 ppm. The single hydrogen atoms adjoining the six-membered heterocyclic ring resonated as a doublet at δ 3.71 ppm, and showed coupling to the adjacent hydrogen on the cyclic ketal ring with a coupling constant of $J = 9.8$ Hz.

The ^{13}C NMR spectrum indicated the presence of a thiocarbonyl fragment at δ 206.5 ppm, and the loss of the sp^2 hybridised carbon signal at δ 130.7 ppm showed the reduction in oxidation level of the carbon due to the formation of the two C-S bonds in the cyclisation reaction giving a signal at δ 44.3 ppm. The infrared spectrum confirmed the thiocarbonyl presence with a strong stretching band at 1066 cm^{-1} , and the $[\text{M} + \text{H}]^+$ ion was observed in the electrospray mass spectrum at 425.0038 Da.

The thiocarbonyl compound **43b** underwent mercuric acetate mediated sulfur-oxygen exchange (Figure 23) in chloroform solution affording the carbonyl compound **44** in good yield, determined by the shift in the ^{13}C NMR spectrum to δ 188.9 ppm indicating the presence of the carbonyl species. The carbonyl compounds have been shown to be more reactive than the thiocarbonyl analogues during the coupling step. Further evidence of the transformation is observable by a shift in the resonance signals for the carbon atoms at the fusion points of the five- and six-membered dithiolo rings from δ 118.9 ppm in **43b** to δ 109.6 ppm in **44**. The stretching frequency of the carbonyl fragment is identifiable in the infrared spectrum as a strong vibration at $\nu = 1683\text{ cm}^{-1}$, and the molecular ion is observed in the high resolution electron impact mass spectrum at 408.0190 Da.

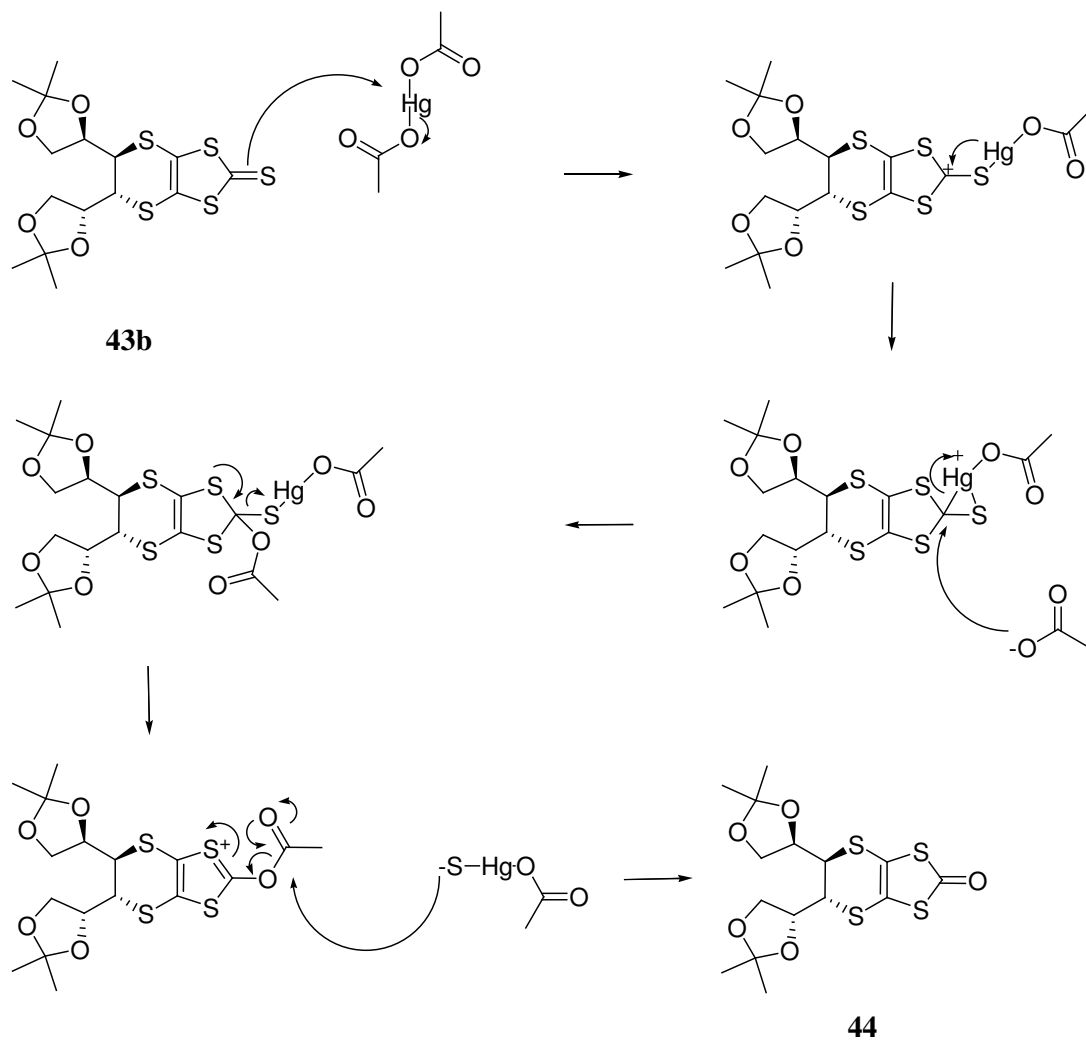


Figure 23: Proposed mechanism for sulfur-oxygen exchange.

The triethyl phosphite-mediated coupling of carbonyl compound **44** either with itself, or with thione **22** affords the chirally pure tetraketal **45** and diketal **46** compounds respectively. The cross-coupled electron donor was isolated and purified by chromatography and characterised by all available methods. The ^1H NMR spectrum of **46** indicates the presence of the four methyl groups, whose hydrogen atoms resonate as two singlets due to their orientations at δ 1.4 and 1.32 ppm, and the ethylene function at the opposite end of the chalcogenic species as a singlet at δ 3.26 ppm. The absence of

peaks in the ^{13}C NMR due to carbonyl and thiocarbonyl confirm that the isolated orange solid is not a composite mixture of both of the reactants. The formation of the central $\text{C}=\text{C}$ bond is observed as an additional resonance in the sp^2 region of the ^{13}C NMR, with the resonances occurring at δ 113.9, 112.3 and 110.4 ppm for the cross-coupled donor **46**. Definite assignment of which carbon is responsible for which resonance was not possible using the NMR techniques available. High resolution electrospray mass spectrometry confirmed the presence of the $[\text{M}+\text{H}]^+$ ion at 584.9507 Da, and the absence of the homo-coupled species **45** and **11**.

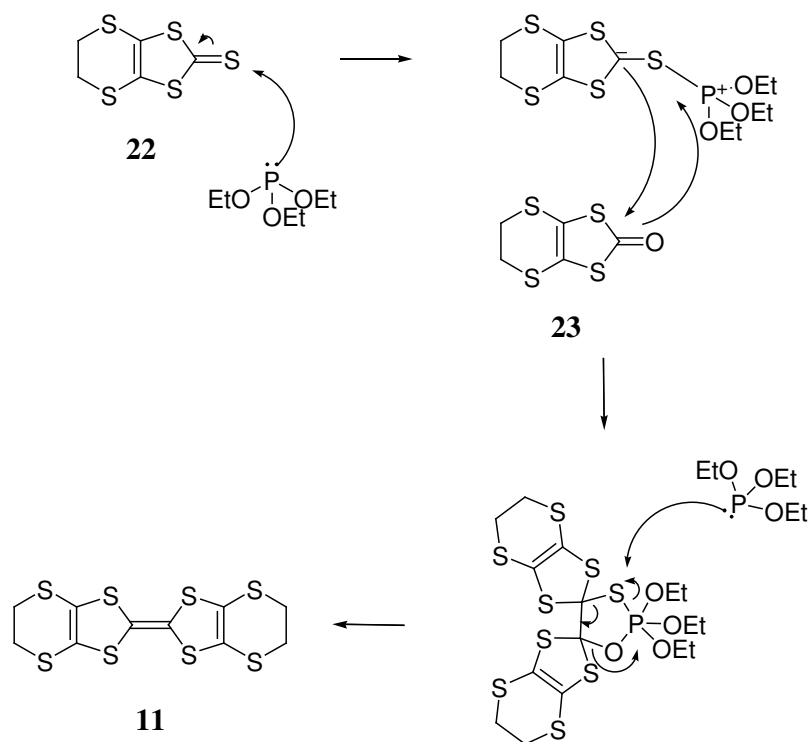


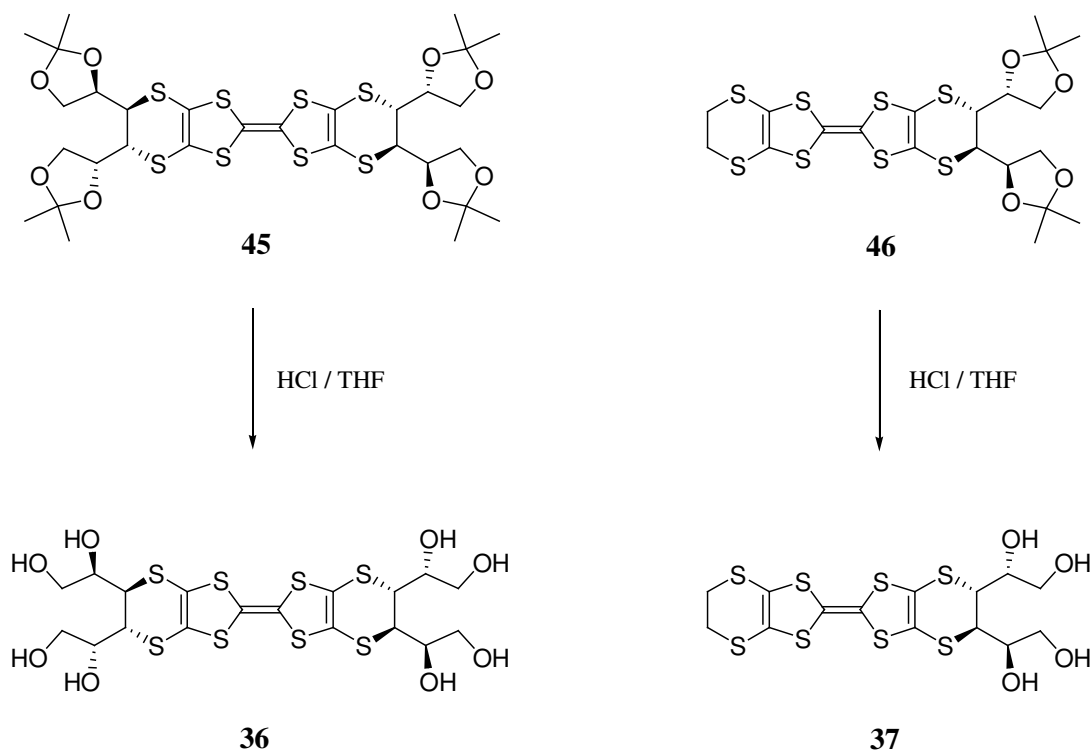
Figure 24: Proposed mechanism for triethyl phosphite coupling reaction to form **11**.

The homo-coupling reaction of carbonyl compound **44** to afford the chiral tetraketal donor **45** proceeded without complication in moderate yield. The pale orange solid isolated after chromatography was identified by its simple ^1H NMR spectrum showing resonances attributable to the hydrogen atoms of eight methyl groups as two singlets at δ 1.43 and 1.35 ppm. The ^{13}C NMR spectrum indicated the symmetry of the species as only two signals at δ 111.0 and 109.9 ppm were observed for the C=C network throughout the core of the electron donor. High resolution electron impact mass spectrometry confirmed the molecular ion as 784.0485 Da.

The deprotection of diketal **46** in tetrahydrofuran solution was achieved readily using aqueous hydrochloric acid, under an atmosphere of nitrogen to give the tetrol **37** as a light brown solid. The identity of **37** was determined from the infrared spectrum, which displayed stretching frequencies attributable to the presence of hydroxyl functions at 3293 cm^{-1} . The ^1H NMR spectrum showed the absence of resonances due to the hydrogen atoms of the methyl groups, and the presence of a signal at δ 3.60 ppm that was partly due to the hydroxyl protons. The ^{13}C NMR indicated a significant shift for the carbon atoms bearing the hydroxyl functions from δ 76.5 and 68.0 ppm in the protected donor **46** to δ 71.8 and 63.3 ppm in the free hydroxyl donor **37**. High resolution electron impact mass spectrometry identified the molecular ion at 503.8818 Da.

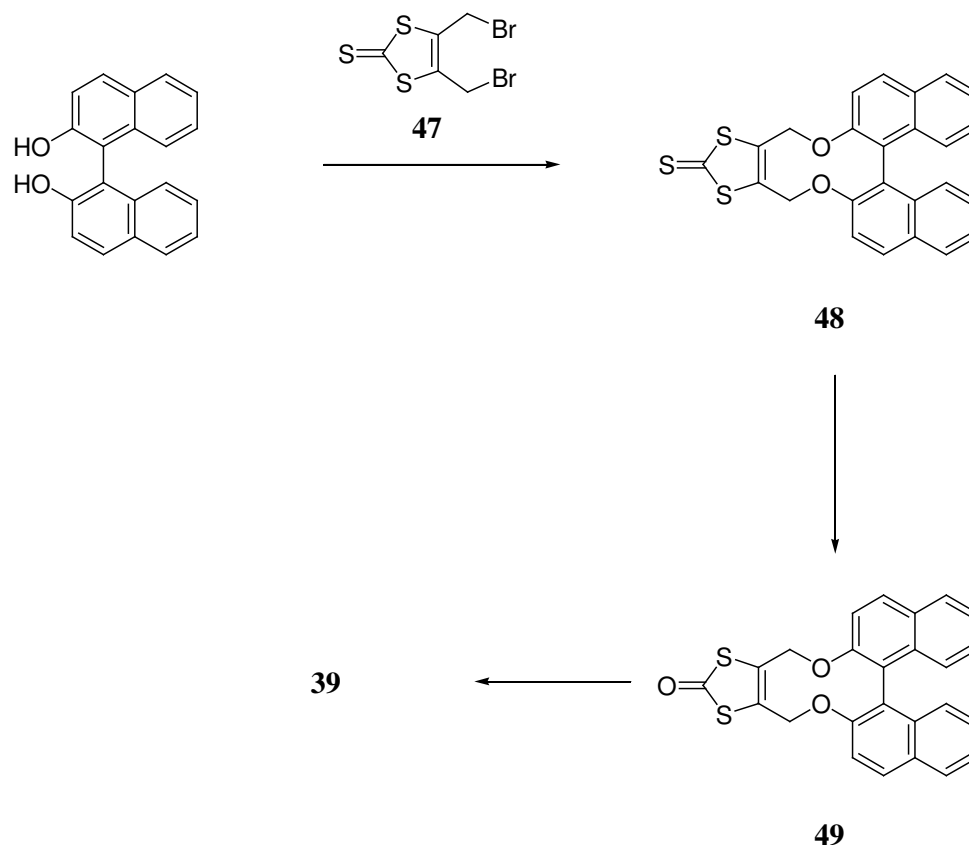
The deprotection of tetraketal **45** proved to be much more difficult. The octol species **36** was found to be very sensitive to air and moisture, rapidly turning dark green - black in colour and giving a highly insoluble material which did not allow characterisation of

the compound. The concentration of acid used in the deprotection was also shown to have an effect and after significant optimisation freshly prepared and thoroughly degassed (by bubbling nitrogen gas through for 20 min) 4 M HCl was determined to be most successful. Monitoring the reaction by TLC, eluting with cyclohexane / ethyl acetate (8:1) and increasing amounts of methanol, allowed the intermediary products to be observed in which some but not all of the ketal fragments had been removed. Careful evaporation under high vacuum at *ca.* 40 °C afforded the octol **36** as a light brown solid. The infrared spectrum indicated the presence of the hydroxyl groups at $\nu = 3254 \text{ cm}^{-1}$. The ^1H NMR spectrum was not as informative as expected, showing only a multiplet at $\delta 3.61$ ppm for all hydrogen resonances. The ^{13}C NMR indicated the presence of free hydroxyl groups as the carbons bearing the functions shifted to $\delta 71.8$ and 63.3 ppm as observed in the deprotection of diketal **46**. High resolution electrospray showed the $[\text{M} + \text{H}]^+$ ion at 624.9315 Da.



Scheme 7: Synthetic route to the final hydroxylated donors 36 and 37.

The preparation of the bis(binaphthyl) decorated donor **39** started from dibromide **47** which was prepared using the literature methods.^{25, 26} Slow addition of a dilute solution of **47** in tetrahydrofuran to a mixture of (*S*)-(-)-2,2-binaphthol and potassium carbonate in tetrahydrofuran afforded the diethereal thiocarbonyl compound **48** as a yellow solid in 83 % yield. The material was characterised by its ¹H NMR which showed aromatic peaks attributable to the binaphthol system, and a shift of the methylene protons from δ 4.35 ppm for **47** to δ 5.03 ppm for thione **48**.



Scheme 8: Synthetic strategy to the formation of donor 39.

The chemical shift for the thiocarbonyl peak in the ^{13}C NMR shifted from δ 208.0 ppm (47) to δ 209.2 ppm (48) indicating the transformation of the starting material had taken place. The stretching frequency for the thiocarbonyl peak was observed in the infrared spectrum at $\nu = 1058\text{ cm}^{-1}$. Elemental analysis confirmed the composition of the material, and the molecular ion was observed using mass spectrometry, at 444.0311 Da.

Subsequently, 48 was converted into the carbonyl analogue 49 using mercuric acetate in tetrahydrofuran. After stirring at room temperature, 49 was isolated in 92 % yield, and characterised by the resonance shifts in the ^{13}C NMR, which showed the absence of the

thiocarbonyl peak at δ 209.2 ppm, and a new peak visible at δ 189.3 ppm, indicative of the sulfur-oxygen exchange reaction having occurred. The strong infrared band for the C=S stretch was not observed, however a broad band was observed at $\nu = 1621 \text{ cm}^{-1}$ attributable to the stretch of a C=O bond. The molecular ion was observed in the mass spectrum at 428.0532 Da, unequivocally confirming the formation of **49**.

The triethyl phosphite mediated homo-coupling reaction of **49** at 100 °C afforded **39**. Chromatography afforded the electron donor species in 32 % yield, identified by the absence of the carbonyl peak in the ^{13}C NMR, and the presence of a resonance for the central C=C bond at δ 108.0 ppm. The purity of the material was confirmed by elemental analysis, and the ammonium adduct of the molecular ion was observed at 842.1523 Da. Compound **39** was found to decompose over a period of two months.

2.3 Materials made by electrocrystallisation

The preparation of radical cation salts of the tetraketal **45** and diketal **46** was investigated in addition to those from the octol **36** and tetrol **37**. The relatively good solubility of **45** and **46** in most common organic solvents proved to inhibit the crystallisation of oxidised species on the electrode. In the case of **45**, the steric bulk of the four ketal groups was also proposed to be inhibitive of crystal growth.

The ease with which the octol **36** species is oxidised makes it very appealing for the preparation of radical cation salts. In practice however, the setting up of electrocrystallisation experiments employing this electron donor proved difficult due to

the aforementioned reason. With every care taken to fully inert and dry the electrocrystallisation experiment, the electron donor was consistently found to turn dark green in colour, and produce no identifiable materials from the experiments.

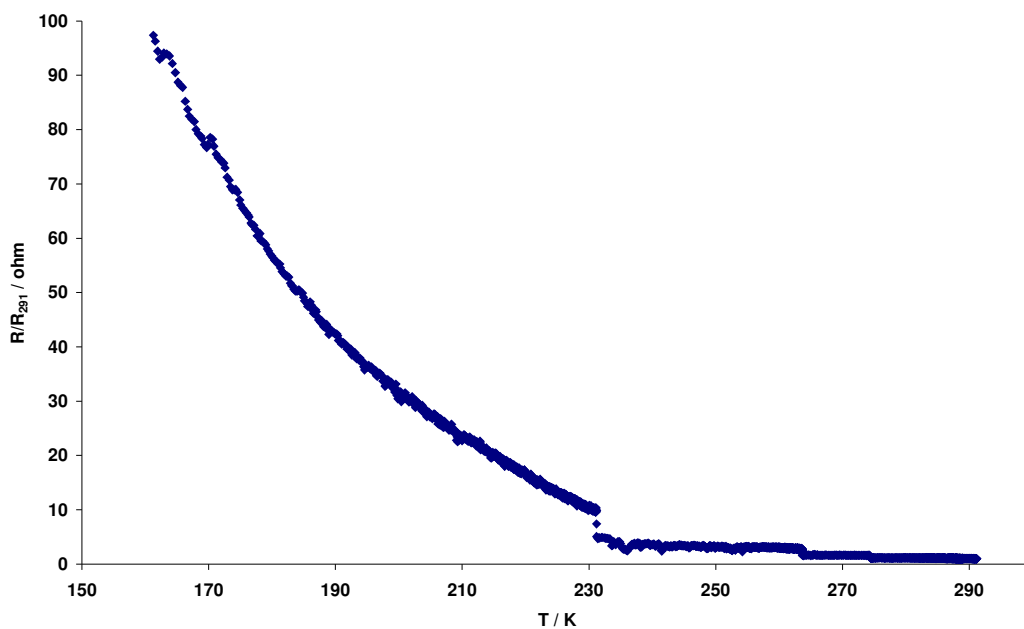


Figure 25: Resistivity as a function of temperature for (37)₂Cl.

In contrast, the tetrol **37** produced a wide range of electrocrystallised materials, although crystals thought to be suitable for single crystal X-ray diffraction were only formed in two cases, with the majority being either twinned or too small. Unfortunately, X-ray crystallographic analysis was unable to provide a structure in either case due to weak diffraction, and thus the materials were characterised by all other methods available.

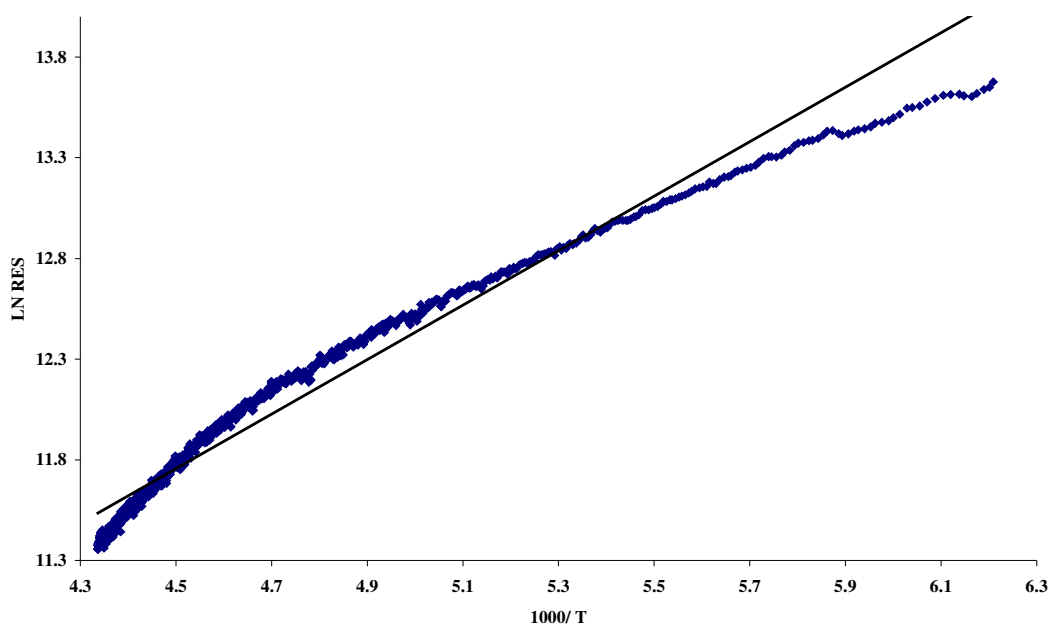


Figure 26: Linear relationship of $(37)_2\text{Cl}$ indicating semiconducting behaviour.

A tetrahydrofuran solution of tetrabutylammonium chloride was used to isolate a radical cation of the tetrol donor **37**. One black diamond shaped crystal was obtained from the anode, and investigated by resistivity measurements. The salt demonstrated semiconductor properties upon cooling from 291-163 K (Figure 25 and Figure 26), at which point the material became insulating. The kink in the resistivity plot against temperature (Figure 25) at around 230 K was determined to be due to the position of the crystal, relative to the liquid nitrogen coolant employed. This is evident from the curve of the temperature profile of the reaction (Figure 27), which exhibits a definite deviation at 233 K. The activation energy was determined to be 0.12 eV, in accordance with other ET-type semiconducting materials. The radical cation salt formed was determined to be of 2:1 stoichiometry by observation of the Raman stretching modes at $\nu_4^a = 1460$, and $\nu_4^b = 1469 \text{ cm}^{-1}$. The ν_3 stretches were not observed.

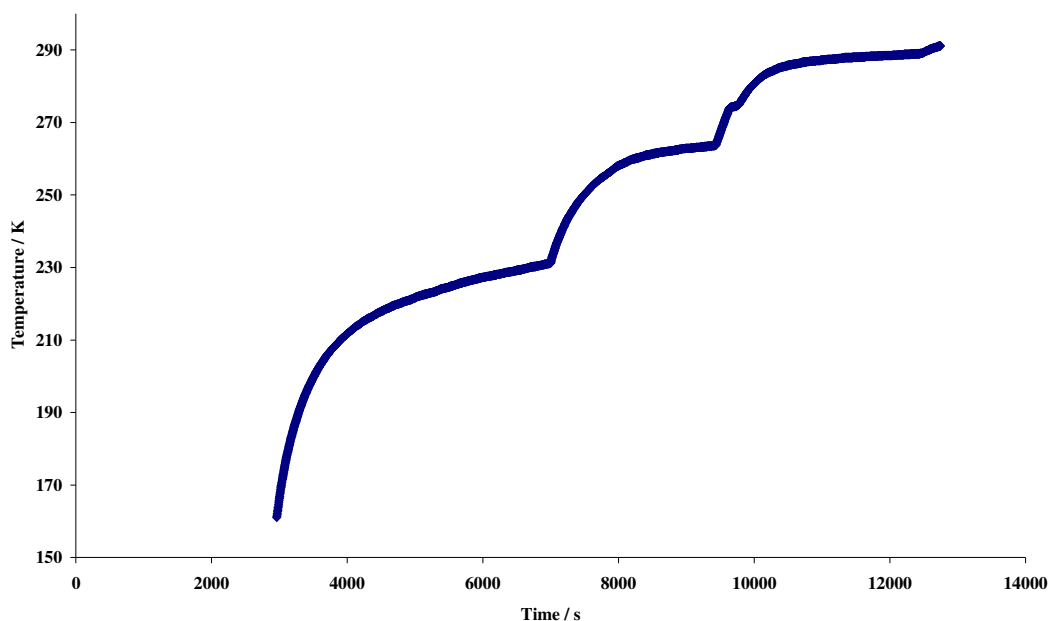


Figure 27: Temperature profile over the period of resistivity data collection for $(37)_2\text{Cl}$.

Further attempts at preparing better quality crystals from **37** with the chloride ion failed.

Salts of tetrol **37** were found to form in a 1:1 stoichiometry when the anion employed was bromide, triiodide, chromium(*R*, *R*-salen)*dis*thiocyanate and iron (III) (tetraphenylporphyrino)*dis*thiocyanate, all identifiable from Raman spectroscopic measurements which indicated the formation of a charge of $Z = +1$ on the electron donor molecule.

Molecular salts of tetrol **37** were found to form in a ratio of 3:1 (donor:anion) when the anion employed was chromium (III) (pyridin-2-yl-4'-(X^*)-isopropyl)oxazoline) tetra*is*thiocyanate, for when X^* = a racemic mixture of *R* and *S* enantiomers, or the *S* enantiomer only. A further 3:1 salt was formed from **37** with chromium (III)

tris(oxalate). All of the salts were identified by Raman spectroscopic measurements as having a charge state of $Z = +1$ on the electron donor molecules.

Molecular salts were synthesised from aluminium tris(oxalate), chromium (III) tris(oxalate), cobalt tetrachloride, and were all identified by Raman spectroscopy as having a charge of $Z = +0.67$ on the electron donor molecule.

A tetrol **37** molecular salt with hexafluorophosphate anion was prepared and determined by elemental analysis to be approximately 4:1 (donor:anion).

2.4 **Experimental**

Nuclear magnetic resonance (NMR) spectra were recorded on a Jeol ECX 400 (^1H : 400 MHz and ^{13}C : 100.6 MHz) spectrometer in the deuterated solvent stated. All chemical shifts (δ) are quoted in ppm and coupling constants (J) in Hz. Residual signals from the solvents were used as an internal reference. Infrared spectra were recorded on either a PerkinElmer Spectrum RX1 FT-IR spectrometer, or a PerkinElmer Spectrum 100 Fourier Transform spectrophotometer (as stated) with Attenuated Total Reflectance (ATR) Sampling Accessory, allowing direct analysis of samples, and are quoted in cm^{-1} . Raman spectra were recorded at room temperature with a Renishaw InVia Raman microscope equipped with a diode laser (785 nm) and a 1200 mm^{-1} grating using a laser power *ca.* 1 mW, or on a Foster and Freeman Foram 685-2 Raman Spectral Comparator using a power setting of 10%, on the 20x magnification averaged over five scans each having an integration time of 20 seconds. Optical rotation measurements were conducted on a PerkinElmer 241 Polarimeter. Elemental analysis (C, H, N) was conducted by Mr Stephen Boyer at London Metropolitan University. Mass Spectrometry measurements were conducted by the EPSRC National Service at the University of Wales Swansea. GC-MS measurements were conducted on an Agilent Technologies 6890N Network GC System fitted to an Agilent Technologies 5975 Inert XL Mass Selective Detector, using the method 'quickorganicstuff' (see Appendix 1). Melting points were collected on a Gallenkamp Melting Point Apparatus and are uncorrected. Single crystal X-ray diffraction measurements were conducted by the EPSRC National X-ray Service at Southampton University, with the exception of the data collection for (ET)Br which was collected by Dr Lee Martin whilst visiting the

research group of Professor Koichi Kikuchi at Tokyo Metropolitan University in Japan. All solvents were dried and distilled prior to use following standard procedures.²⁷ Chemicals obtained from suppliers (SigmaAldrich, Fisher (Acros)) were used as received. Inert atmosphere experiments were performed under dry nitrogen. Chromatography was performed on 40-63 μ silica gel (Fluorochem). Thin Layer Chromatography (TLC) was performed on pre-coated (F₂₅₄) glass-backed silica plates (Fisher). Electrocrystallisation cells, unless otherwise stated, were cleaned by standing in nitric acid overnight, washing with distilled water, then acetone and methanol before drying in a hot oven. Electrocrystallisation electrodes, unless otherwise stated, were cleaned prior to use by passing a current through 1 M sulfuric acid for 10 min, then reversing the current flow for 10 min before washing with distilled water, methanol and drying in air at room temperature. Variable temperature resistivity measurements were conducted on an Oxford MagLab conductivity rig, at University College, London. The crystals were mounted onto an 8-pin chip using annealed gold wire of diameter 0.0025 mm and fixed using carbon conducting cement (Agar Scientific). SQUID measurements were conducted on a Quantum Design MPMS7 SQUID magnetometer at University College, London. The sample was weighed into a gelatine capsule, which was subsequently fitted inside a plastic drinking straw (diamagnetic), using empty gelatine capsules, to the correct level for scanning. The straw was fixed to the instrument probe using diamagnetic tape.

Bis(tetraethylammonium)zinc[di(1,3-dithiolo-2-thione-4,5-dithiolate)], **19**

To a large dried three-necked flask, equipped with overhead stirrer, condensor and nitrogen inlet/outlet, was charged carbon disulphide (240 mL, 3.98 mol) and dry distilled *N,N*-dimethylformamide (480 mL). These were stirred together under nitrogen, and cooled to 0 °C in an ice bath. Finely cut sodium (14.5 g, 0.63 mol) was added in one portion, and the mixture stirred overnight. Remaining sodium metal was destroyed by the addition of methanol (*ca.* 100 mL), and the mixture left to stir for 20 min. Two solutions were prepared: (i) Zinc chloride (21.3 g, 0.16 mol) in a mixture of aqueous 35% ammonia (360 mL) and distilled water (100 mL); (ii) Tetraethylammonium bromide (66.0 g, 0.31 mol) in distilled water (500 mL); and these were added dropwise simultaneously to the reaction flask *via* two addition funnels. A red precipitate formed, and the reaction was allowed to stir overnight. Filtration at the pump, washing with 2-propanol (3 x 200 mL) and then diethyl ether (250 mL) afforded **19** (86.2 g, 75 %) as a red solid Mp 199-200 °C.

[1,3]Dithiolane-2,4,5-trithione, **20**

To a stirred solution of the zinc complex **19** (15.0 g, 20.9 mmol) in acetone (150 mL) at -78 °C, was added dropwise a solution of iodine (10.6 g, 41.8 mmol) in ethanol (300 mL) over 90 min. The reaction was allowed to warm to room temperature overnight, and the precipitate collected by filtration. The mustard-yellow solid was sequentially washed with ethanol (2 x 200 mL), distilled water (2 x 200 mL), acetone (2 x 100 mL),

diethyl ether (2 x 150 mL), and dried under vacuum for 3 h to afford **20** (8.2 g, 100%) as a fine orange-yellow powder Mp 113 °C (dec).

5,6-Dihydro-[1,3]dithiolo[4,5-b][1,4]dithiine-2-thione, 22

To a well-stirred suspension of the zinc complex **19** (40.7 g, 57.0 mmol) in acetonitrile (500 mL) was added 1,2-dibromoethane (12 mL, 0.114 mol). The mixture was heated to reflux at 100 °C under a nitrogen atmosphere and maintained for 7 h, before allowing to cool to room temperature overnight. The reaction mixture was filtered affording a dark yellow shiny solid, which was subsequently washed with methanol (150 mL), and dried on the filter paper for 30 min. The crude solid (*ca.* 33 g) was dissolved in dichloromethane (800 mL) and to this added activated charcoal (*ca.* 20 g). The mixture was heated at 40 °C for 20 min with stirring in air, before filtering (whilst warm) to afford an orange solution. This was evaporated affording **22** (23.4 g, 92%) as a shiny yellow solid Mp 118 °C (lit.²⁸ 120-123 °C); ν_{\max} (ATR)/cm⁻¹ 2951, 2920, 1477, 1418, 1401, 1281, 1253, 1165, 1126, 1057, 1035, 1014, 922, 888, 870, 775, 678, 643, 524, 469, 458; δ_{H} (400 MHz, CDCl₃) 3.43 (4 H, d, $J=1.68$ Hz, 5- H_{α} , 5- H_{β} , 6- H_{α} , 6- H_{β}); δ_{C} (100 MHz, CDCl₃) 212.0 (2- C), 122.8 (2 x sp^2 - C), 29.6 (5-, 6- C).

5R, 6R-5, 6-bis((4'R)-2',2'-dimethyl-1,3-dioxolan-4'-yl)-5,6-dihydro-1,3-dithiolo[4,5-b]1,4-dithiin-2-thione, 43b

The *trans*-diketal alkene **42** was prepared by the literature methods.^{23, 24} A stirred suspension of **42** (1.1 g, 4.82 mmol) was heated with trithione **20** (1.89 g, 9.65 mmol) in

toluene to reflux under nitrogen for 10 h. Removal of the solvent under reduced pressure, afforded the crude material which was purified by chromatography on silica eluting with a mixture of ethyl acetate and cyclohexane (1:5) to give **43b** (0.41 g, 20 %) as a yellow-brown solid; $[\alpha]_D^{25} = +489^\circ \text{ g}^{-1} \text{ mL}^{-1} \text{ dm}^{-1}$ ($c = 0.12$, dichloromethane); ν_{max} (KBr)/ cm^{-1} 2988, 2935, 1488, 1458, 1377, 1368, 1235, 1148, 1066, 830; δ_{H} (400 MHz; CDCl_3) 4.45 (2 H, m, 2 x CHO), 4.18 (2 H, dd, $J=9.1, 6.0$ Hz, 2 x $\text{CH}_\alpha\text{HO}$), 4.03, (2 H, dd, $J=9.1, 4.2$ Hz, 2 x CHH_βO), 3.71 (2 H, d, $J=9.8$ Hz, 5-, 6-H), 1.41 (6 H, s, 2 x CH_3), 1.33 (6 H, s, 2 x CH_3); δ_{C} (100 MHz, CDCl_3) 206.5 (2-C), 118.9 (3a-, 7a-C), 110.6 (2 x 2'-C), 75.9 (2 x 4'-C), 67.8 (2 x 5'-C), 44.3 (5, 6-C), 27.1 (2 x CH_3), 25.3 (2 x CH_3); m/z (ES): found: 425.0038 $[\text{M} + \text{H}]^+$, $\text{C}_{15}\text{H}_{20}\text{O}_4\text{S}_5 + \text{H}$ requires: 425.0035.

5R, 6R-5, 6-bis((4'R)-2',2'-dimethyl-1,3-dioxolan-4'-yl)-5,6-dihydro-1,3-dithiolo [4,5-b]1,4-dithiin-2-one, 44

To a solution of **43b** (0.397 g, 0.94 mmol) in chloroform (30 mL), was added mercuric acetate (0.448 g, 1.40 mmol), and the resultant mixture stirred for 5 h. The mixture was filtered and the precipitate washed with chloroform. The combined organic extracts were washed with water (2 x 30 mL), brine (30 mL) and dried over magnesium sulfate. Slow evaporation of the solvent afforded **44** (0.3 g, 79 %) as yellow-orange needles; $[\alpha]_D^{25} = +206^\circ \text{ g}^{-1} \text{ mL}^{-1} \text{ dm}^{-1}$ ($c = 0.14$, dichloromethane); ν_{max} (KBr)/ cm^{-1} 2988, 2935, 1683, 1381, 1372, 1260, 1245, 1229, 1214, 1074, 822; δ_{H} (400 MHz; CDCl_3) 4.51 (2 H, m, 2 x 4'-H), 4.20 (2 H, dd, $J=8.9, 6.1$ Hz, 2 x 5'- H_α), 4.04, (2 H, dd, $J=9.2, 4.2$ Hz, 2 x 5'- H_β), 3.71 (2 H, d, $J=9.9$ Hz, 5-, 6-H), 1.42 (6 H, s, 2 x CH_3), 1.34 (6 H, s, 2 x CH_3); δ_{C} (100 MHz, CDCl_3) 188.9 (2-C), 110.6 (2 x 2'-C), 109.6 (3a-, 7a-C), 76.1 (2 x 4'-C),

68.0 (2 x 5'-C), 45.7 (5, 6-C), 27.1 (2 x CH₃), 25.4 (2 x CH₃); *m/z* (EI): found: 408.0190, C₁₅H₂₀O₅S₄ requires: 408.0188.

***R, R, R, R*-Tetrakis((4''*R*)-2'',2''-dimethyl-1'',3''dioxolane-4''-yl)-ET, 45**

Carbonyl compound **44** (0.19 g, 0.46 mmol) was heated in triethyl phosphite (3 mL) to 90 °C under nitrogen for 18 h to give an orange solution. Distillation *in vacuo* and purification by chromatography over silica eluting with a mixture of cyclohexane and ethyl acetate (8:1) afforded **45** (0.11 g, 60 %) as a pale orange solid; $[\alpha]_D^{25} = +65.3^\circ \text{ g}^{-1} \text{ mL}^{-1} \text{ dm}^{-1}$ ($c = 0.15$, dichloromethane); (Found C, 46.0; H, 5.1. C₃₀H₄₀O₈S₈ requires C, 45.9; H, 5.1 %); ν_{max} (KBr)/cm⁻¹ 2986, 2933, 2880, 1458, 1382, 1371, 1248, 1215, 1150, 1065, 970, 923, 836, 774, 513; δ_{H} (400 MHz, CDCl₃) 4.38 (4 H, m, 4 x 4''-H), 4.18 (4 H, dd, $J=9.0, 6.0$ Hz, 4 x 5''-H_α), 4.03 (4 H, dd, $J=9.0, 4.3$ Hz, 4 x 5''-H_β), 3.70 (4 H, dd, $J=11.8, 2.0$ Hz, 5-, 6-, 5'-, 6'-H), 1.43 (12 H, s, 4 x CH₃), 1.35 (12 H, s, 4 x CH₃); δ_{C} (100 MHz, CDCl₃) 111.0 & 109.9 (2-,2'-C & 3a-, 7a-, 3a'-, 7a'-C), 110.4 (4 x 2''-C), 76.0 (4 x 4''-C), 68.0 (4 x 5''-C), 44.9 (5-, 6-, 5'-, 6'-C), 27.1 (4 x CH₃), 25.4 (4 x CH₃); *m/z* (EI): found: 784.0485, C₃₀H₄₀O₈S₈ requires: 784.0483.

***R, R, R, R*-Tetrakis((2''*R*)-1'',2''-dihydroxyethyl)-ET, 36**

Tetra ketal **45** (0.04 g, 0.05 mmol) was stirred in a mixture of aq. HCl (4 M, 1.5 mL) and tetrahydrofuran (11 mL) under nitrogen for 24 h. Evaporation and drying *in vacuo* afforded the octol **36** (0.026 g, 82 %) as a light brown solid; $[\alpha]_D^{25} = +187.5^\circ \text{ g}^{-1} \text{ mL}^{-1} \text{ dm}^{-1}$ ($c = 0.048$ in dimethylformamide); (Found C, 34.5; H, 4.1. C₁₈H₂₄O₈S₈ requires C,

34.6; H, 3.9 %); ν_{\max} (KBr)/ cm^{-1} 3254 br, 2962, 1404, 1259, 1082, 1013, 869, 792, 700, 676, 661; δ_{H} (400 MHz, d_6 -DMSO + one drop D_2O) 3.61 (16 H, m, 4 x SCH-CH(OH)- CH_2OH); δ_{C} (100 MHz, d_6 -DMSO + one drop D_2O) 110.5 & 109.8 (3a-, 3a'-, 7a-, 7a'-C & 2',2''-C), 71.8 (4 x -CH(OH)), 63.3 (4 x - CH_2OH), 42.7 (5-, 5'-, 6-, 6'-C); m/z (ES⁺): found: 624.9315 [M + H]⁺, $\text{C}_{18}\text{H}_{24}\text{O}_8\text{S}_8$ + H requires: 624.9310.

R,R*-vic-Bis((4''*R*)-2'',2''-dimethyl-1'',3''-dioxolan-4''-yl)-ET, **46*

A mixture of **44** (0.10 g, 0.25 mmol) and thione **22** (0.08 g, 0.37 mmol) was heated in triethyl phosphite (5 mL) to 90 °C under nitrogen to give an orange solution, and was maintained for 5 h. Distillation *in vacuo* of the residual triethyl phosphite, and purification by chromatography over silica eluting with a mixture of cyclohexane and ethyl acetate (3:1) afforded **46** (0.05 g, 35 %) as an orange solid; $[\alpha]_{\text{D}}^{25} = + 51.2^\circ \text{g}^{-1} \text{mL}^{-1} \text{dm}^{-1}$ ($c = 0.13$, dichloromethane); (Found C, 41.0; H, 4.0. $\text{C}_{20}\text{H}_{24}\text{O}_4\text{S}_8$ requires C, 41.1; H, 4.1%); ν_{\max} (KBr)/ cm^{-1} 2978, 2916, 1654, 1650, 1638, 1618, 1560, 1510, 1456, 1384, 1368, 1249, 1213, 1145, 1062, 1016, 922, 834, 766, 507; δ_{H} (400 MHz, CDCl_3) 4.37 (2 H, m, 2 x 4''-H), 4.13 (2 H, dd, $J=9.1, 5.9$ Hz, 2 x 5''- H_{α}), 4.00, (2 H, dd, $J=9.1, 4.4$ Hz, 2 x 5''- H_{β}), 3.67 (2 H, dd, $J=8.9, 1.0$ Hz, 5-, 6-H), 3.26 (4 H, s, 5', 6'- H_2), 1.40 (6 H, s, 2 x CH_3), 1.32 (6 H, s, 2 x CH_3); δ_{C} (100 MHz, CDCl_3) 113.9, 112.3, 110.4 (sp^2 -C), 109.9 (2 x 2''-C), 76.5 (2 x 4''-C), 68.0 (2 x 5''-C), 44.9 (5, 6-C), 30.2 (5', 6'-C), 27.1 (2 x CH_3), 25.4 (2 x CH_3); m/z (ES): found: 584.9507, $\text{C}_{20}\text{H}_{24}\text{O}_4\text{S}_8$ + H requires: 584.9513.

R,R*-vic-Bis((2''*R*)-1'',2''-dihydroxyethyl)-ET, **37*

A solution of **46** (0.06 g, 0.12 mmol) in tetrahydrofuran (8mL) was stirred under nitrogen, and to it added aq. HCl (4 M, 4 mL) dropwise. The solution was stirred for 12 h. Evaporation and drying *in vacuo* afforded the tetrol **37** (0.049 g, 94 %) as a light brown solid; $[\alpha]_D^{25} = +69^\circ \text{ g}^{-1} \text{ mL}^{-1} \text{ dm}^{-1}$ ($c = 0.035$, tetrahydrofuran); (Found C, 33.3; H, 3.4. $\text{C}_{14}\text{H}_{16}\text{O}_4\text{S}_8$ requires C, 33.3; H, 3.2%); ν_{max} (KBr)/ cm^{-1} 3293, 2920, 1425, 1329, 1296, 1259, 1182, 1109, 1078, 1051, 1026, 958, 870, 818, 766, 626, 523; δ_{H} (400 MHz, d_6 -DMSO) 3.82 (2 H, br d, $J=9.5$ Hz, 5-, 6-*H*), 3.67 (2 H, d, $J=10.2$ Hz, 2 x $\text{CH}_\alpha\text{H}_\beta\text{O}$), 3.60 (6 H, m, 2 x $\text{CHCH}_\alpha\text{CH}_\beta\text{OH}$), 3.34 (4 H, s, 5', 6'- H_2); δ_{C} (100 MHz, d_6 -DMSO) 112.9, 110.5, 110.0, 109.9 (sp^2 -C), 71.8 (2 x $-\text{CH}(\text{OH})$), 63.3 (2 x $-\text{CH}_2\text{OH}$), 42.7 (5, 6-C), 29.5 (5', 6'-C); m/z (EI): found: 503.8818, $\text{C}_{14}\text{H}_{16}\text{O}_4\text{S}_8$ requires 503.8809.

4,5-Dimethylene[(*S*)-2',2''-binaphtholyl]-1,3-dithiole-2-thione, **48**

To a solution of (*S*)-2,2-binaphthol (0.155 g, 0.5 mmol) in tetrahydrofuran (50 mL) was added potassium carbonate (0.97 g, 7.0 mmol). The stirred suspension was heated to 40 °C and to this added a solution of dibromide **47** (0.173 g, 0.5 mmol) in tetrahydrofuran (20 mL) dropwise over 1 h, under an inert atmosphere. Upon complete addition, the temperature was raised to 80 °C for 1 h, then cooled to room temperature and filtered, washing with tetrahydrofuran (*ca.* 50 mL) and chloroform (*ca.* 50 mL). The filtrate was evaporated and the residue purified by chromatography over silica, eluting with tetrahydrofuran/dichloromethane (9:1) to afford **48** (0.2 g, 83 %) as a bright yellow solid Mp 109 °C; $[\alpha]_D^{23} = -74^\circ \text{ g}^{-1} \text{ mL}^{-1} \text{ dm}^{-1}$ ($c = 0.108 \text{ g} / 100 \text{ mL}$ in

tetrahydrofuran); (Found C, 67.7; H, 3.7. C₂₅H₁₆O₂S₃ requires: C, 67.5; H, 3.6); ν_{\max} (ATR/cm⁻¹) 2923, 2849, 1620, 1590, 1506, 1470, 1354, 1325, 1278, 1225, 1207, 1058, 999, 915, 803, 773, 749, 737, 696, 655, 575, 520; δ_{H} (400 MHz, CDCl₃) 7.98 (2 H, d, $J=8.9$ Hz, 5'-, 5''-H), 7.89 (2 H, d, $J=8.2$ Hz, 10'-, 10''-H), 7.41-7.36 (4 H, m, 6'-, 6''-, 9'-, 9''-H), 7.26-7.22 (2 H, m, 8'-, 8''-H), 7.15 (2 H, d, $J=8.5$ Hz, 7'-, 7''-H), 5.03 (4 H, s, 2 x 6-, 2 x 7-H); δ_{C} (100 MHz, CDCl₃) 209.2 (2-C), 153.5 (1'-, 1''-C), 140.1 (4-, 5-C), 133.6 (3'-, 3''-C), 130.3 (4'-, 4''-C), 130.1 (5'-, 5''-C), 128.2 (10'-, 10''-C), 126.9 (7'-, 7''-C), 126.0 (8'-, 8''-C), 124.7 (9'-, 9''-C), 122.3 (2'-, 2''-C), 117.1 (6'-, 6''-C), 63.8 (6-, 7-C); m/z (EI): found: 444.0311 [M]⁺. C₂₅H₁₆O₂S₃ requires: 444.0307.

4,5-Dimethylene[(S)-2',2''-binaphthyl]-1,3-dithiole-2-one, 49

To a solution of **48** (0.18 g, 0.4 mmol) in tetrahydrofuran (50 mL) was added mercuric acetate (0.19 g, 0.6 mmol), and the mixture stirred under nitrogen at room temperature for 2 h. The mixture was filtered, washed with tetrahydrofuran (100 mL), and the combined filtrates evaporated to afford **49** (0.16 g, 92%) as a light yellow solid Mp 118 °C; ν_{\max} (ATR/cm⁻¹) 2874, 1821, 1712, 1621, 1589, 1506, 1431, 1354, 1325, 1279, 1224, 1207, 1120, 1085, 995, 883, 810, 748, 654, 522; δ_{H} (400 MHz, CDCl₃) 7.97 (2 H, d, $J=8.9$ Hz, 5'-, 5''-H), 7.90 (2 H, d, $J=8.2$ Hz, 10'-, 10''-H), 7.41-7.37 (4 H, m, 6'-, 6''-, 9'-, 9''-H), 7.26-7.18 (4 H, m, 7'-, 7''-, 8'-, 8''-H), 4.95 (2 H, d, $J=3.5$ Hz, 2 x 6-, 2 x 7-H); δ_{C} (100 MHz, CDCl₃) 189.3 (2-C), 153.6 (1'-, 1''-C), 133.5 (3'-, 3''-C), 130.2 (4'-, 4''-C), 129.8 (5'-, 5''-C), 129.5 (4-, 5-C), 128.1 (10'-, 10''-C), 126.7 (7'-, 7''-C), 125.9 (8'-, 8''-C), 124.5 (9'-, 9''-C), 122.2 (2'-, 2''-C), 117.2 (6'-, 6''-C), 64.4 (6-, 7-C); m/z (EI): found: 428.0532 [M]⁺. C₂₅H₁₆O₃S₂ requires: 428.0535.

Bis{4,5-dimethylene[(S)-2',2''-binaphtholyl]}tetrathiafulvalene, 39

49 (0.13 g, 0.3 mmol) in triethyl phosphite (5 mL) was heated under nitrogen for 10 h. The solution was cooled to room temperature and the triethyl phosphite removed under reduced pressure. The residue was purified by chromatography over silica eluting with cyclohexane/ethyl acetate (3:1) to afford **39** (0.05 g, 32 %) as a yellow solid Mp 198-200 °C (Found: C, 73.0; H, 4.0. C₅₀H₃₂S₄O₄ requires: C, 72.8; H, 3.9%); ν_{\max} (ATR)/cm⁻¹ 2953, 2917, 1619, 1589, 1506, 1470, 1431, 1353, 1325, 1270, 1222, 1145, 1084, 995, 913, 811, 747, 695, 651, 627; δ_{H} (400 MHz, CDCl₃) 7.95 (4 H, d, $J=8.8$ Hz, 2 x 5'-, 2 x 5''-H), 7.87 (4 H, d, $J=8.1$ Hz, 2 x 10'-, 2 x 10''-H), 7.40-7.34 (8 H, m, 2 x 6'-, 2 x 6''-, 2 x 9'-, 2 x 9''-H), 7.25-7.21 (4 H, m, 2 x 8'-, 2 x 8''-H), 7.16 (4 H, d, $J=8.6$ Hz, 2 x 7'-, 2 x 7''-H), 4.81 (8 H, s, 4 x 6-, 4 x 7-H); δ_{C} (100 MHz, CDCl₃) 153.9 (2 x 1'-, 2 x 1''-C), 133.6 (2 x 3'-, 2 x 3''-C), 130.4 (2 x 4-, 2 x 5-C), 130.2 (2 x 4'-, 2 x 4''-C), 129.8 (2 x 5'-, 2 x 5''-C), 128.1 (2 x 10'-, 2 x 10''-C), 126.6 (2 x 7'-, 2 x 7''-C), 126.1 (2 x 8'-, 2 x 8''-C), 124.4 (2 x 9'-, 2 x 9''-C), 122.3 (2 x 2'-, 2 x 2''-C), 117.5 (2 x 6'-, 2 x 6''-C), 108.0 (2 x 2-C), 64.7 (2 x 6-, 2 x 7-C); m/z (ES): found 842.1523. [C₅₀H₃₂S₄O₄ + NH₄]⁺ requires: 842.1522 Da.

Tetrabutylammonium triiodide, 50

A slight modification to the literature method was employed.²⁹ To a rapidly stirred aqueous solution of potassium iodide (1.7 M, 120 mL) at 65 °C was added tetrabutylammonium iodide (5.0 g, 13.5 mmol). After 10 min, crushed iodine (3.4 g, 13.6 mmol) was added in portions, and heating maintained for a further 25 min.

Cooling and filtration afforded a dark solid, which was recrystallised from hot methanol (80 mL), to give **50** (6.7 g, 80 %) as shiny dark plates (Found C, 30.9; H, 5.8; N, 2.3. C₁₆H₃₆Nl₃ requires: C, 30.8; H, 5.6; N, 2.25 %); δ_{H} (400 MHz, CDCl₃) 3.29 (2 H, m, 1-*H* _{α} , 1-*H* _{β}), 1.71 (2 H, m, 2-*H* _{α} , 2-*H* _{β}), 1.50 (2 H, m, 3-*H* _{α} , 3-*H* _{β}), 1.06 (3 H, t, *J*=7.2 Hz, 4-*H* _{α} , 4-*H* _{β} , 4-*H* _{γ}); δ_{C} (100 MHz, CDCl₃) 59.4 (1-*C*), 24.3 (2-*C*), 20.0 (3-*C*), 13.9 (4-*C*).

2.5 Electrocrystallisation experimental

(37)₃[Cr(NCS)₆]

To the anodic side of a H-shaped electrochemical cell fitted with a glass frit was placed **37** (10 mg, 0.02 mmol), and from the cathodic side of the cell was added a solution of tris(tetrabutylammonium) chromium (III) hexaisothiocyanate (40 mg, 0.04 mmol) in 1,2,4-trichlorobenzene/ethanol (60:40 v/v, 25 mL). The level of solvent in each compartment was allowed to equilibrate, and to each side inserted a platinum-tipped electrode. A constant current of 1.0 μA was applied across the cell for 11 days affording small black multi-layered blocks on the anode; (Raman)/cm⁻¹ $\nu_4 = 1424$, $\nu_3 = 1462$.

(37)₃[Cr(NCS)₆]

To the anodic side of a H-shaped electrochemical cell fitted with a glass frit was placed **37** (10 mg, 0.02 mmol), and from the cathodic side of the cell was added a solution of tris(tetrabutylammonium) chromium (III) hexaisothiocyanate (40 mg, 0.04 mmol) in

chlorobenzene/ethanol (60:40 v/v, 25 mL). The level of solvent in each compartment was allowed to equilibrate, and to each side inserted a platinum-tipped electrode. A constant current of 1.0 μA was applied across the cell for 9 days affording small black plates on the anode; (Raman)/ cm^{-1} $\nu_4 = 1418$, $\nu_3 = 1462$.

(37)[Cr(*R,R*-salen)(NCS)₂]₂

To the anodic side of a H-shaped electrochemical cell fitted with a glass frit was placed **37** (10 mg, 0.02 mmol), and from the cathodic side of the cell was added a solution of tetrabutylammonium chromium (III) (*R,R*-salen)bis(isothiocyanate) (40 mg, 0.04 mmol) in 1,2,4-trichlorobenzene/ethanol (60:40 v/v, 25 mL). The level of solvent in each compartment was allowed to equilibrate, and to each side inserted a platinum-tipped electrode. A constant current of 0.2 μA was applied across the cell for 13 days affording black micro-clusters of blocks on the cell bottom and microcrystalline clusters of black plates on the anode; (Raman)/ cm^{-1} $\nu_4 = 1459$ (weak signal, ν_3 not detected). Repetition of the experiment afforded clusters of small black plates that were observed to be twinned; (Raman)/ cm^{-1} $\nu_4 = 1414$, $\nu_3 = 1466$.

(37)₄[Al(C₂O₄)₃]

To the anodic side of a H-shaped electrochemical cell fitted with a glass frit was placed **37** (10 mg, 0.02 mmol), and from the cathodic side of the cell was added a solution of potassium aluminium tris(oxalate) (100 mg, 0.25 mmol) in 1,2,4-trichlorobenzene/ethanol (60:40 v/v, 25 mL). The level of solvent in each compartment

was allowed to equilibrate, and to each side inserted a platinum-tipped electrode. A constant current of 1.0 μA was applied across the cell for 8 days affording clusters of black blocks on the anode; (Raman)/ cm^{-1} $\nu_4 = 1465$ (only just distinguishable from background noise, ν_3 not observed).

(37)₃[Cr(C₂O₄)₃]

To the anodic side of a H-shaped electrochemical cell fitted with a glass frit was placed **37** (10 mg, 0.02 mmol), and from the cathodic side of the cell was added a solution of potassium chromium (III) tris(oxalate) (100 mg, 0.26 mmol) and 18-crown-6 (50 mg) in tetrahydrofuran (25 mL). The level of solvent in each compartment was allowed to equilibrate, and to each side inserted a platinum-tipped electrode. A constant current of 1.0 μA was applied across the cell for 15 days affording black crystals joined together in an overall ‘Christmas tree’ shape on the anode; (Raman)/ cm^{-1} $\nu_4^{\text{a}} = 1411$, $\nu_4^{\text{b}} = 1459$.

(37)₄[Cr(C₂O₄)₃]

To the anodic side of a H-shaped electrochemical cell fitted with a glass frit was placed **37** (10 mg, 0.02 mmol), and from the cathodic side of the cell was added a solution of ammonium chromium (III) tris(oxalate) (200 mg, 0.54 mmol) and 18-crown-6 (100 mg) in nitrobenzene (25 mL). The level of solvent in each compartment was allowed to equilibrate, and to each side inserted a platinum-tipped electrode. A constant current of 0.1 μA was applied across the cell for 12 days affording black twinned needles on the anode; $\nu_{\text{max}}(\text{ATR})/\text{cm}^{-1}$ 3178, 3052, 2911, 2090, 2003, 1784, 1704, 1640, 1388, 1349,

1256, 1134, 1096, 1055, 958, 900, 835, 801, 705, 690, 542, 478; (Raman)/cm⁻¹ ν_4^a = 1459, ν_4^b = 1465.

(37)Br

To the anodic side of a H-shaped electrochemical cell fitted with a glass frit was placed **37** (10 mg, 0.02 mmol), and from the cathodic side of the cell was added a solution of tetrabutylammonium bromide (40 mg, 0.12 mmol) in 1,2,4-trichlorobenzene/ethanol (60:40 v/v, 25 mL). The level of solvent in each compartment was allowed to equilibrate, and to each side inserted a platinum-tipped electrode. A constant current of 0.4 μ A was applied across the cell for 3 days affording small black 'Roman helmet' shaped clusters on the anode; (Raman)/cm⁻¹ ν_4 = 1402, ν_3 = 1469.

(37)₃Cl₂

To the anodic side of a H-shaped electrochemical cell fitted with a glass frit was placed **37** (10 mg, 0.02 mmol), and from the cathodic side of the cell was added a solution of tetrabutylammonium chloride (40 mg, 0.14 mmol) in dichloromethane (25 mL). The level of solvent in each compartment was allowed to equilibrate, and to each side inserted a platinum-tipped electrode. A constant current of 1.0 μ A was applied across the cell for 3 days affording a black diamond/kite shaped crystal; Mp 210 °C; $\nu_{\max}(\text{ATR})/\text{cm}^{-1}$ 3177, 2873, 1456, 1403, 1298, 1223, 1168, 1030, 960, 875, 771, 615, 527, 496; (Raman)/cm⁻¹ ν_4^a = 1459, ν_4^b = 1469; Similar experiments were conducted at the lower current of 0.2 μ A in dichloromethane, affording black fragile needles after 7

days; Mp 210 °C; $\nu_{\max}(\text{ATR})/\text{cm}^{-1}$ 2285, 1456, 1408, 1292, 1219, 1167, 1076, 1033, 994, 870, 818, 771, 709, 595, 523; (Raman)/ cm^{-1} $\nu_4^a = 1459$, $\nu_4^b = 1469$.

(37)₃[CoCl₄]

To the anodic side of a H-shaped electrochemical cell fitted with a glass frit was placed **37** (10 mg, 0.02 mmol), and from the cathodic side of the cell was added a solution of bis(tetrabutylammonium) cobalt tetrachloride (40 mg, 0.09 mmol) in tetrahydrofuran (25 mL). The level of solvent in each compartment was allowed to equilibrate, and to each side inserted a platinum-tipped electrode. A constant current of 1.0 μA was applied across the cell for 1 week afforded black microcrystalline clusters on the anode; (Raman)/ cm^{-1} $\nu_4^a = 1459$, $\nu_4^b = 1472$.

(37)₃(I₃)₂

To the anodic side of a H-shaped electrochemical cell fitted with a glass frit was placed **37** (10 mg, 0.02 mmol), and from the cathodic side of the cell was added a solution of tetrabutylammonium iodide (40 mg, 0.06 mmol) in chlorobenzene/ethanol (60:40 v/v, 25 mL). The level of solvent in each compartment was allowed to equilibrate, and to each side inserted a platinum-tipped electrode. A constant current of 1 μA was applied across the cell for 11 days affording clusters of small black needles on the anode; (Raman)/ cm^{-1} $\nu_4^a = 1462$, $\nu_4^b = 1468$.

(37)(I₃)

In a similar experiment conducted in 1,2,4-trichlorobenzene/ethanol (60:40 v/v, 25 mL), a black amorphous solid was produced after 11 days; $\nu_{\max}(\text{ATR})/\text{cm}^{-1}$ 3158, 2917, 2346, 2116, 2091, 1989, 1677, 1450, 1407, 1193, 1110, 1069, 1011, 921, 877, 833, 807, 773, 571, 475; (Raman)/ cm^{-1} $\nu_4 = 1405$, $\nu_3 = 1459$.

(37)₄[PF₆]₃

To the anodic side of a H-shaped electrochemical cell fitted with a glass frit was placed **37** (10 mg, 0.02 mmol), and from the cathodic side of the cell was added a solution of tetrabutylammonium hexafluorophosphate (40 mg, 0.06 mmol) in dichloromethane (25 mL). A constant current of 1.0 μA was applied across the cell for 11 days affording clusters of small black needles on the anode (Found: C, 28.75; H, 2.4. $\text{C}_{56}\text{H}_{64}\text{O}_{16}\text{S}_{32}\text{P}_3\text{F}_{18}$ requires: C, 28.5; H, 2.7 %).

(37)₂Cl

To the anodic side of a H-shaped electrochemical cell fitted with a glass frit was placed **37** (10 mg, 0.02 mmol), and from the cathodic side of the cell added a solution of tetrabutylammonium chloride (40 mg, 0.14 mmol) in tetrahydrofuran (25 mL). A constant current of 1.0 μA was applied across the cell for 11 days affording a diamond shaped crystal on the anode: (Raman)/ cm^{-1} $\nu_4 = 1460$, $\nu_3 = 1469 \text{ cm}^{-1}$.

2.6 References

- ¹ N. Saygili, R. J. Brown, P. Day, R. Hoelzl, P. Kathirgamanathan, E. R. Mageean, T. Ozturk, M. Pilkington, M. M. B. Qayyum, S. S. Turner, L. Vorwerg and J. D. Wallis, *Tetrahedron*, **2001**, 57, 5015.
- ² H. Li, D. Zhang, B. Zhang, Y. Yao, W. Xu, D. Zhu and Z. Wang, *J. Mater. Chem.*, **2000**, 10, 2063.
- ³ V. Y. Lee, E. M. Engler, R. R. Schumaker and S. S. P. Parkin, *J. Chem. Soc., Chem. Commun.*, **1983**, 235.
- ⁴ H. Kobayashi, H. Tanaka, E. Ojima, H. Fujiwara, Y. Nakazawa, T. Otsuka, A. Kobayashi, M. Tokumoto and P. Cassoux, *Synth. Met.*, **2001**, 120, 663.
- ⁵ M. Mizuno, A. F. Garito and M. P. Cava, *J. Chem. Soc., Chem. Commun.*, **1978**, 18.
- ⁶ A. M. Kini, U. Geiser, H. H. Wang, K. D. Carlson, J. M. Williams, W. K. Kwok, K. G. Vandervoort, J. E. Thompson, D. L. Stupka, D. Jung and M. -H. Whangbo, *Inorg. Chem.*, **1990**, 29, 2555.
- ⁷ J. M. Williams, H. H. Wang, M. A. Beno, T. J. Emge, L. M. Sowa, P. T. Copps, F. Behroozi, L. N. Hall, K. D. Carlson and G. W. Crabtree, *Inorg. Chem.*, **1984**, 23, 3839.
- ⁸ H. H. Wang, M. A. Beno, U. Geiser, M. A. Firestone, K. S. Webb, L. Nunez, G. W. Crabtree, K. D. Carlson, J. M. Williams, L. J. Azevedo, J. F. Kwak and J. E. Schirber, *Inorg. Chem.*, **1985**, 24, 2465.
- ⁹ D. Jérôme, A. Mazaud, M. Ribault and K. Bechgaard, *J. Phys. Lett. (Paris)*, **1980**, 41, L95.
- ¹⁰ K. Bechgaard, C. S. Jacobsen, K. Mortenson, H. J. Pederson and N. Thorup, *Solid State Communications*, **1980**, 33, 1119.
- ¹¹ K. Bechgaard, K. Carneiro, F. B. Rasmussen, M. Olsen, G. Rindorf, C. S. Jacobsen, H. J. Pedersen and J. C. Scott, *J. Am. Chem. Soc.*, **1981**, 102, 2440.
- ¹² H. Urayamam H. Yamochi, G. Saito, S. Sato, A. Kawamoto, J. Tanaka, T. Mori, Y. Maruyama and H. Inokuchi, *Chem. Lett.*, **1988**, 463.
- ¹³ H. Mori, S. Tanaka, M. Oshima, G. Saito, T. Mori, Y. Maruyama and H. Inokuchi, *Bull. Chem. Soc. Jpn.*, **1990**, 63, 2183.
- ¹⁴ M. Kurmoo, A. W. Graham, P. Day, S. J. Coles, M. Hursthouse, J. L. Caulfield, J. Singleton, F. L. Pratt, W. Hayes, L. Ducasse and P. Guionneau, *J. Am. Chem. Soc.*, **1995**, 117, 12209.
- ¹⁵ S. -X. Liu, A. Neels, H. Stoeckli-Evans, M. Pilkington, J. D. Wallis, S. Decurtins, *Polyhedron*, **2004**, 23, 1185.
- ¹⁶ H. Li, D. Zhang, B. Zhang, Y. Yao, W. Xu, D. Zhu, Z. Wang, *J. Mater. Chem.*, **2000**, 10, 2063.

- ¹⁷ F. Leurquin, T. Ozturk, M. Pilkington and J. D. Wallis, *J. Chem. Soc., Perkin Trans. 1*, **1997**, 3173.
- ¹⁸ S. G. Telfer and R. Kuroda, *Coord. Chem. Rev.*, **2003**, 242, 33.
- ¹⁹ E. F. DiMauro and M. C. Kozlowski, *Org. Lett.*, **2001**, 3, 1641.
- ²⁰ T. Arai, Y. Endo and A. Yanagisawa, *Tetrahedron Asymmetry*, **2007**, 18, 165.
- ²¹ Y. Wang, J. Sun and K. Ding, *Tetrahedron*, **2000**, 56, 4447.
- ²² J. L. Gómez and N. M. Segura, *Org. Lett.*, **2000**, 2, 1585.
- ²³ R. S. Tipson and A. Cohen, *Carbohydr. Res.*, **1968**, 7, 232.
- ²⁴ F. W. Eastwood, K. J. Harrington, J. S. Josan and J. L. Pupra, *Tetrahedron Lett.*, **1970**, 21, 5223.
- ²⁵ J. O. Jeppesen, K. Takimiya, N. Thorup and J. Becher, *Synthesis*, **1999**, 803.
- ²⁶ J. O. Jeppesen, K. Takimiya, F. Jensen, T. Brimert, K. Nielsen, N. Thorup and J. Becher, *J. Org. Chem.*, **2000**, 65, 5794.
- ²⁷ D. D. Perrin and W. L. F. Armarego, “*Purification of Laboratory Chemicals*”, Pergamon Press, Exeter, **1988**, 3 ed.
- ²⁸ C. Jia, *Synthesis*, **2002**, 15, 2177.
- ²⁹ J. M. Williams, T. J. Emge, H. H. Wang, M. A. Beno, P. T. Copps, L. N. Hall, K. D. Carlson and G. W. Crabtree, *Inorg. Chem.*, **1984**, 23, 2558.

Chapter 3

Metal-binding electron donors

3 Metal-binding electron donors

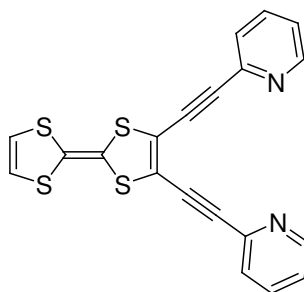
3.1 Introduction

It is increasingly desirable to obtain materials with more than one functionality, *i.e.* more than just electrical conductivity. By the incorporation of a magnetic network into the structure of the conductor, the hybrid materials produced have the potential to find applications in molecular computing, molecular wires, and memory devices. Although it is thought that it is not possible to exhibit both electrical superconductivity and magnetism, as the Cooper pairs formed for superconduction are destroyed by the fields generated in ferromagnetic materials, there have been numerous examples where a hybrid conducting system has been prepared containing localised magnetic moments. A radical cation salt of ET was prepared with iron (III) tris(oxalate),¹ and shown to have $T_C = 7$ K. Similarly, κ -(BETS)₂FeBr₄ was found to exhibit a transition from an antiferromagnetic phase to a superconducting phase at 1.1 K.²

In creating materials with dual functionality, it is necessary to install a spin centre to allow for magnetically induced phenomena to occur. This can either be by incorporation of an organic spin radical unit, or by the incorporation of a metal centre. Although the preparation of radical cation salts with transition metal centre anions has been achieved, the metal atom/complex has not been coordinated to the donor molecule. This raises interesting questions into how the interaction between electrical and magnetic properties will be affected should the metal species be coordinated to, and thus more closely associated with the electron donor species. It is hoped that there is a

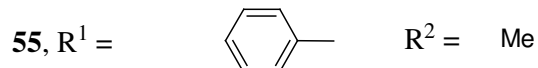
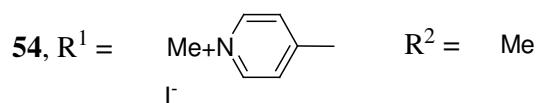
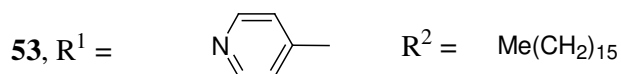
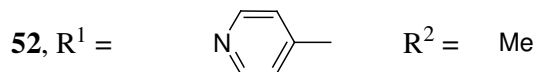
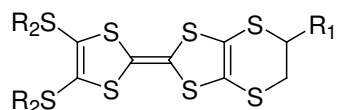
mutual influence of the two properties, allowing for externally controlled dual functionality materials. The coordination of the donor species to the anion may lead to a reduced unit cell volume, which could lead to an increased temperature at which a superconducting phase transition occurs, due to the reduced distance over which short S...S interactions occur.

Materials based upon the tetrathiafulvalene donor have been prepared in which two pyridyl groups are extended from the donor core by acetylene functions **51** serving to retain rigidity and conjugation in the molecule.³ The preparation of a number of copper complexes allowed the authors to demonstrate a charge transfer interaction between the metal centre and the donor core, although the room temperature conductivity measurements on compressed pellets of two of their materials were low, being $\sigma = 1.08 \times 10^{-3} \text{ S cm}^{-1}$ for a Cu (I) bis(triflate) *intramolecular* charge transfer salt, and $\sigma = 1.39 \times 10^{-3} \text{ S cm}^{-1}$ for a Cu (II) dichloride coordination complex with donor **51**.

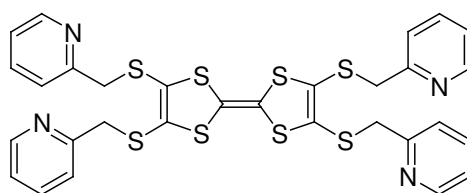


51

Goldenberg *et al.* demonstrated the use of pyridyl substituted organochalcogen donors in the preparation of Langmuir-Blodgett films (**52-55**).⁴ The films produced showed a stable room temperature conductivity of 10^{-3} - $10^{-4} \text{ S cm}^{-1}$ after doping with iodine.



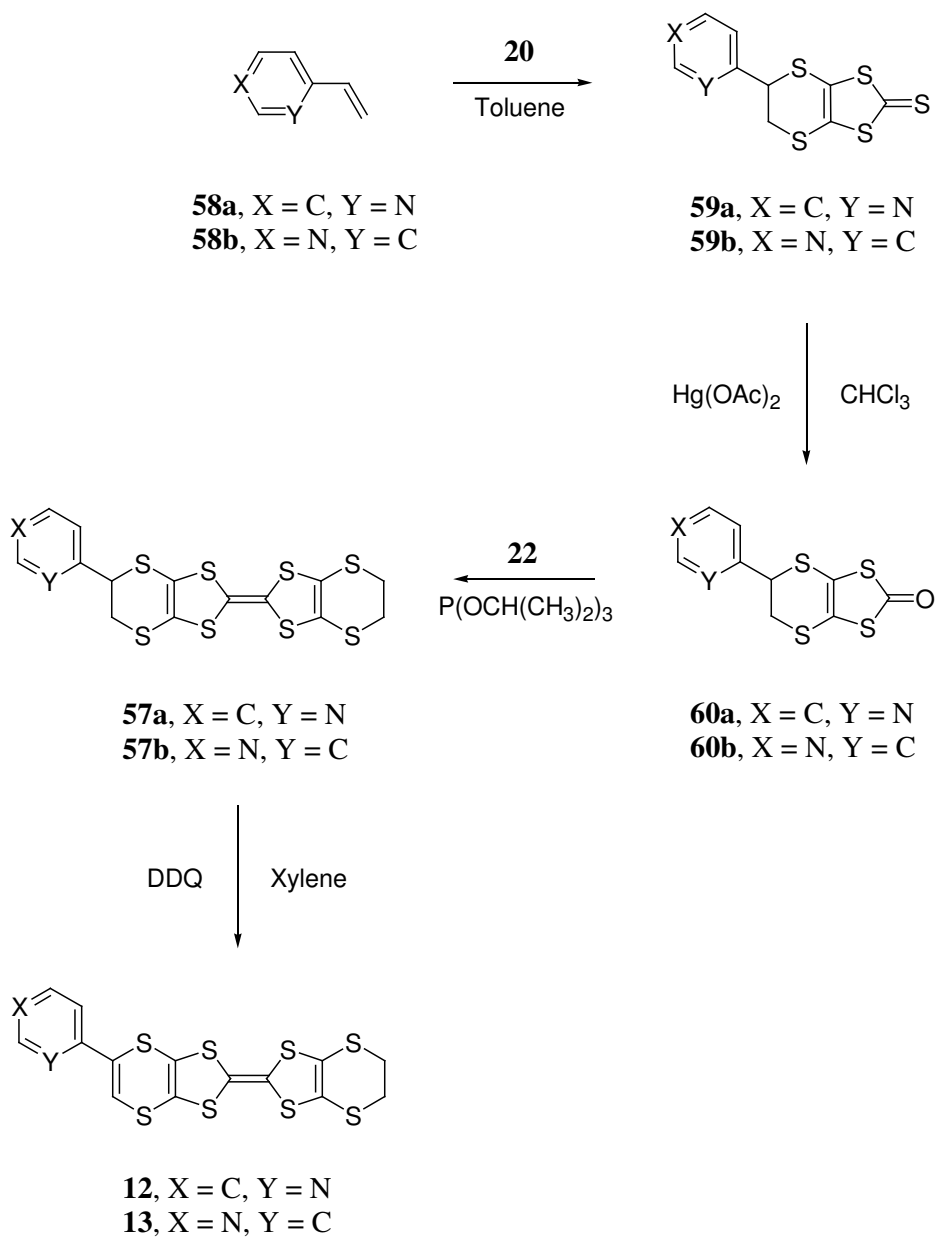
The 2-pyridyl substituted derivative of tetra(thiomethyl)TTF **56** was prepared by Liu and co-workers, using improved methodology to access electron donor species from the tetrathiolate anion, which allows a shorter synthetic scheme to the final target donor materials.⁵



56

Xu *et al.* synthesised the mono-pyridyl substituted ETs **57a** and **57b** and VT analogues **12** and **13** electron donors, starting from the corresponding vinylpyridine **58a** or **58b**, which was reacted with **20** to form the thiocarbonyl compounds **59a** and **59b**.

Conversion to the carbonyl compound using mercuric acetate gave **60a** and **60b**, which could be cross-coupled with **22** to give the donors **57a** and **57b**. Oxidation by DDQ in xylene afforded the VT analogues **12** and **13** from the corresponding precursor ET compounds, as shown in Scheme 9.⁶ The redox potentials for **57a** and **57b** show a slightly increased value relative to that of ET, and **12** and **13** show a value slightly higher still. The higher values required to oxidise the compounds may be explained by the electron withdrawing effect of the pyridine substituent. There is no significant alteration in the redox potentials of the donors when comparing the 4-pyridyl against the 2-pyridyl analogues.



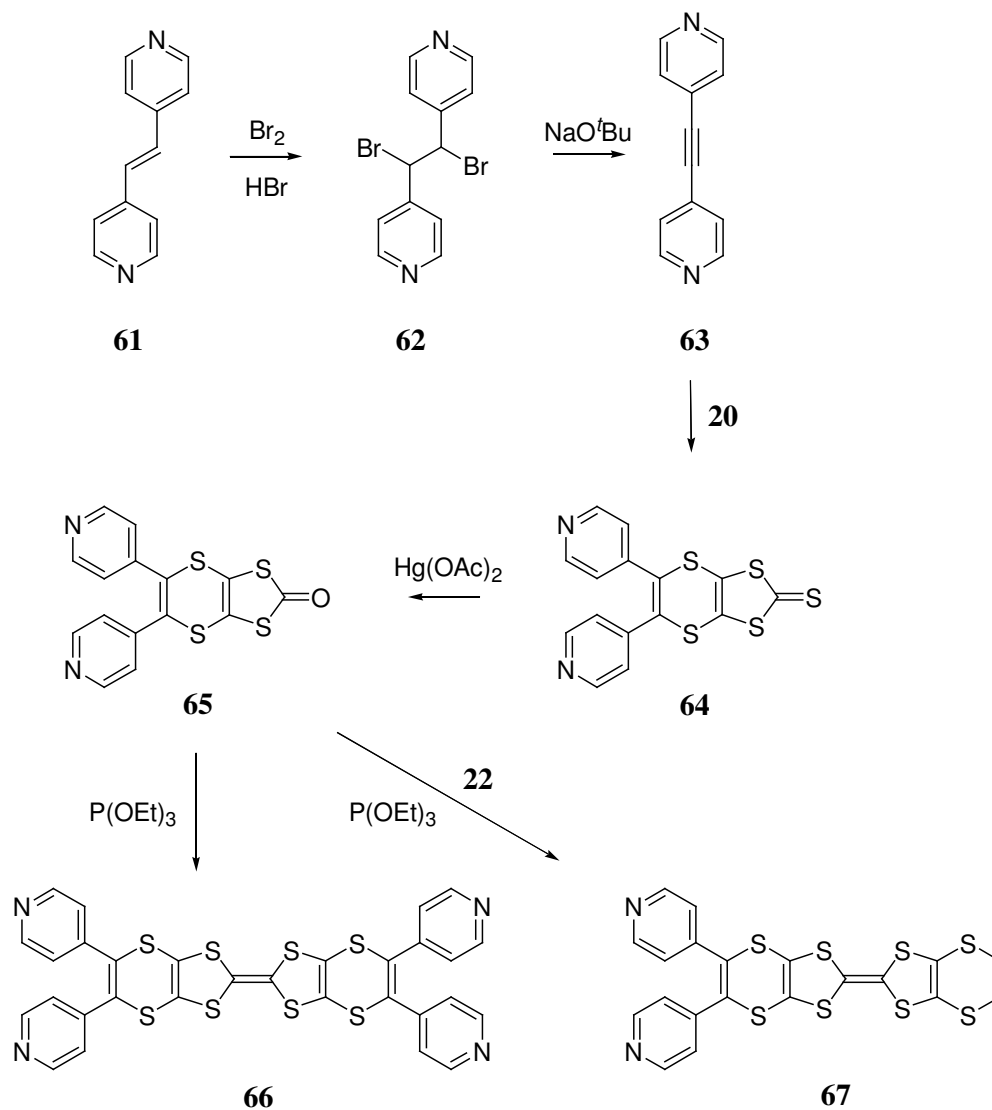
Scheme 9: Preparation of pyridyl substituted donors **57a**, **57b**, **12** and **13**.

Building on this research, it was decided to attempt to prepare the tetrapyridyl-VT donors containing 2-, 3-, or 4-pyridyl groups. In addition, the mixed VT-ET bipyridyl donor systems were identified as target materials.

The objective was to utilise the electron donor molecules in electrocrystallisation experiments and in transition metal coordination chemistry, with a view to obtaining bifunctional hybrid materials exhibiting tuneable conducting and magnetic properties.

3.2 Results and discussion

Incorporation of metal binding pyridyl groups into the bis(ethylenedithio)tetrathiafulvalene core was achieved by a six-step synthesis starting with the bromination of 1,2-bis(4-pyridyl)ethene **61**. This afforded the dibromo compound **62** in good yield, which was isolated readily. The subsequent elimination of HBr to afford the 1,2-bis(4-pyridyl)ethyne dienophile **63** was achieved with isolation of the product by careful chromatography.⁷



Scheme 10: Synthetic route taken to donors 66 and 67.

Alkyne **63** was subjected to a hetero Diels-Alder type 1,4-cycloaddition reaction with the polymeric 'trithione' species **20** in toluene at reflux. After cooling to room temperature, filtration and evaporation of the filtrate, the thione compound **64** was isolated by chromatography over silica eluting with ethyl acetate to give **65** in 92 % yield. The compound was identified by its simple ^1H NMR spectrum in deuterated chloroform, and the presence of the thiocarbonyl peak at δ 204.0 ppm in the ^{13}C NMR,

with the loss of the signal for the two *sp* alkyne carbons at δ 90.6 ppm and the presence of a signal corresponding to the reduced oxidation state of these carbons at δ 135.3 ppm. The structure was confirmed by the C=S stretching band in the infrared spectrum $\nu = 1071 \text{ cm}^{-1}$, and high resolution electrospray mass spectrometry showing the $[M + H]^+$ ion at 376.9365 Da.

Exploratory research determined the possibility of undertaking heteroatom Diels-Alder reactions in a standard domestic 800 W microwave oven. The preparation of **64** was also achieved by subjecting a toluene solution of the Diels-Alder reactants to pulsed microwave irradiation. TLC monitoring indicated the complete consumption of starting materials in less than 2 mins on full power. Evaporation of the solvent (toluene) and extraction into chloroform afforded only the pure product, with identical spectroscopic data and in greater than 99 % yield. The option to employ the microwave reactor enables a more time-efficient and cleaner route to the target material, suitable for use on a small scale. The method does not lend itself easily to larger scales due to the size restriction imposed by the heating compartment of the microwave equipment.

Further studies showed that it was possible to obtain **64** in the solid state, by mixing well equimolar amounts of the alkyne **63** and the solid trithione species **20**. Microwave irradiation (standard domestic 800 W microwave) for less than 3 mins afforded the thione **64** indicated by the TLC that showed complete consumption of the alkyne and the presence of the characteristic yellow compound. Simple extraction into chloroform allowed the separation of the target material from residual trithione species, in greater than 99 % yield.

To allow for the smooth cross-coupling reaction to give donor **67**, the thiocarbonyl compound **64** was converted to the carbonyl analogue **65**. The mercuric acetate mediated sulfur-oxygen exchange was not as straightforward as expected. As with other exchange reactions of this kind, the thiocarbonyl species **64** was treated with one and a half molar equivalents of mercuric acetate in dry chloroform. Upon filtration a yellow solid by-product was removed, and the chloroform solution evaporated to yield a material that was either a solid or an oil on different occasions. Upon inspection of elemental analysis data, it was noticed that for the solid the elemental composition correlated with that of the expected composition **65**, but with some residual acetic acid. The lower solubility of the solid form in chloroform supports the hypothesis of a proportion of the pyridines being protonated. Purification of a chloroform solution of **65** by treatment with weak sodium bicarbonate solution afforded a crude material, that was passed through a short column of silica. A yellow band was collected leading to the isolation of the carbonyl compound **65** as a brown oil, identified by the loss of the signal associated with the thiocarbonyl carbon in the ^{13}C NMR, and the appearance of a signal for the carbonyl carbon at δ 190.8 ppm. The migration of the signals for the sp^2 carbon atoms located at the fusion of the five and six membered rings from δ 129.3 to 120.3 ppm is indicative of an electronic change in the ring system, demonstrating that sulfur-oxygen exchange occurred. The easily distinguished C=O stretching frequency observed at $\nu = 1674\text{ cm}^{-1}$ in the infrared spectrum confirmed the success of the exchange reaction. High resolution electrospray mass spectrometry showed the $[\text{M} + \text{H}]^+$ ion at 360.9594 Da.

The protonation of the pyridine system and subsequent isolation of the solid salt can be eliminated by employing shorter reaction times. Despite the slight colour change of the reaction mixture within a few minutes, indicative of the conversion of the thiocarbonyl to the carbonyl species, typical exchange reactions are allowed to stir for around two hours, to ensure complete exchange. However, in this case, the longer reaction time allows the protonation to occur. By working up the reaction after only 30 mins, the carbonyl compound may be isolated pure without the need for chromatography, and in much higher yields.

The triethyl phosphite-mediated cross coupling reaction of carbonyl **65** with thiocarbonyl **22** afforded the donor **67** after careful chromatography. Dependant upon the volume of triethyl phosphite employed, the location of the donor may be either in solution or in the solid precipitated from the reaction mixture. For dilute reactions, the precipitate contained the homo-coupled products **11** and **66**, and some cross-coupled **67**, whilst the reaction liquors contained homo-coupled **66** and cross-coupled **67**. In concentrated reactions, the precipitated solid contained all products, with <1 % combined products in the reaction liquors based on mass. Optimum yields were obtained with concentrations around 40 g L⁻¹ (of combined solid reactants in triethyl phosphite, *known here as the dilute reaction*) affording *ca.* 50 % of the required cross-coupled donor.

Thus for dilute reactions, the residual triethyl phosphite was distilled off under vacuum, and the residue dried for 5 h under vacuum. The crude material was purified by chromatography over silica, eluting with a mixture of tetrahydrofuran and methanol

(5:2) to give the bis(4-pyridyl) donor **67**, which was identified by the presence of the aromatic and ethylene protons in the ^1H NMR, the absence of carbonyl and thiocarbonyl carbon signals in the ^{13}C NMR along with the presence of signals corresponding to the delocalised π core system of C=C bonds at δ 113.0 and 109.8 ppm. High resolution chemical ionisation mass spectrometry confirmed the chemical structure, with the observation of the $[\text{M} + \text{H}]^+$ ion at 536.8838 Da.

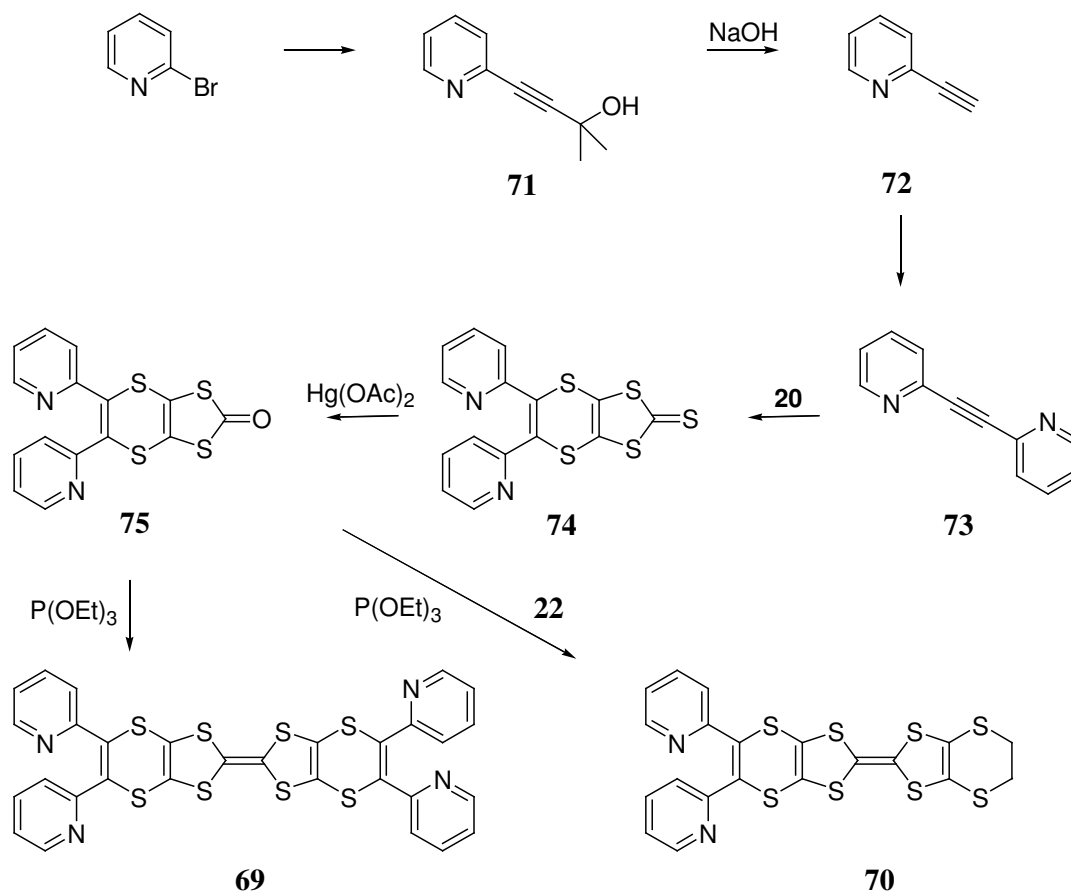
For more concentrated reactions, the precipitate formed was filtered off, and washed with copious amounts of diethyl ether. The orange solid was dissolved in chloroform and loaded onto silica. Purification by chromatography eluting with a mixture of chloroform and tetrahydrofuran (9:1) gave the required donor **67** which was spectroscopically identical to that obtained *via* the dilute method.

The triethyl phosphite mediated homo-coupling reaction of oxo compound **65** proceeded smoothly, in a concentrated solution of around 60 g L^{-1} (solid reactant dissolved in triethyl phosphite). At this concentration, the precipitate formed in the reaction consisted solely of the required product **66**, and the reaction liquors contained no appreciable amount of **66**. The precipitate was washed with copious amounts of diethyl ether and dried under vacuum affording the tetra(4-pyridyl) donor in near quantitative yield. The structure was identified by its simple ^1H NMR spectrum showing the aromatic pyridine protons, and ^{13}C NMR spectrum indicating the absence of carbonyl and thiocarbonyl signals and the observation of the central delocalised π core system of C=C bonds at δ 122.6 and 119.1 ppm. Confirmation was achieved by

observation of the $[M]^+$ ion in the high resolution electron impact mass spectrum at 687.9133 Da.

The coordination chemistry of the bipyridyl donor **67** was initially investigated by reaction with zinc trifluoromethanesulfonate in refluxing acetonitrile under a nitrogen atmosphere. Orange microcrystals were obtained but isolated in low yield. Analysis of the compound by infrared suggested that no metal coordination had taken place, and showed peaks attributable to the neutral donor **67** only. Confirmation of the identity was achieved by observation of the melting point, which showed an identical value to that of the neutral donor. Similar results were obtained when attempting to obtain the copper, nickel and manganese coordination salts.

The silver trifluoromethanesulfonate salt was prepared by stirring a tetrahydrofuran solution of donor **67** under nitrogen in the dark, with the addition of a tetrahydrofuran solution of the silver (I) salt. A light brown precipitate formed which was insoluble in most solvents. Elemental analysis of the complex **68** indicated the formation of a 1:1 salt, and the infra-red spectrum showed peaks attributable to both the donor and the S=O bond of the anion. The attempted recrystallisation of **68** failed to provide crystalline material of any sort. It could be speculated that this afforded a coordination polymer with a silver cation coordinating two pyridyl groups in a linear fashion.

Scheme 11: Synthetic route to donors **69** and **70**.

The analogous electron donors **69** and **70** were formed with the nitrogen atoms of the pyridyl groups in the 2- position, as shown in Scheme 11. The synthetic route proceeded by the initial Sonogashira coupling of 2-bromopyridine with 2-methyl-2-hydroxy-but-3-yne to afford the protected terminal alkynyl derivative **71**, as prepared in the literature.⁸ The ^1H NMR and ^{13}C NMR spectroscopic data obtained were comparable to that obtained in the literature, and the species was confirmed by the observation of the molecular ion 161 $[\text{M}]^+$ by GC-MS.

A toluene solution of the protected alkyne **71** was refluxed with sodium hydroxide pellets to deprotect the alkyne. Filtration and careful evaporation, so as to not sublime over the required compound, afforded the terminal alkyne **72** which was confirmed by the presence of its terminal hydrogen in the ^1H NMR spectrum as a singlet at δ 3.14 ppm, and the loss of the methyl group singlet at δ 1.62 ppm, indicating the loss of the acetone fragment. The ^{13}C NMR spectrum confirmed the deprotection, with a difference in the chemical shifts of the alkyne carbons, from δ 94.9 and 81.0 ppm in **71**, to δ 82.4 and 76.9 ppm in **72**. GC-MS confirmed the structure with a signal for the molecular ion at 103 $[\text{M}]^+$.

Sonogashira coupling of the exposed terminal alkyne **72** with 2-bromopyridine gave after work-up and chromatography the symmetrical alkyne, bis(2-pyridyl)ethyne, **73**, as an oil. The structure was determined by its ^1H NMR spectrum, showing the loss of the terminal hydrogen, and by ^{13}C NMR showing the absence of the terminal carbon peak at δ 76.9 ppm and a shift of the lone signal in the region to δ 87.8 ppm. This was comparable to the data shown in the literature.⁹ GC-MS was used to confirm the structure with the presence of the 180 $[\text{M}]^+$ ion peak clearly visible.

In a similar fashion to that employed in the synthesis of the 4-pyridyl analogue, the treatment of the alkyne **73** with the oligomeric trithione species **20** in refluxing toluene solution afforded, after two chromatography columns, the thiocarbonyl compound **74** as a brown solid in 80 % yield. The C=S stretching band was clearly observable in the infrared spectrum at $\nu = 1063 \text{ cm}^{-1}$. ^1H NMR and ^{13}C NMR confirmed the structure of **74** with the absence of the resonance signals for the *sp* carbons, these carbons now being in a lower oxidation state and having peaks at δ 136.9 ppm. The thiocarbonyl peak resonates at δ 213.9 ppm. High resolution mass spectrometry provided confirmation of the formation of **74** with the ion peak for $[\text{M}]^+$ at 375.9291 Da.

The mercury acetate mediated conversion from thiocarbonyl **74** to carbonyl compound **75** proceeded in a short reaction time in the presence of an excess of the mercury salt. The orange gum isolated in 70 % yield after work-up was characterised by its ^{13}C NMR spectrum, which showed loss of the thiocarbonyl peak and appearance of the carbonyl peak at δ 192.2 ppm, and changes in the electronic nature of the five-membered ring by the shift of the alkene carbons (3a and 7a -C, *carbons enclosed by the sulfurs*) from δ 130.1 to 120.4 ppm. High resolution mass spectrometry unequivocally confirmed the identity of **75**.

The homo-coupling reaction of **75** was achieved in under three hours in triethyl phosphite, and the product precipitated from the reaction mixture. Filtration and washing with copious amounts of diethyl ether gave the tetra(2-pyridyl) donor **69** in 97 % yield, which was identified by the simplicity of the ^1H NMR spectrum, and the lack of a carbonyl resonance in the ^{13}C NMR. The homo-coupling was confirmed by

the presence of two resonances for the core of the organosulfur donor δ 122.2 and 118.8 ppm. The $[M+H]^+$ peak in the high resolution mass spectrum confirmed the species as **69** of molecular weight 688.9215 Da.

The cross-coupling reaction of **75** with thione **22** in triethyl phosphite was completed at a concentration of approximately 90 g L^{-1} , and was treated as a concentrated solution (as defined above). As such, the precipitate formed in the reaction was filtered and washed with a large volume of diethyl ether. The crude solid was purified by chromatographic separation over silica and the cross-coupled donor **70** was isolated as a bright orange solid in 54 % yield, which contained some crystals. The crystals were reserved and investigated by single crystal X-ray crystallography. ^1H NMR analysis showed the presence of aromatic protons, and the ethylene protons were identified as the resonance at δ 3.28 ppm. Observation of the ^{13}C NMR showed the lack of carbonyl and thiocarbonyl peaks, and the required presence of alkenic carbons attributed to the core of the organosulfur donor at δ 122.1, 116.2, 114.2, and 113.7 ppm. High resolution mass spectrometry was used to confirm the structure of **70**, and was indicated by the presence of the $[M]^+$ peak at 535.8763 Da.

The cross-coupled donor **70** crystallised from a mixed solvent system of tetrahydrofuran/chloroform (9:1) as bright orange laths. Crystal data for $\text{C}_{20}\text{H}_{12}\text{N}_2\text{S}_8$, $M = 536.80$, orange lath, $0.31 \times 0.09 \times 0.01 \text{ mm}^3$, monoclinic, space group Pn (No. 7), $a = 4.1894(2)$, $b = 12.7225(5)$, $c = 20.5532(8) \text{ \AA}$, $\beta = 92.917(2)^\circ$, $V = 1094.06(8) \text{ \AA}^3$, $Z = 2$, $D_c = 1.629 \text{ g/cm}^3$, $F_{000} = 548$, MoK α radiation, $\lambda = 0.71073 \text{ \AA}$, $T = 120(2)\text{K}$, $2\theta_{\text{max}} = 55.0^\circ$, 10725 reflections collected, 4553 unique ($R_{\text{int}} = 0.0534$). Final $\text{Goof} =$

1.097, $RI = 0.0554$, $wR2 = 0.1066$, R indices based on 3929 reflections with $I > 2\sigma(I)$ (refinement on F^2), 282 parameters, 8 restraints. Lp and absorption corrections applied, $\mu = 0.829 \text{ mm}^{-1}$. Absolute structure parameter = $0.23(12)$.¹⁰

The asymmetric unit consisted of a single donor molecule, which is flexed about the S...S vector across the dithiin ring as shown in Figure 28. Both the ethylene function and the bis(2-pyridyl)ethylene function were found to be displaced to the same side of the mean plane derived from the central TTF organosulfur core. Positional disorder of the ethylene functions was observed and was modelled effectively, with C1 having an alternative position 0.75 \AA (C1X) away, and C2 having an alternative position 0.63 \AA (C2X) away. This serves to generate the inverted ethylene function, i.e. from $\downarrow\uparrow$ to $\uparrow\downarrow$ (when viewed down the length of the molecule, towards the bis(2-pyridyl) end), and gives two envelope conformations.

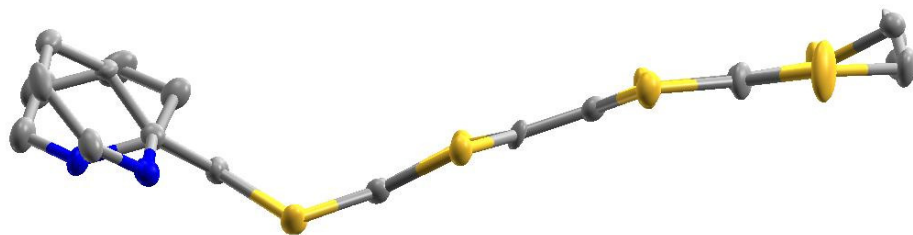


Figure 28: Asymmetric unit of 70, showing slightly bent structure. Hydrogen atoms and the alternative positions for ethylene carbons have been removed for clarity. Thermal ellipsoids are drawn at the 50 % probability level.

The nitrogen atom of one of the pyridine groups in Figure 29 is orientated inwards toward the other pyridyl group, whereas the other pyridine group has the nitrogen atom orientated pointing away from the other 2-pyridyl group (and away from the donor). The lattice structure is composed of isolated stacks of electron donor molecules extending in the crystallographic *a* direction, with each donor molecule exhibiting one S...S intrastack close contact to each of its neighbouring donor molecules (S6...S8 3.564 Å). The stacks are arranged such that the organosulfur molecules have their pyridyl moieties pointing towards the sulfur edge of the adjacent donor molecule, at the unfunctionalised end (Figure 30).

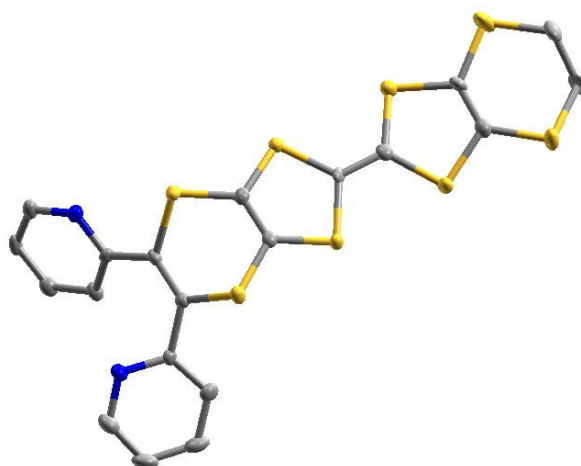


Figure 29: Asymmetric unit of 70. Hydrogen atoms and the alternative positions for ethylene carbons have been removed for clarity. Thermal ellipsoids are drawn at the 50 % probability level.

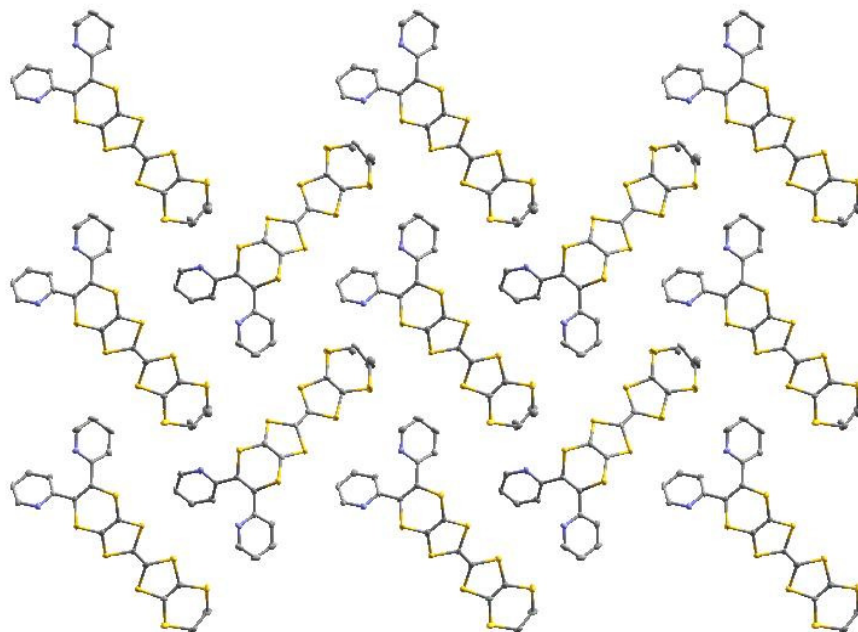


Figure 30: Lattice as viewed down the crystallographic *a* axis. Hydrogen atoms have been removed for clarity. Thermal ellipsoids are drawn at the 50 % probability level.

The stacking of the electron donor molecules is observed when viewing the lattice down the crystallographic *b* axis (Figure 31). The non-planarity of the molecule is readily observed, with the pyridyl moieties adopting positions displaced from the mean plane.

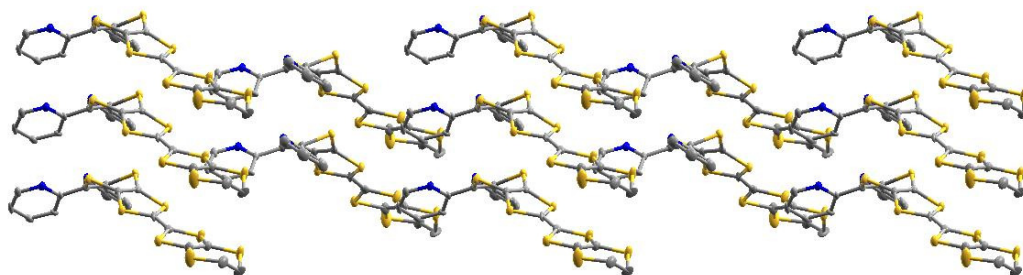
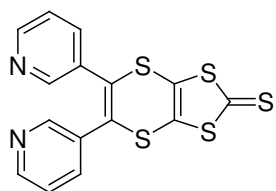


Figure 31: Lattice as viewed down the crystallographic *b* axis. Hydrogen atoms have been removed for clarity. Thermal ellipsoids are drawn at the 50 % probability level.

Viewing the lattice down the crystallographic *c* axis, it is evident that the two 2-pyridyl groups are twisted with respect to each other, caused by their close proximity to each other and the hydrogen atom in the 6-position protruding towards the neighbouring aromatic system.

All non-hydrogen atoms were refined anisotropically, before adding hydrogen atom positions geometrically. Confirmation as to the protonation state of the pyridyl nitrogen atoms was sought from the C-N-C bond angles, which were observed as: (N1) 117.70 ° and (N2) 115.86 ° for the two pyridyl systems. The measurements indicated that the nitrogen atoms were not protonated.

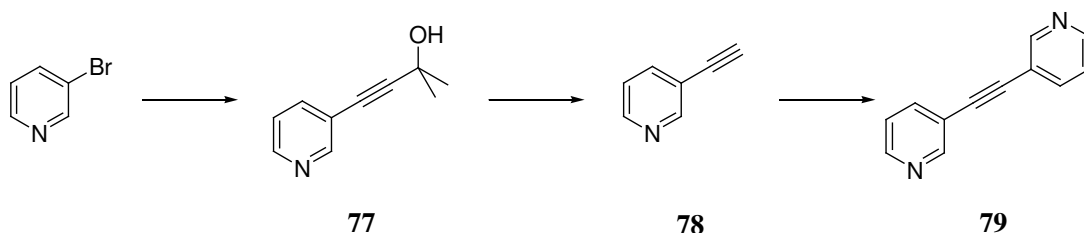
Charge determination of the donor molecule based upon bond length calculations of the core of the organosulfur unit, demonstrated that the charge state was neutral as expected, and confirmed the validity of the method for the determination of charges using this extended ET framework.¹¹



76

It was also decided to attempt to prepare the 3-pyridyl analogue **76**, as the ring nitrogen atoms would be in a preferential geometry for chelation to metal centres. This however, proved unsuccessful at the Diels-Alder cyclisation step. Sonogashira coupling of

3-bromopyridine with 2-methyl-2-hydroxy-but-3-yne afforded **77**, which was deprotected using sodium hydroxide to give terminal alkyne **78**. Sonogashira coupling of **78** with 3-bromopyridine afforded the symmetrical alkyne **79**. Diels-Alder reaction of **79** with oligomeric **20** failed to produce **76**, despite early belief of the formation of the thiocarbonyl compound.



Scheme 13: Preparation of bis(3-pyridyl)ethyne.

TLC analysis of the cycloaddition reaction mixture a few minutes after reaching reflux indicated the presence of a new compound as a yellow spot, which was much more intense than the spot for alkyne **79**. The reaction was maintained for an additional hour to drive the reaction to completion, however at this time the yellow spot was no longer visible. In addition an intense spot with identical R_f to that of 1,2-bis(3-pyridyl)ethyne was visible, suggesting reformation of the reagent materials. It was postulated that this may be possible *via* a retro-Diels-Alder reaction, driven by the thermal energy supplied to the reaction vessel. As such the cycloaddition reaction was re-attempted with short reaction times of less than 10 min, however these reactions proved unsuccessful and the yellow compound was not observed again.

The reactivity of the bis(2-pyridyl) and bis(4-pyridyl) alkenes towards Diels-Alder reactions, is likely to be greater than for the corresponding 3-pyridyl analogue, since the

pyridine rings are able to more effectively remove π -electron density from the π -bond, for the aforementioned two, as illustrated in Figure 32.

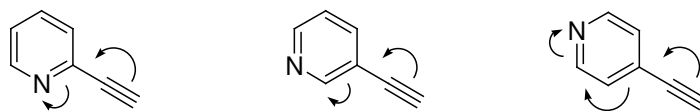


Figure 32: π -electron delocalisation in pyridylethyne analogues.

The redox potentials of the homo-coupled electron donors **66** and **69**, and those of the cross-coupled donors **67** and **70** are given in Table 3. For comparison, the oxidation potentials of ET and VT are given, as described in the literature.^{12, 13} Cyclic voltammetry of the donor **66** showed a pair of quasi reversible redox waves centred at 0.81 V similar to that of the unsubstituted VT, which showed a similar process at 0.79 V. Donors **67**, **69** and **70** showed two separate processes, with higher values compared to ET, with the cross-coupled materials being lower in value than the corresponding homo-coupled electron donors. The typical redox behaviour of the TTF system, showing two pairs of reversible single-electron redox waves, was exhibited.

Compound	$E_{1/2}^1$ [V]	$E_{1/2}^2$ [V]
66	0.81	-
67	0.75	1.07
69	0.77	1.12
70	0.69	1.08
ET ¹²	0.49	0.89
VT ¹³	0.79	-

Table 3: Oxidation potentials for **66**, **67**, **69** and **70**, relative to Ag/ AgCl.

The redox behaviour exhibited by electron donors **67**, **69** and **70** showed that the oxidation and re-reduction of the species were reversible, with a ratio of the corresponding peaks close to unity.

The cyclic voltammetry measurements were made relative to the Ag/AgCl electrode, at room temperature in dichloromethane, containing 0.1 M Bu₄NPF₆. Measurements were made using a Pt working electrode, and a scan rate of 100 mV s⁻¹.

3.3 Materials made by chemical oxidation or electrocrystallisation

3.3.1 (70)(CuCl₂)₃(CH₃CN)_{0.75}(H₂O)_{1.5}

The reaction of the bis(2-pyridyl) electron donor **70** with copper (II) chloride produced a black amorphous material that was characterised, and the magnetic properties investigated. Elemental analysis data showed the composition of the solid to be one donor molecule to three copper dichloride molecules, with the incorporation of acetonitrile and water. SQUID magnetometry identified the copper atoms to be present in the +2 oxidation state, implying the absence of the occurrence of a redox reaction. It could be speculated that coordination of the pyridyl rings to the metal centre had occurred, with the addition of a structurally isolated copper dichloride species. Raman spectroscopy challenges this interpretation, as it identifies the charge state on the donor molecule to be +1, from the observed ν_4 and ν_3 stretching frequencies observed at 1414 and 1466 cm⁻¹ respectively. This result suggested that oxidation had occurred and thus an anionic species must be present to balance the charge within the salt. It is proposed

that one of the three metal centres is present in the +1 oxidation state, as the anion $[\text{CuCl}_2]^-$, and that the remaining two metal centres are each present as $[\text{CuCl}_2]$. This is supported by the observation of the dark precipitate formed in the reaction, which was found to be not soluble in the common organic solvents. The presence of water molecules in the compound was confirmed in the infrared spectrum which displayed a broad band centred at $\nu = 3183 \text{ cm}^{-1}$, indicative of the O-H stretches.

3.3.2 $(70)_x(\text{CoCl}_4)_y$

The electrocrystallisation of **70** with the cobalt (II) tetrachloride anion formed long laths on the anode. The typical dimensions of the crystals were 1 mm x 4 mm x <0.1 mm. Crystals showed a low conductivity along the long axis (Figure 33), which remained constant on cooling, until an insulating phase transition occurred at $T_{\text{M-I}} = 212\text{-}213 \text{ K}$. A small decrease in the conductivity was observed at 261-262 K, which may be attributable to a modification of the crystal lattice.

The crystals obtained were thermo-responsive, having a tendency to curl when cooled or warmed. At 90 °C the crystals started to curl slightly as if starting to melt, however they retained their physical structure up to 206 °C at which point a clear melting point was observed. Upon cooling from room temperature, the crystals were found to curl also.

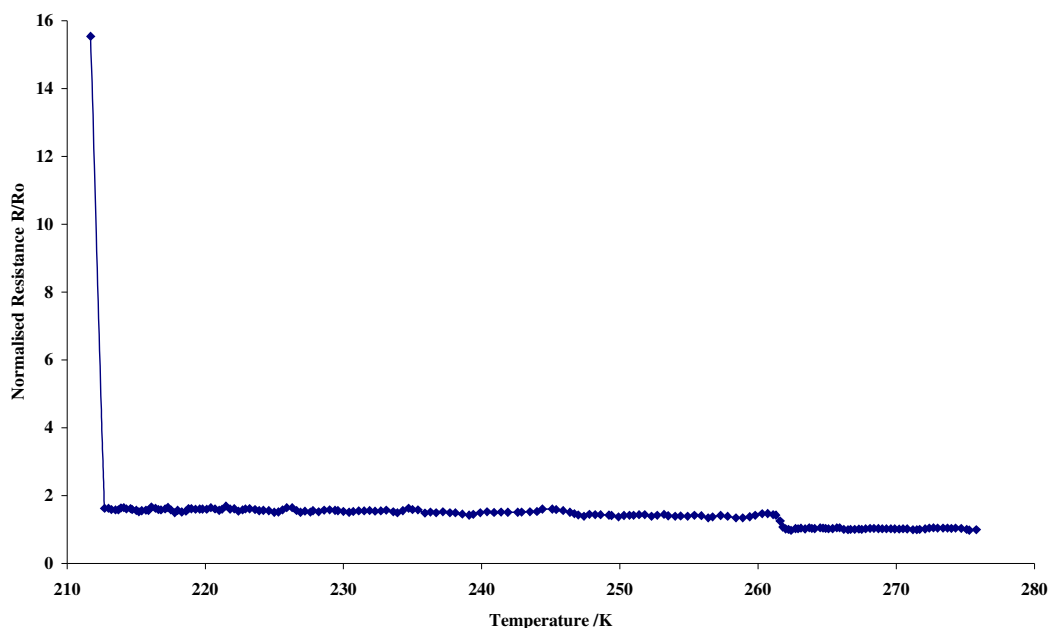


Figure 33: Normalised resistance profile for (70)CoCl₄.

3.3.3 (70-H)⁺(ReO₄)₂·0.5(CH₂Cl₂)

The radical cation salt (70-H)⁺(ReO₄)₂·0.5(CH₂Cl₂) was formed by the constant current (0.1 μA) electrocrystallisation of **70** with tetrabutylammonium perrhenate in dichloromethane. Small dark blades of the salt, of typical dimensions 0.2 x 0.1 x <0.1 mm, crystallised on the anode over 3 weeks. These were harvested and washed with acetone. Resistivity measurements as a function of temperature were not performed on the crystals, as they were too small for the attachment of gold wires.

Structural determination was obtained from two individual crystals, by single crystal X-ray diffraction, and both datasets determined to be identical. Crystal data for C_{20.50}H₁₄ClN₂O₈Re₂S₈, $M = 1080.67$, dark brown blade, 0.16 × 0.07 × 0.02 mm³,

triclinic, space group $P-1$ (No. 2), $a = 7.7886(2)$, $b = 9.2525(2)$, $c = 21.0117(5)$ Å, $\alpha = 94.7170(10)$, $\beta = 90.5190(10)$, $\gamma = 103.2370(10)^\circ$, $V = 1468.36(6)$ Å³, $Z = 2$, $D_c = 2.444$ g/cm³, $F_{000} = 1020$, MoK α radiation, $\lambda = 0.71073$ Å, $T = 120(2)$ K, $2\theta_{\max} = 55.1^\circ$, 21251 reflections collected, 6699 unique ($R_{\text{int}} = 0.0321$). Final $GooF = 1.032$, $RI = 0.0424$, $wR2 = 0.0918$, R indices based on 6182 reflections with $I > 2\sigma(I)$ (refinement on F^2), 374 parameters, 3 restraints. Lp and absorption corrections applied, $\mu = 8.946$ mm⁻¹. All non-hydrogen atoms were refined anisotropically, with hydrogen atoms added geometrically. The asymmetric unit was found to consist of one donor molecule, which was protonated on the pyridine nitrogen atom that pointed towards the other pyridine moiety, two perrhenate anions, and half a molecule of dichloromethane, disordered over two sites approximately equally (Figure 34).

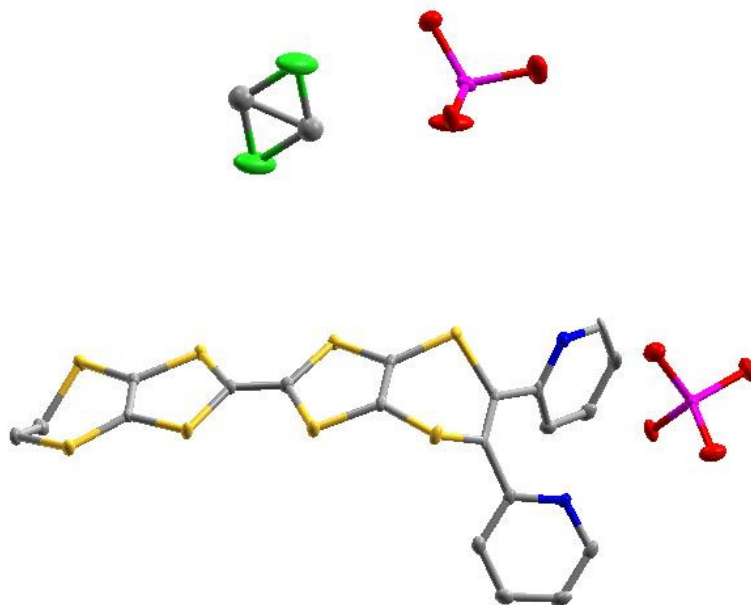


Figure 34: Asymmetric unit of $(70\text{-H})^+(\text{ReO}_4)_2 \cdot 0.5(\text{CH}_2\text{Cl}_2)$. Hydrogen atoms have been removed for clarity. Thermal ellipsoids are shown at the 50 % probability level. Dichloromethane is disordered about a centre of symmetry.

The evidence for the *N*-protonation of one of the pyridine groups is found in the C-N-C bond angles exhibited by the pyridine rings. In the pyridine system, the C-N-C angle is 116.91°, typical for pyridine systems, and as observed for the crystal structure of the neutral donor **70** (C-N-C bond angles 117.70 ° and 115.86 °). The pyridinium system however has a C-N-C angle of 122.79°, much greater than those mentioned previously. The solid state arrangement is represented by sets of dimers (Figure 35), closely associated to adjacent sets of dimers, to form a ‘staircase’ extending in the crystallographic *a* direction. Each step was found to exhibit a short S...S intrastack contact: S1...S8 3.40 Å; S2...S6 3.57 Å; S3...S6 3.41 Å (Figure 36).

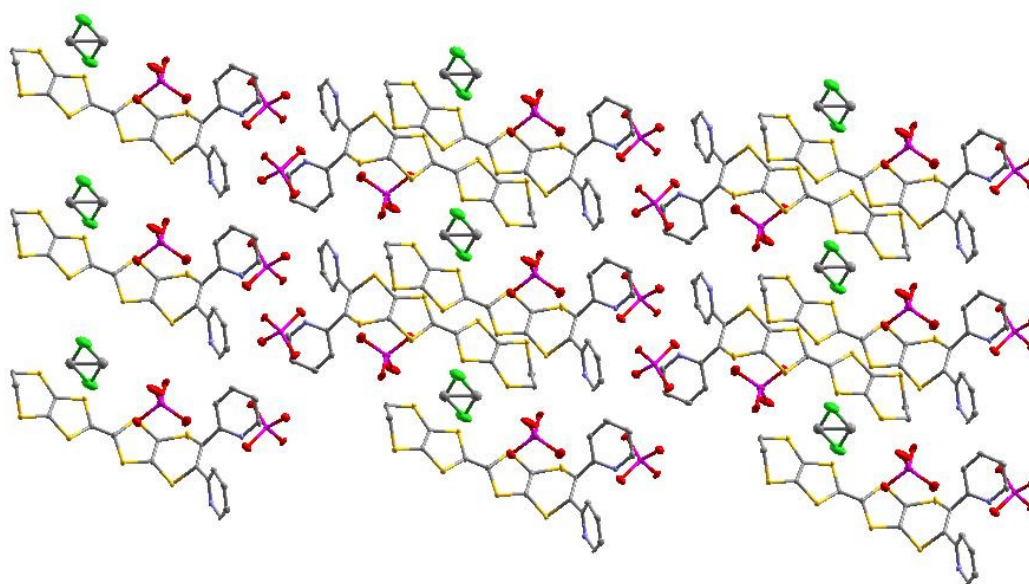


Figure 35: Lattice as viewed down the crystallographic *a* axis, showing dimerisation of the donor molecules. Hydrogen atoms have been removed for clarity. Thermal ellipsoids are shown at the 50 % probability level.

The two perrhenate anions were found to each serve a different function, one type of which is well ordered with respect to its thermal parameters. This type of anion formed

ribbons extending along the crystallographic c axis. The ribbons were located in between the pyridyl fragments, with hydrogen bonding evident from the $H-N^+$ (pyridinium) to the perrhenate anion, with a distance of 1.85 Å.

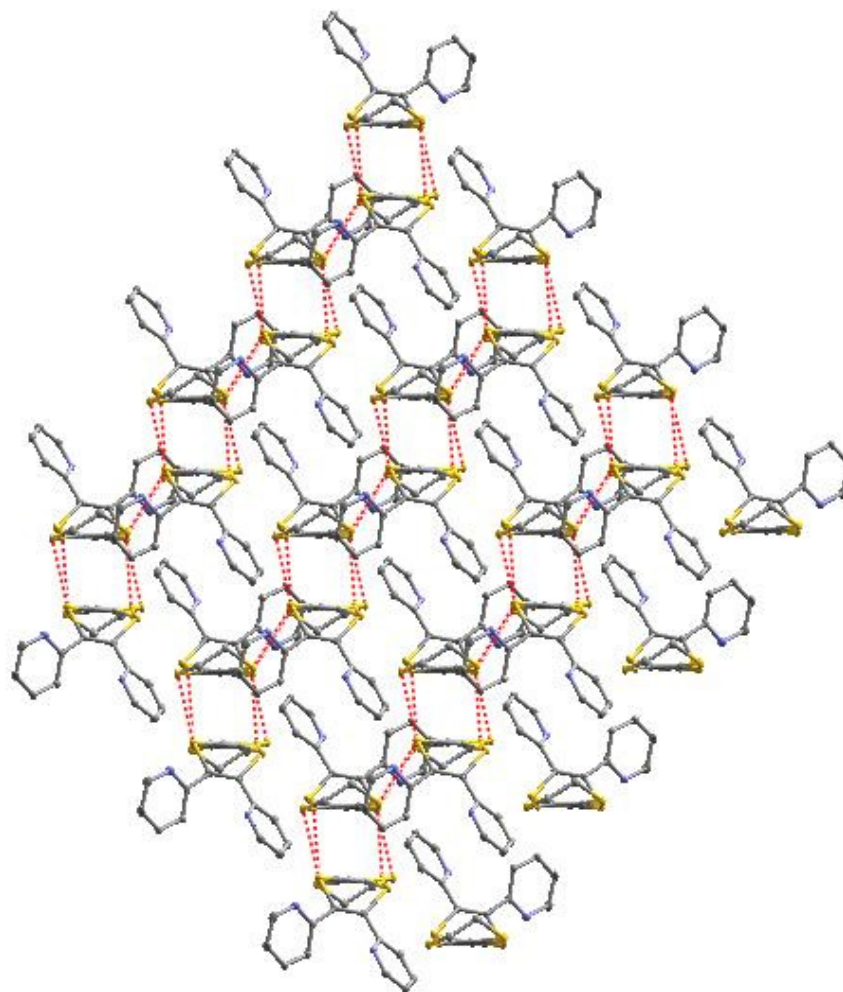


Figure 36: Short S...S contacts (red dashed lines) extending in the crystallographic a direction.

Hydrogen atoms have been removed for clarity. Thermal ellipsoids are shown at the 50 % probability level.

Weak hydrogen bonding was found to exist between $N^+-H...O-Re$ over an $N...O$ distance of 2.70 Å. This linked two donor molecules in a head to tail arrangement

(Figure 37), *via* two perrhenate anions. The absence of hydrogen bonding interactions for the remaining perrhenate anion led to less well-defined atomic positions. This perrhenate served to stabilise the charge associated with the organosulfur donor, determined to be +0.98 from bond length calculations.

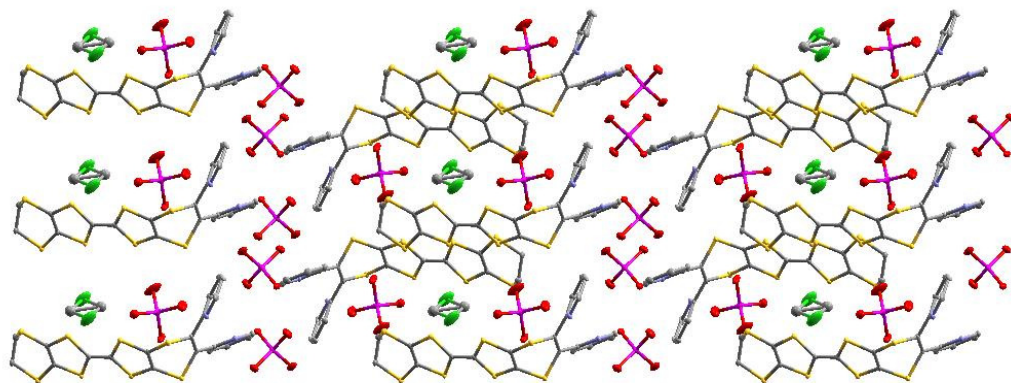


Figure 37: Lattice as viewed down the crystallographic *b* axis. Hydrogen atoms have been removed for clarity. Thermal ellipsoids are shown at the 50 % probability level.

The charge of +1 on the donor molecule is confirmed by the Raman stretches of $\nu_4 = 1418$ and $\nu_3 = 1462$. Figure 38 illustrates the ‘sandwich’ of two centrosymmetrically related perrhenate anions and a disordered dichloromethane molecule between two donor molecules.

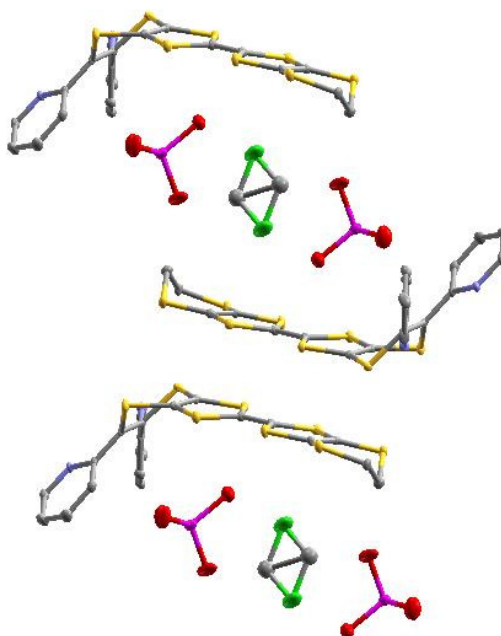


Figure 38: Slice of lattice structure, illustrating the sandwich of perrhenate anions between organosulfur donor molecules. Hydrogen atoms have been removed for clarity. Thermal ellipsoids are shown at the 50 % probability level.

3.3.4 Experimental

1,2-[Bis(4'-pyridyl)]-1,2-dibromoethane, **62**

Trans-1,2-bis(4-pyridyl)ethene **61** (5.0 g, 27.4 mmol) was stirred in 48% hydrobromic acid solution (70 mL), and cooled using an ice-water bath. Bromine (4.9 mL, 96 mmol) was added dropwise, causing an immediate thickening of the reaction mixture. An additional portion of 48% hydrobromic acid (40 mL) was added to aid stirring. The orange suspension was stirred for 20 min, before heating to 120 °C for 90 min. The reaction mixture was cooled to room temperature and stirred overnight. The orange solid was collected by suction filtration, transferred to a flask, and stirred in 2 M sodium

hydroxide solution (180 mL) for 4 h at room temperature, before isolating an off-white solid by suction filtration, from the yellow filtrate. This solid was washed with water (100 mL) and dried *in vacuo* at 55 °C to a constant weight, affording the brominated product **62** (7.77 g, 84%) as an off-white powder; δ_{H} (400 MHz; CDCl₃) 8.63 (4 H, dd, $J=4.7, 1.4$ Hz, 2 x 2'-, 6'-H), 7.33 (4 H, dd, $J=4.5, 1.6$ Hz, 2 x 3'-, 5'-H), 5.21 (2 H, s, 1-, 2-H); δ_{C} (100 MHz; CDCl₃) 150.5 (2 x 2'-, 6'-C), 147.5 (2 x 4'-C), 122.5 (2 x 3'-, 5'-C), 51.8 (1-, 2-C).

1,2-Bis(4'-pyridyl)ethyne, 63

Fresh, finely cut pieces of sodium metal (1.3 g) were dissolved in *t*-butanol (110 mL) at 80 °C under nitrogen. To the solution was added **62** (4.0 g, 11.7 mmol) in portions over 10 min, and the resultant mixture stirred at 80 °C for 24 h. The yellow mixture was allowed to cool to 40 °C, and ethanol (40 mL) added, followed by water (40 mL), giving a brown solution. The mixture was cooled to room temperature, chloroform (100 mL) and water (100 mL) added, and the two layers separated. The extraction was repeated with further portions of chloroform (4 x 100 mL), the extracts combined, washed with water (300 mL), dried using calcium chloride and evaporated to afford the crude product. This was dissolved in a minimal amount of methanol and purified by chromatography over silica, eluting with diethyl ether/tetrahydrofuran (85:15) to afford 1,2-bis(4-pyridyl)ethyne **63** (0.763 g, 36%) as a white crystalline material; δ_{H} (400 MHz; CDCl₃) 8.59 (4 H, dd, $J=4.5, 1.7$ Hz, 2 x 2'-, 6'-H), 7.34 (4 H, dd, $J=4.4, 1.6$ Hz, 2 x 3'-, 5'-H); δ_{C} (100 MHz; CDCl₃) 150.0 (2 x 2'-, 6'-C), 130.2 (2 x 4'-C), 125.6 (2 x 3'-, 5'-C), 90.6 (1-, 2-C).

2-Methyl-4-pyridin-4-yl-but-3-yn-2-ol, 80

The literature method was modified to afford **80**.¹⁴ Thus, to a stirred mixture of 4-bromopyridine hydrochloride (6.74 g, 34.7 mmol) in triethylamine (100 mL) under a nitrogen atmosphere, was added 2-methyl-2-hydroxy-but-3-yne (3.4 mL, 35.1 mmol) and the mixture stirred for 5 min. Bis(triphenylphosphine)palladium dichloride (0.5g, 0.71 mmol) and copper iodide (0.23 g, 1.21 mmol) were added successively, and the orange-brown mixture stirred at room temperature overnight. Distilled water (400 mL) was added and extracted with diethyl ether (3 x 200 mL). The combined ether extracts were washed with distilled water (100 mL), dried over sodium sulfate, and evaporated. The crude material was purified by chromatography over silica eluting with cyclohexane/ethyl acetate (3:1) to afford **80** (4.1 g, 73%) as a slightly yellow oil; δ_{H} (400 MHz, CDCl_3) 8.48 (2 H, dd, $J=4.5, 1.6$ Hz, 2'-, 6'-H), 7.20 (2 H, dd, $J=4.4, 1.7$ Hz, 3'-, 5'-H), 2.91 (1 H, s br, O-H), 1.56 (6 H, s, 2 x CH_3); δ_{C} (100 MHz, CDCl_3) 149.5 (2'-, 6'-C), 131.3 (3'-, 5'-C), 125.7 (4'-C), 98.9 (*sp*-C), 79.5 (*sp*-C), 65.3 ($\text{C}(\text{OH})(\text{CH}_3)_2$), 31.2 (2 x CH_3); m/z (GC-MS): found: 161 $[\text{M}]^+$, 146 $[\text{M}-\text{CH}_3]$, 118, 104. $\text{C}_{10}\text{H}_{11}\text{NO}$ requires: 161.

4-Ethynylpyridine, 81

To a solution of **80** (4.0 g, 24.8 mmol) in toluene (100 mL) was added sodium hydroxide pellets (1 g, 25 mmol). The mixture was rapidly stirred and heated to reflux under nitrogen for 3 h. The reaction was cooled to room temperature, filtered and carefully evaporated on a rotary evaporator with the water bath set at 40 °C to give **81**

(2.48 g, 97%) as a tacky off-white solid; m/z (GC-MS): found: 103 $[M]^+$, 76, 50. C_7H_5N requires: 103.

1,2-Bis(4'-pyridyl)ethyne, 63

To a mixture of **81** (2.4 g, 23.3 mmol) in triethylamine (60 mL) was added 4-bromopyridine hydrochloride (4.0 g, 20.6 mmol). Whilst stirring under nitrogen, bis(triphenylphosphine)palladium dichloride (0.3 g, 0.43 mmol) and copper iodide (0.15 g, 0.79 mmol) were added, and the mixture heated to 70 °C for 4 h. The mixture was cooled to room temperature, poured into distilled water (200 mL) and extracted with dichloromethane (3 x 150 mL). The combined organic extracts were washed with distilled water (80 mL), dried over sodium sulfate, and evaporated. The crude material was purified by chromatography over silica eluting initially with cyclohexane/ethyl acetate (1:1) and then cyclohexane/ethyl acetate (1:2) to give **63** (2.1 g, 57%) as an off-white solid; δ_H (400 MHz; $CDCl_3$) 8.59 (4 H, dd, $J=4.5, 1.7$ Hz, 2 x 2', 6'-H), 7.34 (4 H, dd, $J=4.4, 1.6$ Hz, 2 x 3', 5'-H); δ_C (100 MHz; $CDCl_3$) 150.0 (2 x 2', 6'-C), 130.2 (2 x 4'-C), 125.6 (2 x 3', 5'-C), 90.6 (1-, 2-C); m/z (GC-MS): found: 180 $[M]^+$, 153, 140, 127, 100, 74, 50. $C_{12}H_8N_2$ requires: 180.

5,6-Bis(pyridin-4-yl)-[1,3]dithiolo[4,5-b][1,4]dithiine-2-thione, 64

Alkyne **63** (0.141 g, 0.78 mmol) was dissolved in toluene (25 mL) and heated to reflux (oil bath temp 120 °C) under nitrogen. Addition of the trithione **20** (0.152 g, 0.78 mmol) at reflux in one portion, caused the reaction mixture to turn dark brown with

concurrent evolution of a little white vapour. The resulting mixture was refluxed and monitored by TLC (ethyl acetate). An additional portion of the trithione (0.152 g, 0.78 mmol) was added after 2 h 40 min, and the mixture continued to reflux for a further 2 h at which time TLC (ethyl acetate) indicated complete consumption of the alkyne **63**. The mixture was cooled to room temperature, evaporated and purified by chromatography on silica eluting with ethyl acetate to give **64** (0.27 g, 92%) as a brown solid Mp 177 °C (Found C, 47.9; H, 2.1; N, 7.5. C₁₅H₈N₂S₅ requires C, 47.9; H, 2.1; N, 7.45%); $\nu_{\max}(\text{ATR})/\text{cm}^{-1}$ 1579, 1543, 1403, 1071, 1041, 1017, 847, 823, 768, 627, 602, 538, 510, 461; δ_{H} (400 MHz; CDCl₃) 8.46 (4 H, dd, $J=4.5, 1.6$ Hz, 2 x 2'-, 6'-H), 6.96 (4 H, dd, $J=4.5, 1.6$ Hz, 2 x 3'-, 5'-H); δ_{C} (100 MHz; CDCl₃) 204.0 (2-C), 150.4 (2 x 2'-, 6'-C), 143.4 (2 x 4'-C), 135.3 (5-, 6-C), 129.3 (3a-, 7a-C), 123.5 (2 x 3'-, 5'-C); m/z (ES⁺): found: 376.9365 [M + H]⁺. C₁₅H₈N₂S₅ + H requires: 376.9364.

5,6-Bis(pyridin-4-yl)-[1,3]dithiolo[4,5-b][1,4]dithiine-2-one, 65

Thione **64** (0.63 g, 16.8 mmol) was dissolved in dry chloroform (65 mL), and mercuric acetate (0.801 g, 25.1 mmol) added. The mixture was stirred under nitrogen for 35 min and filtered, washing with a little chloroform. The organic phase was washed with water (30 mL x 2), dried over sodium sulfate and evaporated to give a yellow-brown oil. The crude material was purified by chromatography over silica eluting with ethyl acetate to give **65** (0.35 g, 57%) as a brown oil (Found C, 50.1; H, 2.3; N, 7.8. C₁₅H₈N₂S₄O requires C, 50.0; H, 2.2; N, 7.8%); $\nu_{\max}(\text{ATR})/\text{cm}^{-1}$ 1674, 1584, 1544, 1404, 1062, 990, 910, 843, 822, 786, 748, 627, 602, 538, 508; δ_{H} (400 MHz; CDCl₃) 8.46 (4 H, m, 2 x 2'-, 6'-H), 6.97 (4 H, m, 2 x 3'-, 5'-H); δ_{C} (100 MHz; CDCl₃) 190.8

(2-C), 150.3 (2 x 2'-, 6'-C), 144.1 (2 x 4'-C), 135.2 (5-, 6-C), 124.0 (2 x 3'-, 5'-C), 120.3 (3a-, 7a-C); m/z (ES⁺): found: 360.9594 [M + H]⁺. C₁₅H₈N₂OS₄ + H requires: 360.9592.

Bis[di(4'-pyridyl)vinylenedithio]tetrathiafulvalene, 66

Oxo compound **65** (0.3 g, 0.83 mmol) was heated in triethyl phosphite (5 mL) under nitrogen to 110 °C. An orange precipitate was observed after approximately 1 h, and the reaction maintained at this temperature for a further 5 h. The reaction was cooled to room temperature, and filtered through a glass sinter washing with diethyl ether (*ca.* 100 mL). Drying *in vacuo* at room temperature overnight afforded **66** (0.27 g, 93%) as an orange solid Mp 206 °C (Found C, 52.5; H, 2.2; N, 8.1. C₃₀H₁₆N₄S₈ requires C, 52.3; H, 2.3; N, 8.1%); ν_{\max} (ATR)/cm⁻¹ 1583, 1544, 1403, 1216, 989, 917, 839, 822, 791, 763, 739, 627, 601, 537, 510; δ_{H} (400 MHz, CDCl₃) 8.50 (8 H, dd, $J=6.1, 1.6$ Hz, 4 x 2'-, 6'-H), 7.01 (8 H, dd, $J=6.1, 1.6$ Hz, 4 x 3'-, 5'-H); δ_{C} (100 MHz, CDCl₃) 150.3 (4 x 2'-, 6'-C), 143.7 (4 x 4'-C), 135.8 (5-, 5''-, 6, 6''-C), 123.5 (4 x 3'-, 5'-C), 122.6 (*sp*²C), 119.1 (*sp*²C); m/z (EI): found: 687.9133 [M]⁺. C₃₀H₁₆N₄S₈ requires: 687.9135.

[Bis(4'-pyridyl)vinylenedithio](ethylenedithio)tetrathiafulvalene, 67

Oxo compound **65** (0.1 g, 0.27 mmol) and thione **22** (0.3 g, 1.4 mmol) were dissolved in triethyl phosphite (10 mL) under nitrogen, and heated to 110 °C for 12 h. Distillation *in vacuo* of the triethyl phosphite afforded the crude material which was purified by chromatography over silica eluting with tetrahydrofuran/methanol (5:2) to give **67** (0.07

g, 48%) as a yellow-brown solid Mp 209 °C (dec.) (Found C, 44.6; H, 2.3; N, 5.2. C₁₅H₁₄N₂S₈ requires C, 44.75; H, 2.25; N, 5.2%); ν_{\max} (ATR)/cm⁻¹ 3623, 2956, 1598, 1585, 1543, 1433, 1401, 1232, 1216, 1155, 910, 866, 849, 825, 793, 769, 751, 628, 603, 540, 526, 470; δ_{H} (400 MHz; *d*₆-DMSO) 8.56 (4 H, d, *J*=4.3, 1.8 Hz, 2 x 2'-, 6'-*H*), 7.25 (4 H, d, *J*=4.4, 1.7 Hz, 2 x 3'-, 5'-*H*), 3.48 (4 H, d, *J*=2.0 Hz, 5''-, 6''-*H*); δ_{C} (100 MHz; *d*₆-DMSO) 150.1 (2 x 2'-, 6'-*C*), 143.1 (2 x 4'-*C*), 135.2 (5-, 6-*C*), 123.5 (2 x 3'-, 5'-*C*), 113 (*sp*²*C*), 109.8 (*sp*²*C*), 29.5 (5''-, 6''-*C*); *m/z* (CI⁺): found: 536.8838 [M + H]⁺. C₂₀H₁₂N₂S₈ + H requires: 536.8839.

Coordination salt of 67:Ag(O₃SCF₃), 68

To a solution of **67** (0.023 g, 0.04 mmol) in dry distilled tetrahydrofuran (7 mL), was added a solution of silver trifluoromethanesulphonate (0.011 g, 0.04 mmol) in dry distilled tetrahydrofuran (3 mL) under nitrogen in the dark. A precipitate formed immediately and the reaction was allowed to stir overnight. Filtration afforded **68** (0.015 g, 44%) as a light brown solid (Found C, 31.8; H, 1.6; N, 3.6. C₂₁H₁₂N₂O₃S₉F₃Ag requires C, 31.8; H, 1.5; N, 3.5%); ν_{\max} (ATR)/cm⁻¹ 3457, 3090, 2923, 1634, 1604, 1547, 1497, 1425, 1339, 1271, 1244, 1222, 1154, 1069, 1026, 915, 850, 831, 795, 769, 757, 733, 684, 635, 572, 541, 515.

2-Methyl-4-pyridin-2-yl-but-3-yn-2-ol, 71

The literature method was adapted.¹⁴ Thus, bis(triphenylphosphine)palladium dichloride (0.8 g, 1.14 mmol) was added to a solution of 2-bromopyridine (10 g, 63.3

mmol) and 2-methyl-2-hydroxy-but-3-yne (6.73 g, 80.0 mmol) in triethylamine (100 mL) under nitrogen. Copper iodide (0.54 g, 2.84 mmol) was added in one portion and the mixture stirred at room temperature for 24 h. Distilled water (200 mL) was added and extracted with diethyl ether (3 x 200 mL). The combined extracts were dried over sodium sulfate, and evaporated to give the crude product as a thick brown oil. Purification by chromatography over silica eluting with cyclohexane/ethyl acetate (2:1) gave **71** (6.54 g, 64%) as a yellow oil; δ_{H} (400 MHz, CDCl_3) 8.50 (1 H, d, $J=4.1$ Hz, 6-*H*), 7.56 (1 H, dt, $J=7.8, 1.8$ Hz, 4-*H*), 7.33 (1 H, dd, $J=7.8, 0.9$ Hz, 3-*H*), 7.15 (1 H, dq, $J=2.8, 5.0, 0.9$ Hz, 5-*H*), 4.42 (1 H, s br, O-*H*), 1.62 (6 H, s, 2 x CH_3); δ_{C} (100 MHz, CDCl_3) 149.6 (6-*C*), 143.0 (2-*C*), 136.3 (4-*C*), 127.1 (3-*C*), 122.8 (5-*C*), 94.9 (*sp-C*), 81.0 (*sp-C*), 65.0 (O- $\text{C}(\text{CH}_3)_2$), 31.2 (2 x CH_3); m/z (GC-MS): found 161 $[\text{M}]^+$, 146, 118, 104, 78. $\text{C}_{10}\text{H}_{11}\text{NO}$ requires: 161.

2-Ethynylpyridine, 72

To a solution of **71** (6.5 g, 40.3 mmol) in toluene (150 mL) was added sodium hydroxide pellets (1.7 g, 42.5 mmol) and the mixture rapidly stirred under nitrogen with heating to reflux for 4 h. The reaction was cooled to room temperature, filtered and evaporated carefully on a rotary evaporator with the water bath set at 40 °C, to afford **72** (4.1 g, 99%) as an orange-red oil; δ_{H} (400 MHz, CDCl_3) 8.57 (1 H, d, $J=4.6$ Hz, 6-*H*), 7.64 (1 H, dt, $J=7.8, 1.4$ Hz, 4-*H*), 7.46 (1 H, d, $J=7.8$ Hz, 3-*H*), 7.25 (1 H, t, $J=5.0$ Hz, 5-*H*), 3.14 (1 H, s, C-*H*); δ_{C} (100 MHz, CDCl_3) 150.1 (6-*C*), 142.4 (2-*C*), 136.2 (4-*C*), 127.5 (3-*C*), 123.4 (5-*C*), 82.4 (-CCH), 76.9 (-CCH); m/z (GC-MS): found 103 $[\text{M}]^+$, 76, 50. $\text{C}_7\text{H}_5\text{N}$ requires: 103.

1,2-Bis(2-pyridyl)ethyne, 73

The literature method was slightly modified.¹⁴ Thus, to a stirred solution of **72** (4.1 g, 39.8 mmol) in triethylamine (60 mL) was added bis(triphenylphosphine)palladium dichloride (0.45 g, 0.64 mmol) and copper iodide (0.23 g, 1.21 mmol). The reaction was inerted with nitrogen, 2-bromopyridine (4 mL, 41.9 mmol) added and the mixture heated to 70 °C for 3 h. The reaction was cooled to room temperature, distilled water (100 mL) added and extracted with dichloromethane (3 x 150 mL). The combined extracts were dried over sodium sulfate and evaporated. The material was purified by chromatography over silica eluting initially with cyclohexane/ethyl acetate (1:1) and then cyclohexane/ethyl acetate (1:2) to give **73** (2.3 g, 32 %) as a slightly yellow oil; δ_{H} (400 MHz, CDCl₃) 8.60 (2 H, m, 6-*H*), 7.66 (2 H, m, 4-*H*), 7.58 (2 H, m, 3-*H*), 7.24 (2 H, m, 5-*H*); δ_{C} (100 MHz, CDCl₃) 150.1 (6-*C*), 142.6 (2-*C*), 136.2 (4-*C*), 127.7 (3-*C*), 123.3 (5-*C*), 87.8 (*sp-C*); *m/z* (GC-MS): found 180 [M]⁺, 152, 128, 100, 74, 51. C₁₂H₈N₂ requires: 180.

5,6-Bis(pyridin-2-yl)-[1,3]dithiolo[4,5-b][1,4]dithiine-2-thione, 74

A solution of **73** (0.22 g, 1.20 mmol) in toluene (40 mL) and solid trithione **20** (0.48 g, 2.40 mmol) was stirred under reflux at 135 °C under a nitrogen atmosphere for 15 h. The mixture was allowed to cool to room temperature, filtered washing with chloroform (*ca.* 50 mL), and evaporated. The crude product was first purified by chromatography over silica, eluting with ethyl acetate to afford an orange band, which was collected and evaporated to yield a brown solid. This was further purified by chromatography over

silica, eluting with a mixture of cyclohexane/ethyl acetate (2:1) to afford **74** (0.36 g, 80 %) as a brown solid Mp 181 °C (Found C, 47.95; H, 2.1; N, 7.4. C₁₅H₈N₂S₅ requires C, 47.9; H, 2.1; N, 7.45%); ν_{\max} (ATR)/cm⁻¹ 1578, 1563, 1455, 1428, 1063, 992, 760, 740, 622, 505; δ_{H} (400 MHz, CDCl₃) 8.61 (2 H, dq, $J=4.9, 0.9$ Hz, 2 x 6'-H), 7.46 (2 H, dt, $J=1.8, 7.7$ Hz, 2 x 4'-H), 7.19 (2 H, ddd, $J=7.6, 4.8, 1.04$ Hz, 2 x 5'-H), 6.91 (2 H, td, $J=7.9, 1.0$ Hz, 2 x 3'-H); δ_{C} (100 MHz, CDCl₃) 213.9 (2-C), 154.2 (2 x 2'-C), 150.0 (2 x 6'-C), 136.9 (5-, 6-C), 136.3 (2 x 4'-C), 130.1 (3a-, 7a-C), 124.7 (2 x 3'-C), 123.4 (2 x 5'-C); m/z (EI): found: 375.9291 [M]⁺. C₁₅H₈N₂S₅ requires: 375.9285.

5,6-Bis(pyridin-2-yl)-[1,3]dithiolo[4,5-b][1,4]dithiine-2-one, 75

To a stirred solution of **74** (0.083 g, 0.22 mmol) in dry chloroform (20 mL), was added mercuric acetate (0.105 g, 0.33 mmol) under a nitrogen atmosphere. The suspension was stirred at room temperature for 35 min, filtered washing with dry chloroform (30 mL), and the filtrate washed with saturated sodium bicarbonate solution (10 mL). The organic phase was dried over sodium sulfate before evaporating to give **75** (0.055 g, 70 %) as an orange gum; ν_{\max} (ATR)/cm⁻¹ 1668, 1579, 1564, 1456, 1429, 993, 792, 760, 740, 622, 454; δ_{H} (400 MHz, CDCl₃) 8.61 (2 H, dq, $J=4.8, 0.9$ Hz, 2 x 6'-H), 7.46 (2 H, dt, $J=1.7, 7.6$ Hz, 2 x 4'-H), 7.18 (2 H, ddd, $J=7.6, 4.8, 1.0$ Hz, 2 x 5'-H), 6.93 (2 H, d, $J=7.8$ Hz, 2 x 3'-H); δ_{C} (100 MHz, CDCl₃) 192.2 (2-C), 154.4 (2 x 2'-C), 150.0 (2 x 6'-C), 136.7 (5-, 6-C), 136.3 (2 x 4'-C), 124.7 (2 x 3'-C), 123.3 (2 x 5'-C), 120.4 (3a-, 7a-C); m/z (EI): found: 359.9513 [M]⁺. C₁₅H₈N₂S₄O requires: 359.9514.

Bis[di(2'-pyridyl)vinylenedithio]tetrathiafulvalene, 69

The oxo compound **75** (0.04 g, 0.11 mmol) was heated in freshly distilled triethyl phosphite (3 mL) to 100 °C under a nitrogen atmosphere for 2 h 40 min. The reaction was allowed to cool to room temperature overnight, and filtered through a glass-sintered funnel, washing with diethyl ether (*ca.* 200 mL) to afford **69** (0.037 g, 97 %) as an orange solid Mp 213 °C (Found C, 52.2; H, 2.3; N, 8.1. C₂₀H₁₆N₄S₈ requires C, 52.3; H, 2.3; N, 8.1%); ν_{\max} (ATR)/cm⁻¹ 1581, 1556, 1460, 1422, 1090, 1044, 994, 919, 782, 759, 742, 661, 618; δ_{H} (400 MHz, CDCl₃) 8.58 (4 H, dq, $J=5.0, 0.9$ Hz, 4 x 6'-H), 7.44 (4 H, dt, $J=1.7, 7.6$ Hz, 4 x 4'-H), 7.15 (4 H, ddd, $J=7.6, 4.9, 1.1$ Hz, 4 x 5'-H), 6.92 (4 H, d, $J=7.8$ Hz, 4 x 3'-H); δ_{C} (100 MHz, CDCl₃) 154.7 (4 x 2'-C), 149.8 (4 x 6'-C), 137.4 (5-, 5''-, 6-, 6''-C), 136.2 (4 x 4'-C), 124.6 (4 x 3'-C), 123.1 (4 x 5'-C), 122.2 (*sp*²-C), 118.8 (*sp*²-C); m/z (ES)⁺: found: 688.9215 [M+H]⁺. C₃₀H₁₆N₄S₈ + H requires: 688.9213.

[Bis(2'-pyridyl)vinylenedithio](ethylenedithio)tetrathiafulvalene, 70

A mixture of the oxo compound **75** (0.4 g, 1.11 mmol) and thione **22** (1.00 g, 4.44 mmol) were heated together with stirring in freshly distilled triethyl phosphite (15 mL) under a nitrogen atmosphere to 110 °C. After 6 h the reaction was allowed to cool to room temperature, filtered through a glass-sintered funnel washing with diethyl ether (*ca.* 250 mL). The crude solid collected was purified by chromatography over silica eluting with chloroform/tetrahydrofuran (9:1) to afford **70** (0.32 g, 54 %) as a bright orange solid Mp 208 °C (Found C, 44.8; H, 2.2; N, 5.2. C₂₀H₁₂N₂S₈ requires C, 44.8; H,

2.2; N, 5.2%); ν_{\max} (ATR)/ cm^{-1} 1581, 1552, 1458, 1422, 995, 919, 769, 757, 741, 617, 484; δ_{H} (400 MHz, CDCl_3) 8.56 (2 H, dq, $J=4.9, 0.9$ Hz, 2 x 6'-H), 7.41 (2 H, dt, $J=1.8, 7.7$ Hz, 2 x 4'-H), 7.12 (2 H, ddd, $J=7.6, 4.8, 1.0$ Hz, 2 x 5'-H), 6.90 (2 H, td, $J=7.9, 1.0$ Hz, 2 x 3'-H), 3.28 (4 H, s, 2 x CH_2); δ_{C} (100 MHz, CDCl_3) 154.6 (2 x 2'-C), 149.8 (2 x 6'-C), 137.4 (5-, 6-C), 136.1 (2 x 4'-C), 124.6 (2 x 3'-C), 123.1 (2 x 5'-C), 122.1 (sp^2 -C), 116.2 (sp^2 -C), 114.2 (sp^2 -C), 113.7 (sp^2 -C), 30.1 (2 x CH_2); m/z (EI):found: 535.8763 $[\text{M}]^+$. $\text{C}_{20}\text{H}_{12}\text{N}_2\text{S}_8$ requires: 535.8761.

(70)(CuCl₂)₃(CH₃CN)_{0.75}(H₂O)_{1.5}, 82

A solution of copper (II) chloride (0.005 g, 0.04 mmol) in acetonitrile (4 mL) under an atmosphere of nitrogen was added to a hot solution of **70** (0.02 g, 0.04 mmol) in dichloromethane (5 mL). The mixture turned dark immediately, and was heated for 2 min at reflux. The mixture was allowed to cool to room temperature and filtered, washing with acetonitrile (20 mL) and dichloromethane (50 mL), and dried under high vacuum at room temperature, to afford **82** as a black solid Mp 184 °C (Found C, 25.7; H, 1.65; N, 4.0. (70)(CuCl₂)₃(CH₃CN)_{0.75}(H₂O)_{1.5} requires C, 25.9; H, 1.7; N, 3.9%); ν_{\max} (ATR)/ cm^{-1} 3183, 1594, 1556, 1470, 1425, 1103, 1055, 827, 763, 609; Raman/ cm^{-1} $\nu_4 = 1414, \nu_3 = 1466$.

3.3.5 Electrocrystallisation experimental section

(67)_{>1}(I₃)

To the anodic side of a H-shaped electrochemical cell fitted with a glass frit was placed **67** (10 mg, 0.02 mmol), and from the cathodic side of the cell was added a solution of tetrabutylammonium iodide (64.7 mg, 0.10 mmol) in tetrahydrofuran (25 mL). The level of solvent in each compartment was allowed to equilibrate, and to each side inserted a platinum-tipped electrode. A constant current of 0.1 μA was applied across the cell for 4 weeks giving black needles that grew as clusters in hedgehog shapes. Repetitions of the experiment afforded black crystalline materials visibly suitable for single crystal X-ray diffraction studies. However crystals selected showed no diffraction upon examination at the Daresbury synchrotron. Raman spectroscopy identified the presence of electron donors in the +1 and neutral oxidation states from the symmetrical C=C stretches at $\nu_4 = 1392$ and $\nu_3 = 1469$; and $\nu_4 = 1504$ and $\nu_3 = 1552$ cm^{-1} respectively. The crystals produced were not large enough for the attachment of gold wires for resistivity measurements.

(70)CoCl₄

To the anodic side of a H-shaped electrochemical cell fitted with a glass frit was placed **70** (10 mg, 0.02 mmol), and from the cathodic side of the cell was added a solution of tetrabutylammonium cobalt (II) tetrachloride (40.0 mg, 0.10 mmol) in dichloromethane (25 mL). The level of solvent in each compartment was allowed to equilibrate, and to

each side inserted a platinum-tipped electrode. A constant current of 0.1 μA was applied across the cell for 2 weeks affording black laths on the electrode Mp 206 °C.

(70-H)(ReO₄)₂(CH₂Cl₂)_{0.5}

To the anodic side of a H-shaped electrochemical cell fitted with a glass frit was placed **70** (10 mg, 0.02 mmol), and from the cathodic side of the cell was added a solution of tetrabutylammonium perrhenate (40.0 mg, 0.08 mmol) in dichloromethane (25 mL). The level of solvent in each compartment was allowed to equilibrate, and to each side inserted a platinum-tipped electrode. A constant current of 0.1 μA was applied across the cell for 3 weeks affording small black crystals Mp 173-174 °C (Found C, 21.9; H, 0.8; N, 2.3. C_{20.5}H₁₄ClN₂O₈Re₂S₈ requires C, 21.8; H, 1.3; N, 2.6%); Raman/cm⁻¹ $\nu_4 = 1418$, $\nu_3 = 1462$. Suitable crystals were analysed by single crystal X-ray diffraction.

3.4 References

- ¹ M. Kurmoo, A. W. Graham, P. Day, S. J. Coles, M. Hursthouse, J. L. Caulfield, J. Singleton, F. L. Pratt, W. Hayes, L. Ducasse and P. Guionneau, *J. Am. Chem. Soc.*, **1995**, 117, 12209.
- ² E. Ojima, H. Fujiwara, K. Kato, H. Kobayashi, H. Tanaka, A. Kobayashi, M. Tokumoto and P. Cassoux, *J. Am. Chem. Soc.*, **1999**, 121, 5581; H. Fujiwara, E. Fujiwara, Y. Nakazawa, B. Z. Narymbetov, K. Kato, H. Kobayashi, M. Tokumoto and P. Cassoux, *J. Am. Chem. Soc.*, **2001**, 123, 306.
- ³ E. Isomura, K. -I. Tokuyama, T. Nishinaga and M. Iyoda, *Tetrahedron Lett.*, **2007**, 48, 5895.
- ⁴ L. M. Goldenberg, J. Y. Becker, O. P. Levi, V. Y. Khodorkovsky, L. M. Shapiro, M. R. Bryce, J. P. Cresswell and M. C. Petty, *J. Mater. Chem.*, **1997**, 7, 901.
- ⁵ S. -X. Liu, S. Dolder, M. Pilkington and S. Decurtins, *J. Org. Chem.*, **2002**, 67, 3160.
- ⁶ W. Xu, D. Zhang, H. Li and D. Zhu, *J. Mater. Chem.*, **1999**, 9, 1245.
- ⁷ B. J. Coe, J. L. Harries, J. A. Harris, B. S. Brunshwig, S. J. Coles, M. E. Light and M. B. Hursthouse, *Dalton Trans.*, **2004**, 2935.
- ⁸ G. J. Rodriguez, R. Martin-Villamil, F. H. Cano and I. Fonseca, *J. Chem. Soc., Perkin Trans. 1*, **1997**, 709.
- ⁹ G. R. Newkome, J. M. Roper and M. J. Robinson, *J. Org. Chem.*, **1980**, 45, 4380.
- ¹⁰ H. D. Flack, *Acta Cryst.* **1983**, A39, 876.
- ¹¹ P. Guionneau, C. J. Kepert, G. Bravic, D. Chasseau, M. R. Truter, M. Kurmoo and P. Day, *Synth. Metals*, **1997**, 86, 1973.
- ¹² C. Jia, D. Zhang, Y. Xu, W. Xu, H. Hu, D. Zhu, *Synth. Metals*, **2003**, 132, 249.
- ¹³ T. Nogami, K. Inone, T. Nakamura, S.-i. Iwasaka, H. Nakano, T. Mikawa, *Synth. Metals*, **1987**, 19, 539.
- ¹⁴ S. A. Al-Taweel, *Phosphorus, Sulfur and Silicon*, **2002**, 177, 1041.

Chapter 4

Novel radical cation salts formed from ET

4 Novel radical cation salts formed from ET

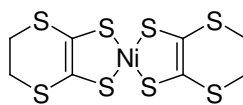
4.1 Synthesis of new radical cation salts of ET with the sulfamate anion

4.1.1 Introduction

The incorporation of hydrogen bonding potential into electron donor molecules or the anions employed in electrocrystallisation experiments, and resultantly in the radical cation salts generated, has been shown to significantly contribute to the crystallographic packing observed.^{1, 2} Weak donor-acceptor systems based upon derivatives of quinine have shown that hydrogen bonding exists to connect ‘ribbon-like’ layers of molecules, giving a three-dimensional supramolecular structure.³ Miyazaki *et al.* synthesised the radical cation salt γ -(ET)₃(HSO₄)₂ and determined it to crystallise in the space group P-1. The material underwent a metal to insulator transition at $T_{M-I} = 126$ K.⁴ The isostructural perchlorate salt exhibited a metal to insulator transition at $T_{M-I} = 170$ K.⁵ It has been shown that for tetrahedral anions, the temperature at which a transition into an insulating state occurs is strongly correlated with the unit cell volume.⁶ However, despite the marked difference in transition temperature for HSO₄⁻ and ClO₄⁻ salts, the unit cell volumes are virtually identical (1182 Å³ and 1181 Å³ respectively).

An explanation for the difference in transition temperatures is proposed in terms of hydrogen bonding. The existence of intermolecular hydrogen bonds between two hydrogensulfate anions enhances the stabilisation of the lattice structure allowing conductivity to persist to lower temperatures. Miyazaki prepared the deuterated

analogue in order to observe the isotope effect, however no significant difference in the transition temperature of the salt was observed. An isostructural system in which the central two carbons (C=C) of the electron donor were removed and replaced by a square planar coordinating transition metal was prepared (Ni(dddt)₂, **83**). The salt formed, [83]₃(HSO₄)₂, was found to undergo a metal to insulator transition at a much lower temperature T_{M-I} = 30 K.

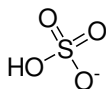


83

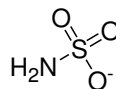
A range of salts in which the hydrogensulfate anion was replaced with the hydrogenselenate anion (HSeO₄⁻), were prepared by Kotov *et al.*⁷ The ET and [Ni(dddt)₂] derivatives with the larger selenium-based anion were synthesised, as was the mixed salt [(ET)_{1-x}[Ni(dddt)₂]_x]₃(HSO₄)₂. (ET)₃(HSeO₄)₂ was found to crystallise in space group P-1, with a unit cell volume of 1206.1 Å³. An insulating transition from a metallic phase is observed at T_{M-I} = 180 K. The asymmetric unit was found to contain two independent ET molecules, one of which lies in a general position and the other on the centre of symmetry. The donor molecules are arranged in stacks with a periodicity of three, with a longitudinal displacement between them. The core section of the donor molecules show that each ET molecule has almost identical bond lengths and thus each bears an equal charge of +2/3. No short intrastack S...S contacts were located, however many interstack S...S contacts were found. The close contacts are generally longer than those observed in the hydrogensulfate analogue, and this can be attributed to the larger anion volume of the hydrogenselenate salt.

The two anions present in the hydrogensulfate and hydrogenselenate salts are related by an inversion centre, forming a dimeric pair *via* two O-H...O hydrogen bonds. The distances between the two oxygen atoms connected by the hydrogen bond varies; (ET)₃(HSeO₄)₂, O...O: 2.574 Å; (ET)₃(HSO₄)₂, O...O: 2.605 Å; [Ni(ddd_t)₂]₃(HSO₄)₂, O...O: 2.615 Å.

Many polyfluorinated sulfonate anions have been incorporated into radical cation salts of ET.^{2, 8} Wang *et al.* prepared a range of salts in which the fluoroalkyl and fluoroaryl groups were systematically studied in determining their conducting properties. (ET)₂(C₆F₅SO₃).(C₂H₃Cl₃) was shown to be a semiconductor, whilst (ET)₂(C₆H₅CH₂SO₃).(H₂O) was found to be metallic in behaviour down to 200 K, below which a transition to an insulating phase occurred. A family of salts were prepared of general formula (ET)₂SF₅(R)SO₃ in which R = CHF₂, CHF, CH₂ and CF₂. The only superconducting salt containing a sulfonate anion is β''-(ET)₂SF₅CH₂CF₂SO₃, exhibiting a transition into a superconducting phase at T_C = 5 K.⁹ (ET)₄(naphthalenedisulfonate) was observed to have a weak semiconductor property from room temperature down to 210 K, at which point a strong metallic transition occurred and dominated to near absolute zero. However a superconducting phase transition was not observed.



84



85

Building on the work on the hydrogensulfate anion **84**, it was decided to attempt to prepare the sulfamate (**85**) salt of ET. The sulfamate ion could be expected to form dimeric pairs linked by N-H...O hydrogen bonds. The presence of the additional N-H bond could lead to further hydrogen bonding in the lattice structure.

4.1.2 Results and Discussion

Initial investigations into the electrocrystallisation of ET with tetrabutylammonium sulfamate were carried out in a range of uni-solvent systems consisting of acetonitrile, acetophenone, chlorobenzene, chloroform, dichloromethane, ethanol, methanol and tetrahydrofuran. Mixed bi-solvent systems were also investigated in chlorobenzene-ethanol (60:40 v/v) and 1,2,4-trichlorobenzene-ethanol (60:40 v/v). From these systems, only dichloromethane and tetrahydrofuran afforded oxidised crystalline material. Non-crystalline phases were isolated from anhydrous systems and identified by elemental analysis.

4.1.3 (ET)₃(H₂NSO₃)₂·2H₂O

Needle-shaped crystals of dimensions 2-4 mm x 1 mm x <0.1 mm were collected from the anode of the experiment conducted in dichloromethane. Suitable crystals were characterised by single crystal X-ray diffraction, Raman spectroscopy and elemental analysis.

(ET)₃(H₂NSO₃)₂·2H₂O was found to crystallise in the centrosymmetric space group P-1, with 1.5 donor molecules per asymmetric unit. The structure (Figure 39) is similar to those reported in the literature for the HSO₄⁻ and HSeO₄⁻ anions.^{4, 5, 7}

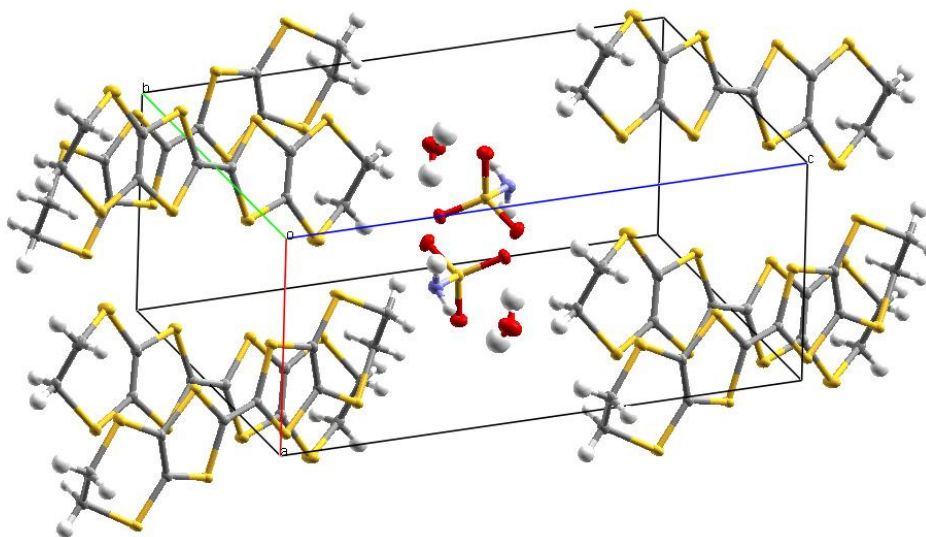


Figure 39: Representative diagram of the expanded unit cell of (ET)₃(H₂NSO₃)₂·2H₂O.

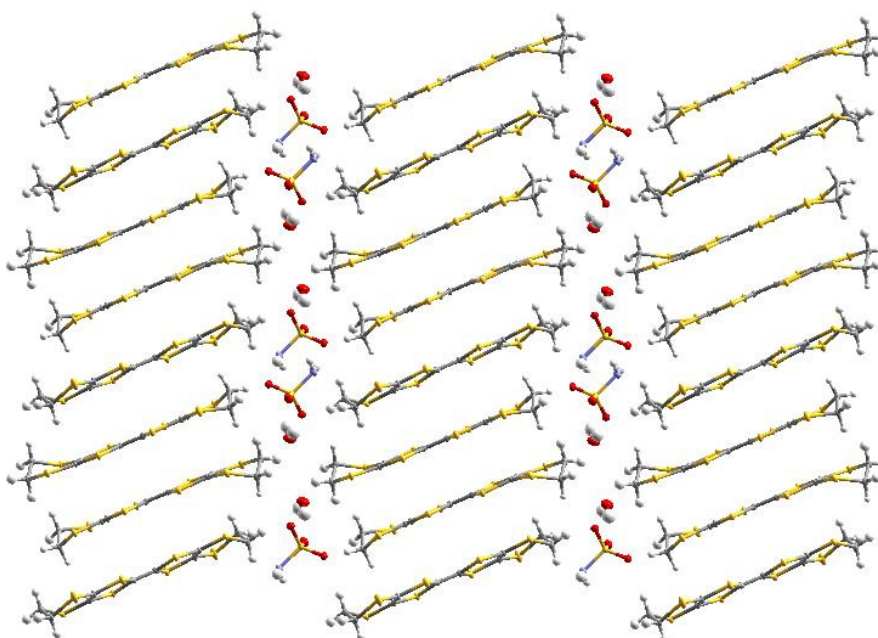


Figure 40: Crystal structure as viewed down the crystallographic *a* axis. Thermal ellipsoids are shown at the 50 % probability level.

There exist stacks of organosulfur electron donors extending along the crystallographic *b* axis (Figure 40 and Figure 41), with a repeating pattern involving three donor molecules.

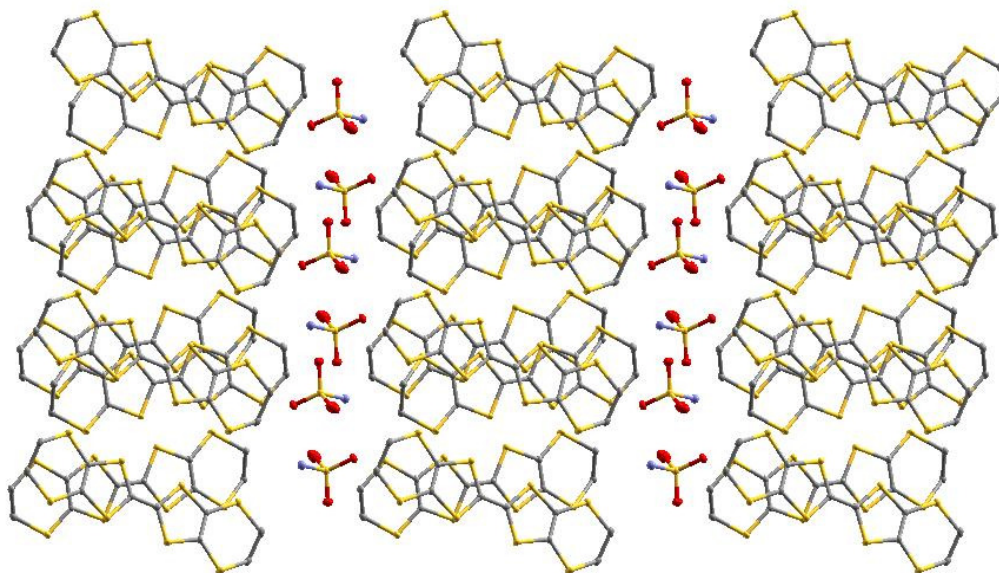


Figure 41: Organosulfur donors form stacks along the crystallographic *b* axis, as viewed down the *b* axis. Hydrogen atoms have been removed for clarity. Thermal ellipsoids are shown at the 50 % probability level.

The reflection data for the X-ray crystal structure was sufficiently good to allow the hydrogen atoms to be found and refined.

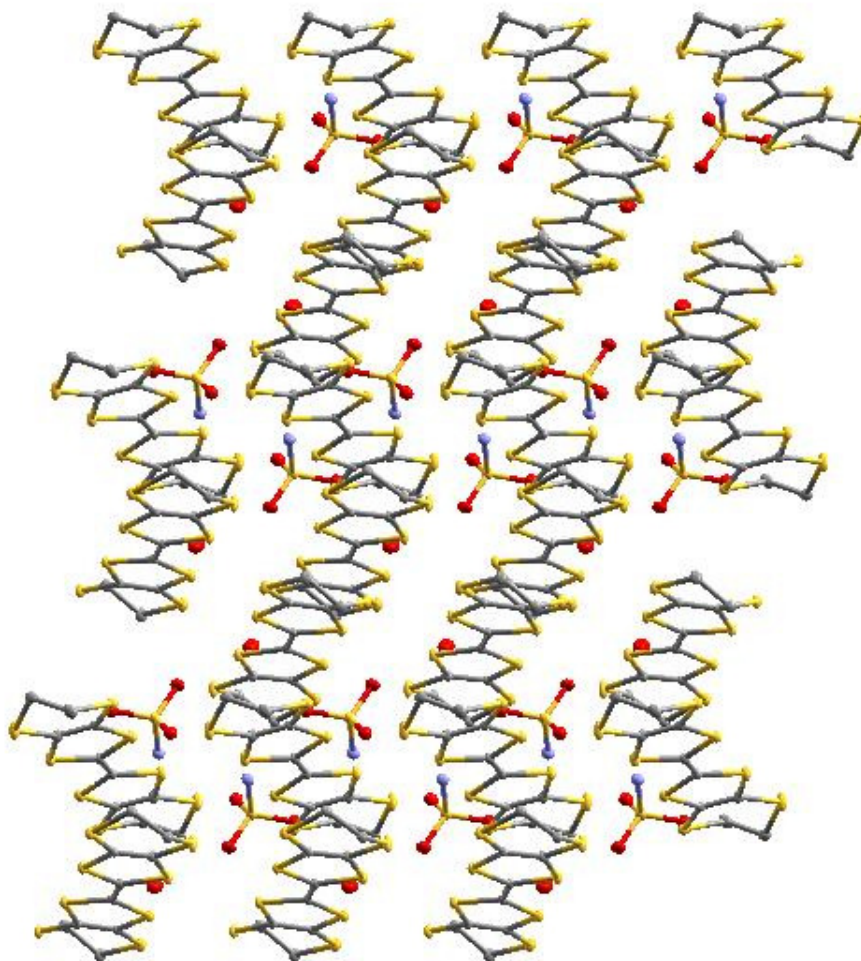


Figure 42: Crystal structure as viewed down the crystallographic *c* axis. Hydrogen atoms have been removed for clarity. Thermal ellipsoids are shown at the 50 % probability level.

A semi-twisted arrangement of donor molecules is observed (Figures 43 and 44) in the intrastack direction, with two electron donors (type I) lying more or less above each other orientated slightly to one direction and the third (type II) orientated (still within the stack of donors) with an observable twist in the opposite orientation.

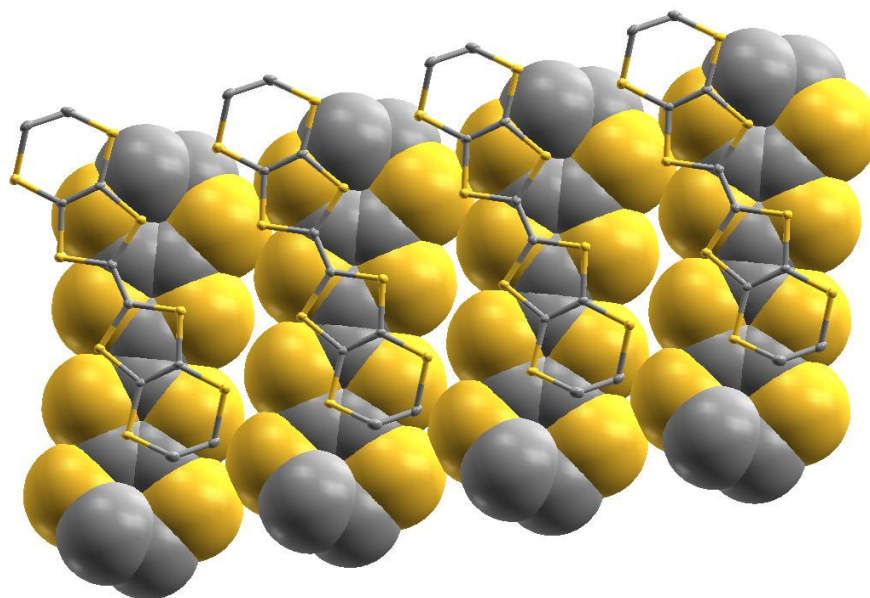


Figure 43: Twisted arrangement of the donor stacks, as viewed down the crystallographic *b* axis.

The stacks are separated from each other in the *c* direction by a network of anions and water molecules extending throughout the *ab* plane. The network of anions and water molecules consists of extensive hydrogen bonding, forming ribbons that extend in the crystallographic *a* direction, and are repeated in the *b* direction.

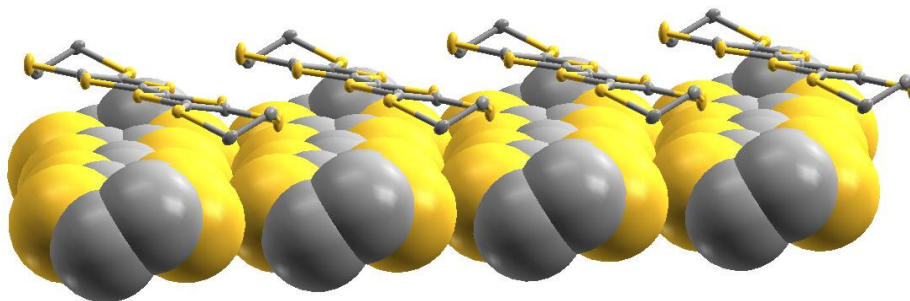


Figure 44: Twisted arrangement of the donor stacks, as viewed down the crystallographic *c* axis.

There are no short S...S contacts observed in the intrastack direction. There are, however, many short S...S contacts in the interstack direction. These vary between sheets, and are shown in Figure 45 and Figure 46.

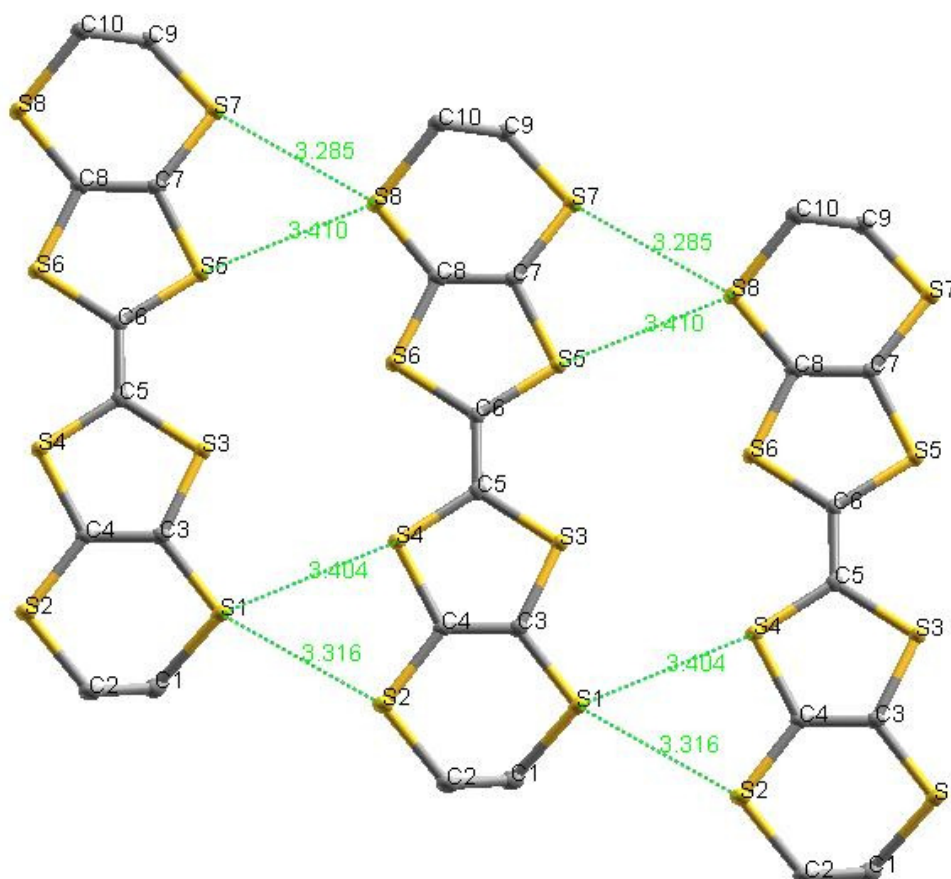


Figure 45: Interstack S...S close contacts in type I donor in the salt $(ET)_3(H_2NSO_3)_2 \cdot 2H_2O$. Thermal ellipsoids are shown at the 50 % probability level.

In the type I donor sheets (Figure 45), 75% of the sulfur atoms are involved in close contact interactions with sulfur atoms of the neighbouring donor molecule in the adjacent stack. The short contacts exist between S1...S2* (3.32 Å), S1...S4* (3.40 Å),

S5...S8* (3.41 Å) and S7...S8* (3.29 Å). Only S3 and S6 are shown to not experience short contact interactions.

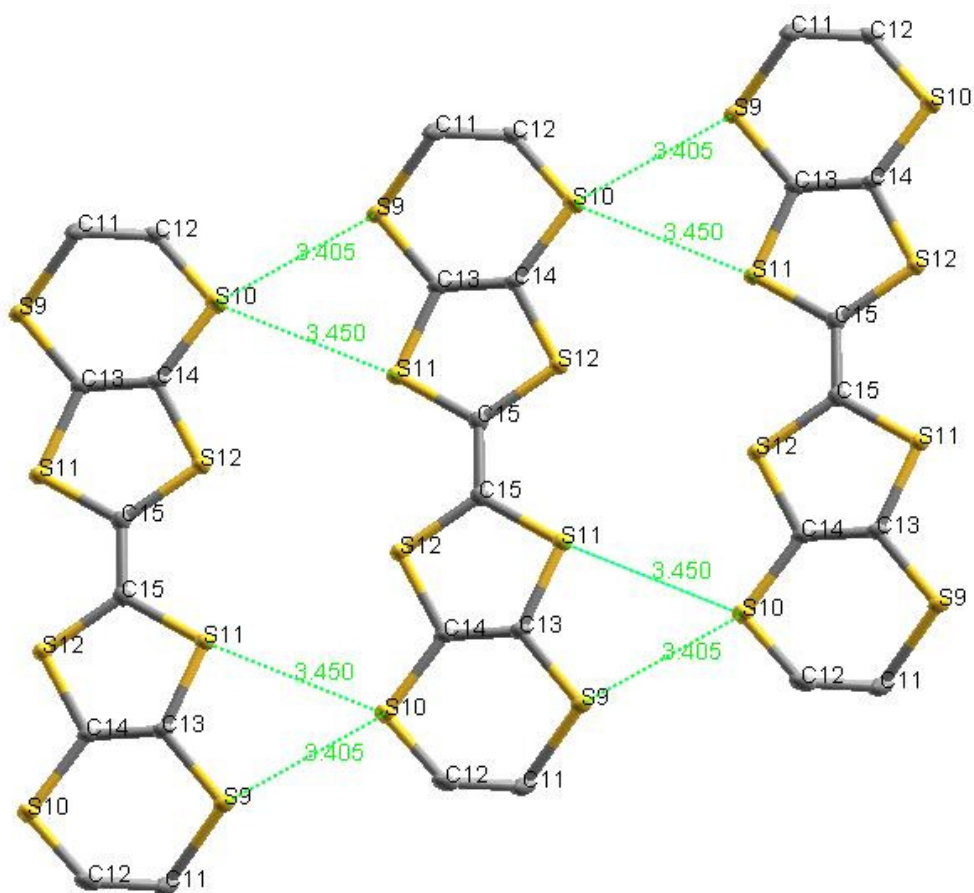


Figure 46: Interstack S...S close contacts in type II donor in the salt $(ET)_3(H_2NSO_3)_2 \cdot 2H_2O$.

Thermal ellipsoids are shown at the 50 % probability level.

In type II donor sheets (Figure 46), 75 % of the sulfur atoms are involved in close contact interactions with sulfur atoms of the neighbouring donor molecule in the adjacent stack. The short contacts exist between S9...S10* (3.41 Å), S11...S10* (3.45 Å), and the atoms generated by the symmetry operation due to the space group classification (having identical close contact distances). Only S12 and its symmetry generated equivalent do not participate in short contact interactions.

The close S...S contacts exhibited by the twisted overlapped donors of types I and II are shown overlaid in Figure 47.

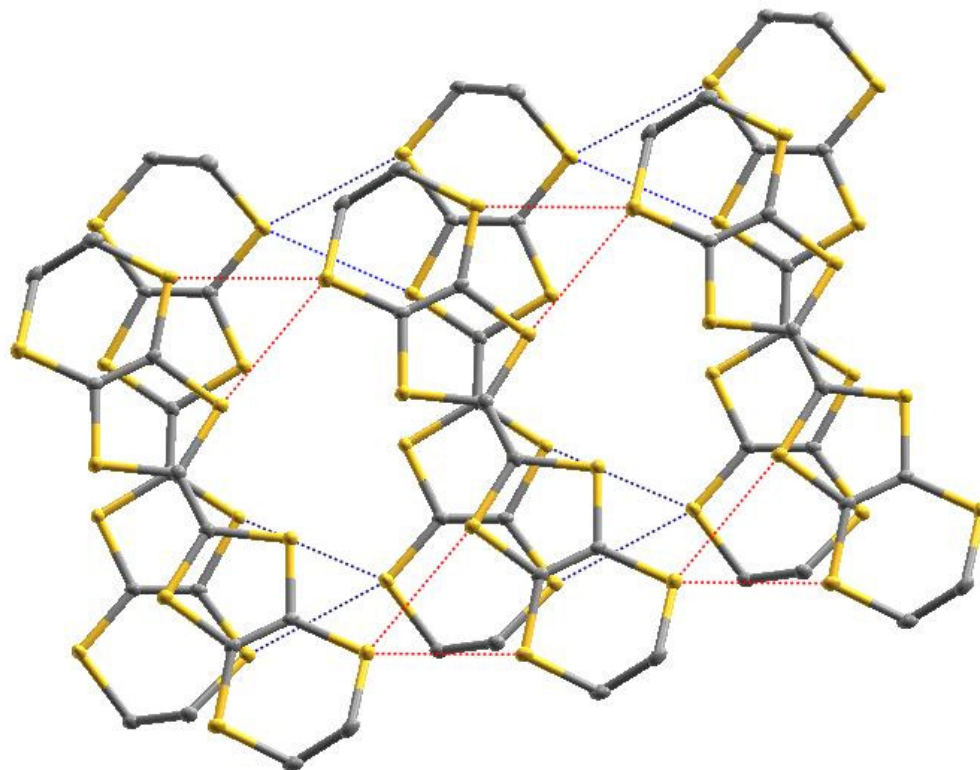


Figure 47: Overlapping of types I and II of donor molecule, with S...S short contacts shown.

From the X-ray crystal structure, it is expected that the radical cation salt would conduct electricity in one dimension only. By observation of the locations of the close contact interactions throughout the lattice structure, two parallel zones can be identified that represent the likely pathways of conductivity. The zones extend along the crystallographic a axis, i.e. in an interstack direction, perpendicular to the stacks. Measurements on the width of the pathways indicate close contacts that cover 8.29 Å of the c axis, accounting for approximately 50 % of this dimension.

The mixed anion-water layer showed an extensive hydrogen bonding network, as shown in Figure 48 and Figure 49. Water molecules were found to bridge between the anions *via* hydrogen bonding to sulfamate oxygens. The ribbons formed were well defined, evident from the small thermal ellipsoids of the atomic positions. The sulfamate was found to be hydrogen bonded through the oxygen atoms to the two neighbouring water molecules, O1...H4B and O3...H4A having distances 2.02 and 2.05 Å respectively. The sulfamate anion was shown to bond to a symmetry generated anion (labelled *) forming a dimeric species which exhibited N-H...O hydrogen bonding from O2...H3A* (2.24 Å), and O1...H3B* (2.25 Å).

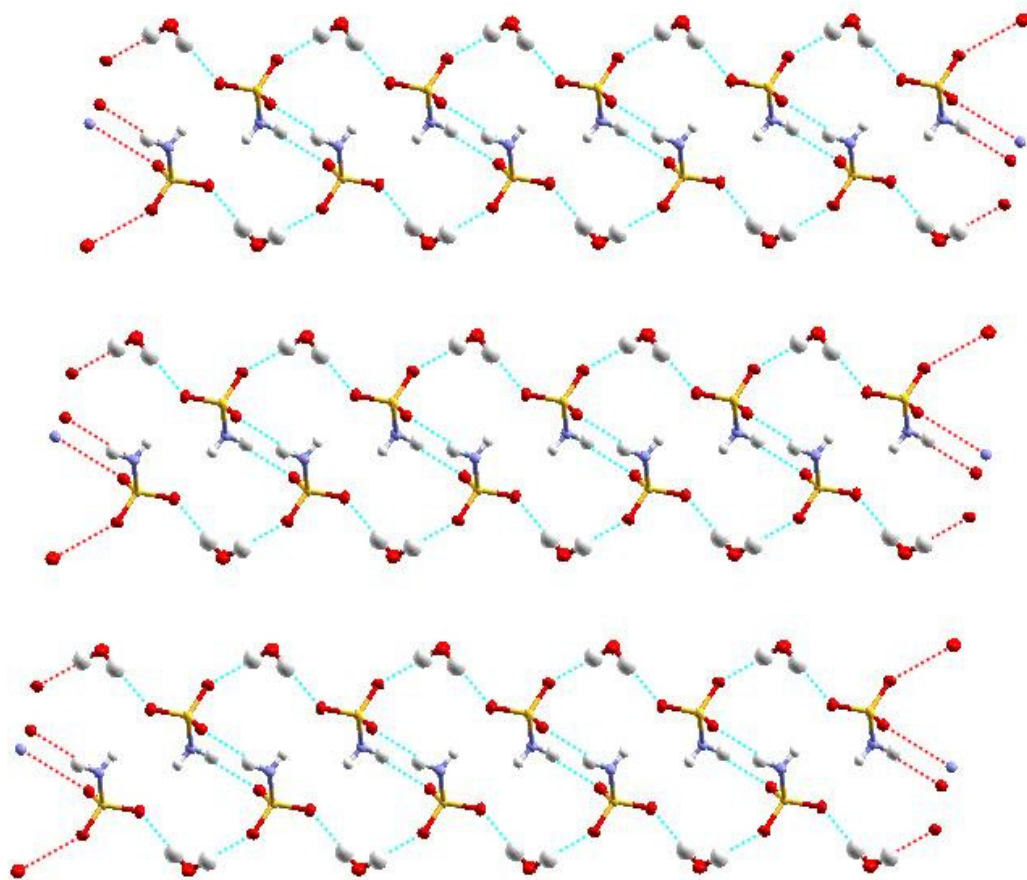


Figure 48: Supramolecular anion ribbons (left to right) of H_2NSO_3^- and H_2O , as viewed down the crystallographic c axis. Thermal ellipsoids are shown at the 50 % probability level.

The mixed anion-water channel dimensions were calculated from the X-ray crystal structure as an infinite channel running throughout the crystal lattice in the *a* direction, 8.04 Å wide in the *b* direction and 2.97 Å wide in the *c* direction.

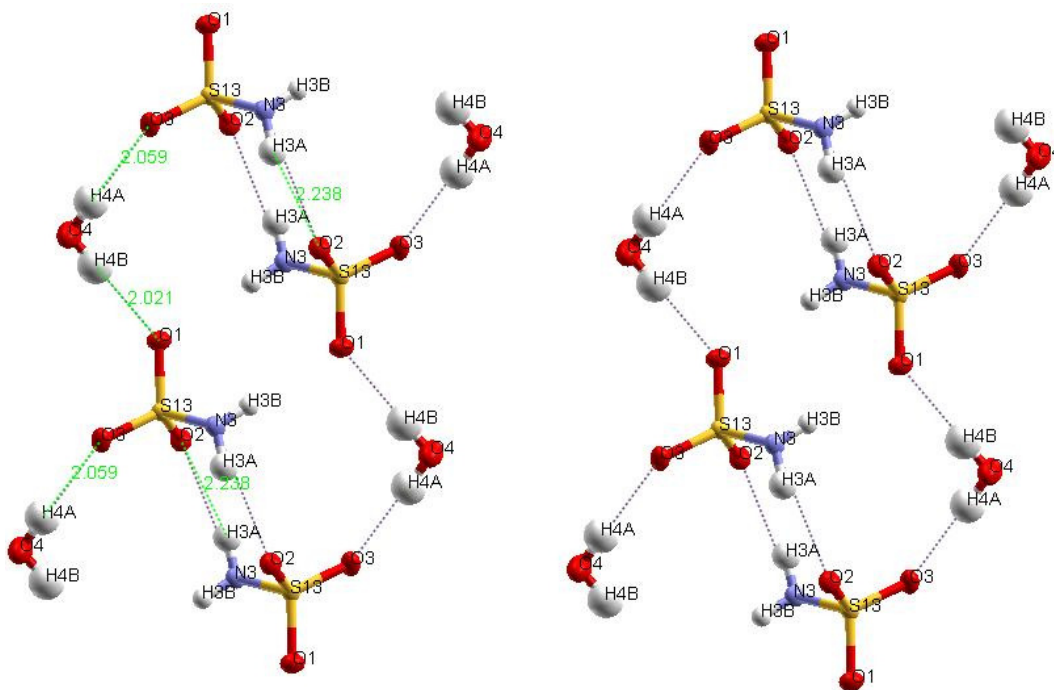


Figure 49: Numbering scheme and hydrogen bonding interactions within two anion channels (channels run top to bottom), as viewed down the crystallographic *c* axis. Thermal ellipsoids are shown at the 50 % probability level.

The encapsulated hydrated sulfamate anion ribbons are shown in Figure 50. The ethylene groups residing on the organosulfur donor molecules form the outer rim of the channel with eight donor molecules circling two anions. At its narrowest point, the channel was found to have a width (in the *c* plane) of 2.32 Å, whilst the largest section had a width of 4.72 Å. The length of channel (in the *b* plane) available for occupation in the channel was 8.55 Å. Each channel has a displacement from the next channel of 2.84 Å.

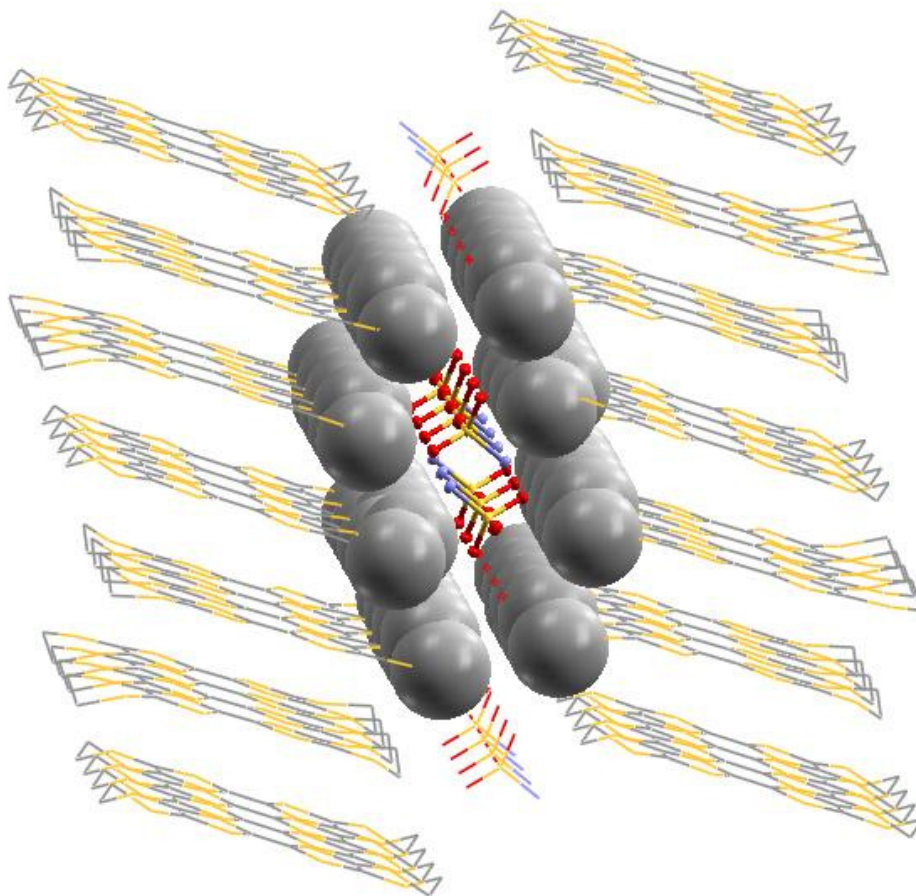


Figure 50: Encapsulation of the channel of hydrated dimeric H_2NSO_3^- anions by the ethylene functions. As viewed just off the crystallographic a axis.

4.1.4 Electron transfer properties of $(\text{ET})_3(\text{H}_2\text{NSO}_3)_2 \cdot 2\text{H}_2\text{O}$

The electron transport properties of the salt were initially investigated by the two-probe resistivity method. The resistivity profile is shown in Figure 51 as a function of temperature. Upon cooling from room temperature, the conductivity of the material increased to a maximum at around 200 K. Below this temperature the conductivity gently decreased. The profile suggests metallic behaviour that would probably result in

an insulating transition below liquid nitrogen temperatures, based on the electron donor packing motif.

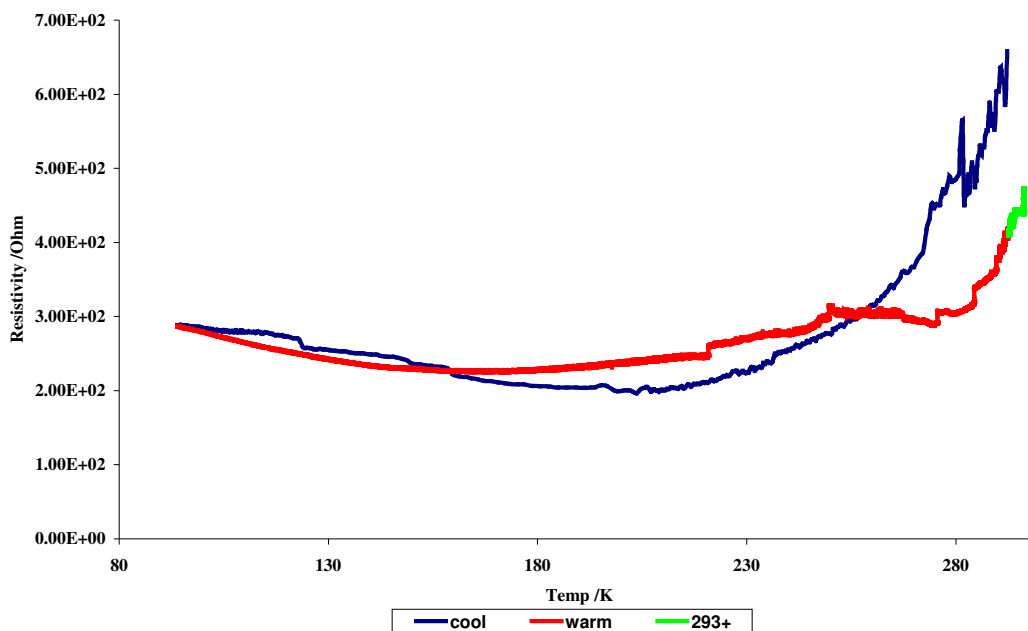


Figure 51: Resistivity data for $(\text{ET})_3(\text{H}_2\text{NSO}_3)_2 \cdot 2\text{H}_2\text{O}$ as a function of temperature.

The three colours used in Figure 51 indicate data collection upon cooling (blue) and re-warming (red). A sustained temperature of over 293 K is identified by the green data points. Resistivity measurements on a further sample revealed semiconductor behaviour (Figure 52) to around 111 K, with $E_a = 0.08$ eV in the range 111 – 275 K. X-ray crystallographic analysis was not performed on this sample, although Raman spectroscopy and measurement of the melting point suggested the composition to be the same as the determined $(\text{ET})_3(\text{H}_2\text{NSO}_3)_2 \cdot 2\text{H}_2\text{O}$.

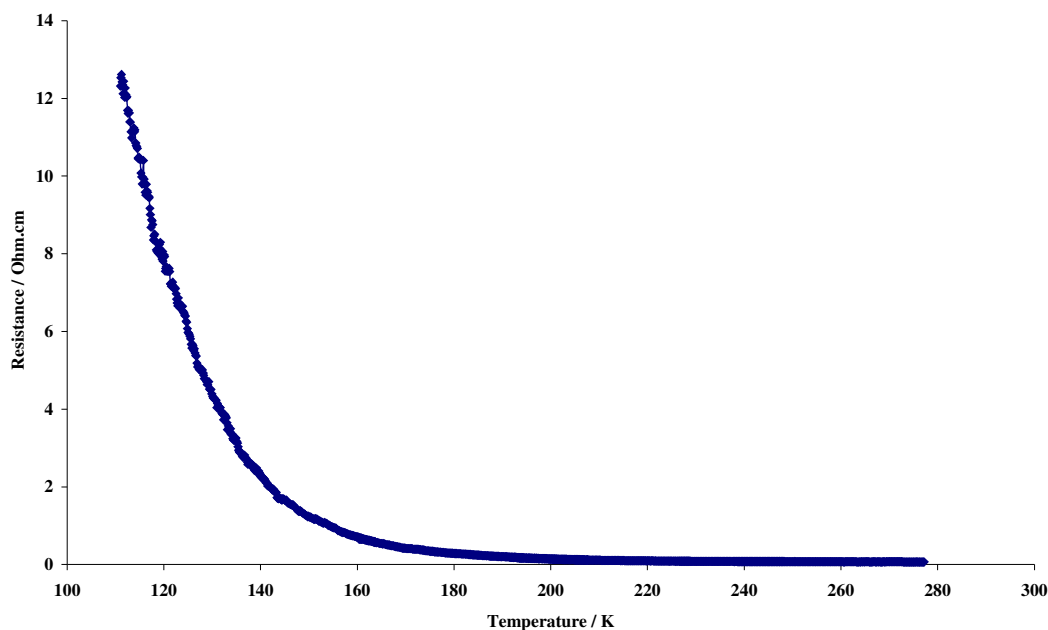


Figure 52: Resistivity against temperature for a further sample of $(\text{ET})_3(\text{H}_2\text{NSO}_3)_2 \cdot 2\text{H}_2\text{O}$.

4.1.5 Charge state of the donor species

Raman spectroscopy measured on multiple crystals identified symmetrical stretching modes of the central C=C bond as $\nu = 1421, 1460, 1476$ and 1490 cm^{-1} , and indicated the oxidation state of the donor molecules to be in the region of +0.5 to +0.9, as according to the method of Wang *et al.*¹⁰ Confirmation of the charge states was achieved from bond length measurements in the X-ray crystal structure, according to the method of Guionneau *et al.*¹¹ The two type I donors lying almost directly above each other each carry a charge of +0.5, and the remaining type II donor carries a charge of +0.8. The total charge calculated is +1.8 in good agreement with that expected (+2.0) for the summed charge of the three donor atoms. Elemental analysis on the bulk sample

was in agreement with the results inferred by Raman spectroscopy and the X-ray crystal structure.

4.1.6 Experimental

5,6-Dihydro-[1,3]dithiolo[4,5-b][1,4]dithiine-2-one, **23**

To a stirred solution of thione **22** (5.0 g, 22.3 mmol) in chloroform (100 mL) was added mercuric acetate (10.68 g, 33.5 mmol) and the mixture stirred under nitrogen for 2 h. The reaction was filtered, washing with chloroform (*ca.* 50 mL), and the filtrate washed with saturated sodium bicarbonate solution (10 mL), dried over magnesium sulfate and evaporated to give **23** (3.94 g, 85%) as a yellow solid Mp 123 °C (lit.¹² 125 °C); δ_{H} (400 MHz, CDCl₃) 3.37 (4 H, s, 2 x CH₂); δ_{C} (100 MHz, CDCl₃) 188.7 (2-C), 113.3 (2 x sp²-C), 31.0 (2 x CH₂).

Bis(ethylenedithio)tetrathiafulvalene, ET, **11**

Carbonyl compound **23** (3.5 g, 16.8 mmol) was heated in freshly distilled triethyl phosphite (15 mL) under nitrogen for 6 h. The reaction was allowed to cool to room temperature, and filtered washing with *n*-hexane (*ca.* 100 mL) and diethyl ether (*ca.* 50 mL). Drying *in vacuo* gave **11** (3.07 g, 95%) as an orange solid laced with orange-red crystals. Recrystallisation from chloroform afforded orange-red crystals Mp 248 °C (lit. 245-247 °C); ν_{max} (ATR)/cm⁻¹ 2963, 2922, 1508, 1422, 1407, 1283, 1260, 1173, 1126,

997, 918, 906, 889, 875, 819, 771, 686, 653, 624, 498; (Raman)/ cm^{-1} $\nu_4 = 1498$, $\nu_3 = 1552$ (lit.¹³ 1495, 1554).

To the anodic side of a H-shaped electrochemical cell fitted with a glass frit was placed **11** (10 mg, 0.02 mmol), and from the cathodic side of the cell was added a solution of tetrabutylammonium sulfamate (40 mg, 0.12 mmol) in dichloromethane (25 mL). The level of solvent in each compartment was allowed to equilibrate, and to each side inserted a platinum-tipped (length 15 mm, diameter 1mm) electrode. A constant current of 0.1 μA was applied across the cell for two weeks, and then increased to 1.0 μA for one week after which time shiny black needles had formed on the anode. These were collected from the electrode, and characterised by single crystal X-ray diffraction. Two probe resistivity measurements were performed along the long axis of the crystal, corresponding to the crystallographic *c* axis.

An identical experiment was carried out in tetrahydrofuran (25 mL), which afforded microcrystalline needles on the electrode that were subsequently determined to be twinned. Raman spectroscopy identified the material as $(\text{ET})_3(\text{H}_2\text{NSO}_3)_2$ with identical bands being observed (within the error on the machine) as for the determined structure $(\text{ET})_3(\text{H}_2\text{NSO}_3)_2 \cdot 2\text{H}_2\text{O}$. The salt exhibited an identical Mp 218-220 °C to the crystals formed in dichloromethane.

Further experiments were conducted with the rigorous exclusion of water, thus in each case the reagents were dried under vacuum, and the solvents (dichloromethane, tetrahydrofuran) freshly dried, distilled and de-gassed prior to use.¹⁴ The

electrochemical cells were well dried in an oven and allowed to cool under a flow of nitrogen gas. The electrocrystallisation experiments were set up according to the procedure outlined above, and inerted with nitrogen gas before inserting electrodes and sealing. The current was set at 0.1 μA , and after one week, dark material grew on the electrodes in both the dichloromethane and tetrahydrofuran experiments. After a further week, the materials were harvested and found to consist completely of amorphous solids. Elemental analysis data, melting points and Raman spectroscopy were performed on the compounds, and the materials subsequently determined:

From tetrahydrofuran: Mp 219-220 $^{\circ}\text{C}$; Found C, 27.4; H, 1.9; N, 2.3. $(\text{ET})_3(\text{H}_2\text{NSO}_3)_2$ requires: C, 26.8; H, 2.1; N, 2.1%; (Raman)/ cm^{-1} $\nu_{4(a)}$ 1440, $\nu_{4(b)}$ 1450, $\nu_{4(c)}$ 1460, $\nu_{3(a)}$ 1465, $\nu_{3(b)}$ 1478, $\nu_{3(c)}$ 1500.

From dichloromethane: Found C, 19.3; H, 2.1; N, 5.8. $(\text{ET})_2(\text{H}_2\text{NSO}_3) \cdot (\text{H}_2\text{NSO}_3\text{H})_4$ requires: C, 19.2; H, 2.4; N, 5.6%; (Raman)/ cm^{-1} $\nu_{4(a)}$ 1450, $\nu_{4(b)}$ 1460, $\nu_{3(a)}$ 1469, $\nu_{3(b)}$ 1494.

The oxidation states for the ET molecules in the salt formed in tetrahydrofuran, as determined by Raman spectroscopy, are +0.8, +0.7 and +0.5, with a total charge of +2.0. This agrees with the elemental analysis data obtained.

The oxidation states of the organosulfur electron donor in the salt formed in dichloromethane, as determined by Raman spectroscopy, are +0.7 and +0.5, with a total charge of +1.2. The elemental analysis data suggests a stoichiometry of 2:5 electron

donors to anions, thus the remaining charge must be counteracted by the presence of protons. The proposed structure fits the data reasonably well and accounts for the charges observed, with one anion stabilising the combined charge of the two donors, and the addition four anions present as their corresponding acid forms.

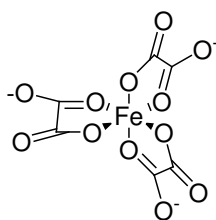
4.2 Electrochemical synthesis of new structures of ET chromium hexathiocyanate, (ET)₄[Cr(NCS)₆]

4.2.1 Introduction

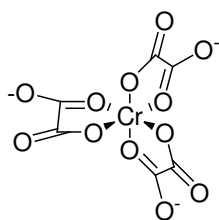
Over recent years, a dramatic increase in research into bifunctional materials exhibiting electron-conducting and magnetic properties has occurred. Such materials could offer themselves to applications in molecular computing, memory devices and switches.

The introduction of the magnetic properties (magnetic spin) may be included by two different means:

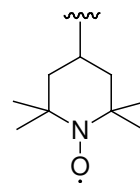
- 1) Inclusion of metal centres (such as **86** and **87**, where the metal atoms are in oxidation state III) within the lattice structure of the material; or
- 2) Incorporation of a spin radical unit, such as ‘TEMPO’ **88**.



86



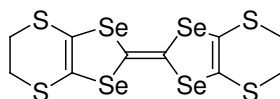
87



88

The incorporation of metal centres has seen the larger share of research, no doubt due to the large variation in magnetic properties achievable simply by changing the metal employed in the synthesis. Metal halide salts have been employed in radical cation salt

formation and have led to materials such as the bis(ethylenedithio)tetraselenafulvalene (BETS, **89**) salt, λ -(BETS) $_2$ FeCl $_4$, in which the interactions of the π - and d- electrons are found to have important roles in the magnetic properties observed, with superconductivity being induced by an applied magnetic field.^{15, 16} The κ -phase of the salt has also been shown to exhibit antiferromagnetism and superconductivity.^{17, 18, 19}



89

Metal thiocyanate complexes have been widely investigated also. Electrical-insulating TTF-based materials have been prepared by electrocrystallisation, that display ferromagnetic or antiferromagnetic phases, and investigation into the X-ray crystal structure allowed the determination of the reasons for the low conductivity observed.²⁰ The derivation of the magnetic properties could not however, be easily interpreted from the lattice coordinates.

Similar radical cation salts, in which chromium- and iron- tetra*is*thiocyanate complexes have their octahedral coordination environments further furnished with either phenanthroline or isoquinoline ligands, have been shown to exhibit long range ferromagnetic ordering.^{21, 22} The materials again demonstrated low electrical conductivity due to the isolated donor units reducing orbital overlap capability *via* S \cdots S close contacts. Comparable magnetic properties were observed when the electron donor molecule employed was ET.²³

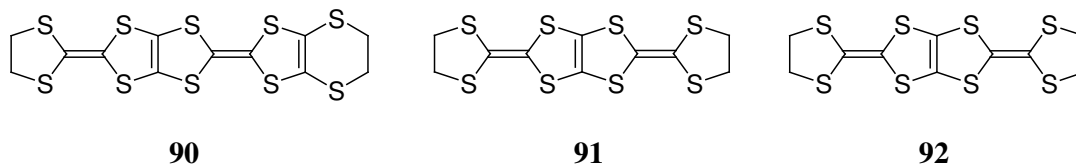
Carlson *et al.* prepared the salt $(\text{ET})_2[\text{Cu}(\text{NCS})_2]$ and the analogous compounds where the Cu had been exchanged for Ag and Au.²⁴ Superconducting salts exhibiting a κ -type packing motif were formed for the copper salt over a wide range of conditions, and the transition into a superconducting phase occurred at $T_C = 9.4 \pm 0.3$ K.

Müller *et al.* observed a deviation in the T_C for $(\text{ET})_2[\text{Cu}(\text{NCS})_2]$ in the range of 7.75-9.3 K and was able to attribute this to a dependency upon the method of preparation of the electron donor molecule, the source of the anion in the experiment *cf.* CuSCN/KSCN *vs.* $[\text{Cu}(\text{SCN})_2]^-$ and the solvent employed.²⁵

High ratios of donor to anion have also been observed in radical cation salts obtained from chromium hexaisothiocyanate. Salts with stoichiometries of up to 5.5:1 have been observed.²⁶ Bérézovsky *et al.* synthesised $(\text{ET})_{5.5}[\text{Cr}(\text{NCS})_6]$ by electrocrystallisation and found that it exhibited normal paramagnetic behaviour between 300-50 K, below which the material deviated from the Curie law. The crystal structure was determined to be centrosymmetric, having space group P-1. A stacked motif was observed for the ET molecules, although each donor moiety had a different valence state, with mixed organic/inorganic layers comprised of the anionic metal centre and ET^0 molecules.

Semiconducting and metallic salts have been isolated when employing the electron donors 2-(4,5-ethylenedithio-1,3-dithiol-2-ylidene)-5-(1,3-dithiolan-2-ylidene)-1,3,4,6-tetrathiapentalene (EDDH-TTP, **90**) and 2,5-bis(1,3-dithiolan-2-ylidene)-1,3,4,6-tetrathiapentalene (BDH-TTP, **91**). They were found to exhibit Curie-Weiss behaviour indicating weak exchange interactions occurring between the magnetic centres.²⁷ Weak

ferromagnetism has also been observed in ferromagnetic chains derived from the electron donor 2-(1,3-dithiolan-2-ylidene)-5-(1,3-dithiole-2-ylidene)-1,3,4,6-tetrathiapentalene (DTDH-TTP, **92**).²⁸



Over the last decade there has been a re-focussing of the research away from the thiocyanate complexes since the discovery of the metal Δ - and Λ -trisoxalate complexes and the first molecular superconductor containing paramagnetic metal centres.²⁹ Kurmoo *et al.* synthesised the radical cation salt β'' -(ET)₄[(H₃O)Fe(C₂O₄)₃].C₆H₅CN in 1995, and demonstrated for the first time an organic superconducting lattice with isolated localised magnetic moments present on the anionic centres. A transition into a superconducting phase was observed at T_C = 8.3 K (guest molecule = benzonitrile), however isomorphous structures containing different guest molecules were found to demonstrate alternative T_Cs. Thus when the guest solvent molecule was replaced with nitrobenzene, there was a decrease to T_C = 5.8 K,³⁰ and when the guest was pyridine no superconductivity was observed at all, with the metallic character being lost as the material became semiconducting at 116 K.³¹ Sun *et al.* have also reported β -(ET)₄[(H₂O)Fe(C₂O₄)₃].C₆H₅NO₂ a semiconducting magnetic radical cation salt, which remained conducting at 20 K.³² Since then, the mixed metal salt (ET)₃[MnCr(C₂O₄)₃] has been prepared and shown to exhibit both metallic conductivity, and a coexisting ferromagnetic state.³³

Thétiot and co-workers prepared the hexaisothiocyanate salt $(\text{ET})_4[\text{Cr}(\text{NCS})_6] \cdot \text{C}_6\text{H}_5\text{CN}$ and found that it exhibited semiconducting properties.³⁴ X-ray crystallographic analysis showed that the salt crystallised in the space group $P2_1$, exhibiting four unique donor molecules, a metal anion and a solvent molecule. Magnetic data shows the presence of antiferromagnetic coupling between organic components, which are independent of the inorganic components, supported by analysis of the lattice structure.

Recently, the emphasis has been on the incorporation of chirality into the lattice in the hope of reducing positional disorder. There exist two avenues with which molecular chirality can be achieved, by:

- 1) Employing enantiopure electron donor molecules, and
- 2) Employing enantiopure anions/ electron acceptor molecules.

A third option is available which may lead to supramolecular chirality:

- 3) Induction by the local presence of chiral species.

Martin *et al.* prepared the radical cation salt $\beta''\text{-(ET)}_4[(\text{H}_3\text{O})\text{M}^{3+}(\text{C}_2\text{O}_4)_3]$ ($\text{M} = \text{Cr}, \text{Fe}$), in which the two enantiomers of the metal trisoxalate existed in separate discrete channels (Figure 53).³⁵

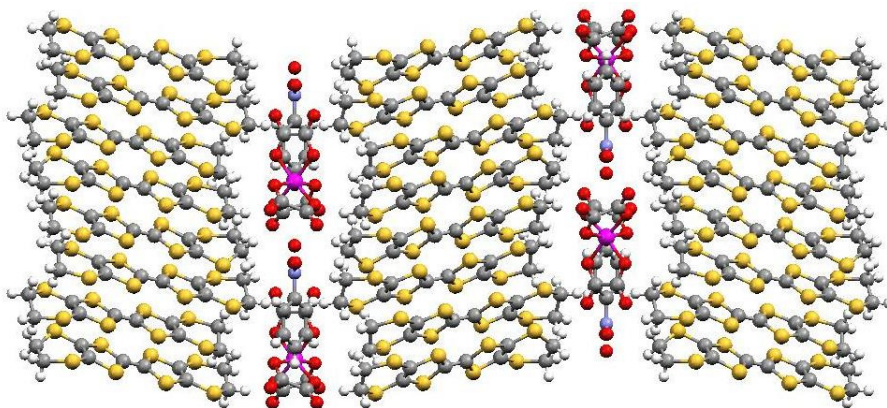


Figure 53: $\beta''\text{-(ET)}_4[(\text{H}_3\text{O})\text{M}^{3+}(\text{C}_2\text{O}_4)_3]$ ($\text{M} = \text{Cr}, \text{Fe}$), showing isolated channels of D- and L-enantiomers of the trisoxalate, thus overall the material is racemic [Reproduced with permission of Dr Lee Martin].

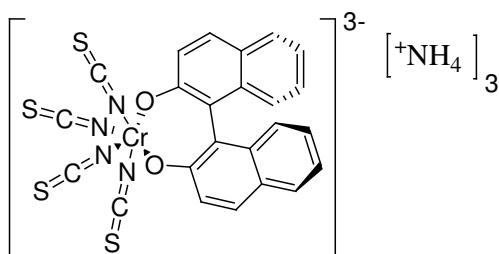
In addition to the increased occupational ordering possible, the incorporation of chirality may lead to other interesting phenomena, such as magnetochiral anisotropy.³⁶

Building on this work, it was decided to prepare transition metal complexes bearing chiral bidentate ligands. The incorporation of chirality in this fashion should significantly reduce the possibility of racemisation, a problem which was encountered with the Δ and Λ enantiomers of some metal trisoxalates.^{37, 38}

4.2.2 Results and Discussion

It was decided to synthesise three coordination complexes derived from Reinecke's Salt. One complex would contain the sterically bulky chirally pure (*R*)-(+)-2,2-bi(naphthol) ligating species, another the 2-(4'-(*S*)-Isopropyl-4',5'-dihydro-oxazol-2'-yl)-pyridine ligand, and the third the 2'-Pyridin-2-yl-4',5'-dihydro-thiazole-4'-(*S*)-carboxylic acid ligand.

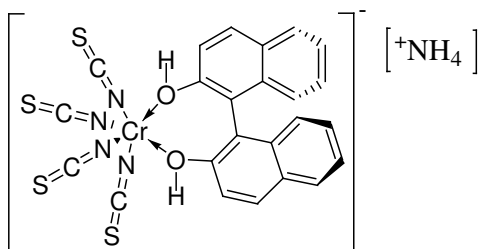
The large steric requirements of the binaphthol ligand were expected to greatly influence the packing arrangement exhibited, and ready access to both enantiopure ligands could allow for comparisons to be made with regard to the conducting properties for each enantiomer. The large π -electron system of the ligand also affords access to π/π bonding interactions, which could serve to stabilise the structure and hence increase the conductivity of the material. The preparation of coordination complex **93** was attempted by refluxing an acetonitrile solution of ammonium chromium-bis(ammine)-tetraisothiocyanate ‘Reinecke’s Salt’ with (*R*)-(+)-2,2-bi(naphthol). A purple precipitate was isolated which showed from elemental analysis and infrared data that the coordinated ammonia molecules had been displaced. The product formed was determined to be either the $[\text{NH}_4][\text{H}^+]_2$ salt (in which the metal complex has an overall charge of -3), or the complex in which the bi(naphthol) ligand had formed dative bonds through the electron lone pairs on the oxygen atoms, giving a metal complex of overall -1 charge (stabilised by the ammonium cation).



93

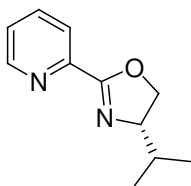
Mass spectrometry did not conclusively determine the identity of the metal complex, but confirmed the presence of the {bi(naphthol)-2H} species with a peak at m/z 284.8,

and the presence of the $\{\text{Cr}(\text{NCS})_4\}$ species with a peak at 283.8. The salt was tentatively assigned as the lone-pair coordinated mono-anionic species **94**.

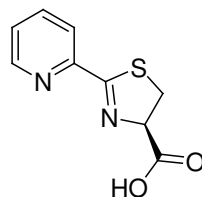


94

Employing microwave chemistry, the ligands **95** and **96** were prepared by heating 2-cyanopyridine with either *L*-valinol or *L*-cysteine respectively. After purification, the ligands were isolated and characterised.

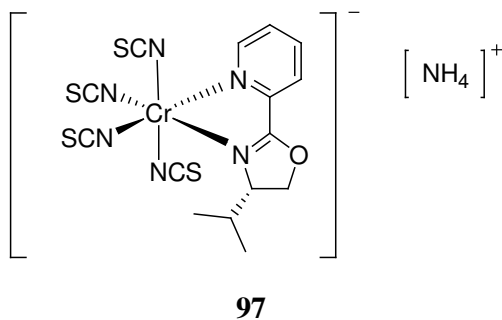


95



96

Coordination of the ligands was attempted by refluxing an acetonitrile solution of Reinecke's salt with the corresponding ligand in a 1:1 stoichiometry. Coordination complex **97** was isolated after reaction and characterised by elemental analysis and infrared spectroscopy, however the material produced from Reinecke's salt and ligand **96** could not be identified by elemental analysis, mass spectrometry or infrared spectroscopy.



The constant current electrocrystallisation of ET with **94** was performed at room temperature in a mixed solvent system of nitrobenzene and acetonitrile. The dark crystals produced were harvested from the electrode and studied by single crystal X-ray diffraction. Most notably, the structure was found to not contain the chiral metal complex, but instead the chromium hexaisothiocyanate complex.

Crystal data for $C_{52}H_{37}CrN_7O_2S_{38}$, $M = 2062.17$, black block, $0.20 \times 0.20 \times 0.10 \text{ mm}^3$, monoclinic, space group $P2_1$ (No. 4), $a = 11.795(2)$, $b = 20.144(4)$, $c = 16.395(3) \text{ \AA}$, $\beta = 101.03(3)^\circ$, $V = 3823.5(13) \text{ \AA}^3$, $Z = 2$, $D_c = 1.791 \text{ g/cm}^3$, $F_{000} = 2092$, Bruker SMART APEX2 CCD diffractometer, synchrotron radiation, $\lambda = 0.6942 \text{ \AA}$, $T = 120(2)\text{K}$, $2\theta_{\text{max}} = 61.1^\circ$, 39216 reflections collected, 20865 unique ($R_{\text{int}} = 0.0356$). Final $Goof = 1.032$, $R1 = 0.0507$, $wR2 = 0.1382$, R indices based on 19698 reflections with $I > 2\sigma(I)$ (refinement on F^2), 901 parameters, 1 restraint. Lp and absorption corrections applied, $\mu = 1.235 \text{ mm}^{-1}$.

The salt exhibited a columnar motif of ET molecules extending in the crystallographic b direction, with a periodic nitrobenzene molecule incorporated in a central position (of

the donor molecule stack). Observation of the lattice along the crystallographic *a* axis (Figure 54) showed the columnar arrangement of the donor stacks, with the chromium hexaisothiocyanate anions extending parallel to the electron donor stacks. The orientation of the nitrobenzene molecule is inverted due to the symmetry exhibited within the crystal.

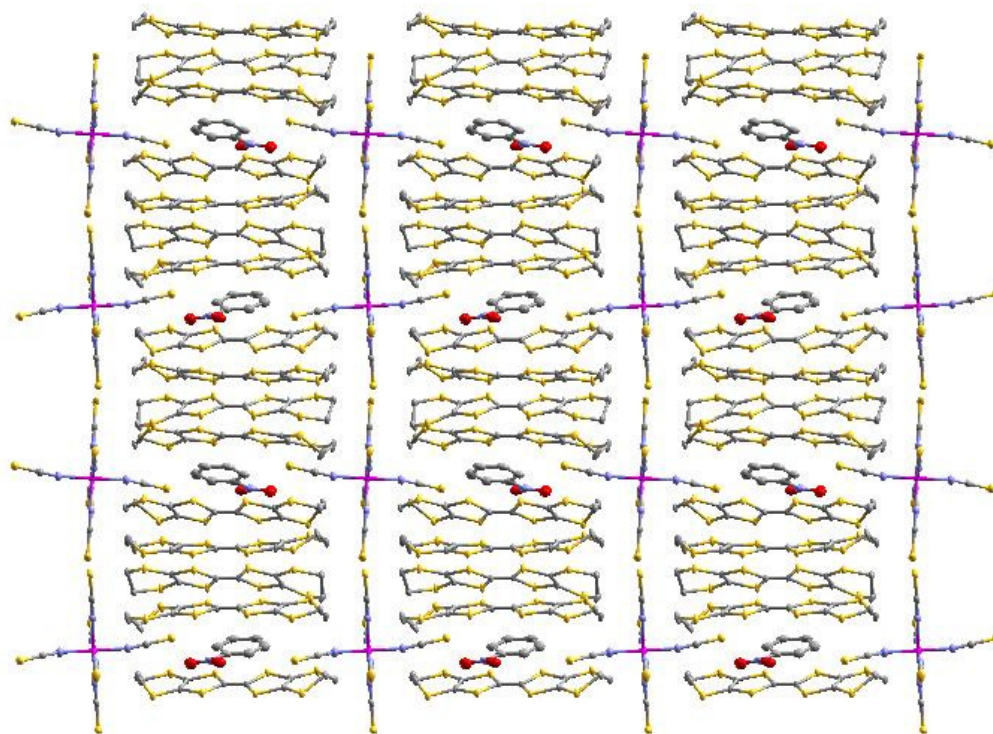


Figure 54: $(\text{ET})_4[\text{Cr}(\text{NCS})_6] \cdot \text{C}_6\text{H}_5\text{NO}_2$ as viewed down the crystallographic *a* axis. Thermal ellipsoids are shown at the 50 % probability level. Hydrogen atoms have been removed for clarity.

The electron donor molecules were found to not exist in a side-by-side arrangement with respect to each other within the plane, however overall the molecules were found to arrange latitudinally as portrayed in Figure 55.

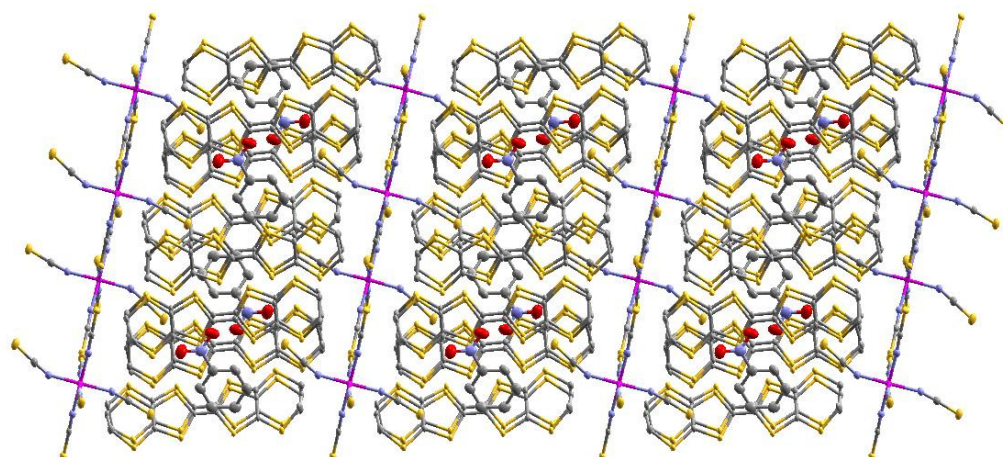


Figure 55: $(\text{ET})_4[\text{Cr}(\text{NCS})_6] \cdot \text{C}_6\text{H}_5\text{NO}_2$ as viewed down the crystallographic b axis. Thermal ellipsoids are shown at the 50 % probability level. Hydrogen atoms have been removed for clarity.

Figure 56 illustrates the non-planar arrangement of donor molecules when viewed down the crystallographic c axis. There are few short S...S contacts extending along the b axis, due to the displacement of donor molecules relative to each other. There is however an extensive network of short S...S present in the material, evident from the crystal structure as portrayed in Figure 57 and Figure 58, and these are given in Table 4. The structure is isomorphous with Thétiot's structure with the guest solvent molecule differing by replacement of a nitrile group (Thétiot) with a nitro group (this work).³⁴

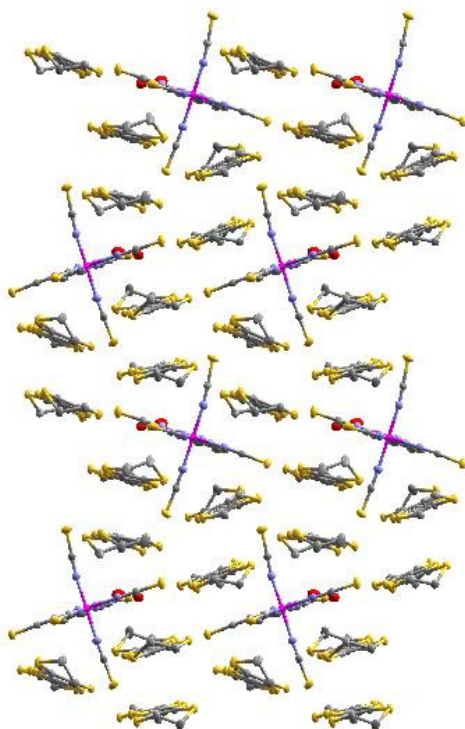


Figure 56: (ET)₄[Cr(NCS)₆].C₆H₅NO₂ as viewed down the crystallographic *c* axis. Thermal ellipsoids are shown at the 50% probability level. Hydrogen atoms have been removed for clarity.

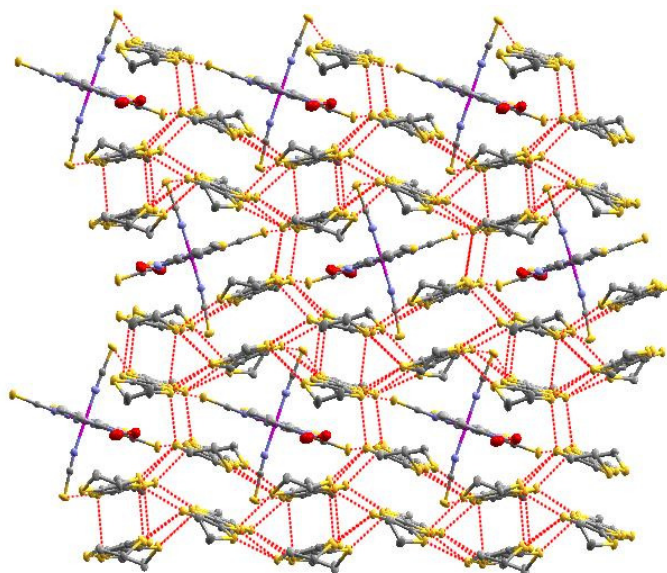


Figure 57: S...S short contacts, as viewed down the *c* axis. Thermal ellipsoids are shown at the 50 % probability level. Hydrogen atoms have been removed for clarity.

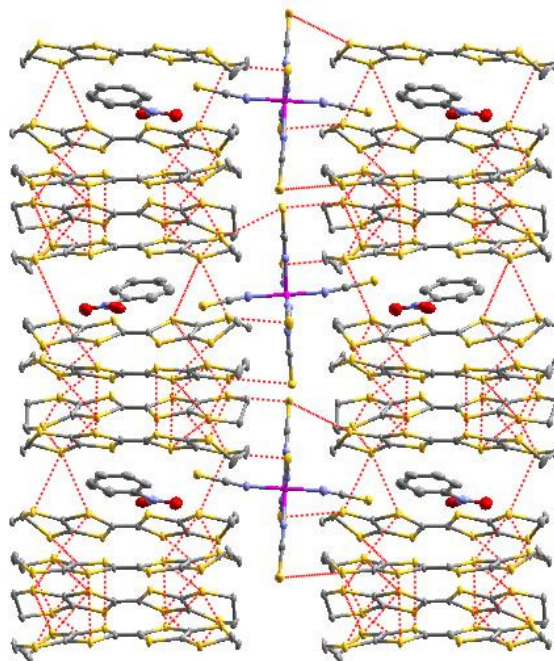


Figure 58: S...S short contacts, as viewed down the *a* axis. Thermal ellipsoids are shown at the 50 % probability level. Hydrogen atoms have been removed for clarity.

S...S close contact	Close contact length / Å
S4-S9	3.44
S8-S13	3.35
S8-S15	3.44
S10-S17	3.31
S12-S17	3.38
S16-S21	3.36
S16-S23	3.40
S17-S26	3.50
S17-S28	3.51
S23-S32	3.54
S18-S37	3.58

Table 4: S...S close contacts observed in $(\text{ET})_4[\text{Cr}(\text{NCS})_6] \cdot \text{C}_6\text{H}_5\text{NO}_2$.

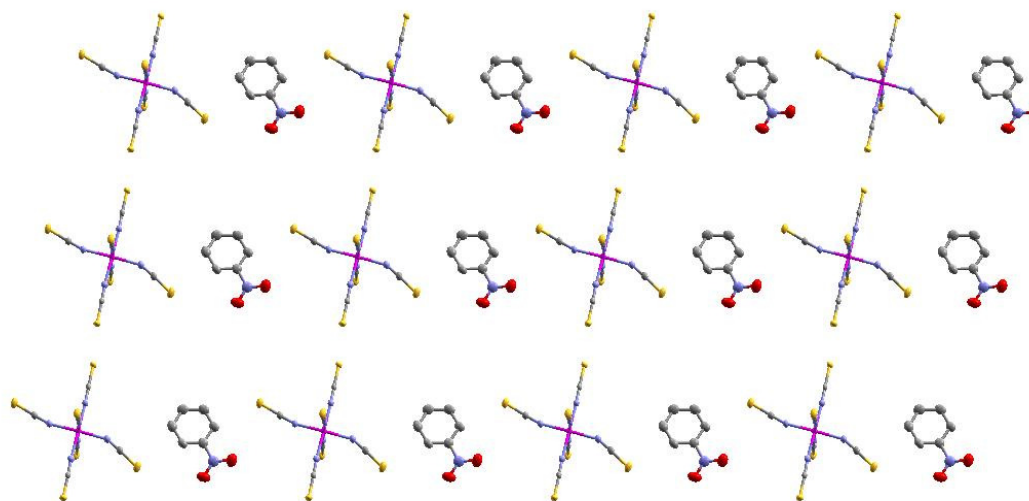


Figure 59: Anion and solvent sheet. Thermal ellipsoids are shown at the 50% probability level.

Hydrogen atoms have been removed for clarity.

The *isothiocyanate* ligands extending towards the nitrobenzene molecule are slightly distorted from the expected linear configuration by an angle of either 27.0° for the *isothiocyanate* extending towards the nitro group, or 17.3° for the *isothiocyanate* extending away from the nitro group (Figure 59). Both of these *isothiocyanate* functions protrude into the electron donor stacks, as seen in such related salts as $(\text{ET})_4[\text{Fe}(\text{NCS})_6] \cdot \text{CH}_2\text{Cl}_2$,³⁹ and $(\text{ET})_2[\text{Cr}(\text{NCS})_4(\text{NH}_3)_2]$.⁴⁰ The guest nitrobenzene molecule sits comfortably within an ET pocket, as depicted in Figure 60.

The distortion of *isothiocyanate* groups is also observed in the results published by Thétiot.³⁴ Thétiot observed that the *isothiocyanate* functions protruded into the donor stacks and exhibited bond angles of (Cr-N-C) 22.2° and 12.6° , similar to those observed in this salt.

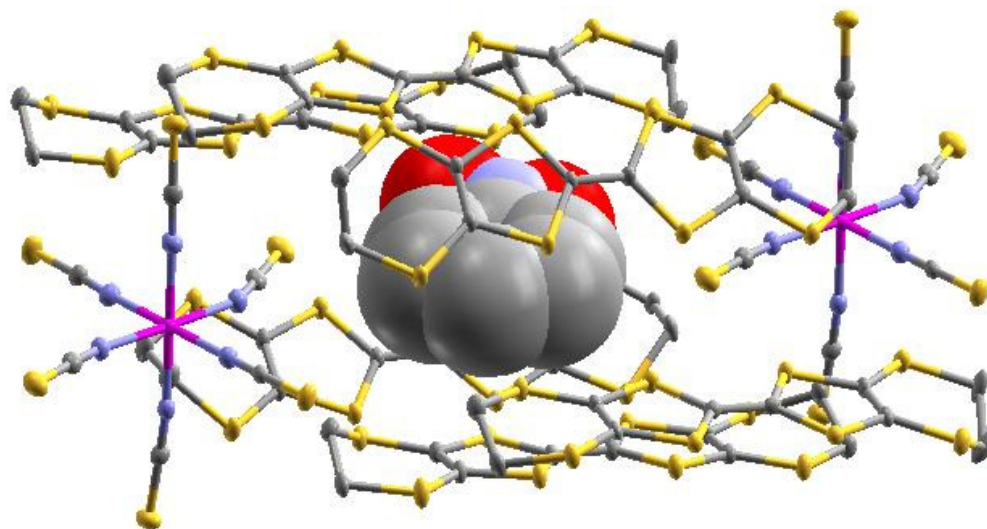


Figure 60: Nitrobenzene molecule (spacefill representation) within the ET pocket. Thermal ellipsoids (donors and anions) are shown at the 50 % probability level. Hydrogen atoms have been removed for clarity.

Charge determination based upon bond length calculations show that the four organosulfur donor molecules in this salt exist in slightly different charge states.¹¹ The donor consisting of S1-S8 shows a charge of +0.99, the donor consisting of S9-S16 has a much lower charge associated with it at +0.23. Donor molecules S17-S24 and S25-S32 carry charges of +0.98 and +1.08 respectively. Total charge residing on donor molecules in the X-ray crystal structure = +3.28. The $[\text{Cr}(\text{NCS})_6]^{3-}$ anion stabilises charge. The results of the charge determination are similar to those observed by Thétiot *et al.*, being +0.94, +1.06, +1.02 and +0.13 (total = +3.15).³⁴

Confirmation of the charge residues was sought from Raman spectroscopic measurements, which identified two peaks in the region in which the active symmetric stretch for the central C=C occur. One broad peak was exhibited at $\nu = 1430\text{-}1465$ and

a minor peak at $\nu = 1493\text{-}1497\text{ cm}^{-1}$, indicating the presence of ET molecules in oxidation states +0.6-1.0 and +0.1-0.2 as according to the method of Wang *et al.*¹⁰ Despite the broadness of the spectral peaks, the results do confirm the oxidation states of the ET molecules as calculated from the X-ray crystal structure.

Electrical resistivity measurements were performed as a function of temperature, by the standard two-probe method technique. The resistance of the gold wires attached to the crystal, and of the copper wires attached to the MagLab were assumed to be negligible in comparison to the resistance within the crystal when its electron transport behaviour was observed, thus a measurement by the four-probe technique was not conducted.

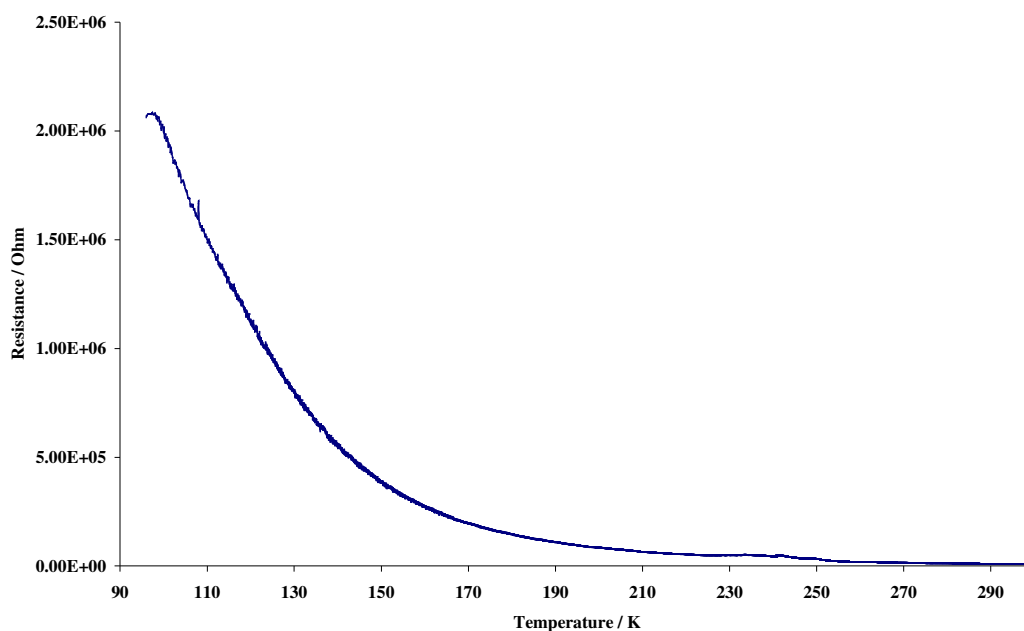
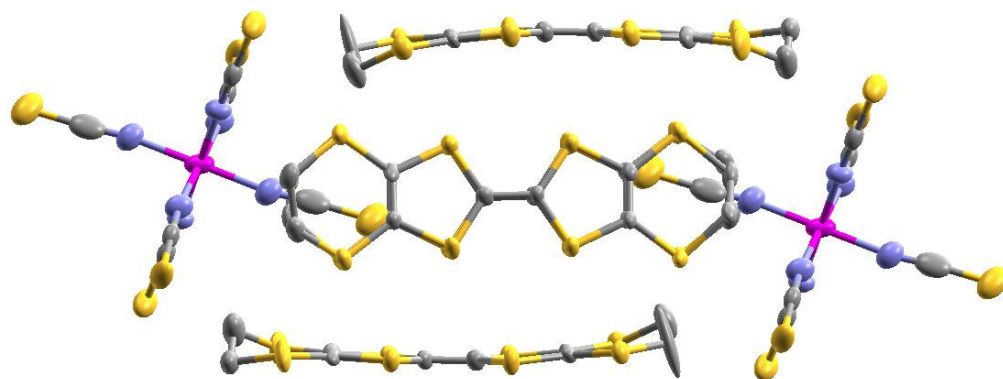


Figure 61: Resistivity data for $(\text{ET})_4[\text{Cr}(\text{NCS})_6]\cdot\text{C}_6\text{H}_5\text{NO}_2$ as a function of temperature.

The measurements were obtained over the temperature range 298-96 K, by immersing the probe, upon which the crystal was mounted in a standard 8-pin chip, into liquid nitrogen whilst collecting the resistance data both as the material cooled down and as it returned to room temperature. The semiconducting nature of the salt is displayed (Figure 61). Below 143 K a least-squares fit to the plot of the logarithm of the resistivity against the reciprocal of the temperature indicated that the material exhibited $E_a = 0.04$ eV. Above this temperature, a least-squares best fit to the data indicated $E_a = 0.11$ eV.

A slight deviation from the curve exhibited when $T = 250-222$ K was attributed to the position of the crystal changing with respect to the liquid nitrogen coolant, rather than a structural modification occurring. This is evident as a stepped temperature/ time profile is observed with more rapid warming occurring at the temperatures at which the resistivity deviations occur. Due to this evidence, single crystal X-ray diffraction measurements were not performed at these temperatures.

The electrocrystallisation of ET with **97** afforded a similar product, in which the chiral ligand was again absent. In this instance, an elongated box-like tube structure was exhibited, although the '*contents of the box*' (species encapsulated within the electron donor molecules) has thus far been undetermined. The crystallographic structure is notably different from those reported elsewhere, in that two electron donor molecules lie perpendicular to each other, and the other two sides of the box are generated by a symmetry relationship, as shown in Figures 62 to 65.



**Figure 62: ET box-like tube structure. Thermal ellipsoids are shown at the 50% probability level.
Hydrogen atoms have been removed for clarity.**

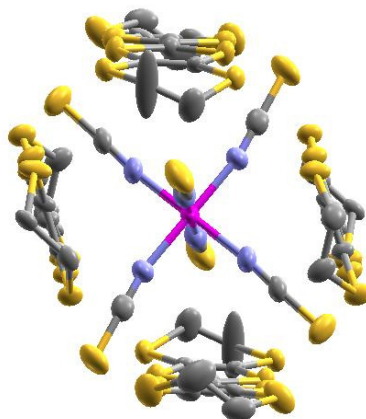


**Figure 63: ET tube, end-on view. Thermal ellipsoids are shown at the 50% probability level.
Hydrogen atoms have been removed for clarity.**

Due to the incomplete structure solution, a detailed discussion of the X-ray crystal structure will not be undertaken. Suffice it to say, that bond length calculations performed on the electron donor molecules indicate that for each box, two donors

exhibit a charge of +0.8 each, and the remaining two donors exhibit a charge of +0.6 each. These values correspond well with the expected values, and thus it can be concluded that the species residing inside the box, which is unknown, has neutral charge. Raman spectroscopy confirmed the charges, with weak ν_4 stretches at 1416 and 1460 cm^{-1} indicative of charge states between +0.8 to +1.0, and +0.6 to +0.7 respectively. The ν_3 stretches were not distinguishable from the background.

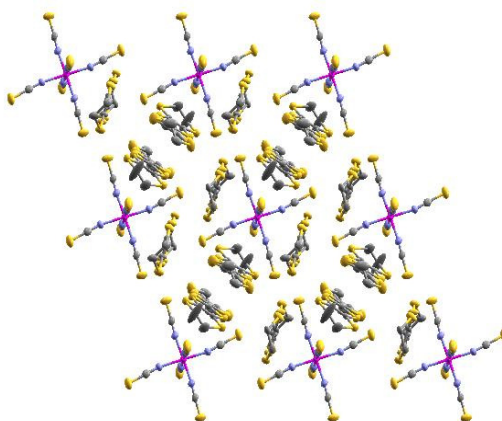


Figure 64: Crystalline packing of ET tube, end-on view. Thermal ellipsoids are shown at the 50% probability level. Hydrogen atoms have been removed for clarity.

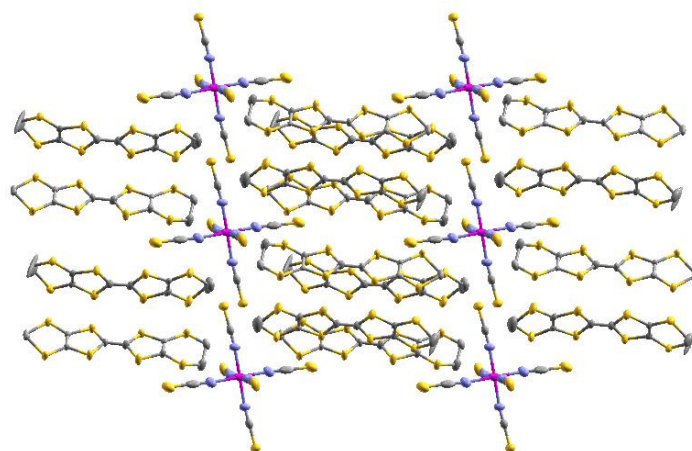


Figure 65: Crystalline packing of ET tube, side-on view. Thermal ellipsoids are shown at the 50% probability level. Hydrogen atoms have been removed for clarity.

Resistivity measurements were not performed on the plates, due to the small size and fragile nature.

4.2.3 Experimental



Reinecke's Salt (1.0 g, 2.97 mmol) and (*R*)-(+)-2,2-bi(naphthol) (0.85 g, 2.97 mmol) in acetonitrile (40 mL) were heated to reflux under a nitrogen atmosphere for 12 h. Over the course of the reaction, a colour change from pink to purple was observed. The reaction was cooled to room temperature, and evaporated under reduced pressure to around 5 mL. Standing in the fridge overnight afforded a precipitate, which was isolated by filtration and dried *in vacuo* at room temperature to afford **94** (1.80 g, 97%) as a purple solid Mp 188 °C (Found: C, 48.7; H, 3.5; N, 12.0).

[Cr(NCS)₄(C₂₀H₁₄O₂)] [NH₄] requires: C, 49.0; H, 3.1; N, 11.9%; ν_{\max} (ATR)/cm⁻¹ 3509, 3432, 3153, 2077, 1617, 1595, 1511, 1383, 1318, 1272, 1257, 1219, 1181, 1148, 1024, 823, 814, 748, 564.

2-(4'-(S)-Isopropyl-4',5'-dihydro-oxazol-2'-yl)-pyridine, 95

L-valinol (0.7 g, 6.78 mmol), 2-cyanopyridine (0.71 g, 6.78 mmol) and a few crystals of 4-toluenesulfonic acid were heated together in a conventional 800 W microwave oven for 2 min. The crude material was allowed to cool, and purified by chromatography over silica eluting with ethyl acetate/methanol (15:1) affording **95** (0.26 g, 20 %) as a colourless oil; δ_{H} (400 MHz, CDCl₃) 8.71 (1 H, dq, $J=4.92, 0.92, 0.76$ Hz, 6-*H*), 8.07 (1 H, d, $J=7.92$ Hz, 3-*H*), 7.78 (1 H, dt, $J=7.76, 1.84$ Hz, 4-*H*), 7.39 (1 H, ddd, $J=4.72, 2.76, 1.14$ Hz, 5-*H*), 4.52 (1 H, q, $J=7.48, 1.4$ Hz, 4'-*H*), 4.22 (1 H, q, $J=8.16, 7.8$ Hz, 5'-*H*_α), 4.17 (1 H, m, 5'-*H*_β), 1.90 (1 H, m, C-*H*), 1.06 (3 H, d, $J=6.88$ Hz, CH₃), 0.95 (3 H, d, $J=6.84$ Hz, CH₃); δ_{C} (100 MHz, CDCl₃) 162.5 (2'-*C*), 149.7 (6-*C*), 146.9 (2-*C*), 136.6 (4-*C*), 125.4 (3-*C*), 123.9 (5-*C*), 72.9 (4'-*C*), 70.7 (5'-*C*), 32.7 (CH), 19.0 (CH₃), 18.4 (CH₃); m/z (GC-MS): found: 190 [M]⁺, 171, 147, 119, 92, 69, 51. C₁₁H₁₄N₂O requires: 190.

2'-Pyridin-2-yl-4',5'-dihydro-thiazole-4'-(S)-carboxylic acid, 96

2-Cyanopyridine (0.5 g, 4.75 mmol) and *L*-cysteine (0.595 g, 4.76 mmol) were mixed together in distilled water (10 mL), and heated in a conventional 800 W microwave oven for 2 min on half-power. The reaction was allowed to cool for 2 min, methanol

(30 mL) added, and the mixture filtered. The filtrate was evaporated and the crude material purified through a short column of silica eluting with chloroform/methanol (5:1) to give **96** (0.76 g, 77 %) as a slightly-yellow solid; ν_{\max} (ATR)/ cm^{-1} 2809, 1706, 1565, 1461, 1436, 1382, 1300, 1272, 1258, 1240, 1214, 1146, 1058, 1014, 994, 972, 949, 901, 868, 801, 785, 740, 712, 693, 620, 608, 560, 539, 480; δ_{H} (400 MHz, CD_3OD) 8.58 (1 H, d, $J=4.9$ Hz, 6-*H*), 8.15 (1 H, d, $J=8.5$ Hz, 3-*H*), 7.89 (1 H, t, $J=7.9$ Hz, 4-*H*), 7.49 (1 H, m, 5-*H*), 5.29 (1 H, t, $J=9.5$ Hz, 4'-*H*), 5.07 (1 H, s *br*, CO_2H) 3.65 (2 H, m, 5'-*H*); δ_{C} (100 MHz, CD_3OD) 176.5 (C=O), 173.5 (2'-*C*), 152.1 (2-*C*), 150.2 (6-*C*), 138.3 (4-*C*), 127.2 (5-*C*), 123.2 (3-*C*), 82.1 (4'-*C*), 35.9 (5'-*C*).

Ammonium chromium [2-(4'-(*S*)-Isopropyl-4',5'-dihydro-oxazol-2'-yl)-pyridine]tetrathiocyanate, 97

Ligand **95** (1.0 g, 5.3 mmol) and Reinecke's Salt (1.77 g, 5.3 mmol) were heated to reflux in acetonitrile (60 mL) under an atmosphere of nitrogen overnight. The reaction was allowed to cool to room temperature, and the solvent evaporated. Drying under high vacuum at room temperature afforded **97** (2.58 g, 99 %) as a purple gum (Found C, 36.5; H, 3.7; N, 19.9. $\text{C}_{15}\text{H}_{18}\text{CrN}_7\text{OS}_4$ requires: C, 36.6; H, 3.7; N, 19.9 %); ν_{\max} (ATR)/ cm^{-1} 3151, 2964, 2053, 1651, 1593, 1526, 1414, 1392, 1256, 1166, 923, 749, 668, 480.

4.2.4 Electrocrystallisation experimental

(11)₄[Cr(NCS)₆].C₆H₅NO₂

To the anodic side of a H-shaped electrochemical cell fitted with a glass frit was placed **11** (10 mg, 0.02 mmol), and from the cathodic side of the cell was added a solution of **94** (40 mg, 0.07 mmol) in nitrobenzene/acetonitrile (50:50 v/v, 25 mL). The level of solvent in each compartment was allowed to equilibrate, and to each side inserted a platinum-tipped electrode. A constant current of 0.2 μA was applied across the cell for two weeks affording black blocks on the anode. These were harvested, washed with acetone and dried Mp 208 °C; Raman/ cm^{-1} $\nu_4 = 1430\text{-}1465$ (broad); $\nu_3 = 1493\text{-}1497$.

(11)₄[Cr(NCS)₆].X (where X is an undetermined, neutral guest molecule/ solvent)

To the anodic side of a H-shaped electrochemical cell fitted with a glass frit was placed **11** (10 mg, 0.02 mmol), and from the cathodic side of the cell was added a solution of **97** (40 mg, 0.07 mmol) in nitrobenzene/acetonitrile (50:50 v/v, 25 mL). The level of solvent in each compartment was allowed to equilibrate, and to each side inserted a platinum-tipped electrode. A constant current of 1.0 μA was applied across the cell for one week affording black needles on the anode. These were harvested, washed with acetone and dried Mp 211 °C; Raman/ cm^{-1} $\nu_4 = 1416$, $\nu_3 = 1460 \text{ cm}^{-1}$.

4.3 Chiral packing of achiral components

4.3.1 Introduction

The volume of the anionic species employed in electrocrystallisation, which serves to trap and stabilise the radical cations of electron donor molecules formed by oxidation, has been correlated against the resulting cell volume of the salt. It is believed that similar cell volumes to the salts which exhibit superconductivity could produce further superconducting materials.^{41, 42} The influence of the anion is important in determining the packing characteristics observed in the crystalline state, and as such the incorporation of hydrogen bonding capability is desirable in attempting to control the motifs exhibited by crystalline materials.

Furthermore, over recent years there has been a marked increase in the number of researchers approaching the preparation of enantiopure molecular conducting systems, in the hope that there may be an increased control over the supramolecular chirality inferred by the chiral species. This could lead to higher temperatures at which superconductivity is observed, or new physical phenomena such as that of ‘Magnetochiral Anisotropy’ observed by Rikken *et al.*³⁶

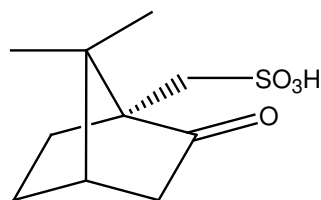
There exists a vast array of organic compounds that are small in size and exhibit a chiral centre. In addition, there is a large subset of these that have hydrogen bonding capabilities installed, such as amino acids.

The preparation of a completely organic radical cation salt could lead to a more stable lattice structure being observed, which in turn decreases the possibility of phonon interactions onto the lattice. This may allow access to a range of superconducting species in which the transition into a superconducting phase occurs at a much higher temperature than that previously observed.

Building on these ideas, it was decided to attempt to prepare the radical cation salt in which the anion employed was a derivative of camphor. Camphorsulfonic acid is readily available in enantiopure form, and has previously been employed in the preparation of chiral conducting polymers, such as poly(aniline). In addition chiral nanotubes have been prepared by the *in-situ* polymerisation of poly(aniline) in the presence of camphorsulfonic acid.^{43, 44, 45, 46, 47, 48} In addition, camphor exhibits a bicyclic structure, having a relatively small volume that can be roughly approximated to a sphere with side-arm for attachment. This should allow siting in small voids created in the lattice. Furthermore, the bicyclic structure of camphor imposes a certain degree of rigidity, which would serve to decrease phonon interactions.

4.3.2 Results and Discussion

The enantiopure camphorsulfonic acid **98** was derivatised as its tetrabutylammonium, and (separately) as its tetramethylammonium salt, by neutralisation with the appropriate tetraalkylammonium hydroxide.



98

Electrocrystallisation of ET with tetrabutylammonium (1R)-(+)-camphorsulfonate in a mixed solvent system of 1,2,4-trichlorobenzene/ethanol (60:40) afforded in one instance elongated black rods of typical dimension 4.1 x 2.0 x 1.5 mm on the anode. These were harvested and investigated by Raman spectroscopy, X-ray crystallography and resistivity measurements. On other occasions, no crystalline material was observed, with dark amorphous solids forming over the bottom of the electrocrystallisation cell, mixed in with un-dissolved ET. Raman spectroscopy on the elongated black rods showed C=C symmetrical stretching frequencies at $\nu_4 = 1420$ and $\nu_3 = 1450$ cm^{-1} , indicating a uniform charge state of +1 on the organosulfur units. This was subsequently confirmed by X-ray crystallographic analysis, in which the bond lengths on the organosulfur donor indicated a charge of +1, by the method of Guionneau *et al.*¹¹ Remarkably however, the X-ray crystal structure identified the absence of the camphorsulfonate anion. The structure was eventually determined to be a bromide salt of ET. This was initially confusing, as the possibility of the material containing bromide ions was thought to be impossible. Every care had been taken to thoroughly clean the glassware and electrodes, and the solvents had been purified by distillation prior to use. The source of the bromide ions was eventually attributed to the tetrabutylammonium hydroxide employed in the synthesis of tetrabutylammonium camphorsulfonate. Inspection of the analysis sheet provided for the reagent indicated

the presence, albeit in low concentrations, of bromide ions, presumably from the method of synthesis.

Crystal data for (ET)Br: $C_{40}H_{32}Br_4S_{32}$, $M = 1858.22$, black cut rod, $0.03 \times 0.01 \times 0.01$ mm³, monoclinic, space group $C2$ (No. 5), $a = 12.867(3)$, $b = 11.036(2)$, $c = 11.270(2)$ Å, $\beta = 103.66(3)^\circ$, $V = 1555.0(5)$ Å³, $Z = 1$, $D_c = 1.984$ g/cm³, $F_{000} = 924$, MoK α radiation, $\lambda = 0.71073$ Å, $T = 173(2)$ K, $2\theta_{max} = 46.6^\circ$, 3459 reflections collected, 2113 unique ($R_{int} = 0.0126$). Final $Goof = 1.052$, $R1 = 0.0217$, $wR2 = 0.0562$, R indices based on 2021 reflections with $I > 2\sigma(I)$ (refinement on F^2), 174 parameters, 1 restraint. Lp and absorption corrections applied, $\mu = 3.698$ mm⁻¹. Absolute structure parameter = 0.141(16).⁴⁹

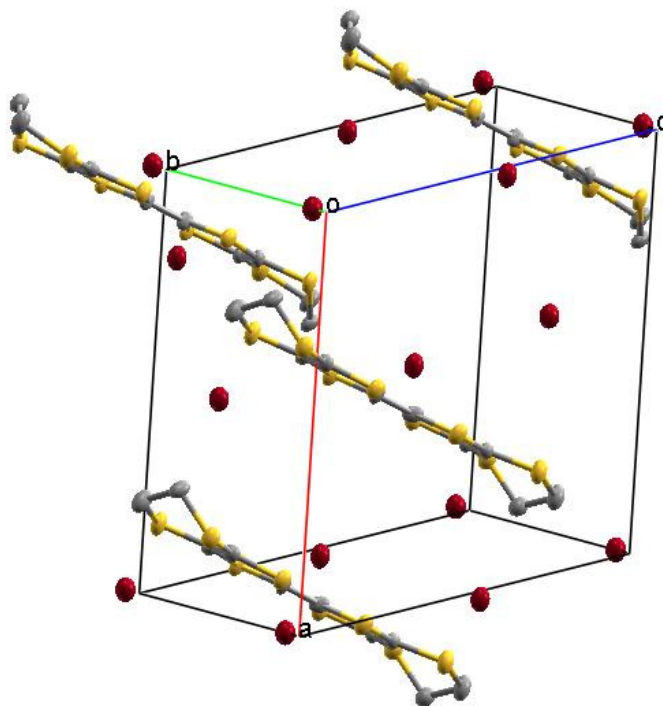


Figure 66: Filled unit cell, showing the arrangement of ET molecules and bromide ions.

Bromide ions lie on two-fold axes parallel to the *b* axis. Successive bromide ions along a row are displaced by 2.05 Å in the *b* direction and 5.64 Å in the *c* direction, so they form a chiral arrangement in the crystal structure (Figure 66).

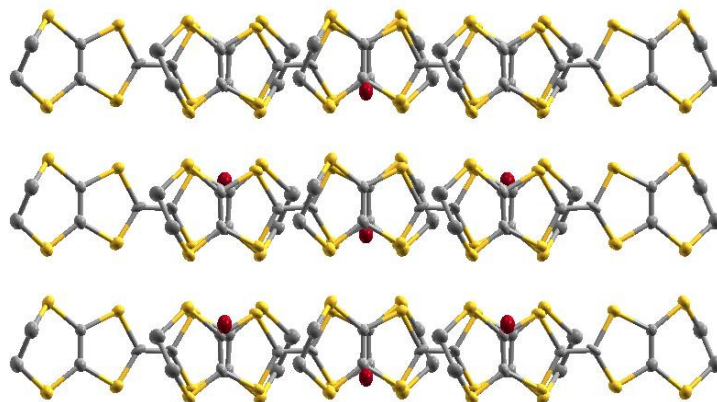


Figure 67: (ET)Br as viewed along the crystallographic *a* axis. Thermal ellipsoids are shown at the 50 % probability level. Hydrogen atoms have been removed for clarity.

There exists a stacked arrangement of organosulfur donor molecules (Figures 67 to 70), with numerous short S...S contacts observed, and listed in Table 5. The short contacts also extend in the other two directions creating a 3-D network.

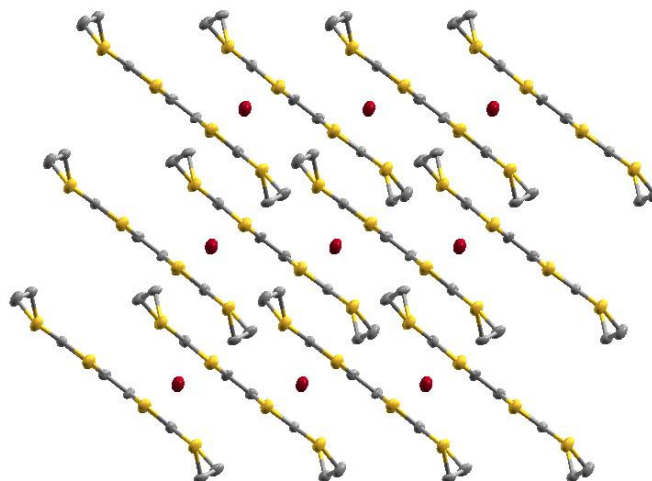


Figure 68: (ET)Br as viewed along the crystallographic *b* axis. Thermal ellipsoids are shown at the 50 % probability level. Hydrogen atoms have been removed for clarity.

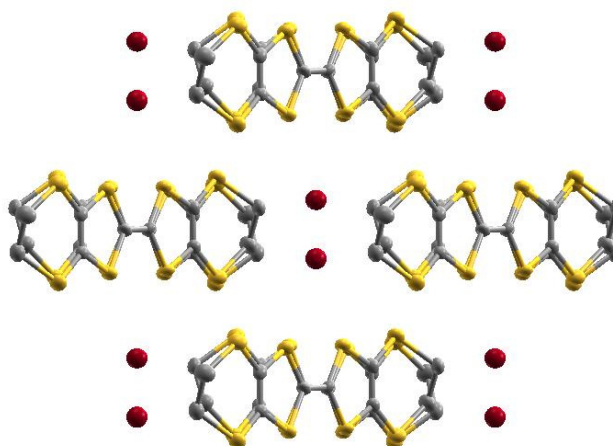


Figure 69: (ET)Br as viewed along the crystallographic *c* axis. Thermal ellipsoids are shown at the 50% probability level. Hydrogen atoms have been removed for clarity.

S...S close contact	Distance / Å
S1...S8	3.29
S1...S4	3.41
S5...S8	3.41
S2...S7	3.46
S2...S3	3.53
S6...S7	3.56

Table 5: S...S close contacts present in (ET)Br

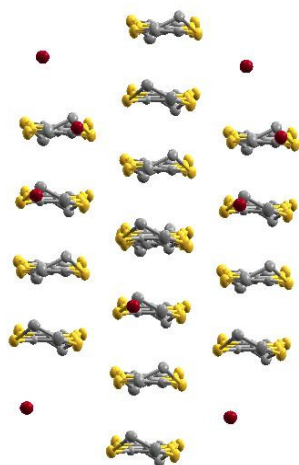


Figure 70: (ET)Br as viewed along the length of the ET molecule.

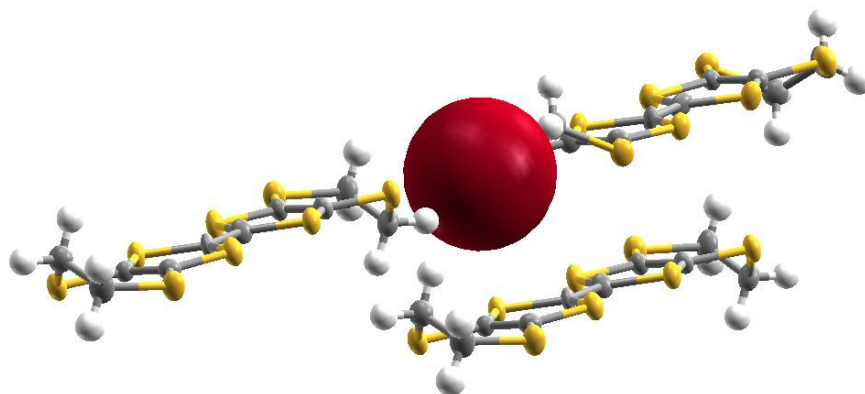


Figure 71: The ethylene groups on the ET molecules are displaced to accommodate the bromide ion.

Figure 71 illustrates the orientation of the ethylene functions at the end of the ET molecules, which exist in one envelope conformation to accommodate the local bromide ion.

The resistivity of (ET)Br was measured as a function of temperature, by the two probe method. The insulating transition was sufficiently high to neglect the contribution to the resistance from the gold wires used in the measurement. Contacts were made using carbon conducting cement. The resistivity was measured along the long axis on the 4.1 x 2.0 mm face, with contacts made 3.1 mm apart. The salt exhibited semiconducting behaviour upon cooling from room temperature, as shown in Figure 72.

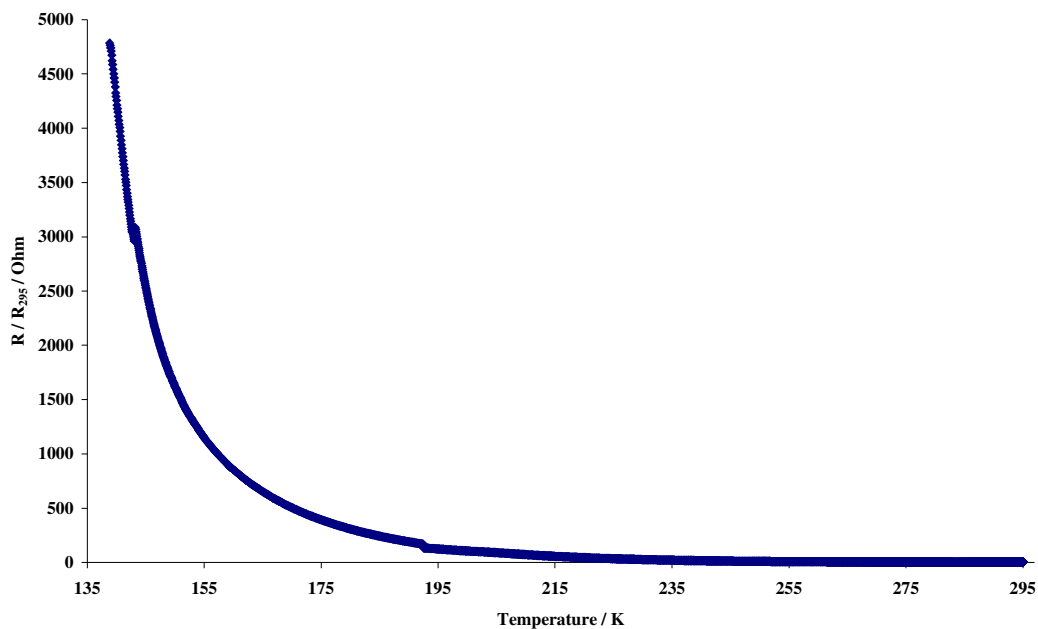


Figure 72: Normalised resistivity data for (ET)Br as a function of temperature.

Two regions may be determined from the data. From room temperature to 192 K, a plot of the natural log of the normalised resistance as a function of $1/T$ affords a straight line (least square best fit $R^2 = 0.9971$) of gradient 1573.4 K^{-1} . This corresponds to $E_a = 0.26 \text{ eV}$. Below 192 K, the data for the crystal indicates $E_a = 0.13 \text{ eV}$. Both of these values are in the range for an ET semiconductor. Inspection of the temperature/ resistance profile (Figure 73) indicates a sudden increase in resistance at $T = 192 - 193 \text{ K}$. This is attributed to a structural change within the crystal, as a positional change of the crystal with respect to the surface of the liquid nitrogen coolant would be indicated as a deviation in the temperature/ time profile (Figure 74), and no such deviation is observed. Confirmation of this structural modification by X-ray crystallography at different temperatures was not investigated.

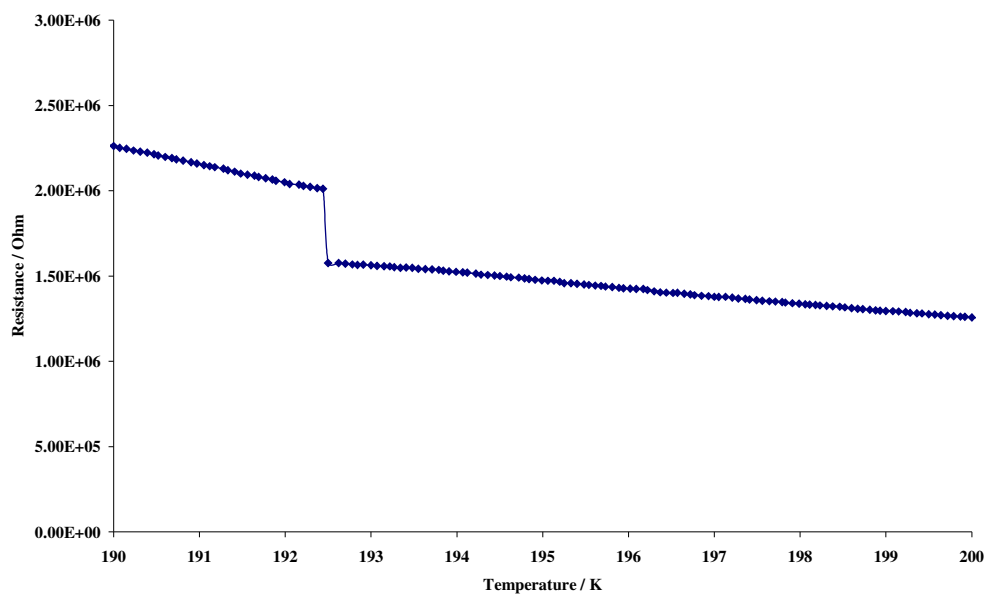


Figure 73: Expanded data section illustrating large increment in resistance at 192 K.

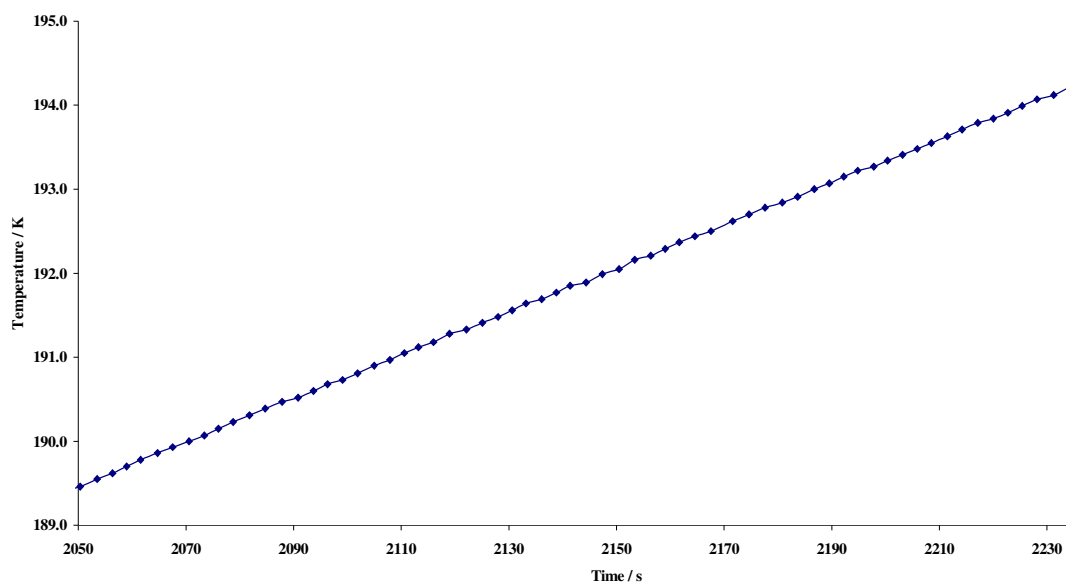


Figure 74: Temperature profile (as a function of time) in the region of the increment of resistance at 192 K, showing the absence of a deviation in the cooling/ warming rate.

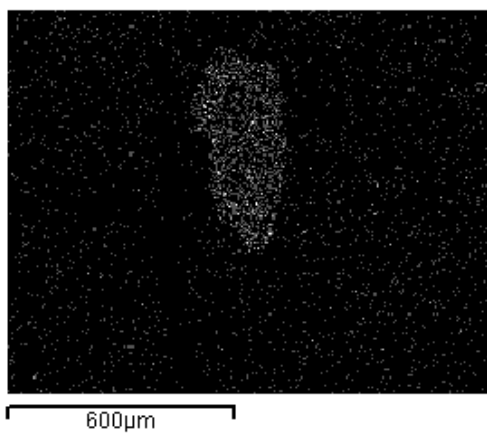


Figure 75: Electron microprobe analysis using X-ray diffuse scattering, on the scanning electron microscope indicating the presence of bromine.

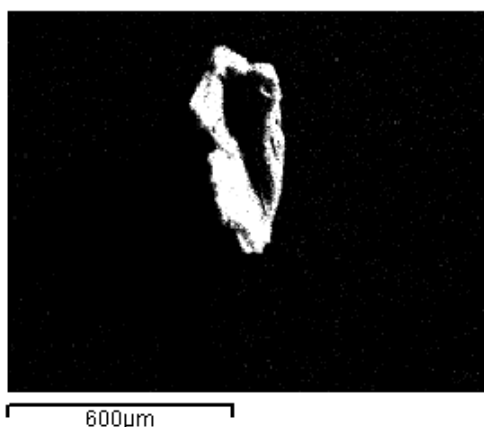


Figure 76: Electron microprobe analysis using X-ray diffuse scattering, on the scanning electron microscope indicating the presence of sulfur.

The presence of bromine was confirmed using electron microprobe analysis on the Scanning Electron Microscope (SEM). The image generated for the detection of bromine is displayed in Figure 75. Similarly, the presence of sulfur was confirmed and the image is shown in Figure 76.

Electrocrystallisation experiments employing ET with the camphorsulfonate anion in acetonitrile gave, from the same batch of tetrabutylammonium camphorsulfonate, a needle that also showed semiconducting behaviour (Figure 77), with an insulating phase becoming dominant at 117 K. The slight step in the resistivity curve at 236 to 237 K coincided with a deviation in the temperature profile (Figure 78), suggesting that the position of the crystal had changed relative to the level of liquid nitrogen. The activation energy of the semiconductor was determined to be $E_a = 0.11$ eV in the temperature range 134 to 236 K.

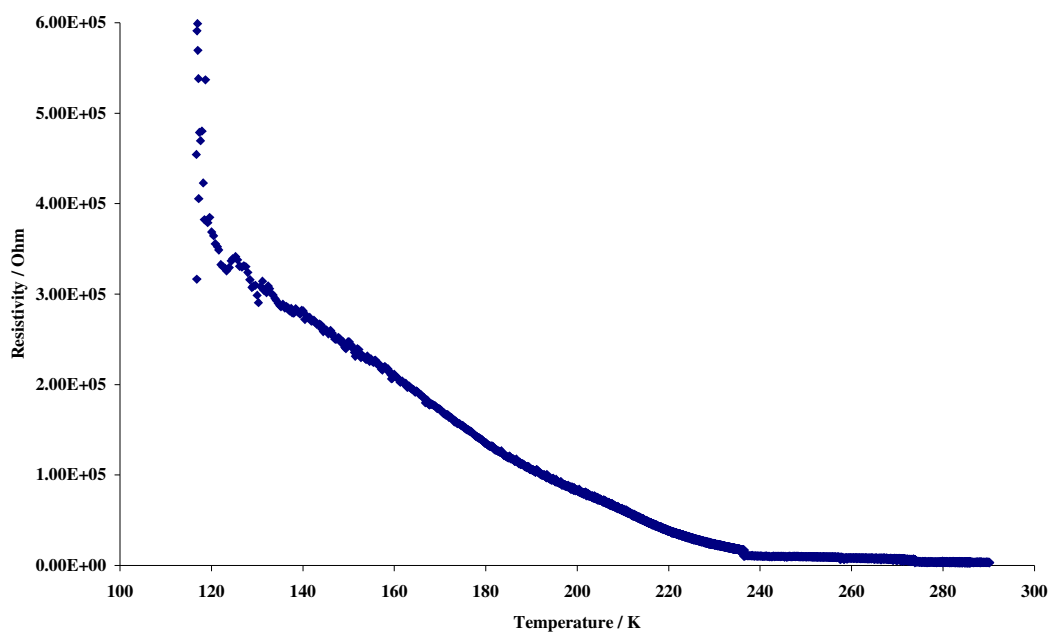


Figure 77: Resistivity data for (ET)Br grown in acetonitrile, as a function of temperature.

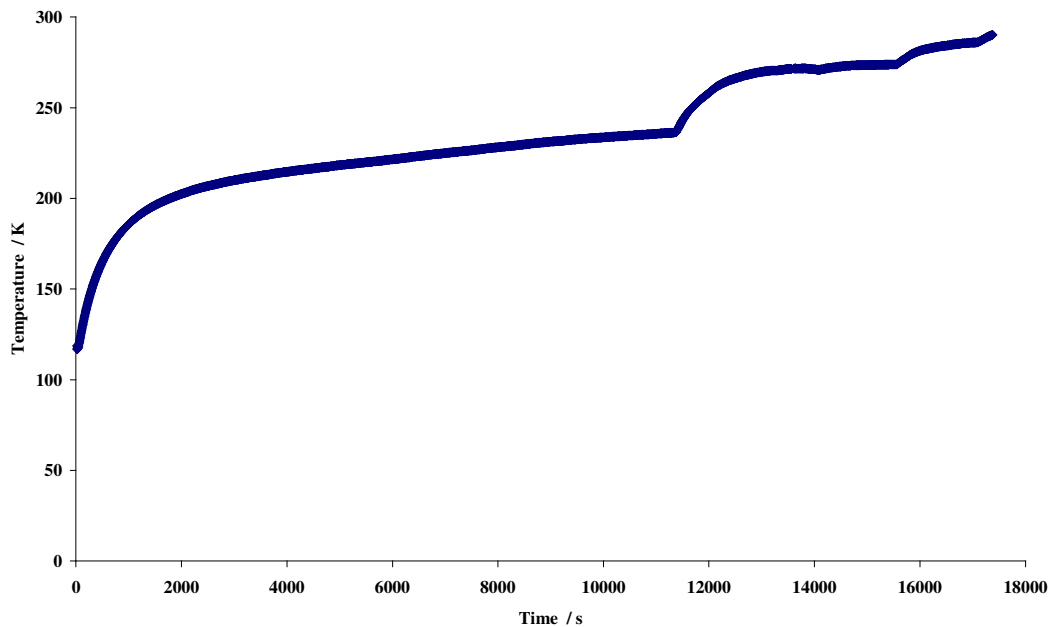


Figure 78: Temperature profile of the resistivity measurements for (ET)Br grown in acetonitrile.

The structure of the crystal was not determined by X-ray crystallography, however, Raman spectroscopy demonstrated symmetrical stretches for the central C=C bond at $\nu_4 = 1460$ and $\nu_3 = 1469$, indicative of a charge state between +0.67 and +0.5, i.e. a salt of composition between 3:2 and 2:1 (donor:anion).

Attempts to recreate the conditions from which the (ET)Br salt grew in the C2 form, focussed on the synthesis of the bromide source. Thus, tetrabutylammonium bromide was mixed with (1*R*)-(+)-camphorsulfonic acid in acetonitrile, and evaporated to dryness. The white solid isolated was employed in electrocrystallisation experiments without success. However, by heating the two reagents to reflux in acetonitrile afforded a yellow-brown solid upon evaporation of the solvent. The electrocrystallisation of the yellow-brown mixed salt with ET under identical conditions to those used to synthesise the chiral ET(Br) above, afforded dark rods on the anode. However these grew in length only to the region 2 to 2.5 mm. Raman spectroscopy ($\nu_4 = 1430$, $\nu_3 = 1465$) demonstrated a charge state of +1, and the melting point (206 – 207 °C) of the material was identical to that observed previously. Structural characterisation by X-ray single crystal diffraction was not performed, due to the inability to isolate a crystal that did not visibly appear twinned.

In a similar fashion to that employed above for the formation of the yellow-brown salt, the opposite enantiomer, (1*S*)-(-)-camphorsulfonic acid, was prepared and employed in the electrocrystallisation experiments under identical conditions. Needles grew on the anode and were harvested, washed with acetone and characterised by single crystal X-ray diffraction and Raman spectroscopy. The ν_4 and ν_3 symmetrical stretches were

observed at 1420 and 1469 cm^{-1} respectively, indicating a +1 charge state on the ET molecules. However, the crystal structure revealed a new $(\text{ET})_4\text{Br}_4(\text{H}_3\text{O})(\text{H}_2\text{O})$ salt, in which there exists a square of bromide anions with a $\text{H}_2\text{O}\cdots\text{H}^+\cdots\text{OH}_2$ unit inside it in two possible orientations.

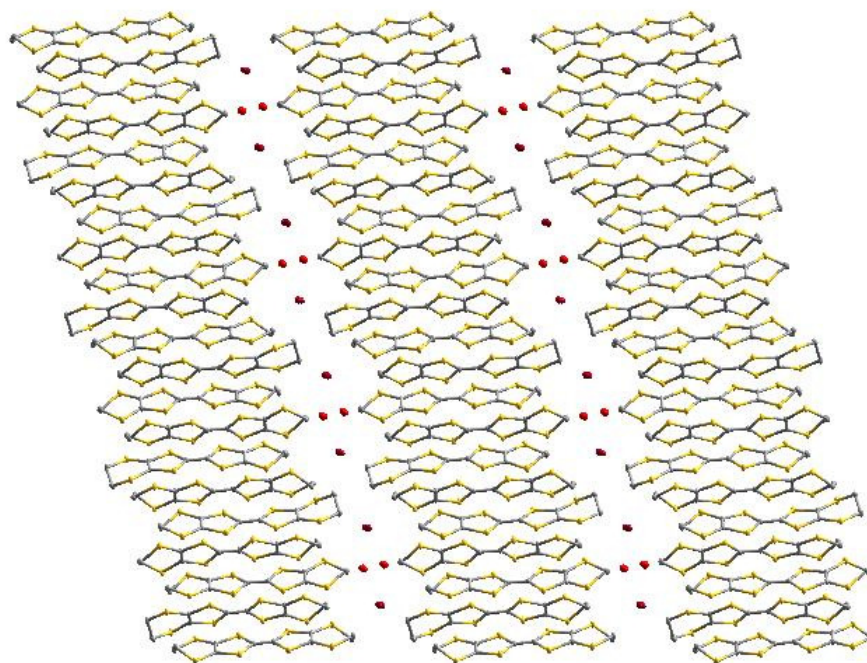


Figure 79: Hydrated ET bromide salt, as viewed down the crystallographic a axis.

Crystal data for $\text{C}_{11.11} \text{H}_{10} \text{Br}_{0.89} \text{O}_{0.44} \text{S}_{8.89}$, $M = 506.04$, $0.13 \times 0.10 \times 0.08 \text{ mm}^3$, monoclinic, space group P-1, $V = 3844.19(13) \text{ \AA}^3$, $Z = 9$, $D_c = 1.970 \text{ g/cm}^3$, $F_{000} = 2282$, Bruker-Nonius APEX II CCD camera on κ -goniostat, $\text{MoK}\alpha$ radiation, $\lambda = 0.71073 \text{ \AA}$, $T = 120 \text{ K}$, $2\theta_{\text{max}} = 55.2^\circ$, 62725 reflections collected, 17619 unique ($R_{\text{int}} = 0.0396$). Final $\text{Goof} = 1.359$, $R1 = 0.0497$, $wR2 = 0.1138$, R indices based on 15225 reflections with $I > 2\sigma$ (refinement on F^2), 893 parameters, 24 restraints.

The very large unit cell showed extensive S...S short contacts down the stacks of electron donors.

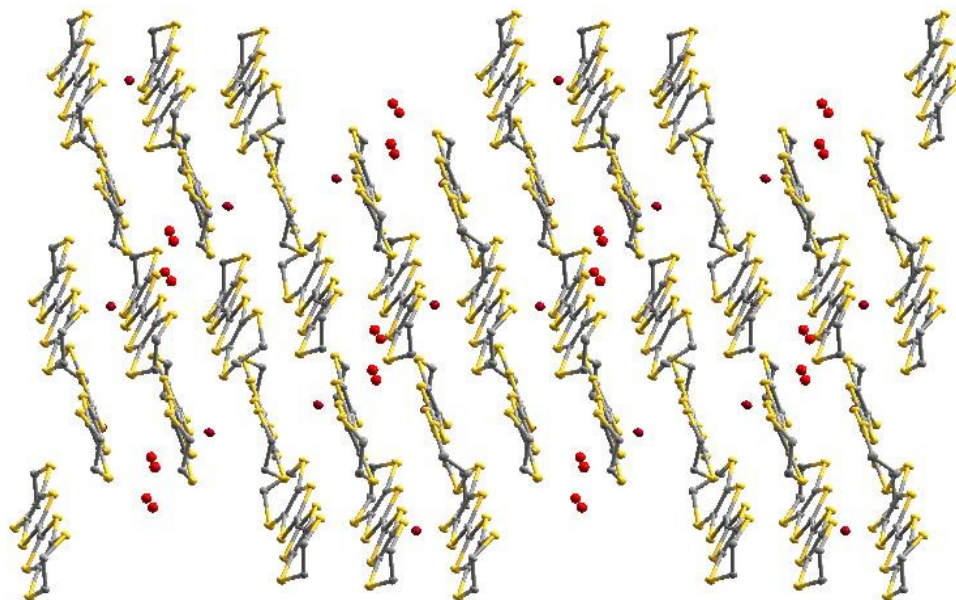


Figure 80: Hydrated ET bromide salt, as viewed down the crystallographic *b* axis.

Bond length calculations using the method of Guionneau *et al.* from the X-ray crystal structure indicated the charge on the donor molecules to be in the range $Z = +0.4$ to $Z = +0.7$, with each donor bearing a slightly different charge.¹¹ Although the charges determined by Raman spectroscopy and from X-ray bond lengths differ, the results are roughly the same. Resistivity measurements were not performed on the salt due to the small crystal size obtained.

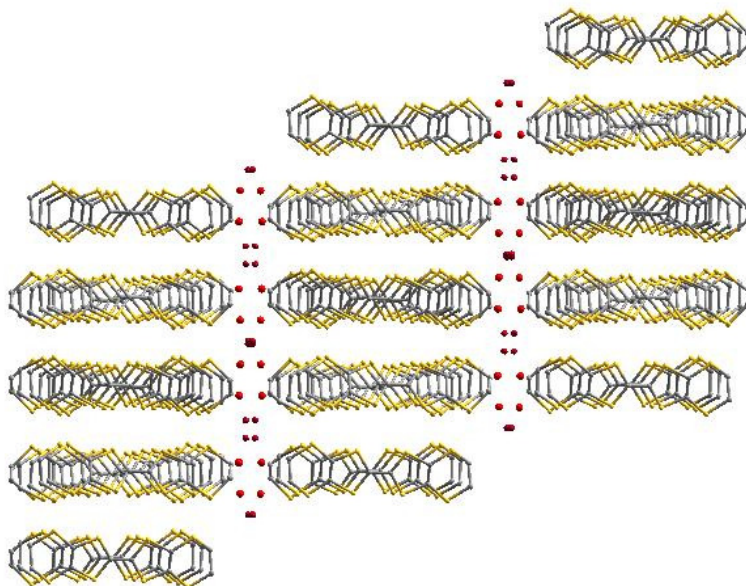


Figure 81: Hydrated ET bromide salt, as viewed down the crystallographic *c* axis.

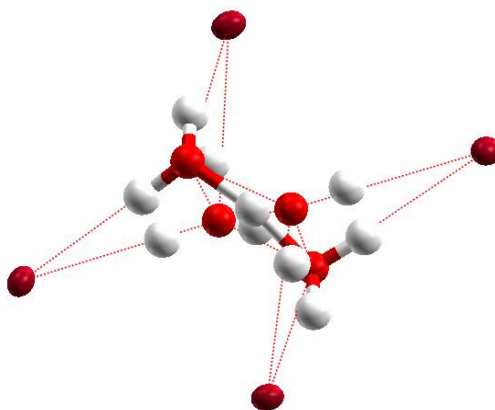


Figure 82: Cluster of bromides (deep red) and waters with short contacts shown as red lines.

The preparation of tetramethylammonium salts of both enantiomers of camphorsulfonic acid was achieved by neutralisation of the acidic aqueous solutions. The use of these salts in electrocrystallisation proved unsuccessful, and no radical cation salts were

formed when the solvent employed was nitrobenzene, chlorobenzene, 1,2,4-trichlorobenzene, acetophenone, dichloromethane, tetrahydrofuran, ethanol, and the mixed solvent systems 1,2,4-trichlorobenzene-ethanol (60:40 v/v) and chlorobenzene-ethanol (60:40 v/v).

4.3.3 Experimental

(1*R*)-(+)-camphorsulfonic acid, (1*S*)-(-)-camphorsulfonic acid, tetrabutylammonium hydroxide, and tetrabutylammonium bromide were purchased from SigmaAldrich. Tetramethylammonium hydroxide was purchased from Fisher Scientific. All reagents were used without further purification.

Tetrabutylammonium camphorsulfonate, 99

A solution of tetrabutylammonium hydroxide (3.44 g, 4.3 mmol) in distilled water (30 mL) was added to a stirred solution of camphorsulfonic acid (1.0 g, 4.3 mmol) in distilled water (30 mL). The solution was stirred at room temperature for 15 min, and the pH was tested (pH = 7). The water was evaporated under reduced pressure to afford an off-white viscous gel, which proved to be extremely hygroscopic. Before use in electrocrystallisation experiments, this material was dried at room temperature under vacuum for at least 15 h.

Tetramethylammonium (1R)-(+)-camphorsulfonate, 100

A 25% w/w solution of tetramethylammonium hydroxide in distilled water (23.6 mL, 64.7 mmol) was added to a stirred solution of (1R)-(+)-camphorsulfonic acid (15.0 g, 64.7 mmol) in distilled water (50 mL). The solution was stirred at room temperature for 30 min, and the pH was tested (pH = 7). Acetone (300 mL) was added to precipitate a white solid which was dried under vacuum at room temperature, to afford **100** (19.36 g, 98%) as a white solid Mp >280 °C (Found C, 55.1; H, 8.9; N, 4.5. C₁₄H₂₇NO₄S requires: C, 55.1; H, 8.9; N, 4.6%); ν_{\max} (ATR)/cm⁻¹ 3033, 2953, 1753, 1736, 1499, 1489, 1227, 1190, 1169, 1036, 952, 781, 760, 616, 610, 599, 577, 522, 508.

Tetramethylammonium (1S)-(-)-camphorsulfonate, 101

Tetramethylammonium (1S)-(-)-camphorsulfonate was prepared following an identical procedure to that used for **100**, affording **101** (18.96 g, 96%) as a white solid Mp > 280 °C; ν_{\max} (ATR)/cm⁻¹ 3033, 2953, 1753, 1736, 1499, 1489, 1227, 1190, 1169, 1036, 952, 781, 760, 616, 610, 599, 577, 522, 508.

Tetrabutylammonium bromide/ (1R)-(+)-camphorsulfonic acid mix, 102

To a solution of (1R)-(+)-camphorsulfonic acid (0.72g, 3.1 mmol) in acetonitrile (40 mL), was added tetrabutylammonium bromide (1.0 g, 3.1 mmol) and the solution stirred overnight under a nitrogen atmosphere. Evaporation of the solvent afforded **102** (1.7 g, 99 %) as a white viscous gum (Found C, 57.3; H, 7.6 %); δ_{H} (400 MHz, CDCl₃) 3.60 (1

H, q, $J=7.6, 7.1$ Hz), 3.21 (7H, m), 2.77 (1 H, m), 2.67 (1 H, d, $J=14.7$ Hz), 2.24 (0.5 H, t, $J=3.8$ Hz), 2.19 (0.5 H, t, $J=3.5$ Hz), 1.93 (2 H, m), 1.76 (1 H, d, $J=18.1$ Hz), 1.58 (7 H, m), 1.36 (6 H, m), 1.24 (1 H, m), 1.13 (2 H, t, $J=6.85$ Hz), 1.06 (3 H, s), 0.92 (9-10 H, t, $J=7.2$ Hz), 0.75 (3 H, s); δ_C (100 MHz, $CDCl_3$) 217.1, 58.4, 57.5, 47.6, 46.6, 42.8, 42.5, 26.9, 24.3, 23.8, 20.1, 19.7, 19.5, 18.1, 13.5.

Tetrabutylammonium bromide/ (1R)-(+)-camphorsulfonic acid mix, 103

(1R)-(+)-camphorsulfonic acid (1.44 g, 6.2 mmol) was added to a solution of tetrabutylammonium bromide (2.0 g, 6.2 mmol) in acetonitrile (60 mL), and the solution refluxed under a nitrogen atmosphere for 3 h. Evaporation of the solvent afforded a yellow-brown solid, which was used without further purification.

Tetrabutylammonium bromide/ (1S)-(-)-camphorsulfonic acid mix, 104

Prepared using an identical method to that shown for **103**.

4.3.4 Electrocrystallisation experimental

To the anodic side of a H-shaped electrochemical cell fitted with a glass frit was placed **11** (10 mg, 0.02 mmol), and from the cathodic side of the cell was added a solution of **99** (40 mg, 0.08 mmol) in 1,2,4-trichlorobenzene/ethanol (60:40 v/v, 25 mL). The level of solvent in each compartment was allowed to equilibrate, and to each side inserted a platinum-tipped (10 mm x 1 mm diameter) electrode. A constant current of 0.1 μ A was

applied across the cell for two weeks affording two dark rods on the anode. These were carefully collected, washed with acetone and dried in air. The crystal chosen for measurements was a black rod of dimensions 4.1 x 2.0 x 1.5 mm. This crystal was structurally determined by X-ray crystallography, and the composition confirmed by electron microprobe analysis on the SEM. Mp 206 °C; Raman /cm⁻¹ $\nu_4 = 1420, \nu_3 = 1450$.

In a similar experiment, black needles and fragile thin plates grew on the anode from acetonitrile. The needle used in the resistivity measurements was 3.5 x 0.8 x 0.9 mm. ν_{\max} (ATR)/cm⁻¹ 2680, 2334, 2120, 1992, 1653, 1330; Raman /cm⁻¹ $\nu_4^a = 1460$, $\nu_4^b = 1469$.

The plates were too fragile to be investigated.

To the anodic side of a H-shaped electrochemical cell fitted with a glass frit was placed **11** (10 mg, 0.02 mmol), and from the cathodic side of the cell was added a solution of **104** (40 mg) in 1,2,4-trichlorobenzene/ethanol (60:40 v/v, 25 mL). The level of solvent in each compartment was allowed to equilibrate, and to each side inserted a platinum-tipped (10 mm x 1 mm diameter) electrode. A constant current of 0.1 μ A was applied across the cell for two weeks affording small dark plates on the anode. These were carefully collected, washed with acetone and dried in air. Mp 209 °C.

4.4 (ET)₃(CoCl₄)₂

4.4.1 Introduction

There has been an extensive amount of research into the radical cation salts formed by the electrocrystallisation of ET, with a wide variety of anionic species. Tetrahedral anions have been investigated as the small volume occupied is believed to enhance the possibility of the existence of a superconducting phase, due to the closer packing motifs allowed.^{50, 51, 52, 53} In addition, the incorporation of paramagnetic centres is desirable due to the potential formation of dual functionality materials, or even a synergistic material, which may exhibit conductivity that responds cooperatively to the local magnetic environment.

The cobalt tetrachloride dianion has been investigated in the preparation of radical cation salts. Mixed radical cation salts of ET with [GaCl₄]⁻ and [CoCl₄]²⁻ were prepared,⁵⁴ and found to be isostructural with the salts formed with tetrachloride anions containing manganese and zinc.^{55, 56} Salts containing only the cobalt tetrachloride anion, with ET, were found to crystallise with included trichloroethane solvent.

4.4.2 Results and discussion

The electrocrystallisation of ET in a mixed solvent system of tetrahydrofuran and dichloromethane with [NBu₄]₂[CoCl₄] formed black needles on the electrode, which were suitable for analysis by single crystal X-ray diffraction. Resistivity measurements

were performed upon cooling from room temperature, and the material was found to show semiconductor behaviour down to 82 K, at which point the conductivity became negligible. The activation energy, calculated from the least squares best-fit linear relationship, was determined as $E_a = 0.034$ eV.

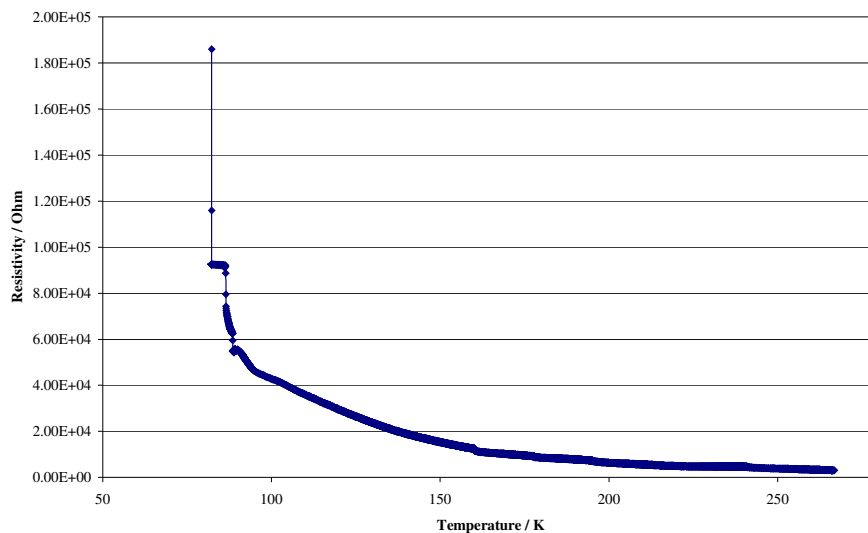


Figure 83: Resistivity profile for $(ET)_3(CoCl_4)_2$.

The crystal lattice is isostructural to those observed for mixed Ga/ Co salts of ET.^{54, 55, 56} Two distinct types of donor molecule were found to exist in the crystal structure. An overall columnar motif, with donor molecules slightly dimerised in a more local environment extended in the crystallographic *c* direction. The second donor type occupied positions interlaced between the columns and being isolated from surrounding molecules. This donor molecule was found to carry a charge of $Z = +1.7$, and for every one of these molecules, there was found to exist two donor molecules present in the columnar motif each carrying a charge of $Z = +0.8$. The charge states as determined by X-ray crystallographic measurements were supported by the investigation of the

material by Raman spectroscopy. The stoichiometry of 3:2 was also supported by the ν_4 symmetrical C=C stretch at 1465 cm^{-1} in the Raman spectrum.¹⁰

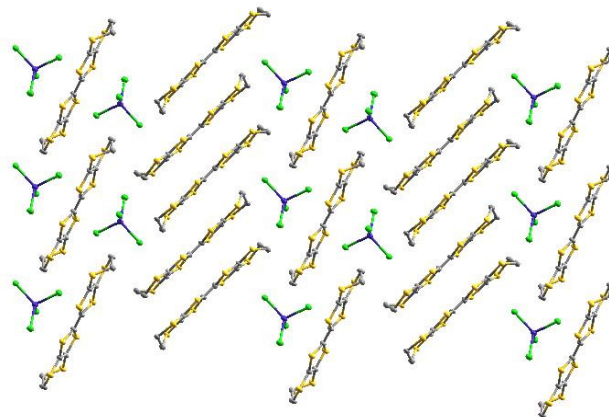


Figure 84: $(\text{ET})_3(\text{CoCl}_4)_2$ as viewed down the crystallographic a axis.

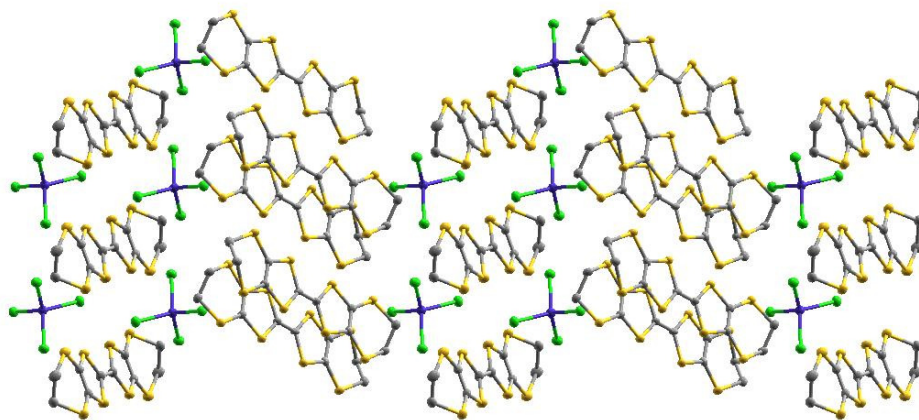


Figure 85: $(\text{ET})_3(\text{CoCl}_4)_2$ as viewed down the crystallographic b axis.

4.4.3 Experimental

Bis(tetrabutylammonium) [cobalt (II) tetrachloride], **105**

To a solution of cobalt (II) chloride (3.0g, 23.1 mmol) in ethanol (30 mL), was added a solution of tetrabutylammonium chloride (12.84g, 46.2 mmol) in ethanol (40 mL). The solution was heated to reflux under a nitrogen atmosphere for 1 h, and then cooled to -5°C overnight. Crystallisation had not occurred, and thus the blue solution was evaporated to yield a blue oil. Recrystallisation from acetonitrile failed, and so the oil was dissolved in acetone (30 mL), and petroleum ether 40-60 added to precipitate the product (15.83 g, >99%) as a light blue solid, which was collected by filtration and washed with additional petroleum ether 40-60 and dried Mp $169-170^{\circ}\text{C}$ (Found C, 56.2; H, 10.4; N, 4.15. $\text{C}_{32}\text{H}_{72}\text{N}_2\text{Cl}_4\text{Co}$ requires: C, 56.05; H, 10.6; N, 4.1 %); ν_{max} (ATR)/ cm^{-1} 3485, 2959, 2874, 1649, 1481, 1381, 1152, 1106, 1057, 1026, 881, 797, 735.

(ET)₃(CoCl₄)₂

To the anodic side of a H-shaped electrochemical cell fitted with a glass frit was placed **11** (10 mg, 0.02 mmol), and from the cathodic side of the cell was added a solution of **105** (40 mg, 0.06 mmol) in tetrahydrofuran/dichloromethane (50:50 v/v, 25 mL). The level of solvent in each compartment was allowed to equilibrate, and to each side inserted a platinum-tipped electrode. A constant current of $1.0\ \mu\text{A}$ was applied across

the cell for two days affording black needles on the anode Mp 216 °C; Raman/cm⁻¹ ν_4 = 1465.

4.5 References

- ¹ H. Yamochi, T. Komatsu, N. Matsukawa, G. Saito, T. Mori, M. Kusunoki and K. Sakaguchi, *J. Am. Chem. Soc.*, **1993**, 115, 11319.
- ² H. H. Wang, U. Geiser, J. A. Schlueter, B. H. Ward, J. P. Parakka, A. M. Kini, J. L. O'Malley, S. Y. Thomas, E. Morales, J. D. Dudek, J. M. Williams and G. L. Gard, *Synthetic Metals*, **1999**, 102, 1666.
- ³ M. Hashimoto, K. Yamamura and J. Yamane, *Tetrahedron*, **2001**, 57, 10253.
- ⁴ A. Miyazaki, T. Enoki and G. Saito, *Synthetic Metals*, **1995**, 70, 793.
- ⁵ H. Kobayashi, R. Kato, T. Mori, A. Kobayashi, Y. Sasaki, G. Saito, T. Enoki and H. Inokuchi, *Chem. Lett.*, **1984**, 179.
- ⁶ N. D. Kush, V. N. Laukhin, A. I. Schegolev, E. B. Yagubskii, E. Y. Alikberova and N. S. Rukk, *J. Phys. France*, **1991**, 1, 1365.
- ⁷ A. I. Kotov, L. I. Buravov, E. B. Yagubskii, S. S. Khasanov, L. V. Zorina, R. P. Shibaeva and E. Canadell, *Synthetic Metals*, **2001**, 124, 357.
- ⁸ U. Geiser, J. A. Schlueter, A. M. Kini, H. H. Wang, B. H. Ward, M. A. Whited, J. Mohtasham and G. L. Gard, *Synthetic Metals*, **2003**, 133-134, 401.
- ⁹ U. Geiser, J. A. Schlueter, H. H. Wang, A. M. Kini, J. M. Williams, P. P. Sche, H. I. Zakowicz, M. L. Vanzile, J. D. Dudek, P. G. Nixon, R. W. Winter, G. L. Gard, J. Ren and M. -H. Wangbo, *J. Am. Chem. Soc.*, **1996**, 118, 9996.
- ¹⁰ H. H. Wang, J. R. Ferraro, J. M. Williams, U. Geiser and J. A. Schlueter, *J. Chem. Soc., Chem Commun.*, **1994**, 1893.
- ¹¹ P. Guionneau, C. J. Kepert, G. Bravic, D. Chasseau, M. R. Truter, M. Kurmoo and P. Day, *Synth. Met.*, **1997**, 86, 1973.
- ¹² K. Hartke, *Chemische Berichte*, 1980, Volume 113, 5, 1898.
- ¹³ M. Meneghetti, R. Bozio and C. Pecile, *J. Phys. (Paris)*, **1986**, 47, 1377.
- ¹⁴ D. D. Perrin and W. L. F. Armarego, "Purification of Laboratory Chemicals", Pergamon Press, Exeter, **1988**, 3 ed.
- ¹⁵ H. Kobayashi, A. Kobayashi and P. Cassoux, *Chem. Soc. Rev.*, **2000**, 29, 325.
- ¹⁶ S. Uji, H. Shinagawa, T. Terashima, T. Yakabe, Y. Terai, M. Tokumoto, A. Kobayashi, H. Tanaka and H. Kobayashi, *Nature*, **2001**, 410, 908.

- ¹⁷ T. Otsuka, A. Kobayashi, Y. Miyamoto, J. Kiuchi, N. Wada, E. Ojima, H. Fujiwara and H. Kobayashi, *Chem. Lett.*, **2000**, 732.
- ¹⁸ H. Fujiwara, E. Fujiwara, Y. Nakazawa, B. Zh. Narymbetov, K. Kato, H. Kobayashi, A. Kobayashi, M. Tokumoto and P. Cassoux, *J. Am. Chem. Soc.*, **2001**, 123, 306.
- ¹⁹ H. Kobayashi, H. Tanaka, E. Ojima, H. Fujiwara, Y. Nakazawa, T. Otsuka, A. Kobayashi, M. Tokumoto and P. Cassoux, *Synthetic Metals*, **2001**, 120, 663.
- ²⁰ S. S. Turner, D. Le Pévelen, P. Day and K. Prout, *J. Chem. Soc., Dalton Trans.*, **2000**, 2739.
- ²¹ S. S. Turner, C. Michaut, S. Durot, P. Day, T. Gelbrich and M. B. Hursthouse, *J. Chem. Soc., Dalton Trans.*, **2000**, 905.
- ²² S. S. Turner, D. Le Pévelen and P. Day, *Synthetic Metals*, **2003**, 133-134, 497.
- ²³ S. S. Turner and P. Day, *J. Mater. Chem.*, **2005**, 15, 23.
- ²⁴ K. D. Carlson, U. Geiser, A. M. Kini, H. H. Wang, L. K. Montgomery, W. K. Kwok, M. A. Beno, J. M. Williams, C. S. Cariss, G. W. Crabtree, M. –H. Whangbo and M. Evain, *Inorg. Chem.*, **1988**, 27, 965.
- ²⁵ H. Müller, C. –P. Heidmann, W. Biberacher and K. Andres, *Synthetic Metals*, **1991**, 41-43, 1943.
- ²⁶ F. Bérézovsky, S. Triki, J. Sala Pala, J. R. Galán-Mascarós, C. J. Gómez-García, E. Coronado, *Synthetic Metals*, **1999**, 102, 1755.
- ²⁷ F. Setifi, L. Ouahab, S. Golhen, O. Hernandez, A. Miyazaki, T. Enoki, T. Toita, J. Yamada, H. Nishikawa, A. Łapiński and R. Świetlik, *Inorg. Chem.*, **2002**, 41, 3761.
- ²⁸ F. Setifi, L. Ouahab, S. Golhen, A. Miyazaki, T. Enoki and J. Yamada, *C. R. Chimie*, **2003**, 6, 309.
- ²⁹ M. Kurmoo, A. W. Graham, P. Day, S. J. Coles, M. B. Hursthouse, J. L. Caulfield, J. Singleton, F. L. Pratt, W. Hayes, L. Ducasse and P. Guionneau, *J. Am. Chem. Soc.*, **1995**, 117, 12209.
- ³⁰ S. Rashid, S. S. Turner, P. Day, J. A. K. Howard, P. Guionneau, E. J. L. McInnes, F. E. Mabbs, R. J. H. Clark, S. Firth and T. Biggs, *J. Mater. Chem.*, **2001**, 11, 2095.
- ³¹ S. S. Turner, P. Day, K. M. A. Malik and M. B. Hursthouse, *Inorg. Chem.*, **1999**, 38, 3543.
- ³² S. Sun, P. Wu, Q. Zhang and D. Zhu, *Synthetic Metals*, **1998**, 94, 161.
- ³³ E. Coronado, J. R. Galan-Mascaros, C. J. Gómez-García, V. N. Laukhin, *Nature*, **2000**, 408, 447.
- ³⁴ F. Thétiot, F. Bérézovsky, S. Triki, J. Sala Pala, C. J. Gómez-García, A. A. Hajem, S. Bouguessa and J. –M. Fabre, *C. R. Chimie*, **2003**, 6, 291.

- ³⁵ L. Martin, S. S. Turner, P. Day, P. Guionneau, J. A. K. Howard, D. E. Hibbs, M. E. Light, M. B. Hursthouse, M. Uruichi, K. Yakushi, *Inorg. Chem.*, **2001**, 40, 1363.
- ³⁶ G. L. J. A. Rikken, E. Raupach, V. Krstic and S. Roth, *Molec. Phys.*, **2002**, 100, 1155.
- ³⁷ A. Werner, *Ber.*, **1912**, 45, 3061.
- ³⁸ F. M. Jaeger, *J. Chem. Soc. Abstracts*, **1919**, 116, Pt. 1, 5.
- ³⁹ S. S. Turner, P. Day, T. Gelbrich and M. B. Hursthouse, *J. Solid-State Chem.*, **2001**, 159, 385.
- ⁴⁰ C. J. Kepert, M. Kurmoo, M. R. Truter and P. Day, *J. Chem. Soc. Dalton Trans.*, **1997**, 607.
- ⁴¹ J. M. Williams and K. Carneiro, *Adv. Inorg. Chem. Radiochem.*, **1985**, 29, 249.
- ⁴² J. M. Williams, *J. Phys (Paris) Colloq.*, **1983**, 44, C3-941.
- ⁴³ L. Zhang and M. Wan, *Thin Solid Films*, **2005**, 477, 24.
- ⁴⁴ H. H. Havinga, M. M. Bouman, E. W. Meijer, A. Pomp and M. M. J. Simenon, *Synthetic Metals*, **1994**, 66, 93.
- ⁴⁵ V. Abantanos, L. A. P. Kane-Magime and G. G. Wallace, *Synthetic Metals*, **2000**, 114, 313.
- ⁴⁶ V. Egan, R. Bernstein, L. Hohmann, T. Trau and R. B. Koner, *Chem. Comm.*, **2001**, 801.
- ⁴⁷ M. R. Majidi, L. A. P. Kane-Magime and G. G. Wallace, *Polymer*, **1994**, 35, 3113.
- ⁴⁸ M. R. Majidi, L. A. P. Kane-Magime and G. G. Wallace, *Polymer*, **1995**, 36, 3597.
- ⁴⁹ H. D. Flack, *Acta Cryst.* **1983**, A39, 876.
- ⁵⁰ K. Bechgaard, D. O. Cowan and A. N. Bloch, *J. Chem. Soc. Chem. Comm.*, **1974**, 938.
- ⁵¹ D. Jérôme, A. Mazaud, M. Ribault and K. Bechgaard, *J. Phys. Lett. (Paris)*, **1980**, 41, L95.
- ⁵² K. Bechgaard, C. S. Jacobsen, K. Mortenson, H. J. Pederson and N. Thorup, *Solid State Communications*, **1980**, 33, 1119.
- ⁵³ K. Bechgaard, K. Carneiro, F. B. Rasmussen, M. Olsen, G. Rindorf, C. S. Jacobsen, H. J. Pedersen and J. C. Scott, *J. Am. Chem. Soc.*, **1981**, 103, 2440.
- ⁵⁴ H. Mori, M. Kamiya, M. Haemori, H. Suzuki, S. Tanaka, Y. Nishio, K. Kajita and H. Moriyama, *J. Am. Chem. Soc.*, **2002**, 124, 1251.
- ⁵⁵ T. Mori, H. Inokuchi, *Bull. Chem. Soc. Jpn.*, **1988**, 61, 591.
- ⁵⁶ R. P. Shibaeva, R. M. Lobkovskaya, V. E. Korotkov, N. D. Kuahxh, E. B. Yagubskii and M. K. Makova, *Synth. Met.*, **1988**, 27, A457.

Chapter 5

Chiral metal anion complexes

5 Chiral metal anion complexes

5.1 Introduction

In order to study whether control of the crystalline packing arrangement of radical cation salts was achievable by the selection of component species based on their electronic properties, a range of anionic species containing delocalised π -electron fragments were prepared and employed in electrocrystallisation experiments. It was hoped that π - π interactions between the radical cations and the anion, would lead to closer association of molecular species, reducing the unit cell volume and increasing the number of short contacts, specifically S...S interactions. The increased number of short contact interactions would reduce the electrical resistivity of the crystal, due to increased orbital overlap. In these electrocrystallised salts, metal coordination complexes containing such ligands as *isoquinoline*, 2,2-bipyridine and 1,10-phenanthroline were investigated.^{1, 2, 3}

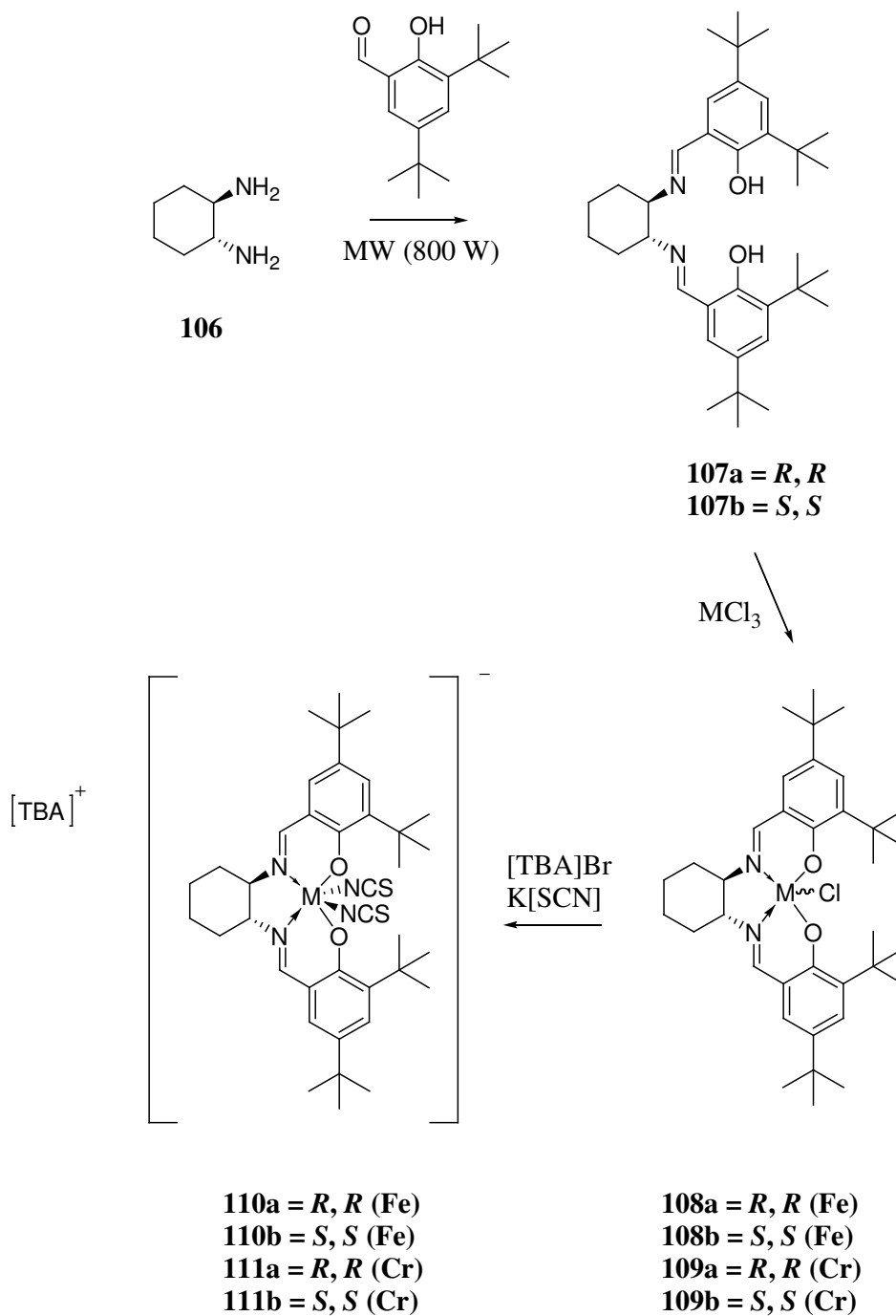
More recently, transition metal complexes containing a series of aromatic bis-Schiff base ligands have been synthesised and employed in the preparation of radical cation salts by electrocrystallisation with organosulfur electron donor molecules.⁴ There exists a large family of salen-type ligands, and these have been extensively reviewed, with a specific focus on their employment in fields such as catalysis, where Jacobsen and others have created chiral catalysts for the asymmetric oxidation of alkenes.^{5, 6, 7, 8} Building on the extensive work with salen structures, it was decided to synthesise chiral (at carbon) metal anionic species. This type of ligand, being tetradentate, was chosen

specifically as there are then no possibilities of obtaining Δ and Λ isomers of the metal coordination complex, a problem which was encountered when attempting to prepare single enantiomers of the tris(oxalate) species which rapidly racemise.^{9, 10} These materials could then be utilised in electrocrystallisation to promote more ordered packing within the lattice, and potentially lead to superconductors at more readily accessible temperatures.

5.2 Results and Discussion

It was decided to prepare the chiral, sterically bulky transition metal complexes in which the metal employed was either Cr (III) or Fe (III). These were chosen as there is the potential to obtain a material that exhibits bi-functionality, conductivity and magnetism, and possibly even with the two properties able to work cooperatively, creating a tuneable device. In addition the steric bulk should assist in inducing a greater chiral influence on the crystal lattice, which could lead to greater packing control and interesting properties such as chiral conduction anisotropy. As such, enantiopure *R, R* and *S, S* salen-type ligands *N,N'*-bis(3,5-di-*tert*-butylsalicylidene)-1,2-cyclohexanediamine were coordinated to the paramagnetic transition metals and the remaining axial coordination sites in the octahedral complex taken up by isothiocyanate ligands. This approach (Scheme 14) serves to give the complex anion an overall charge of -1 , which is stabilised by the tetrabutylammonium cation, allowing for increased solubility in the electrocrystallisation experiments.

The *R, R* enantiomer of the tetradentate ligand was prepared by the microwave heating (domestic microwave, 800 W) of neat *R, R*-1,2-cyclohexyldiamine **106** with 2-hydroxy-3,5-di(*t*-butyl)benzaldehyde. Upon colour change, the hot viscous liquid was removed from the microwave oven and ethanol added. As the mixture cooled, yellow crystals formed. These were subsequently collected by filtration when cold, and washed with ethanol to afford the tetradentate ligand **107a** in 98 % yield, identified by infrared spectroscopy with comparison to a known sample. The opposite enantiomer **107b** was purchased from SigmaAldrich, as the precursor enantiopure diamine was unavailable. Coordination of the tetradentate ligand to a metal centre was achieved by adding dropwise a solution of the corresponding metal (III) chloride in methanol, to a chloroform solution of the ligand, under a nitrogen atmosphere. Heating to reflux and addition of sodium carbonate, followed by evaporation and recrystallisation from hot methanol afforded the metal coordination complexes **108a**, **108b**, **109a** and **109b** individually in near quantitative yield.



Scheme 14: Synthetic route to enantiopure anions 110, 110a, 111 and 111a.

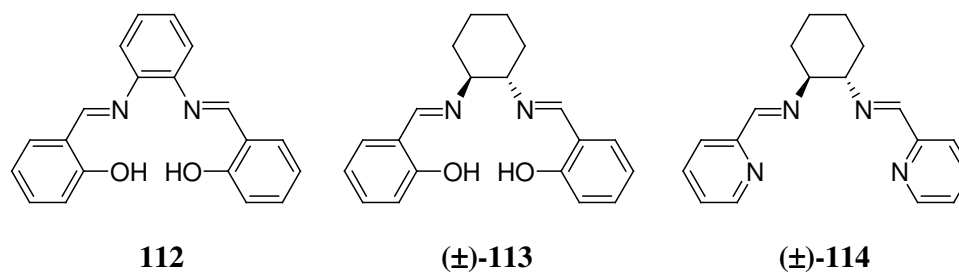
Formation of the anionic metal complex was achieved by refluxing the appropriate metal coordination complex **108a**, **108b**, **109a** or **109b**, with two equivalents of potassium thiocyanate and one equivalent of tetrabutylammonium bromide in acetone. After filtration and concentration of the filtrate, the desired salts **110a**, **110b**, **111a** and **111b** were isolated in near quantitative yield, and characterised by elemental analysis, infrared spectroscopy and mass spectrometry.

Despite all spectroscopic data supporting the formation of the desired complexes, the determination of the structures of **110a** and **111a** by X-ray crystallography showed formation of the neutral complex, and no evidence in the crystal structure for the additional *isothiocyanate* coordinated ligand or the charge-stabilising tetrabutylammonium cation. Crystals of **111a** grown from a tetrahydrofuran solution, showed that one of the axial *isothiocyanate* ligands had been replaced by a solvent molecule. It could be concluded that dissociation of one of the *isothiocyanate* ligand occurs readily in solution. Further evidence for this is presented by the low quantities of oxidised material produced by electrocrystallisation, as a low concentration of anions in solution can only crystallise out a low amount of radical cations.

The salen complexes synthesised **110a**, **110b**, **111a** and **111b** were employed in electrocrystallisation experiments with ET and tetrol **37**. As mentioned above, in all instances in which a visibly dark material was produced on the anode, only a low yield (<1 mg) was achieved. As such, only Raman spectroscopy was suitable for the characterisation of the materials, as according to the method of Wang *et al.*¹¹ For radical cation salts of **11** the stoichiometry was shown to be 1:1, for several of the

enantiopure salen complexes. When **37** was electrocrystallised with a salen compound, a 3:2 salt was produced as determined by Raman spectroscopy. Resistivity measurements were not possible on any of the compounds synthesised, due to the small nature of the radical cation salts.

Further salen-type Schiff base ligands were synthesised in the microwave to test the validity of the method of synthesis. As such, phenylene-1,2-diamine and *trans*-cyclohexyl-1,2-diamine were reacted with salicylaldehyde to give the corresponding bis-Schiff bases **112** and **113**, and pyridine-2-carboxaldehyde was reacted with *trans*-cyclohexyl-1,2-diamine to give **114**.



5.3 Experimental

(*S,S*)-(+)-*N,N'*-Bis(3,5-di-*tert*-butylsalicylidene)-1,2-cyclohexanediamine, 1,2-phenylenediamine, *trans*-1,2-cyclohexanediamine and (*R,R*)-1,2-cyclohexanediamine were purchased from SigmaAldrich and used as received.

(*R,R*)-(-)-*N,N'*-Bis(3,5-di-*tert*-butylsalicylidene)-1,2-cyclohexanediamine, 107a

2-Hydroxy-3,5-di(*t*-butyl)benzaldehyde (2.0 g, 8.5 mmol) was placed in a 250 mL beaker, and to it was carefully added **106** (0.49 g, 4.25 mmol). The mixture was swirled briefly, placed in a conventional 800 W microwave oven and heated on half-power for 1 min, before being removed from the microwave and allowed to stand for 1 min. Ethanol (50 mL) was added to the flask and left to precipitate the product, which was subsequently collected by filtration to afford **107a** (2.3 g, 99%) as yellow crystals; ν_{\max} (ATR)/ cm^{-1} 2950, 2863, 1629, 1593, 1468, 1449, 1437, 1390, 1361, 1323, 1269, 1252, 1240, 1202, 1173, 1135, 1085, 1063, 1037, 975, 940, 906, 879, 862, 828, 804, 772, 732, 711, 644, 595, 559, 544, 509, 492, 458.

(*S,S*)-(+)-*N,N'*-Bis(3,5-di-*tert*-butylsalicylidene)-1,2-cyclohexanediamine, 107b

Purchased from SigmaAldrich, gave (for comparison): ν_{\max} (ATR)/ cm^{-1} 2951, 2863, 1629, 1591, 1467, 1437, 1390, 1361, 1324, 1308, 1269, 1252, 1239, 1202, 1173, 1135, 1116, 1085, 1063, 1037, 1005, 975, 939, 906, 879, 862, 827, 804, 772, 732, 711, 644, 595, 559, 545, 509, 492, 460.

[((*R,R*)-(-)-*N,N'*-Bis(3,5-di-*tert*-butylsalicylidene)-1,2-cyclohexanediamine) iron (III) chloride], 108a

Ligand **107a** (0.4 g, 0.73 mmol) was dissolved in chloroform (20 mL) and to this added a solution of iron (III) chloride hexahydrate (0.2 g, 0.73 mmol) in methanol (20 mL).

The resultant dark solution was heated to reflux for 10 min before addition of sodium carbonate (0.054 g, 0.51 mmol). Reflux was continued for an additional 6 h, before cooling to room temperature overnight. Solvents were removed under reduced pressure, and hot methanol (40 mL) added. The reaction was allowed to cool, and a deep purple solid **108a** (0.32 g, 69%) collected by filtration. The residual methanolic solution was concentrated further to yield additional **108a** as a purple solid, in quantitative yield (Found C, 67.9; H, 8.1; N, 4.4. $\text{FeC}_{36}\text{H}_{52}\text{N}_2\text{O}_2\text{Cl}$ requires C, 68.0; H, 8.2; N, 4.4%); ν_{max} (ATR)/ cm^{-1} 2958, 2867, 1599, 1553, 1534, 1459, 1430, 1409, 1385, 1361, 1341, 1312, 1270, 1253, 1217, 1199, 1171, 1131, 1097, 1029, 976, 917, 888, 874, 862, 840, 814, 781, 750, 722, 641, 594, 573, 553, 541, 481, 461, 418, 388.

(((S,S)-(+)-N,N'-Bis(3,5-di-tert-butylsalicylidene)-1,2-cyclohexanediamine) iron (III) chloride], 108b

Purple solid (98 %); ν_{max} (ATR/ cm^{-1}) 2957, 2868, 1645, 1599, 1555, 1533, 1462, 1434, 1410, 1385, 1361, 1341, 1313, 1270, 1252, 1229, 1199, 1171, 1133, 1080, 1025, 976, 965, 929, 888, 874, 862, 840, 814, 800, 782, 769, 749, 713, 642, 594, 574, 552, 541, 482.

[[*(R,R)*-(-)-*N,N'*-Bis(3,5-di-*tert*-butylsalicylidene)-1,2-cyclohexanediamine) chromium (III) chloride], 109a

Dark orange solid (85 %); ν_{\max} (ATR)/ cm^{-1} 2950, 2867, 1615, 1532, 1460, 1434, 1409, 1386, 1360, 1318, 1271, 1254, 1235, 1199, 1169, 1135, 1027, 970, 916, 873, 837, 814, 784, 749, 725, 667, 639, 564, 543, 511, 480, 426, 412, 396.

[[*(S,S)*-(+)-*N,N'*-Bis(3,5-di-*tert*-butylsalicylidene)-1,2-cyclohexanediamine) chromium (III) chloride], 109b

Dark orange solid (87 %); ν_{\max} (ATR)/ cm^{-1} 2951, 2906, 2866, 1615, 1548, 1532, 1460, 1435, 1409, 1386, 1360, 1319, 1271, 1254, 1235, 1199, 1168, 1136, 1049, 1026, 969, 927, 915, 873, 837, 814, 784, 748, 726, 668, 639, 563, 543, 512, 484, 467, 451, 419, 413, 402, 294.

Tetrabutylammonium [[*(R,R)*-(-)-*N,N'*-bis(3,5-di-*tert*-butylsalicylidene)-1,2-cyclohexanediamine) iron (III) diisothiocyanate], 110a

Complex **108a** (0.3 g, 0.47 mmol), potassium thiocyanate (0.09 g, 0.94 mmol) and tetrabutylammonium bromide (0.15 g, 0.47 mmol) were dissolved in acetone (50 mL) and heated to reflux for 5 h. The reaction was allowed to cool to room temperature and filtered, washing with cold acetone. The filtrate was concentrated to around 10 mL and left at room temperature overnight, affording long dark needles of **110a** (0.16 g, 35 %), further concentration and standing afforded additional **110a** (0.27 g, 59%) as a dark

microcrystalline solid (Found C, 67.7; H, 9.3; N, 7.2. $\text{FeC}_{54}\text{H}_{88}\text{N}_5\text{O}_2\text{S}_2$ requires C, 67.6; H, 9.25; N, 7.3%); ν_{max} (ATR/ cm^{-1}) 3406, 2958, 2869, 2033, 1711, 1598, 1557, 1534, 1461, 1431, 1408, 1384, 1360, 1341, 1321, 1309, 1270, 1252, 1224, 1199, 1172, 1131, 1096, 1027, 976, 927, 918, 885, 874, 862, 839, 814, 781, 749, 724, 640, 594, 573, 553, 541, 531, 482, 460; m/z (FAB): found: 714.2928 $[\text{M-NBu}_4]^+$. $\text{FeC}_{38}\text{H}_{52}\text{N}_4\text{O}_2\text{S}_2$ requires 714.2933.

Tetrabutylammonium **[[*(S,S)*-(+)-*N,N'*-bis(3,5-di-*tert*-butylsalicylidene)-1,2-cyclohexanediamine) iron (III) diisothiocyanate], 110b**

Red-brown powder (93 %) (Found C, 67.6 H, 9.1 N, 7.4. $\text{FeC}_{54}\text{H}_{88}\text{N}_5\text{O}_2\text{S}_2$ requires C 67.6, H 9.25, N 7.3%); ν_{max} (ATR)/ cm^{-1} 3404, 2956, 2867, 2035, 1710, 1599, 1557, 1536, 1462, 1431, 1408, 1385, 1360, 1342, 1309, 1271, 1252, 1224, 1199, 1174, 1028, 977, 918, 875, 863, 839, 815, 781, 749, 641, 594, 555, 543, 531, 483, 438, 419, 403, 391.

Tetrabutylammonium **[[*(R,R)*-(-)-*N,N'*-bis(3,5-di-*tert*-butylsalicylidene)-1,2-cyclohexanediamine) chromium (III) diisothiocyanate], 111a**

Orange-brown powder (89 %) (Found C, 67.8 H, 9.2 N, 7.4. $\text{CrC}_{54}\text{H}_{88}\text{N}_5\text{O}_2\text{S}_2$ requires C, 67.9; H, 9.3; N, 7.3%); ν_{max} (ATR)/ cm^{-1} 3363, 2947, 2904, 2867, 2102, 1615, 1552, 1531, 1464, 1433, 1409, 1386, 1361, 1343, 1317, 1271, 1254, 1235, 1201, 1169, 1138, 1099, 1013, 971, 917, 888, 875, 864, 837, 814, 783, 748, 725, 668, 639, 592, 562, 541,

509, 487, 465, 448, 427, 416. m/z (FAB): found: 712.2941 $[M-NBu_4]^+$.
 $CrC_{38}H_{52}N_4O_2S_2$ requires 712.2942

Tetrabutylammonium [(*S,S*)-(+)-*N,N'*-bis(3,5-di-*tert*-butylsalicylidene)-1,2-cyclohexanediamine) chromium (III) diisothiocyanate], **111b**

Orange-brown powder (94 %) (Found C, 67.8 H, 9.1 N, 7.3. $CrC_{54}H_{88}N_5O_2S_2$ requires C, 67.9 H, 9.2 N, 7.3 %); ν_{max} (ATR)/ cm^{-1} 3351, 2950, 2907, 2866, 2100, 1614, 1552, 1532, 1459, 1433, 1409, 1386, 1361, 1343, 1318, 1294, 1270, 1254, 1234, 1200, 1169, 1138, 1099, 1014, 971, 961, 926, 917, 888, 875, 864, 837, 814, 783, 748, 725, 668, 640, 592, 563, 542, 509, 487, 465, 448, 427, 415, 395. m/z (FAB): found: 712.2946 $[M-NBu_4]^+$. $CrC_{38}H_{52}N_4O_2S_2$ requires 712.2942

N,N'*-Bis(salicylidene)-1,2-phenylenediamine, **112*

1,2-Phenylenediamine (8.87 g, 81.9 mmol) was placed in a 250 mL beaker, and to it was added salicylaldehyde (20 g, 0.164 mol). The mixture was swirled gently and placed in a conventional 800 W microwave oven. The reaction was heated on half-power for 30 s, the flask swirled, and then heated for a further 1 min. The flask was removed, and ethanol (130 mL) added. Filtration afforded the product **112** (25.4 g, 98%) as bright orange crystals; ν_{max} (ATR)/ cm^{-1} 1610, 1585, 1561, 1480, 1276, 1191, 1150, 909, 759, 745, 501; δ_H (400 MHz, $CDCl_3$) 8.62 (2 H, s, 7-, 7'-*H*), 7.39-7.31 (6 H, overlapping m, 3-, 4-, 5-, 6-, 13-, 13'-*H*), 7.25-7.20 (2 H, m, 11-, 11'-*H*), 7.04 (2 H, d, $J=8.12$ Hz, 12-, 12'-*H*), 6.91 (2 H, dt, $J=7.44, 1.04, 1.0$ Hz, 10-, 10'-*H*); δ_C (100 MHz,

CDCl₃) 163.7 (7-, 7'-C), 161.3 (9-, 9'-C), 142.5 (1-, 2-C), 133.3 (11-, 11'-C), 132.3 (13-, 13'-C), 127.7 (4-, 5-C), 119.7 (3-, 6-C), 119.2 (8-, 8'-C), 118.9 (12-, 12'-C), 117.5 (10-, 10'-C); *m/z* (GCMS): found: 314 [M-2H]⁺, 285, 269, 255, 221, 207, 194, 167, 157, 139, 115, 91, 77. C₂₀H₁₆N₂O₂ -2H requires: 314.

***Trans-N,N'*-bis(salicylidene)-1,2-cyclohexanediamine, 113**

Salicylaldehyde (20.0 g, 0.164 mol) was placed in a 250 mL beaker, and to it was carefully added *trans*-1,2-cyclohexyldiamine (9.35 g, 81.9 mmol). The mixture was swirled briefly, placed in a conventional 800 W microwave oven and heated on half-power for 1 min, before being removed from the microwave and allowed to stand for 1 min. Ethanol (150 mL) was added to the flask and left to precipitate the product, which was subsequently collected by filtration to afford **113** (26.1g, 99%) as bright yellow crystals; ν_{\max} (ATR)/cm⁻¹ 2941, 2921, 2848, 1626, 1580, 1500, 1416, 1278, 1216, 1148, 1095, 1045, 844, 758, 659; δ_{H} (400 MHz, CDCl₃) 8.25 (2 H, s, 7-, 7'-H), 7.25 (2 H, dt, *J*=7.44, 1.04, 1.72 Hz, 13-, 13'-H), 7.16 (2 H, dd, *J*=7.68, 1.72 Hz, 11-, 11'-H), 6.89 (2 H, d, *J*=8.28 Hz, 12-, 12'-H), 6.80 (2 H, dt, *J*=7.48, 0.92 Hz, 10-, 10'-H), 3.36-3.29 (2 H, m, 1-, 2-H), 1.97-1.86 (4 H, m, 3 α -, 3 β -, 6 α -, 6 β -H), 1.78-1.69 (2 H, m, 4 α -, 5 α -H), 1.51-1.46 (2 H, m, 4 β -, 5 β -H); δ_{C} (100 MHz, CDCl₃) 164.7 (7-, 7'-C), 160.9 (9-, 9'-C), 132.1 (11-, 11'-C), 131.4 (13-, 13'-C), 118.6 (12-, 12'-C), 116.7 (10-, 10'-C), 72.6 (1-, 2-C), 33.1 (3-, 6-C), 24.1 (4-, 5-C); *m/z* (GC-MS): found: 322 [M]⁺, 201, 184, 159, 122, 107, 77. C₂₀H₂₂N₂O₂ requires: 322.

Trans-*N,N'*-bis(2', 2''-pyridylidene)-1,2-cyclohexanediamine, 114

Pyridine-2-carboxaldehyde (2 g, 18.7 mmol) and *trans*-1,2-cyclohexyldiamine (1.07 g, 9.35 mmol) were swirled together in a 100 mL beaker and placed in a conventional 800 W microwave oven. The reaction was heated on half-power for 2 min, the flask removed from the oven, and ethanol (30 mL) added to precipitate **114** (2.0 g, 73%) as an off-white solid; $\nu_{\max}(\text{ATR})/\text{cm}^{-1}$ 3052, 3007, 2935, 2851, 1644, 1586, 1567, 1467, 1436, 1369, 1339, 1305, 1283, 1236, 1199, 1135, 1097, 1078, 1039, 993, 974, 935, 865, 839, 790, 769, 740, 667, 619, 534, 511, 489, 460; δ_{H} (400 MHz, CDCl_3) 8.50 (2 H, ddd, $J=4.92, 1.60, 0.92$ Hz, 6'-, 6''-*H*), 8.28 (2 H, s, *CHN*), 7.85 (2 H, d, $J=7.92$ Hz, 4'-, 4''-*H*), 7.60 (2 H, ddd, $J=7.8, 7.6, 1.5$ Hz, 3', 3''-*H*), 7.17 (2 H, m, 5'-, 5''-*H*), 3.50 (2 H, m, 1-, 2-*H*), 1.81 (6 H, m, cyclohexyl-*H*), 1.48 (2 H, m, cyclohexyl-*H*); δ_{C} (100 MHz, CDCl_3) 161.3 (*CHN*), 154.5 (2'-, 2''-*C*), 149.1 (6'-, 6''-*C*), 136.3 (4'-, 4''-*C*), 124.4 (5'-, 5''-*C*), 121.2 (3'-, 3''-*C*), 73.5 (1-, 2-*C*), 32.6 (3-, 6-*C*), 24.3 (4-, 5-*C*); m/z (GC-MS): found: 292 $[\text{M}]^+$, 275, 249, 214, 200, 186, 171, 158, 145, 131, 119, 107, 92, 79, 65, 51. $\text{C}_{18}\text{H}_{20}\text{N}_4$ requires: 292. Data comparable to that of the literature.¹²

5.4 Electrocrystallisation experiments**(11)[111b]**

To the anodic side of a H-shaped electrochemical cell fitted with a glass frit was placed **11** (10 mg, 0.02 mmol), and from the cathodic side of the cell was added a solution of **111b** (40 mg, 0.04 mmol) in chlorobenzene/tetrahydrofuran (50:50 v/v, 25 mL). The

level of solvent in each compartment was allowed to equilibrate, and to each side inserted a platinum-tipped electrode. A constant current of 0.1 μA was applied across the cell for one week affording a few black micro-clusters of needles on the electrode.

Raman/ cm^{-1} $\nu_4 = 1424$, $\nu_3 = 1462$.

(11)[110a]

To the anodic side of a H-shaped electrochemical cell fitted with a glass frit was placed **11** (10 mg, 0.02 mmol), and from the cathodic side of the cell was added a solution of **110a** (40 mg, 0.04 mmol) in dichloromethane (25 mL). The level of solvent in each compartment was allowed to equilibrate, and to each side inserted a platinum-tipped electrode. A constant current of 1 μA was applied across the cell for eight days affording flat half-arrow heads (elongated right-angled triangle) on the anode:

Raman/ cm^{-1} $\nu_4 = 1424$, $\nu_3 = 1464$.

(11)[110b]

To the anodic side of a H-shaped electrochemical cell fitted with a glass frit was placed **11** (10 mg, 0.02 mmol), and from the cathodic side of the cell was added a solution of **110b** (40 mg, 0.04 mmol) in dichloromethane (25 mL). The level of solvent in each compartment was allowed to equilibrate, and to each side inserted a platinum-tipped electrode. A constant current of 0.1 μA was applied across the cell for six days affording brittle thin dark plates: Raman/ cm^{-1} $\nu_4 = 1411$, $\nu_3 = 1459$.

(37)₃[111a]₂

To the anodic side of a H-shaped electrochemical cell fitted with a glass frit was placed **37** (10 mg, 0.02 mmol), and from the cathodic side of the cell was added a solution of **111a** (40 mg, 0.04 mmol) in 1,2,4-trichlorobenzene/ethanol (60:40 v/v, 25 mL). The level of solvent in each compartment was allowed to equilibrate, and to each side inserted a platinum-tipped electrode. A constant current of 0.2 μA was applied across the cell for thirteen days affording black micro-clusters of blocks on the cell bottom and microcrystalline clusters of black plates on the anode: Raman/ cm^{-1} $\nu_4 = 1460$, $\nu_3 = 1475$.

5.5 References

- ¹ S. S. Turner, C. Michaut, S. Durot, P. Day, T. Gelbrich and M. B. Hursthouse, *J. Chem. Soc., Dalton Trans.*, **2000**, 905.
- ² S. S. Turner and P. Day, *J. Mater. Chem.*, **2005**, 15, 23.
- ³ S. S. Turner, D. Le Pévelen and P. Day, *Synthetic Metals*, **2003**, 133-134, 497.
- ⁴ S. Wang, P. Day, J.D. Wallis, P.N. Horton, M.B. Hursthouse, *Polyhedron*, **2006**, 25, 2583.
- ⁵ R. I. Kureshy, I. Ahmad, N. H. Khan, S. H. R. Abdi, K. Pathak and R. V. Jasra, *Tetrahedron Asymmetry*, **2005**, 16, 3562.
- ⁶ M. North, *Asymmetric Phase Transfer Catalysis*, **2008**, 161.
- ⁷ T. R. J. Achard, L. A. Clutterbuck and M. North, *Synlett*, **2005**, 1828.
- ⁸ D. A. Atwood and M. J. Harvey, *Chem. Rev.*, **2001**, 101, 37.
- ⁹ A. Werner, *Ber.*, **1912**, 45, 3061.
- ¹⁰ F. M. Jaeger, *J. Chem. Soc. Abstracts*, **1919**, 116, Pt.1, 5.
- ¹¹ H.H. Wang, J.R. Ferraro, J.M. Williams, U. Geiser, J.A. Schlueter, *J. Chem. Soc., Chem. Commun.*, **1994**, 1893.
- ¹² S. Schoumacker, O. Hamelin, J. Pécaut and M. Fontecave, *Inorganic Chemistry*, **2003**, 42, 8110.

Chapter 6

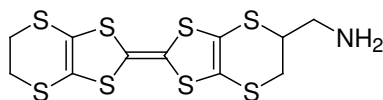
Aldehyde functionalised organosulfur electron donors

6 Aldehyde functionalised organosulfur electron donors

6.1 Introduction

The synthetic route to organosulfur electron donors is extensive and low yielding, consisting of at least five steps with an overall yield of between 15-30 %. Other researchers have developed methodologies to reduce the number of synthetic steps, however they require the use of unstable species handled under highly controlled conditions.¹

Another approach is to synthesise a donor molecule, which can be easily functionalised as required at a later stage, such as the aminomethyl **115**,² methyl methanoate **15**,³ and hydroxymethyl **14**,⁴ derivatives of ET. These however provide access only to a limited number of derivatives.



115

Compounds functionalised with aldehyde groups allow a wide range of materials to be accessed, some of the pathways of which are shown in Figure 86.

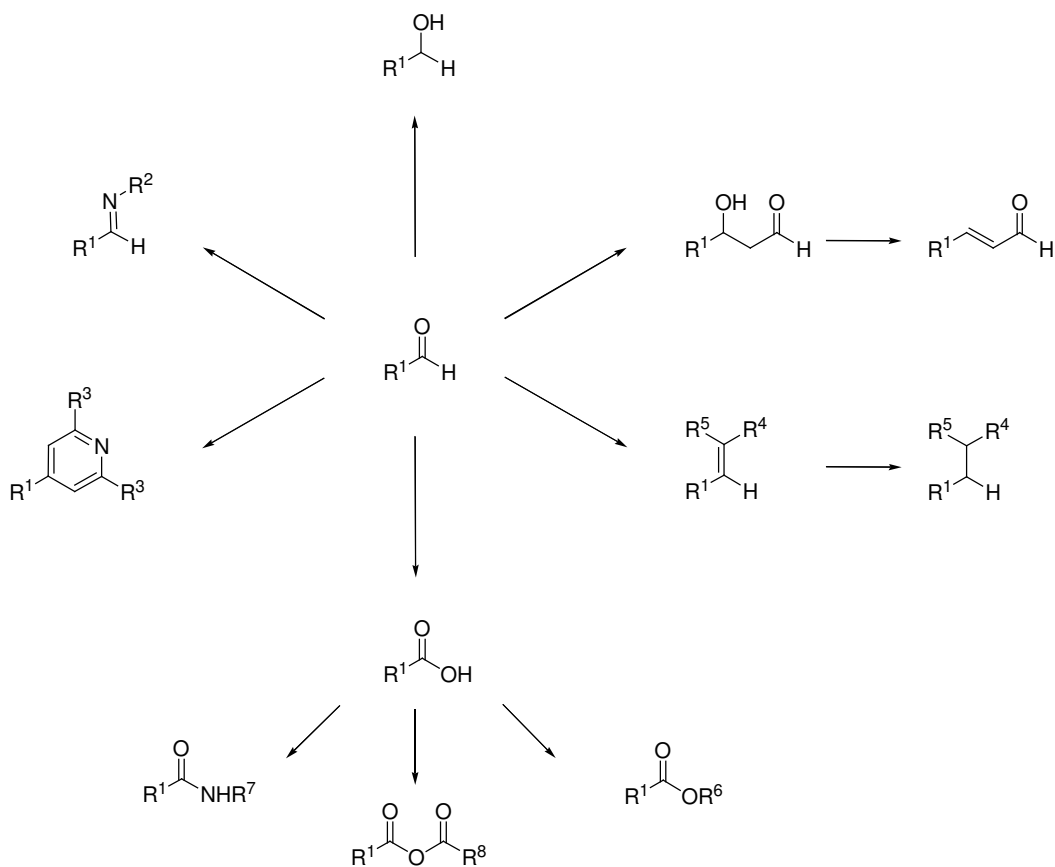
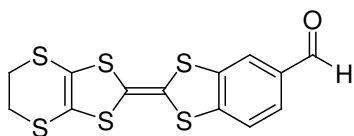
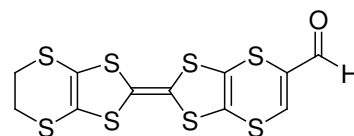


Figure 86: Versatility of the aldehyde function as a reaction centre.

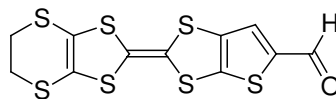
Ishikawa *et al.* reported three aldehyde functionalised electron donors **116-118**,⁵ although little research has been achieved in the further functionalisation of such molecules.



116



117



118

Three electron donor species have been synthesised with functionalities that could be expanded at a later stage *via* the use of the aldehyde group incorporated. Specific targets in this work are the formation of Schiff bases, which can be readily prepared from achiral, racemic or chirally pure amines, and diamines such as those demonstrated in Chapter 5. The bis-Schiff bases are particularly interesting, as they are possible metal coordinators, binding metals strongly through their 5-membered chelate ring systems. The salen-type ligands have found extensive use in asymmetric catalysis particularly in oxidation chemistry.^{6, 7}

The aldehyde functionality also presents the opportunity to prepare alcohol substituted organosulfur donors, *via* the reduction of the aldehyde group. The hydroxy groups are highly desirable moieties in low dimensionality conducting materials, as they may influence the packing motifs exhibited in the crystalline state, as discussed in Chapter 2.

By incorporating two aldehyde functions on adjacent carbon atoms, there is the possibility to prepare heterocyclic compounds, such as furans, pyrroles and thiophenes.

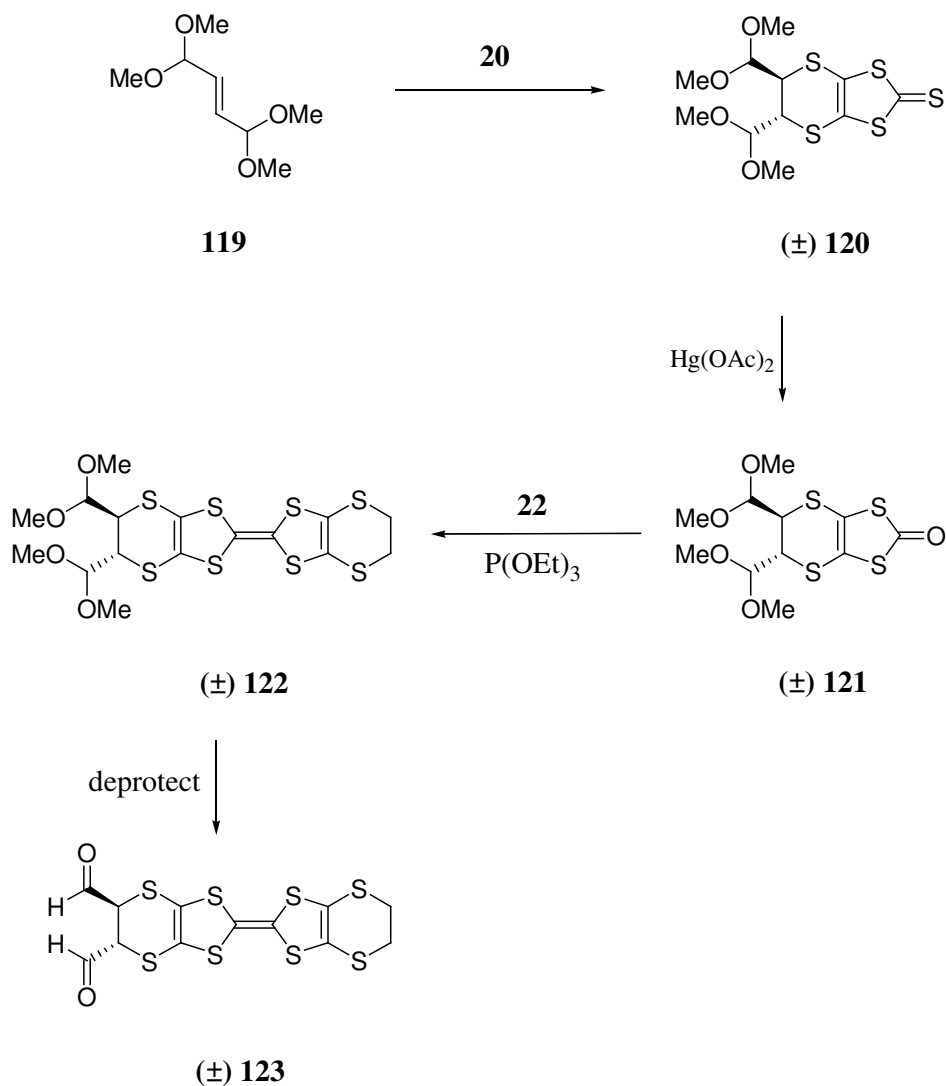
These in turn can be further reacted with electrophiles to produce a wide range of functionalised molecules.

Taking these considerations into account, it was decided to attempt to prepare three organosulfur electron donors, each of which was significantly different to the other two, other than incorporating an aldehyde function. The first synthesis was to prepare an ET derivative functionalised with two aldehyde groups on adjacent carbons, giving access to a range of heterocyclic derivatives upon deprotection of the masked aldehyde groups. The synthetic approach taken is shown in Scheme 15.

6.2 Results and Discussion

The Diels-Alder reaction of bis(dimethylacetal)fumaraldehyde **119** with oligomeric trithione **20** afforded the thione species **120** as a mixture of the *trans* isomers, after refluxing a toluene solution of the reagents for 12 h. Purification by chromatography gave the thiocarbonyl compound **120** in fairly low yield (17 %) as a reddish-brown solid, which was identified by infrared and NMR techniques. The C=S stretching frequency in the infrared spectrum was observed at $\nu = 1047 \text{ cm}^{-1}$, and the simple ^1H NMR spectrum exhibited two singlet resonances for the methyl groups of the acetal functions at δ 3.45 and 3.40 ppm, and a doublet of triplets at δ 3.74 ppm attributed to the hydrogen atoms of the dithiin ring. The acetal hydrogen resonated as a doublet of triplets at δ 4.49 ppm. The ^{13}C NMR confirmed the presence of the thiocarbonyl group with a resonance at δ 207.8 ppm, and the unsaturated ring carbons at δ 122.9 ppm.

Electron impact mass spectrometry confirmed the identity with a $[M+H]^+$ peak at 372.9725 Da, and elemental analysis confirmed the purity of the material isolated.



Scheme 15: Synthetic approach to racemic dialdehyde functionalised donor (\pm) 123.

Conversion of thiocarbonyl compound **120** into carbonyl compound **121** was achieved using the mercuric acetate mediated sulfur-oxygen exchange reaction in chloroform. The reaction was complete within 1 h, and a brown solid was isolated in 97 % yield and

determined to be the carbonyl species by observation of the C=O stretching frequency in the infrared spectrum at $\nu = 1657 \text{ cm}^{-1}$. The ^1H and ^{13}C NMR spectra confirmed the exchange reaction with loss of the resonance attributed to the thiocarbonyl fragment in the ^{13}C NMR, and observation of the carbonyl function at $\delta 188.7 \text{ ppm}$. There is also a shift in the unsaturated ring carbons by around 10 ppm to $\delta 113.7 \text{ ppm}$ indicating a change in the electronic nature of the organochalcogen unit. Elemental analysis and electrospray mass spectrometry unequivocally confirmed the formation of **121**.

The triethyl phosphite-mediated cross coupling reaction of carbonyl compound **121** with thiocarbonyl **22** was achieved in 18 h, and the cross-coupled electron donor **122** isolated in 49 % yield after purification by chromatography. The light orange solid produced was characterised by the absence of thiocarbonyl and carbonyl infrared stretching frequencies, and the absence of the corresponding ^{13}C NMR resonances. Four resonances attributable to the unsaturated carbons comprising the delocalised π system were observed in a close region of the carbon spectrum $\delta 114.0, 113.8, 112.2$ and 111.2 ppm indicating the reasonably even distribution of electronic character across the TTF core. The presence of the two dimethyl acetal functions was confirmed by the singlet resonances at $\delta 3.46$ and 3.39 ppm , and the unsubstituted dithiin ring protons evident as a singlet at $\delta 3.29 \text{ ppm}$. Elemental analysis confirmed the composition, and the molecular ion was observed in the electron impact mass spectrum at 531.9122 Da .

Particular difficulty was encountered in the deprotection of the acetal groups to give electron donor **123**, and no spectroscopic evidence was obtained to confirm the

formation of the donor, nor a derivative formed from it. A range of concentrations of aqueous hydrochloric acid in tetrahydrofuran solution were unsuccessfully employed, as were various concentrations of *p*-toluenesulfonic acid (*p*-TSA) in acetone. In each case, starting material was isolated and determined by analysis of the ^1H and ^{13}C NMR spectra. The absence of reaction could perhaps be attributable to stacking of the electron donors in solution, causing the reaction centres to be inaccessible. Other notable examples of such a lack of reactivity at the carbon α - to the dithiin ring, are the absence of a reaction of aminomethyl-ET with acid chlorides.

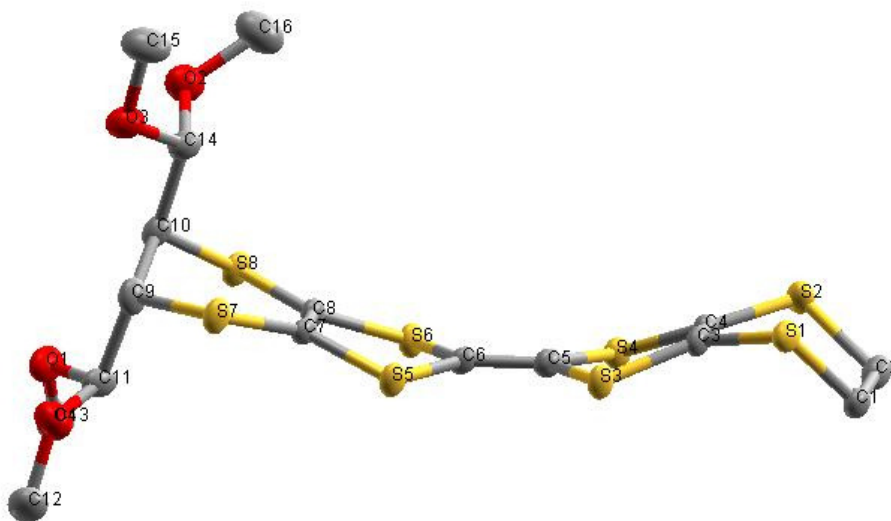


Figure 87: Crystallographic image of 122, showing the bent structure. Thermal ellipsoids are shown at the 50 % probability level.

Crystals of **122** suitable for single crystal X-ray analysis grew upon cooling of a hot acetonitrile solution. The bright yellow needles were shown to consist of each of the two *trans*- stereoisomers (Figure 87) as a centrosymmetrically related pair of donor molecules, packed in the space group P-1 (Figure 88). The crystalline structure showed

that the organosulfur residue adopted a bowed structure, with a flexing about the S3-S4 vector (162.8 °) and the S5-S6 vector (160.4 °), to the same side of the central plane. The unsubstituted dithiin ring sp^3 carbon atoms exhibit a further flexing about the S1-S2 vector (119.9 °) in the opposite sense to the natural bow of the donor molecule.

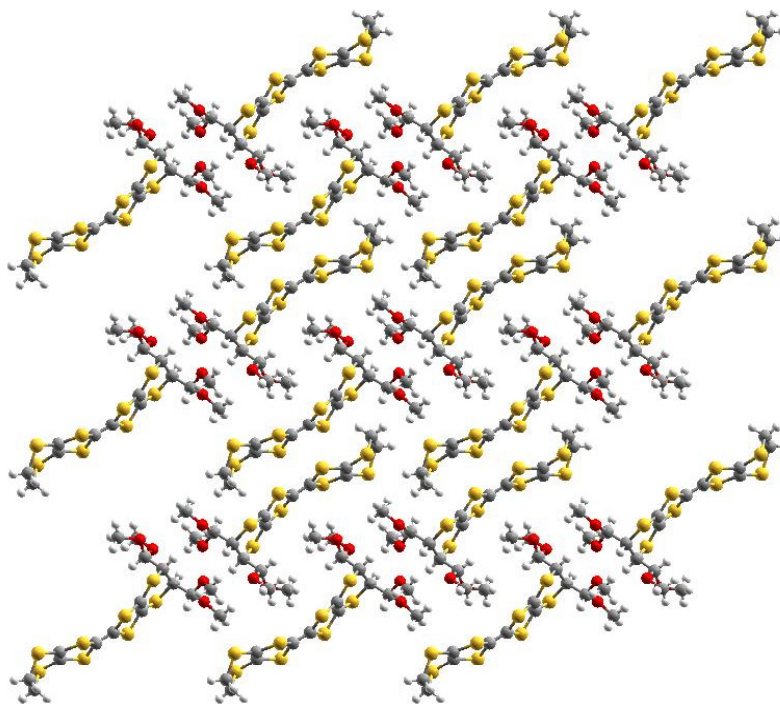


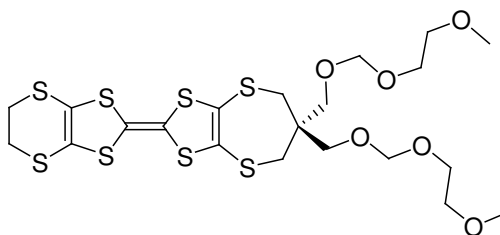
Figure 88: X-ray crystallographic image of **122** as viewed down the crystallographic a axis.

Thermal ellipsoids are shown at the 50 % probability level.

Attempts at the electrocrystallisation of organosulfur donor **122** with simple non-magnetic anions proved unsuccessful. This could have been due to the large steric requirements of the bis(dimethylacetal) functions. From the crystal structure of the neutral donor **122**, it would be expected that the formation of a stacked network of donor molecules would not be possible, with a high probability for the formation of a

dimeric species, with electrically insulating or weakly semiconducting properties. In the crystal structure of the neutral donor, only one sulfur-sulfur contact is shorter than the sum of their van der Waals radii, and exists between S4 and S3*, of length 3.571 Å. Between planes of donor molecules there exists three short contacts, S8-S7* (3.432 Å), S6-S7* (3.393 Å) and S1-S2* (3.646 Å), which indicates that electron transfer could happen across donor molecules in the planar direction.

The crystal shows similarities in the structure to that observed for (ethylenedithio)-(2,2-bis(methoxyethoxymethoxymethyl)propylenedithio)tetrathiafulvalene **124** (Figure 89).⁸



124

The MEM protected *gem*-dihydroxymethyl substituted donor exhibits a bent structure, with the S5-S6-S7-S8 plane deviated from the central S3-S4-S5-S6 plane by 22.6°. To the same side, the ethylene moiety represented by the S1-S2-S3-S4 plane is deviated from the central plane by 19.2° (Figure 90).

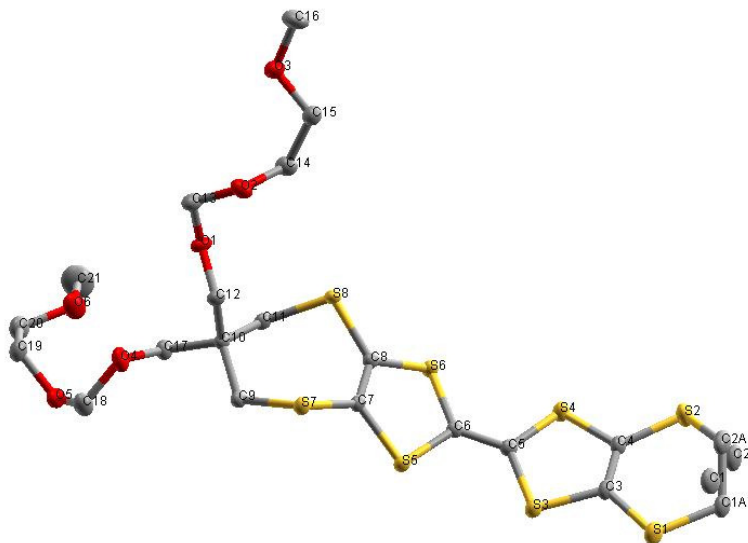


Figure 89: Asymmetric unit for 124, showing atom numbering scheme. Hydrogen atoms have been removed for clarity. Thermal ellipsoids are shown at the 50 % probability level. The ethylene function C1/C1A and C2/C2A exhibits positional disorder as shown (isolated carbon atoms).

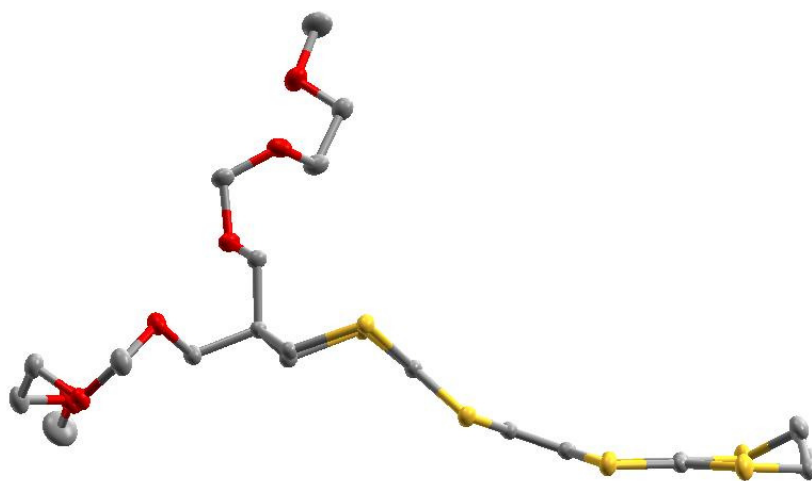


Figure 90: Asymmetric unit for 124, showing the bent structure with displacement of exterior sulfur atoms to the same side of the central mean plane. Hydrogen atoms have been removed for clarity. Thermal ellipsoids are shown at the 50 % probability level.

The crystal structure of **124** was shown to crystallise in the space group $P2_1/n$, with centrosymmetrically related pairs of donor molecules 3.28 Å apart (Figure 91). The pairs are in an isolated environment with respect to each other. The side chains extend in the bc plane and also into the a direction as the alkoxy chain twists. The alkoxy chains of several pairs of donor molecules cluster together forming tunnels extending in the crystallographic a direction, with each tunnel being separated by the donor molecules.

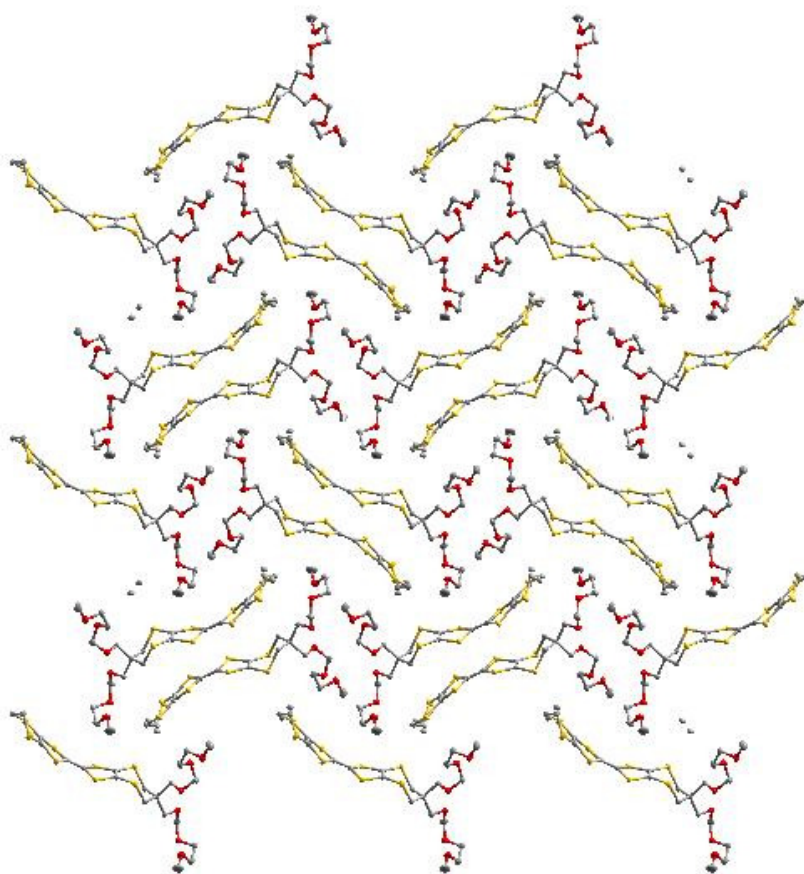
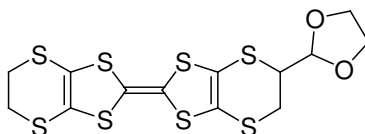


Figure 91: Packing of donor **124** as viewed down the crystallographic a axis. Hydrogen atoms have been removed for clarity. Thermal ellipsoids are shown at the 50 % probability level. The ethylene function C1/C1A and C2/C2A exhibits positional disorder as shown (isolated carbon atoms).

The inability to remove the cyclic-acetal protecting group from electron donor **122** paralleled difficulty in the deprotection of **125**.⁴ As such, it was decided to synthesise a donor bearing an aldehyde function greatly displaced from the electron rich TTF core. It was postulated that the displacement should allow for ready cleavage of the acetal group, revealing the aldehyde upon which further construction could be undertaken.



125

A chain of eight carbons between the core of the donor and the aldehyde fragment was utilised due to the ready availability of the corresponding alkene species. This length of displacement should isolate and nullify any stabilising effect of the TTF core, and in addition, the length of chain was postulated to be that required to synthesise a ‘greasy’ electron donor.

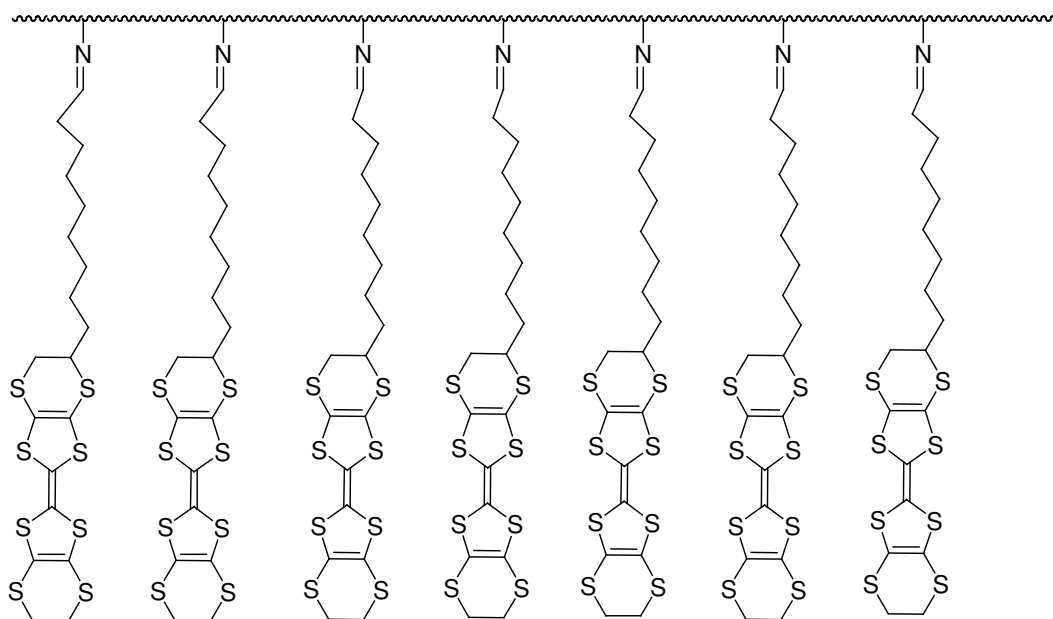


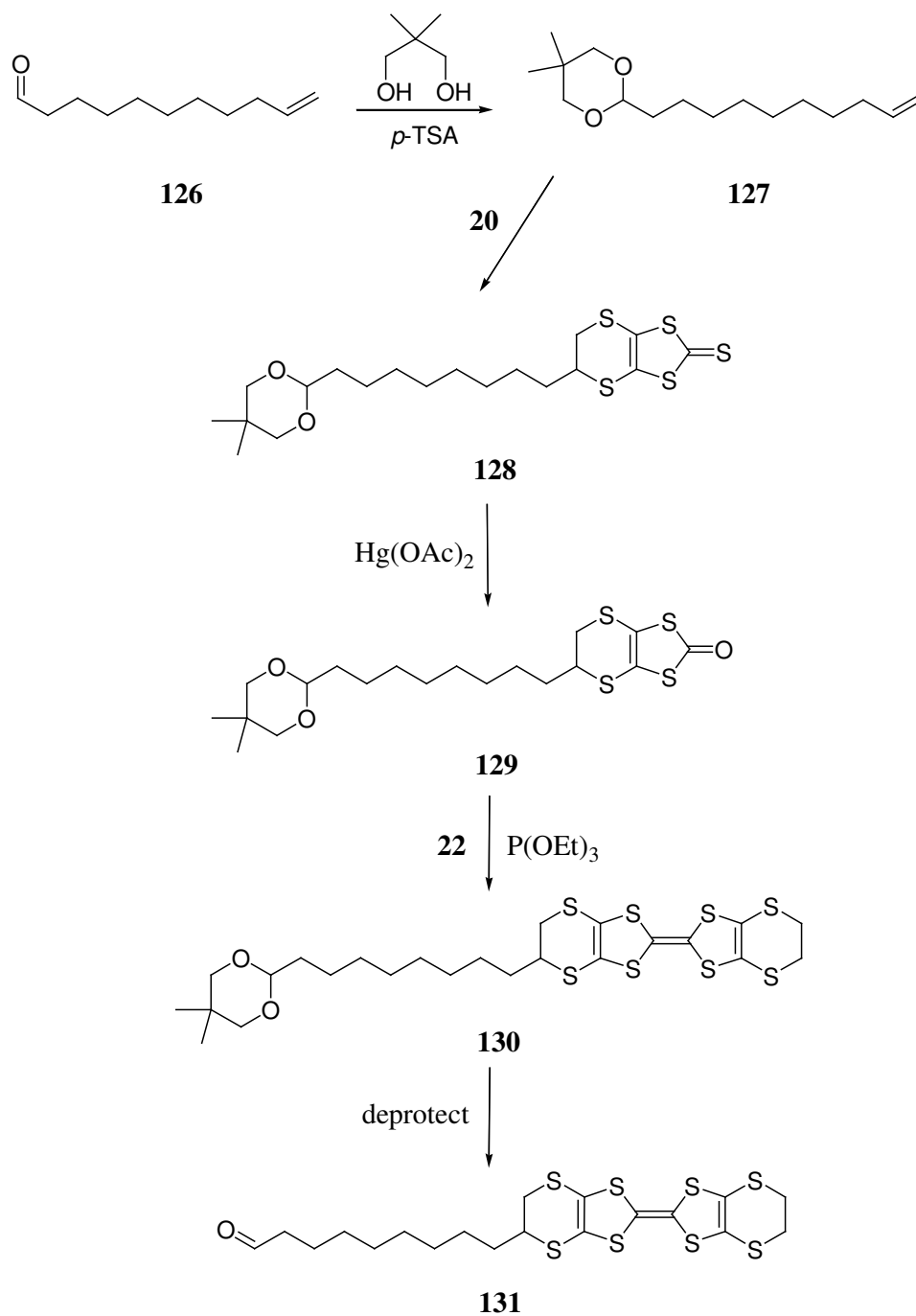
Figure 92: Extended hydrocarbon donors attached to polyamine backbone.

This type of species could find application in the preparation of thin film materials and displays due to its physical character, and expected increased solubility in highly volatile solvents. In addition, this structure was chosen as it resembles part of the hypothesised structure proposed by Little.⁹ Through the deprotection of the donor, and coupling to a polymer support, such as imine formation onto a polyamine core (Figure 92), a material similar in character to Little's model could be achieved.

The synthetic approach taken in the synthesis of the long chain functionalisable donor is shown in Scheme 16. The protection of undec-10-enal **126** as its cyclic acetal **127** was achieved under microwave conditions using neopentyl glycol.^{10, 11, 12} The reaction, catalysed by a small amount of *p*-TSA acid, proceeded in less than 1 min, to yield the product **127** in 98 % yield after simple workup. The protection of the aldehyde was confirmed by the shift in the ¹³C NMR of the carbon of the aldehyde function to δ 102.2

ppm, with the carbon atoms adjacent to the oxygen atoms resonating at δ 77.1 ppm. The presence of two methyl groups was identifiable from the ^1H NMR spectrum as two singlets at δ 1.11 and 0.64 ppm. Analysis of the colourless oil by GC-MS confirmed the molecular ion as 254, with the fragmentation pattern: 181, 167, 130, 115, 95, 69, 56. In addition, the absence of the C=O stretching frequency in the infrared spectrum confirmed protection of the carbonyl fragment.

The formation of the thiocarbonyl compound **128** was performed by addition of the oligomeric trithione **20** to a solution of **127** in toluene, with heating to reflux. After filtration and chromatography over silica, **128** was isolated in 85 % yield as a brown oil. Characterisation of the material was possible from the ^1H NMR spectrum, which indicated the loss of resonances attributable to the hydrogen atoms of the alkene at δ 5.72 (1 H) and 4.92-4.84 (2 H) ppm. The thiocarbonyl function was easily observed at δ 208.2 ppm, and confirmed by the infrared spectrum. The alkenic carbons at the fusion points of the five and six membered rings were found to resonate at δ 123.6 and 121.7 ppm, in the typical region for a thiocarbonyl species of this type. The protecting group of the aldehyde function remained intact, observable by peaks in the ^{13}C NMR for the acetal carbon at δ 102.2 ppm, the O-CH₂X carbon at 77.2 ppm, and from the ^1H NMR, which demonstrated the two methyl groups clearly as singlets at δ 1.17 and 0.70 ppm. Elemental analysis and electron impact mass spectrometry confirmed the purity and identity, with the molecular ion $[\text{M}]^+$, evident at 450.0845 Da.



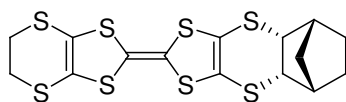
Scheme 16: Synthetic approach taken to donor 131.

The oxymercuration of **128** was performed in chloroform solution with 1.5 molar equivalents of mercuric acetate. After stirring at room temperature for two hours, the carbonyl compound **129** was isolated after simple workup as a brown oil in 84 % yield. Evidence for the exchange of sulfur for oxygen was shown in the ^{13}C NMR, which demonstrated a shift to δ 189.1 ppm for the carbonyl species. The carbon atoms at the fusion of the five and six membered rings showed a shift to δ 113.9 and 112.1 ppm, indicative of the electronic change in the π system. Infrared analysis of compound **129** showed a strong stretching band for C=O at $\nu = 1678\text{ cm}^{-1}$. Elemental analysis of the oil confirmed the purity, and the molecular ion $[\text{M}]^{+}$ was observed as 434.1068 Da in the electron impact mass spectrum.

It was decided that the homo-coupling of compound **129** would not be of benefit, as the two positional isomer generated would be difficult to separate, *without* consideration of the stereochemistry at the tertiary carbon atom functionalised with the alkyl substituent. As such, the cross coupling reaction of carbonyl compound **129** with the thiocarbonyl compound **22** (in a two-fold excess) was undertaken in triethyl phosphite at 110 °C. Purification by chromatography over silica afforded the required species **130** as an orange gum-oil in 53 % yield, which was characterised by the absence of the thiocarbonyl and carbonyl fragments in the NMR and infrared data. The presence of five resonances at δ 114.3, 113.8, 112.7, 112.1 and 111.1 ppm in the ^{13}C NMR spectrum attributable to the central π electron core of the donor molecule indicated formation of the double bond between the substituted and unsubstituted fragments. The identification of the molecular species was confirmed by electrospray mass

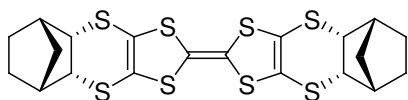
spectrometry which demonstrated the $[M+H]^+$ peak at 611.0396 Da. Elemental analysis confirmed the chemical composition of the material.

The deprotection of the cyclic acetal to give **131** did not occur readily, consistently failing despite using increasingly vigorous conditions, contrary to the author's previous experience. Hydrochloric acid/tetrahydrofuran solutions ranging in acidity were investigated, however NMR showed no evidence for the reformation of the aldehyde species. Solutions of the protected donor in acetone did not react with high concentrations of *p*-TSA acid. The distant position of the aldehyde fragment from the organosulfur core unit was believed to allow deprotection to occur readily, and the lack of reactivity was again surprising, especially under the strongly acidic aqueous-tetrahydrofuran solutions employed. In each case, starting material **130** was isolated.

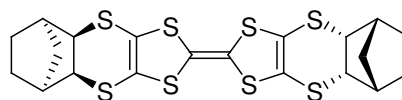


132

The group of Wallis *et al.* had previously attempted to prepare the ET derivative bearing the norbornene cage **132**. Difficulties with purification however, led to a mixture of the two isomeric homo-coupled donors **133a** and **133b** being isolated.



133a



133b

Building on this, and the observation that by moving the reactive centre from the α -position to the β - position (as indicated in Figure 93) with respect to the electron donor core, greatly increases the success with which derivation can occur, it was decided to prepare the bicyclic donor functionalised with an aldehyde fragment which could serve to allow future elaboration. The synthetic route taken is shown in Scheme 17.

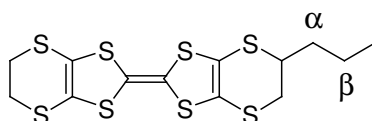
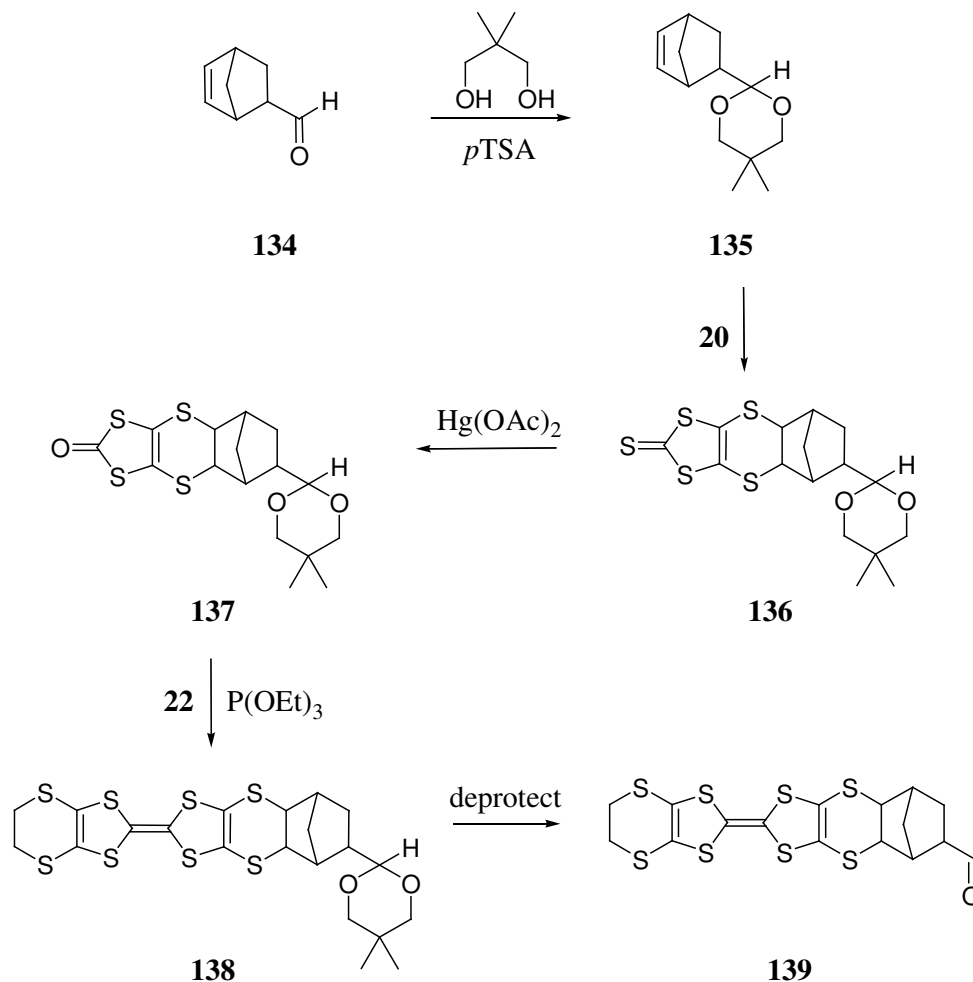


Figure 93: Chemical structure indicating the α - and β - positions.

5-Norborene-2-carboxaldehyde **134** was protected using the same methodology as that employed for the protection of undec-10-enal, thus the aldehyde and neopentyl glycol were subjected to microwave irradiation in the presence of a catalytic amount of *p*-TSA, to afford after simple workup **135** as a beige solid in 96 % yield. Observation of the ^1H NMR for **135** determined the solid to be a mixture of the *exo* and *endo* isomers in approximately a 5:1 ratio. GC-MS analysis showed two peaks with very close retention times, 17.16 and 17.31 minutes in the chromatogram, with both peaks exhibiting an extremely similar mass spectrum fragmentation pattern from the clearly identifiable molecular ion at 208 Da. The GC-MS chromatogram indicated a ratio of approximately 4:1 for the two isomers, from the integration (uncalibrated, but relative). Protection of the carbonyl function was confirmed by the absence of a stretching band in the infrared spectrum for C=O. The ^1H NMR showed the alkenic protons for the major isomer at δ 6.14 and 5.88 ppm. Also observable was the minor isomer with alkenic resonances at δ 6.10 and 6.07 ppm. The two methyl groups of the neopentyl function were observable

at δ 1.17 and 0.68 ppm. The ^{13}C NMR showed the absence of the aldehyde peak, and resonances were observed at δ 106.4 and 105.8 ppm attributable to the formation of the acetal for the two isomers. The complexity of the NMR spectrum focussed the determination of the compound identity on mass spectrometry, elemental analysis and infrared spectroscopy.



Scheme 17: Synthetic route taken to donor **139** as a mixture of isomers.

Compound **135**, as a mixture of isomers, was dissolved in toluene and to this added the oligomeric trithione species **20**. After heating under reflux over two days, the

thiocarbonyl species **136** was isolated after chromatography over silica in 69 % yield as a brown solid. The ^{13}C NMR identified the thiocarbonyl resonance at δ 210.0 ppm, with the alkenic carbon atoms at the fusion of the five and six membered rings resonating at δ 136.7 and 136.5 ppm, in the region expected for this type of species. The molecular ion was identified in the electron impact mass spectrum as 404.0066 Da, and the material purity was confirmed by elemental analysis.

Conversion of thiocarbonyl **136** into carbonyl compound **137** was achieved using 1.5 molar equivalents of mercuric acetate in chloroform solution. Evaporation of the filtrate after removal of the mercury salts, afforded **137** as an orange-brown solid in 75 % yield. ^{13}C NMR showed substitution had occurred by the shift in the resonance for the carbon to δ 190.0 ppm. Alongside this, the alkenic carbon atoms at the fusion points of the five and six membered rings, exhibited a shift in their resonances to δ 127.4 and 127.2 ppm. The electrospray mass spectrum indicated the ammonium adduct $[\text{M}+\text{NH}_4]^+$ of the molecular ion as 405.0632 Da, and elemental analysis confirmed the purity.

The cross coupling of carbonyl **137** with thione **22** was undertaken on a 1:3 molar scale respectively, in triethyl phosphite with heating at 95 °C for 22 h. After purification by chromatography over silica, **138** was isolated as a bright orange solid in 46 % yield as a mixture of stereoisomers. Elemental analysis confirmed the correct composition, and electron impact mass spectrometry identified the molecular ion at 563.9538 Da. The ^1H NMR data showed the presence of the ethylene protons at δ 3.24 ppm as a singlet protruding from a region in which several other protons co-resonated as multiplet signals. The ^{13}C NMR indicated the absence of carbonyl and thiocarbonyl resonances,

and six sp^2 alkenic carbon atoms resonating at δ 127.1, 126.8, 113.8, 113.7, 112.2 and 111.7 ppm.

Deprotection of the acetal species was attempted using 2 M, 4 M, 8 M and 10 M concentrations of HCl/ tetrahydrofuran, and also *p*TSA in acetone (10 % w/v, 25 % w/v, 50 % w/v), but the starting material was consistently isolated, even after refluxing the 10 M HCl/ tetrahydrofuran solution for 48 h.

6.3 Experimental

5,6-Bis-dimethoxymethyl-3a,7a-dihydro-[1,3]dithiolo[4,5-b][1,4]dithiine-2-thione, 120

Fumaraldehyde bis(dimethylacetal) **119** (0.98 g, 5.6 mmol) and trithione **20** (2.3 g, 11.7 mmol) were heated to reflux in toluene (60 mL) under an inert atmosphere for 12 h. The reaction was cooled to room temperature and filtered, washing with dichloromethane (*ca.* 50 mL). The combined filtrate was evaporated, and the material purified by chromatography over silica eluting with cyclohexane/ethyl acetate (3:1) to afford **120** (0.35 g, 17 %) as a red-brown solid Mp 88 °C (Found C, 35.5; H, 4.3. $C_{11}H_{16}O_4S_5$ requires C, 35.5; H, 4.3%); ν_{\max} (ATR)/ cm^{-1} 2925, 2830, 1442, 1395, 1351, 1266, 1186, 1110, 1047(C=S), 957, 900, 887, 819, 726, 562, 544, 515; δ_H (400 MHz, $CDCl_3$) 4.49 (2 H, dt, $J=6.76$, 1.6 Hz, $CH(CH_3)_2$), 3.74 (2 H, dt, $J=7.92$, 1.61, 5-, 6-*H*), 3.45 (6 H, s, 2 x CH_3), 3.40 (6 H, s, 2 x CH_3); δ_C (100 MHz, $CDCl_3$) 207.8 (2-*C*), 122.9

(3a, 7a-C), 104.1 (CH(CH₃)₂), 55.9 (2 x CH₃), 55.0 (2 x CH₃), 45.6 (5, 6-C); *m/z* (EI) [M+H]⁺ 372.9723. [C₁₁H₁₆O₄S₅+H]⁺ requires 372.9725.

5,6-Bis-dimethoxymethyl-3a,7a-dihydro-[1,3]dithiolo[4,5-b][1,4]dithiin-2-one, 121

To a stirred solution of **120** (0.35 g, 0.94 mmol) in chloroform (50 mL) under an inert atmosphere, was added mercuric acetate (0.45 g, 1.4 mmol). After 1 h the reaction was filtered, the solid washed with a little chloroform (*ca.* 20 mL) and the filtrate evaporated to afford **121** (0.32 g, 97 %) as a red-brown solid Mp 83 °C (Found C, 37.0; H, 4.45. C₁₁H₁₆O₅S₄ requires C, 37.1; H, 4.5%); ν_{\max} (ATR)/cm⁻¹ 2938, 2830, 1701, 1657 (C=O), 1627, 1507, 1443, 1357, 1188, 1109, 1056, 965, 891, 804, 749, 728, 678, 546; δ_{H} (400 MHz, CDCl₃) 4.54 (2 H, dt, *J*=7.76, 1.54 Hz, CH(CH₃)₂), 3.75 (2 H, dt, *J*=7.92, 1.58 Hz, 5-, 6-*H*), 3.47 (6 H, s, 2 x CH₃), 3.42 (6 H, s, 2 x CH₃); δ_{C} (100 MHz, CDCl₃) 188.7 (2-C), 113.7 (3a, 7a-C), 104.0 (CH(CH₃)₂), 55.6 (2 x CH₃), 54.8 (2 x CH₃), 46.9 (5, 6-C); *m/z* (ES)⁺ [M+NH₄]⁺ 374.0223. [C₁₁H₁₆O₅S₄+NH₄]⁺ requires 374.0219.

5,6-Bis-dimethoxymethyl-5,6,5',6'-tetrahydro-[2,2']bi[[1,3]dithiolo[4,5-b][1,4]dithiinylidene], 122

Oxo compound **121** (0.3 g, 0.84 mmol) and thione **22** (0.57 g, 2.53 mmol) were heated to 100 °C in triethyl phosphite (15 mL) under an inert atmosphere. After approximately 30 min an orange precipitate was observed. Heating was continued for 18 h, before cooling to room temperature. The precipitate was filtered washing with *n*-hexane (50 mL) and then chloroform (50 mL). The filtrate was evaporated affording the crude

material as a deep orange oil, which was purified by chromatography over silica eluting with cyclohexane/ethyl acetate (2:1) to give **122** (0.22 g, 49 %) as a light orange solid Mp 133 °C (Found C, 36.2; H, 3.7. C₁₆H₂₀S₈O₄ requires C, 36.1; H, 3.8%); ν_{\max} (ATR)/cm⁻¹ 2922, 2869, 2829, 1439, 1344, 1180, 1112, 1060, 959, 914, 875, 771, 731, 563; δ_{H} (400 MHz, CDCl₃) 4.41 (2H, dt, $J=8.04, 1.78$ Hz, CH(CH₃)₂), 3.71 (2H, dt, $J=8.0, 1.84$ Hz, 5-, 6-H), 3.46 (6H, s, 2 x CH₃), 3.39 (6H, s, 2 x CH₃), 3.29 (4H, s, 2 x CH₂); δ_{C} (100 MHz, CDCl₃) 114.0 (*sp*²C), 113.8 (*sp*²C), 112.2 (*sp*²C), 111.2 (*sp*²C), 104.2 (CH(CH₃)₂), 56.0 (2 x CH₃), 54.7 (2 x CH₃), 46.3 (5, 6-C), 30.2 (2 x CH₂); *m/z* (EI) [M]⁺ 531.9122. [C₁₆H₂₀S₈O₄]⁺ requires 531.9122.

2-Dec-9-enyl-5,5-dimethyl-[1,3]dioxane, 127

Undec-10-enal **126** (5g, 29.7 mmol), neopentyl glycol (3.09 g, 29.7 mmol) and *p*-TSA (0.1 g, 0.58 mmol) were heated in a conventional 800 W microwave oven on half-power for 40 seconds. After cooling, chloroform (*ca.* 100 mL) was added and the solution washed with saturated sodium bicarbonate solution (*ca.* 20 mL) to afford **127** (7.4 g, 98%) as a colourless oil; ν_{\max} (ATR)/cm⁻¹ 2925, 2853, 1641, 1467, 1393, 1123, 1017, 991, 908, 791, 722, 666, 510; δ_{H} (400 MHz, CDCl₃) 5.72 (1 H, m, 10-H), 4.92-4.84 (2 H, m, 2 x 11-H), 4.33 (1 H, t, $J=5.04$ Hz, 1-H), 3.52 (2 H, d, $J=11.12$ Hz, 3 $_{\alpha}$ '-, 3 $_{\alpha}$ ''-H), 3.34 (2 H, d, $J=11.0$ Hz, 3 $_{\beta}$ '-, 3 $_{\beta}$ ''-H), 1.95 (2 H, m, 9-H), 1.54 (2 H, m, 8-H), 1.30 (4 H, m *br*, 2 x 2-, 3-H), 1.21 (8 H, s *br*, 2 x 4-, 5-, 6-, 7-H), 1.11 (3 H, s, CH₃), 0.64 (3 H, s, CH₃); δ_{C} (100 MHz, CDCl₃) 139.0 (10-C), 114.0 (11-C), 102.2 (1-C), 77.1 (3'-, 3''-C), 34.8, 33.7, 29.4, 29.3, 29.2, 29.0, 28.8, 23.8 (CH₃), 22.9 (CH₃), 20.9; *m/z* (GC-MS): found: 254 [M]⁺. C₁₆H₃₀O₂ requires: 254.

5-[8-(5,5-Dimethyl-[1,3]dioxan-2-yl)-octyl]-5,6-dihydro-[1,3]dithiolo[4,5-b][1,4]dithiine-2-thione, 128

To a stirred solution of alkene **127** (1.32 g, 5.20 mmol) in toluene (60 mL) was added trithione **20** (2.04 g, 10.4 mmol) and the mixture heated to reflux at 135 °C under nitrogen for 18 hours. The reaction was cooled to room temperature, and filtered washing with chloroform. The filtrate was evaporated, and the crude material purified by chromatography over silica eluting with cyclohexane/ethyl acetate (5:1) to give **128** (2.0 g, 85%) as a brown oil (Found C, 50.7; H, 6.6. C₁₉H₃₀S₅O₂ requires: C, 50.6; H, 6.7%); δ_{H} (400 MHz, CDCl₃) 4.39 (1 H, t, $J=5.06$ Hz, 1-*H*), 3.58 (2 H, d, $J=11.12$ Hz, 3 α' -, 3 α'' -*H*), 3.40 (2 H, d, $J=10.64$ Hz, 3 β' -, 3 β'' -*H*), 1.76 (2 H, m, aliphatic-*H*), 1.60 (2 H, m, aliphatic-*H*), 1.40 (2 H, m, aliphatic-*H*), 1.28 (13 H, s, aliphatic-*H*), 1.17 (3 H, s, CH₃), 0.70 (3 H, s, CH₃); δ_{C} (100 MHz, CDCl₃) 208.2 (2-*C*), 123.6 & 121.7 (3a-, 7a-*C*), 102.2 (1-*C*), 77.2 (3'-, 3''-*C*), 44.0, 34.9, 34.8, 34.7, 29.4, 29.3, 29.2, 29.1, 26.8, 23.9 (CH₃), 23.0 (CH₃), 21.8; m/z (EI): found: 450.0845 [M]⁺. C₁₉H₃₀S₅O₂ requires: 450.0844.

5-[8-(5,5-Dimethyl-[1,3]dioxan-2-yl)-octyl]-5,6-dihydro-[1,3]dithiolo[4,5-b][1,4]dithiin-2-one, 129

To a stirred solution of the thione **128** (2.0 g, 4.44 mmol) in chloroform (50 mL) under nitrogen, was added mercuric acetate (2.12 g, 6.66 mmol). The mixture was stirred for 2 h at room temperature, filtered washing with chloroform (*ca.* 30 mL), and the filtrate washed with saturated sodium bicarbonate solution (10 mL). The organic phase was

dried over magnesium sulphate and evaporated to afford **129** (1.62 g, 84%) as a brown oil (Found C, 52.6; H, 6.8. C₁₉H₃₀S₄O₃ requires: C, 52.5; H, 7.0%); ν_{\max} (ATR)/cm⁻¹ 2924, 2851, 1678, 1628, 1507, 1465, 1393, 1362, 1125, 1016, 972, 890, 759, 666, 541; δ_{H} (400 MHz, CDCl₃) 4.39 (1 H, t, $J=5.04$ Hz, 1-*H*), 3.59 (2 H, d, $J=9.96$ Hz, 3 α' -, 3 α'' -*H*), 3.41 (2 H, d, $J=10.56$ Hz, 3 β' -, 3 β'' -*H*), 1.76 (2 H, m, aliphatic-*H*), 1.60 (2 H, m, aliphatic-*H*), 1.45-1.30 (X H, s *br*, aliphatic-*H*), 1.28-1.25 (X H, s *br*, aliphatic-*H*), 1.17 (3 H, s, CH₃), 0.70 (3 H, s, CH₃); δ_{C} (100 MHz, CDCl₃) 189.1 (2-*C*), 113.9 & 112.1 (3a-, 7a-*C*), 102.2 (1-*C*), 77.2 (3'-, 3''-*C*), 45.6, 36.0, 35.1, 34.8, 29.4, 29.3, 29.2, 29.1, 28.9, 26.6, 23.9, 22.9, 22.1, 21.8; m/z (EI): found: 434.1068 [M]⁺. C₁₉H₃₀S₄O₃ requires: 434.1072.

5,5-Dimethyl-2-[8-ET-octyl]-[1,3]dioxane, 130

A mixture of oxo compound **129** (1.5 g, 3.46 mmol) and thione **22** (2.32 g, 10.4 mmol) were heated together in freshly distilled triethyl phosphite (20 mL) under a nitrogen atmosphere to 110 °C. After heating for 18 h the reaction was allowed to cool to room temperature and filtered. The precipitate was washed with chloroform (50 mL), and the filtrate evaporated. The crude material was purified by chromatography over silica, eluting with cyclohexane/chloroform (3:1) to afford **130** (1.12 g, 53%) as an orange gum (Found C, 47.3; H, 5.4. C₂₄H₃₄S₈O₂ requires: C, 47.2; H, 5.6%); ν_{\max} (ATR)/cm⁻¹ 2922, 2848, 1466, 1392, 1285, 1161, 1124, 1019, 967, 822, 772; δ_{H} (400 MHz, CDCl₃) 4.37 (1 H, t, $J=5.04$ Hz, 1-*H*), 3.56 (2 H, d, $J=9.6$ Hz 3 α' -, 3 α'' -*H*), 3.39 (2 H, d, $J=10.56$ Hz, 3 β' -, 3 β'' -*H*), 3.26 (4 H, s, 2 x CH₂), 1.73-1.66 (2 H, m, aliphatic-*H*), 1.62-1.56 (2 H, m, aliphatic-*H*), 1.43-1.31 (2 H, m, aliphatic-*H*), 1.25 (13 H, s *br*, aliphatic-

H), 1.15 (3 H, s, CH_3), 0.69 (3 H, s, CH_3); δ_C (100 MHz, $CDCl_3$) 114.3 (sp^2C), 113.8 (sp^2C), 112.7 (sp^2C), 112.1 (sp^2C), 111.1 (sp^2C), 102.2 (1-C), 77.2 (3'-, 3''-C), 44.4, 35.4, 34.9, 34.8, 30.1, 29.4, 29.3, 29.2, 29.1, 26.7, 23.9, 22.9, 21.8; *m/z* (ES): found: 611.0396 [M+H]⁺. $C_{24}H_{34}S_8O_2 + H$ requires: 611.0397.

2-Bicyclo[2.2.1]hept-5-en-2-yl-5,5-dimethyl-[1,3]dioxane, 135

5-Norborene-2-carboxaldehyde **134** (3.0 g, 24.6 mmol) and neopentyl glycol (2.56 g, 24.6 mmol) were heated in the presence of *p*-toluenesulfonic acid (0.05 g, 0.3 mmol) in a conventional 800 W microwave oven on half-power for 20 seconds, the flask removed and gently shaken, and subjected to further microwave heating for an additional 20 seconds on half-power. The residue was dissolved in chloroform (100 mL), washed with sodium bicarbonate (1 M, 20 mL), dried over magnesium sulfate and evaporated to give a brown oil which solidified upon cooling affording a mixture of isomers of **135** (4.91 g, 96%, determined to be 5:1 mixture of isomers by NMR and GC-MS) as a beige solid Mp 54 °C; ν_{max} (ATR)/ cm^{-1} 3060, 2952, 2866, 2846, 1471, 1405, 1393, 1362, 1337, 1318, 1230, 1253, 1239, 1201, 1188, 1154, 1107, 1040, 1020, 1007, 996, 975, 957, 943, 926, 918, 854, 831, 814, 789, 775, 718, 683, 659, 559, 531, 484, 457; δ_H (400 MHz, $CDCl_3$) *Major isomer* 6.14 (1 H, dd, $J=3.04, 2.6$ Hz, alkenic-*H*), 5.88 (1 H, dd, $J=2.82, 2.76$ Hz, alkenic-*H*), 3.74 (1 H, d, $J=8.68$ Hz, 2'-*H*), 3.33 (2 H, d, $J=7.64$ Hz, 4 α '-, 6 α '-*H*), 3.30 (2 H, d, $J=7.64$ Hz, 4 β '-, 6 β '-*H*), 2.95 (1 H, s br), 2.79 (1 H, s br), 2.32 (1 H, m), 1.83 (1 H, m), 1.37 (1 H, m), 1.22 (1 H, d, $J=8.12$ Hz), 1.17 (3 H, s, CH_3), 0.83 (1 H, dt, $J=11.92, 3.8, 3.2$ Hz), 0.68 (3 H, s, CH_3); δ_C (100 MHz, $CDCl_3$) *Major isomer* 137.5 (sp^2C), 132.7 (sp^2C), 106.4 (2'-*C*), 77.3 (4'-, 6'-*C*), 49.2, 43.6, 43.5,

42.2, 30.1, 28.4, 23.0 (CH₃), 21.9 (CH₃); δ_{H} (400 MHz, CDCl₃) *Minor isomer* 6.10 (1 H, dd, $J=3.04, 2.6$ Hz, alkenic-*H*), 6.07 (1 H, dd, $J=2.82, 2.76$ Hz, alkenic-*H*), 4.22 (1 H, d, $J=7.48$ Hz, 2'-*H*), 3.43 (1 H, d, $J=3.2$ Hz), 3.41 (1 H, d, $J=3.2$ Hz), 2.85 (1 H, s br), 2.82 (1 H, s br), 1.17 (3 H, s, CH₃), 0.71 (3 H, s, CH₃); δ_{C} (100 MHz, CDCl₃) *Minor isomer* 137.2 (*sp*²-C), 136.5 (*sp*²-C), 105.8 (2'-C), 77.1 (4'-, 6'-C), 45.7, 43.4, 43.2, 41.7, 30.2, 22.9 (CH₃), 21.3 (CH₃). Other peaks that were not observed were assumed to co-resonate with those of the major isomer; m/z (GC-MS): found: 208 [M]⁺. C₁₃H₂₀O₂ requires: 208.

The GC-MS method used for analysis showed two fully-resolved peaks in the chromatogram at retention times 17.16 minutes and 17.31 minutes, in an approximate 4:1 ratio. Both peaks showed comparable mass spectra.

5,6-[2'-Bicyclo[2.2.1]hept-2'-yl-5',5'-dimethyl-[1',3']dioxane]-5,6-dihydro-[1,3]-dithiolo-[4,5-b-[1,4]dithiin-2-thione, 136

To a solution of **135** (0.53 g, 2.55 mmol) in toluene (60 mL) was added trithione **20** (1.0 g, 5.10 mmol) and the mixture heated to reflux at 125 °C under nitrogen for 60 h. The reaction was allowed to cool to room temperature, filtered washing with chloroform and evaporated. The crude material was purified by chromatography over silica eluting with cyclohexane/ethyl acetate (4:1) to give **136** (0.71 g, 69%) as a brown solid Mp 155 °C (Found C, 47.5; H, 5.1. C₁₆H₂₀O₂S₅ requires C, 47.45; H, 4.9%); ν_{max} (ATR)/cm⁻¹ 2953, 2922, 2849, 1463, 1448, 1408, 1393, 1363, 1308, 1281, 1235, 1216, 1201, 1182, 1152, 1112, 1099, 1061, 1039, 1025, 1018, 999, 959, 945, 928, 892, 861, 836, 783, 665, 516,

508, 483, 461; δ_{H} (400 MHz, CDCl_3) 4.29 (1 H, d, $J=6.5$ Hz, 2'-H), 3.89 (1 H, d, $J=7.7$ Hz), 3.59-3.57 (2 H, m, 4 $_{\alpha}'$ -, 6 $_{\alpha}'$ -H), 3.48 (1 H, m), 3.39-3.35 (2 H, m, 4 $_{\beta}'$ -, 6 $_{\beta}'$ -H), 2.55 (1 H, m), 2.50 (1 H, m), 2.40 (1 H, m), 2.24 (1 H, m), 1.89 (1 H, m), 1.45 (1 H, d, $J=10.5$ Hz), 1.27-1.22 (1 H, m), 1.14 (3 H, s, CH_3), 0.69 (3 H, s, CH_3); δ_{C} (100 MHz, CDCl_3) 210.0 (2-C), 136.7 & 136.5 (3a-, 7a-C), 102.4 (2'-C), 77.2 (4'-, 6'-C), 60.1, 55.4, 46.0, 45.0, 44.5, 36.7, 31.7, 30.1, 26.9, 22.9 (CH_3), 21.8 (CH_3), m/z (EI): found: 404.0066 $[\text{M}]^+$. $\text{C}_{16}\text{H}_{20}\text{O}_2\text{S}_5$ requires: 404.0061.

5,6-[2'-Bicyclo[2.2.1]hept-2'-yl-5',5'-dimethyl-[1',3']dioxane]-5,6-dihydro-[1,3]-dithiolo-[4,5-b-[1,4]dithiin-2-one, 137

To a stirred solution of **136** (0.37 g, 0.92 mmol) in chloroform (30 mL) was added mercuric acetate (0.45 g, 1.38 mmol) and the mixture stirred under nitrogen for 2 h. The reaction was filtered washing with chloroform (*ca.* 50 mL), and the filtrate subsequently evaporated to afford **137** (0.27 g, 75%) as an orange-brown solid Mp 108 °C, (Found C, 49.5; H, 5.1. $\text{C}_{16}\text{H}_{20}\text{O}_3\text{S}_4$ requires C, 49.45; H, 5.2%); $\nu_{\text{max}}(\text{ATR})/\text{cm}^{-1}$ 2947, 2869, 2837, 1824, 1755, 1667, 1638, 1618, 1459, 1414, 1392, 1363, 1323, 1307, 1280, 1251, 1232, 1212, 1201, 1181, 1153, 1117, 1097, 1075, 1040, 1020, 996, 962, 941, 927, 888, 867, 789, 756, 677, 665, 642, 593, 545, 480, 462; δ_{H} (400 MHz, CDCl_3) 4.24 (1 H, d, $J=6.7$ Hz), 3.86 (1 H, dd, $J=5.4, 1.4$ Hz), 3.55-3.46 (3 H, overlapping multiplets), 3.33 (2 H, q, $J=5.7$ Hz), 2.47 (2 H, m), 2.32 (1 H, m), 1.86-1.75 (1 H, m), 1.60-1.43 (1 H, m), 1.39 (1 H, d, $J=10.7$ Hz), 1.19 (1 H, m), 1.09 (3H, s), 0.65 (3 H, s); δ_{C} (100 MHz, CDCl_3) 189.8 (2-C), 127.3 & 127.1 (3a-, 7a-C), 102.3 (2'-

C), 77.2 (4'-, 6'-C), 60.1, 55.4, 46.0, 45.0, 44.5, 36.7, 31.7, 30.1, 26.9, 22.9 (CH₃), 21.8 (CH₃), *m/z* (ES): found: 406.0632 [M+NH₄]⁺. C₁₆H₂₀O₃S₄ + NH₄ requires: 406.0639.

5'',6''-Ethylenedithio-[1,3]-dithiolo-[4,5-b][1,4]dithiin-2-ethene-5,6-[2'-bicyclo[2.2.1]hept-2'-yl-5',5'-dimethyl-[1',3']dioxane]-5,6-dihydro-[1,3]-dithiolo-[4,5-b][1,4]dithiine, 138

Oxo compound **137** (0.1 g, 0.26 mmol) and thione **22** (0.17 g, 0.77 mmol) were heated together in freshly distilled triethyl phosphite (8 mL) under nitrogen to 95 °C for 22 h. The reaction was allowed to cool to room temperature, filtered through a glass-sintered funnel washing with petroleum ether 40-60 °C. The filtrate was evaporated, and the crude material purified by chromatography over silica eluting with cyclohexane/ethyl acetate (2:1) to afford un-separable isomers of **138** (0.07 g, 46 %) as a bright orange solid Mp 215-216 °C, (Found C, 44.7; H, 4.3. C₂₁H₂₂O₂S₈ requires C, 44.65; H, 4.3%); δ_{H} (400 MHz, CDCl₃) 4.27 (1 H, d, *J*=6.8 Hz), 3.78 (1 H, d, *J*=6.6 Hz), 3.64-3.54 (2 H, m), 3.42-3.22 (9 H, overlapping multiplets and singlet), 2.46 (1 H, s), 2.40 & 2.38 (combined 1 H, 2 x s), 2.31 (1 H, s), 2.22 & 2.16 (combined 1 H, m & s), 1.93 & 1.87 (combined 1 H, s & m), 1.17 (3 H, s), 0.72 (3 H, s); δ_{C} (100 MHz, CDCl₃) 127.1, 126.8, 113.8, 113.7, 112.2, 111.7, 102.6, 77.2, 64.2, 64.1, 59.6, 54.6, 46.1, 45.0, 44.5, 36.5, 31.5, 23.0, 21.8, 15.9, 15.8; *m/z* (EI): found: 563.9538 [M]⁺. C₂₁H₂₄O₂S₈ requires: 563.9536.

6.4 References

- ¹ S. -X. Liu, S. Dolder, M. Pilkington and S. Decurtins, *J. Org. Chem.*, **2002**, 67, 3160.
- ² J.-P. Griffiths, A. A. Arola, G. Appleby, and J. D. Wallis, *Tetrahedron Lett.*, **2004**, 45, 2813.
- ³ R. J. Brown, G. Camarasa, J.-P. Griffiths, P. Day and J. D. Wallis, *Tetrahedron Lett.*, **2004**, 45, 5103.
- ⁴ N. Saygili, R. J. Brown, P. Day, R. Hoelzl, P. Kathirgamanathan, E. R. Mageean, T. Ozturk, M. Pilkington, M. M. B. Qayyum, S. S. Turner, L. Vorweg and J. D. Wallis, *Tetrahedron*, **2001**, 57, 5015.
- ⁵ Y. Ishikawa, T. Miyamoto, A. Yoshida, Y. Kawada, J. Nakazaki, A. Izuoka and T. Sugawara, *Tetrahedron Lett.*, **1999**, 40, 8819.
- ⁶ D. J. Darensbourg, C. G. Ortiz and D. R. Billodeaux, *Inorganica Chimica Acta*, **2004**, 357, 2143.
- ⁷ A. R. Silva, C. Freire and B. de Castro, *New J. Chem.*, **2004**, 28, 253.
- ⁸ A. C. Brooks, P. Day and J. D. Wallis, *Acta Cryst.*, **2008**, C64, o245.
- ⁹ W. A. Little, *Phys. Rev.*, **1964**, 134, 6A, 1416.
- ¹⁰ A. Diaz-Ortiz, P. Prieto, A. Loupy and D. Abenheim, *Tetrahedron Lett.*, **1996**, 37, 1695.
- ¹¹ S. Rostamizadeh and G. S. A. Housaini, *Tetrahedron Lett.*, **2004**, 45, 8753.
- ¹² A. Procopio, M. Gaspari, M. Nardi, M. Oliverio, A. Tagarelli and G. Sindona, *Tetrahedron Lett.*, **2007**, 48, 8623.

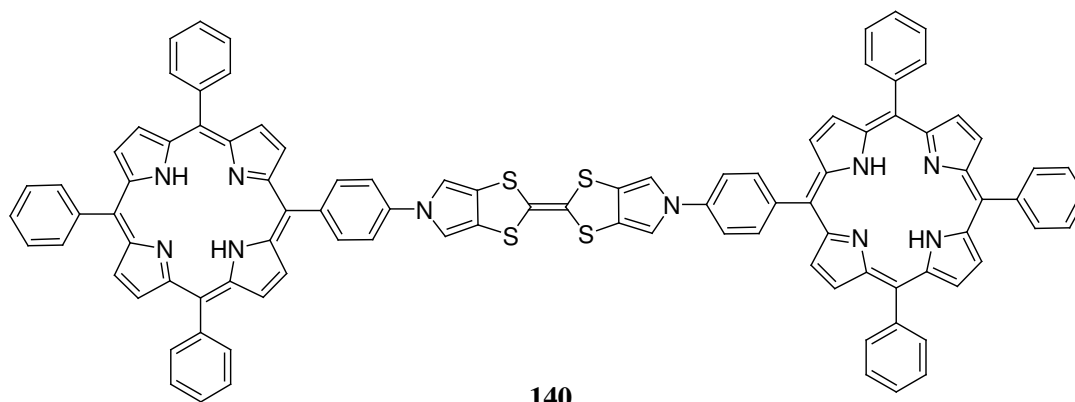
Chapter 7

A Porphyrin based electron donor

7 Porphyrin based electron donor

7.1 Introduction

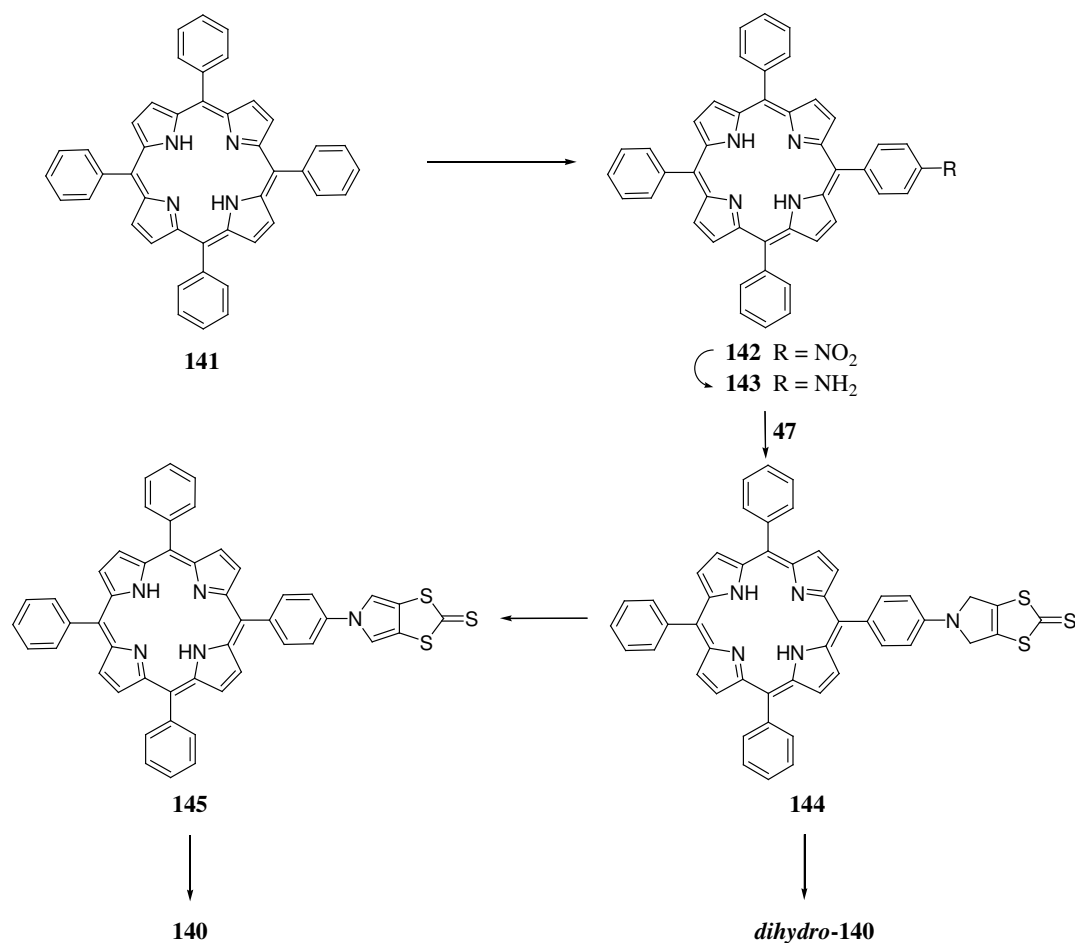
Porphyrins are a distinct class of organic compound that not only attract interest due to their presence in biological systems, but also as they exhibit properties which make them desirable in modern functional materials. The extensive π -aromatic ring system is included in chlorophyll, which forms part of the process for converting light into chemical energy. Until now researchers have tethered these large aromatic systems at distal positions to the core electron donor molecule, but not directly adjacent to the organosulfur moiety. As such, it was decided to attempt the preparation of **140**. It was proposed that the intense aromatic character of the compound would assist in the crystalline packing of the donor species, both in the neutral and radical cation state.



The porphyrin systems could also be metallated to incorporate specific magnetic functionality close to the electron conducting zone of the molecule. The potential synergistic properties of which, would be of extreme interest, especially if the electronic

conductivity could be tuned by the application of a moderate external magnetic field.

The synthetic route to the preparation of **140** is shown in Scheme 18.



Scheme 18: Synthetic route to donor **140**.

7.2 Results and discussion

Meso-tetraphenylporphyrin was synthesised by the literature method.¹ The condensation of benzaldehyde with pyrrole formed the macro cyclic species **141**, in low yield (17 %), which was identifiable from the simple ¹H NMR and the infrared spectrum, which were comparable to that in the literature. Mono nitration of **141** was

undertaken by slight modification of the literature procedure.^{2, 3, 4} The acid mediated reaction of sodium nitrite on the aromatic ring proceeded at the *para*- position affording **142** in 72 % yield. The compound was identified by the more complex ¹H NMR spectrum, which indicated that substitution on one of the phenyl rings had occurred. Furthermore, confirmation of the nitration was observed in the infrared spectrum which showed the N=O stretching frequency at $\nu = 1514 \text{ cm}^{-1}$.

Reduction of nitro compound **142** to the corresponding amino porphyrin **143** was achieved using tin chloride in concentrated hydrochloric acid. Simple workup and extraction afforded pure **143** without the need for purification by chromatography. The reduction was confirmed by the appearance of a resonance for the NH₂ functionality in the ¹H NMR spectrum as a singlet at $\delta 4.01 \text{ ppm}$, and by the lack of the N=O stretching band in the infrared spectrum.

The nucleophilic substitution of two bromines on the dibromide **47** by the amine function on **143** afforded the dihydropyrrole species **144** in moderate yield. The insolubility of the compound made it difficult to fully characterise, however the appearance of a singlet at $\delta 4.71 \text{ ppm}$ in the ¹H NMR spectrum suggested that the bromomethyl functions had undergone a substitution reaction, and the absence of a resonance for the free amine hydrogen atoms at $\delta 4.01 \text{ ppm}$ supported the formation of **144**. Further evidence was found in the infrared spectrum which showed the C=S stretching frequency as a band at $\nu = 1059 \text{ cm}^{-1}$. Mass spectrometry unequivocally confirmed the presence of **144** with observation of the molecular ion peak at 787.1890 Da.

Oxidation to the pyrrole ring system was undertaken prior to formation of the electron donor central C=C bond, as it was thought that a charge transfer salt may form if **140** was reacted with DDQ. As such, **144** was converted into the pyrrole analogue **145** in good yield (84 %). The ^1H NMR spectrum indicated the absence of the dihydropyrrole methylene system at δ 4.71 ppm and mass spectrometry confirmed the oxidised species, with the molecular ion at 785.1738 Da observed. The purity of the material was confirmed by elemental analysis, which correlated exceptionally well with that expected.

The triethyl phosphite mediated homo-coupling reaction of **145** was attempted, however after workup, the purple solid isolated was unable to be determined as **140**. The infrared suggested that formation may have occurred, due to the absence of the corresponding C=S stretching band, however mass spectrometry showed no evidence for the symmetrical species formed. Raman spectroscopy could not determine a symmetrical stretch for the central C=C bond, and NMR results were inconclusive. The formation of *dihydro-140* was also attempted, however the spectroscopic data obtained for the solid isolated did not satisfactorily confirm the formation of the symmetrical donor.

The lack of reactivity in these instances may have been due to the C=S not being as activated as the C=O bond that is normally utilised in the triethyl phosphite coupling step. The sulfur-oxygen exchange reaction mediated by mercuric acetate was not attempted in this case, as it was believed that the porphyrin ring systems could bind the

mercury atom, and that the highly acidic conditions required for de-metallation may present issues in terms of electron donor stability, particularly with respect to oxidation.

Future researchers may wish to re-visit this molecule, and may obtain better results by metallating the aminoporphyrin species **143** prior to reaction with **47**, with a metal such as zinc.

7.3 Experimental

***Meso*-5,10,15,20-tetraphenylporphyrin, 141**

Benzaldehyde (10.0 g, 94.3 mmol) was stirred into propionic acid (150 mL) and heated to reflux for 5 min. At reflux, pyrrole (6.3 g, 94.3 mmol) was added carefully down the inside of the condenser. The resulting dark mixture was allowed to reflux for a further 2 h, before being cooled to room temperature. Methanol (300 mL) was added, and the flask stored in the freezer overnight. Filtration afforded **141** (2.46 g, 17 %) as purple microcrystals; ν_{\max} (ATR/cm⁻¹) 3315, 3055, 3024, 1595, 1574, 1556, 1472, 1441, 1349, 1072, 979, 964, 795, 785, 721, 695, 656; δ_{H} (400 MHz, CDCl₃) 8.84 (8 H, s, 4 x 3-, 4 x 4-*H*), 8.22 (8 H, m, 4 x 3'-, 4 x 5'-*H*), 7.75 (12 H, m, 4 x 2'-, 4 x 4'-, 4 x 6'-*H*).

5-(4-Nitrophenyl)-10,15,20-triphenylporphyrin, 142

To a rapidly stirred solution of **142** (3.04 g, 4.95 mmol) in trifluoroacetic acid (60 mL) at room temperature was added sodium nitrite (0.75 g, 8.81 mmol) under an atmosphere

of nitrogen. The reaction was allowed to stir for 5 min, and then poured into distilled water (300 mL). The crude product was extracted with chloroform (3 x 100 mL) and the combined organic phases washed with saturated sodium bicarbonate solution (100 mL), and then brine (50 mL). The organic phase was dried over sodium sulfate, evaporated to dryness and purified by chromatography over silica eluting with chloroform to give **142** (2.35 g, 72 %) as a dark purple solid; Mp >330 °C; ν_{\max} (ATR)/cm⁻¹ 3315, 3053, 1594, 1514, 1472, 1441, 1344, 979, 964, 846, 794, 720, 695, 639, 560; δ_{H} (400 MHz, CDCl₃) 8.89-8.84 (6 H, m, pyr-H), 8.73 (2 H, d, *J*=4.7 Hz, pyr-H), 8.63 (2 H, d, *J*=8.7 Hz, nitrophenyl-H), 8.39 (2 H, d, *J*=8.7 Hz, nitrophenyl-H), 8.21 (6 H, m, phenyl-H), 7.77 (9 H, m, phenyl-H), -2.79 (2 H, s, pyr-NH).

5-(4-Aminophenyl)-10,15,20-triphenylporphyrin, 143

To a rapidly stirred mixture of **142** (2.0 g, 3.0 mmol) in HCl (37 % v/v, 80 mL) at 70 °C was added SnCl₂ (0.63 g, 3.3 mmol). The mixture was heated for 90 min, then cooled to room temperature and poured into ice cold water (150 mL). The mixture was then neutralised by the careful addition of NH₄OH to pH 7. A mixture of chlorobenzene (50 mL) and chloroform (100 mL) was added to extract **143**. The extraction of the aqueous phase was repeated, and the combined filtrates washed with brine (100 mL), dried over Na₂SO₄, and evaporated to afford **143** (1.83 g, 97 %) as a purple solid; Mp >330 °C; ν_{\max} (ATR)/cm⁻¹ 3460, 3319, 3052, 2930, 1724, 1616, 1595, 1471, 1440, 1348, 1279, 1176, 1071, 1000, 979, 965, 796, 729, 700; δ_{H} (400 MHz, CDCl₃) 8.92 (2 H, s, pyr-H), 8.82 (6 H, d, *J*=5.8 Hz, pyr-H), 8.19 (6 H, m, phenyl-H), 8.00 (2 H, m,

aminophenyl-*H*), 7.74 (9 H, m, phenyl-*H*), 7.04 (2 H, m, aminophenyl-*H*), 4.01 (2 H, s, NH₂), -2.77 (2 H, s, pyr-NH).

4,5-Dimethylene(4'-aminophenyl(triphenyl)porphyrino)-1,3-dithiole-2-thione, 144

To a solution of **143** (1.5 g, 2.4 mmol) in tetrahydrofuran (100 mL) was added **47** (0.76 g, 2.4 mmol), Na₂CO₃ (0.51 g, 4.8 mmol) and tetrabutylammonium iodide (0.1 g, 0.3 mmol). The mixture was heated to reflux under nitrogen for 2 days, and then cooled to room temperature. The mixture was filtered washing the solid with tetrahydrofuran, and the solid dried under high vacuum to give **144** (1.21 g, 64 %) as a relatively insoluble purple solid Mp 320 °C (dec.); ν_{\max} (ATR)/cm⁻¹ 3409, 1605, 1596, 1509, 1472, 1463, 1440, 1355, 1326, 1194, 1059, 1001, 980, 966, 803, 739, 702; δ_{H} (400 MHz, DMSO) 8.85 (2 H, s *br*, pyr-NH), 8.72 (6 H, s *br*, pyr-NH), 8.13 (6 H, s *br*, phenyl-*H*), 8.00 (2 H, s *br*, aminophenyl-*H*), 7.75 (9 H, s *br*, phenyl-*H*), 6.91 (2 H, s *br*, aminophenyl-*H*), 4.71 (4 H, s *br*, dihydropyrrole-*H*), -2.80 (2 H, s *br*, pyr-NH); m/z (EI): found: 787.1890 [M]⁺. C₄₉H₃₃N₅S₃ requires: 787.1893.

4,5-Dimethine(4'-aminophenyl(triphenyl)porphyrino)-1,3-dithiole-2-thione, 145

To a solution of **144** (0.3 g, 0.4 mmol) in chlorobenzene (100 mL) at -5 °C, was added dropwise a solution of DDQ (0.13 g, 0.6 mmol) in chlorobenzene (50 mL) over 1 h. The solution was allowed to warm to room temperature and stirred overnight. Sodium carbonate solution (1 M, 300 mL) was added and the mixture stirred rapidly for 15 min, and then transferred to a separating funnel. Chloroform (100 mL) was added to dilute

the organic phase. The phases were separated and the aqueous phase washed with chloroform (2 x 60 mL). The combined organic phases were washed successively with sodium bicarbonate solution (1 M, 100 mL), distilled water (60 mL), and brine (60 mL), and dried over magnesium sulfate before evaporating to give **145** (0.25 g, 84 %) as a purple solid (Found C, 74.8; H, 4.0; N, 8.9. C₄₉H₃₁N₅S₃ requires: C, 74.9; H, 4.0; N, 8.9); ν_{\max} (ATR)/cm⁻¹ 1706, 1597, 1559, 1512, 1472, 1440, 1350, 1154, 1068, 1001, 980, 965, 798, 727, 700, 657, 638, 619, 560; δ_{H} (400 MHz, CDCl₃) 8.78 (8 H, s *br*, pyrr-*H*), 8.68 (2 H, s *br*, pyrr-*H*), 8.13 (6 H, s *br*, phenyl-*H*), 8.07 (2 H, s *br*, aminophenyl-*H*), 7.68 (9 H, s *br*, phenyl-*H*), 7.42 (2 H, s *br*, aminophenyl-*H*), -2.83 (2 H, s *br*, pyrr-NH); *m/z* (EI) found: 785.1738 [M]⁺. C₄₉H₃₁N₅S₃ requires: 785.1736.

Bis[4,5-dimethine(4'-aminophenyl(triphenyl)porphyrino)-tetrathiafulvalene], 140

145 (0.2 g, 0.3 mmol) was stirred in triethyl phosphite (5 mL) and heated to 110 °C under a nitrogen atmosphere for 1 day. The reaction mixture was cooled to room temperature and the residual triethyl phosphite removed under reduced pressure. Addition of ethanol (10 mL) precipitated a solid, which was collected by filtration and washed with ethanol (30 mL) and then *n*-hexane (50 mL). Drying under vacuum at room temperature afforded a purple solid whose structure could not be conclusively confirmed by NMR, infrared or mass spectrometry.

**Bis[4,5-dimethylene(4'-aminophenyl)(triphenyl)porphyrino]-tetrathiafulvalane],
*dihydro-140***

144 (0.2 g, 0.3 mmol) was stirred in triethyl phosphite (5 mL) and heated to 110 °C under a nitrogen atmosphere for 28 h. The reaction was allowed to cool to room temperature and the residual triethyl phosphite removed under reduced pressure. The crude material was stirred in a mixture of *n*-hexane (25 mL) and diethyl ether (3 mL). A purple solid (0.1g) was isolated by filtration, however definite identity could not be determined Mp >300 °C (Found C, 62.4; H, 5.0; N, 6.5%); *m/z* inconclusive.

7.4 References

- ¹ A. D. Adler, F. R. Longo, R. D. Finarelli, J. Goldmacher, J. Assour, and L. Korsakoff, *J. Org. Chem.*, **1976**, 32, 476.
- ² A. U. Spitzer and R. Stewart, *J. Org. Chem.*, **1974**, 39, 3936.
- ³ S. Uemura, A. Toshimistu and M. Okano, *J. Chem. Soc., Perkin Trans. 1*, **1978**, 9, 1076.
- ⁴ R. Luguay, L. Jaquinod, F. R. Fronczek, M. G. H. Vicente and K. M. Smith, *Tetrahedron*, **2004**, 60, 2757.

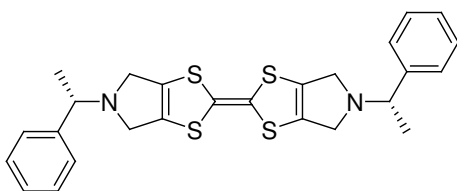
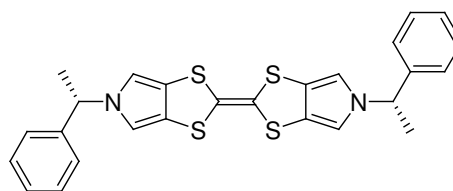
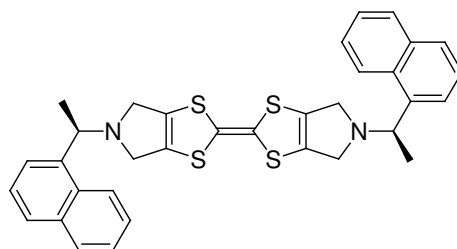
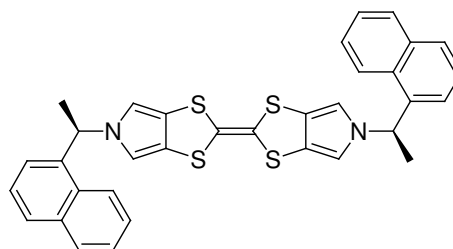
Chapter 8

A spiro organosulfur compound

8 A spiro organosulfur compound

8.1 Introduction

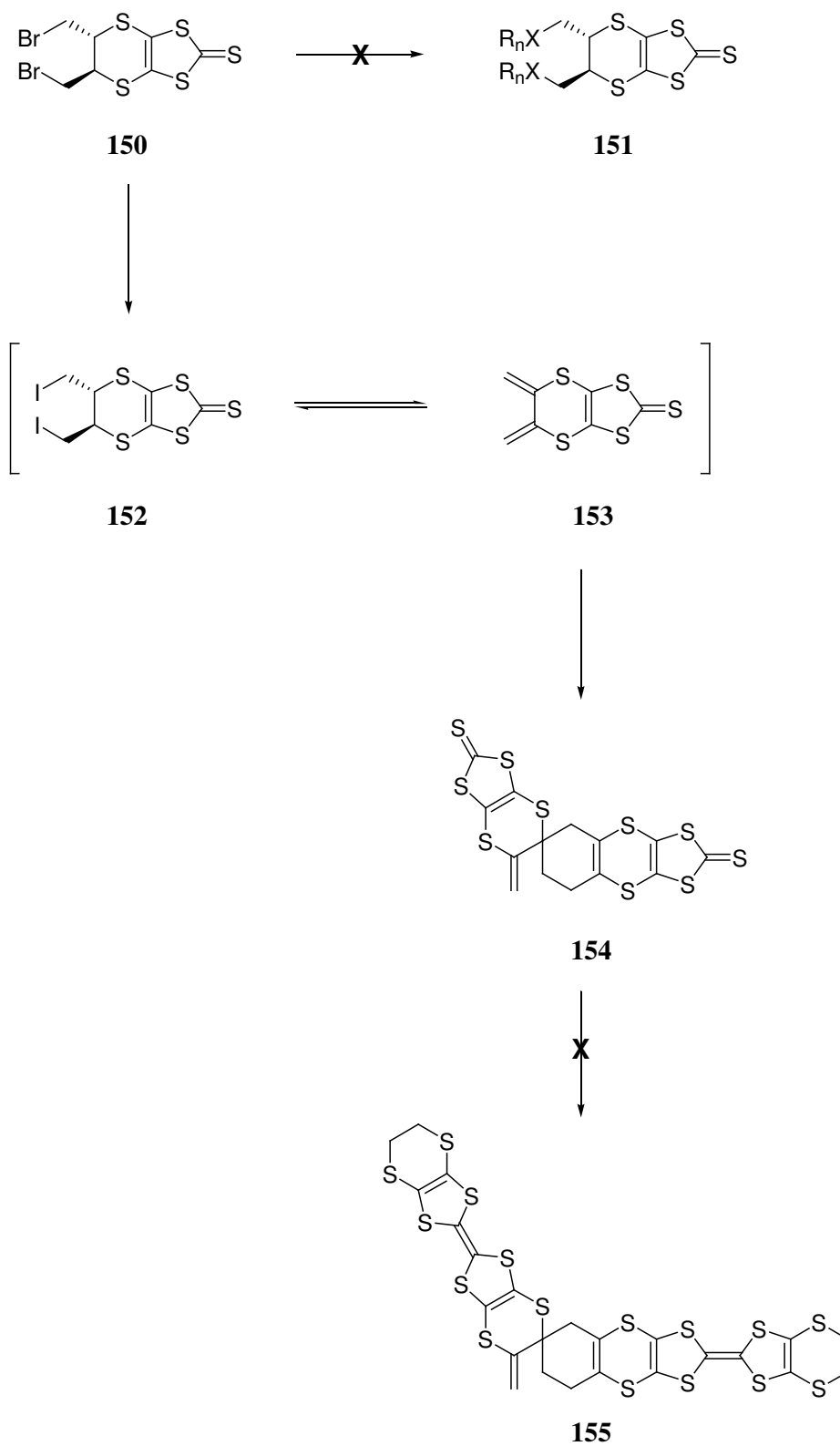
Nucleophilic substitution reactions of bromides are an excellent way of installing functionality into compounds. The synthesis of dibromo **47** has allowed access to a variety of compounds such as molecule **144**, presented in Chapter 7, and the chiral benzyl and naphthyl substituted pyrrole and dihydro pyrrole TTF donors **146-149**.¹

**146****147****148****149**

Compound **47** does however, provide access to a range of other compounds *via* an elimination mechanism to form the diene, which is subsequently able to undergo cycloaddition reactions. Hudhomme *et al.* have demonstrated the versatility of the route by preparing the C₆₀ appended donor molecule **6**,^{2, 3} and a *p*-benzoquinone derived donor.⁴

8.2 Results and discussion

The chemical versatility of dibromo compound **150** made it an attractive precursor with which to prepare a variety of functionalised electron donor molecules. Initial experiments were designed to substitute the bromides with simple amine compounds, such as ethylamine, to test the validity of the synthetic route. It was observed however, that by heating a solution of dibromo **150** in the presence of base, an unknown solid was isolated whose NMR spectra did not resemble the expected compound. Alkenic protons were observed at δ 5.41 and 5.13 ppm in the ^1H NMR spectra, indicating that elimination had occurred. The two resonances indicated that the protons were in different environments, and 2-D NMR indicated that both of these protons resided on the carbon resonating at δ 111.9 ppm. The observation of two resonances for thiocarbonyl species at δ 213.1 and 207.6 ppm indicated that the unknown species was formed by reaction of two molecules of starting material dibromo **150**, and that the organosulfur ring systems had slightly different electronic environments. Mass spectra data was collected and this indicated that the species had a molecular ion at 495.9 Da, and the absence of typical bromine isotope patterns suggested that no bromine was present in the material. The observed isotope pattern of 495.9 (100 %), 496.9 (42 %), 497.9 (53 %), 498.9 (18 %), corresponded well with the theoretical isotope pattern for compound **154** of 495.9 (100 %), 496.9 (29 %), 497.9 (39 %), 498.9 (11 %), which was enforced by the NMR data observed.



Scheme 19: Preparation of spiro organosulfur electron donor 155.

To test the hypothesis, reactions were conducted without employing a base, and separately, without heating. In both instances no reaction was detected. Further studies showed that nucleophilic substitution of the bromine was not favoured, as attempts at reacting **150** with ethanedithiol, aniline and ammonia gave **154** consistently, although in varying yields.

It was then thought that it would be possible to trap the diene formed *in-situ* using either an alkene or an alkyne, and as such a range of unsaturated compounds were employed. Formation of **154** was observed in each case as the only product detected.

8.3 Experimental

5,6-Bis-bromomethyl-5,6-dihydro-[1,3]dithiolo[4,5-b][1,4]dithiine-2-thione, 150

The dibromo compound was prepared and donated by Dr Songjie Yang at Nottingham Trent University. The compound was supplied as a mixture of the *trans*- isomers, and used without further purification.

Spiro compound, 154

To a stirred solution of dibromide **150** (0.2 g, 0.49 mmol) in tetrahydrofuran (15 mL) at room temperature was added potassium carbonate (0.182 g, 1.32 mmol) and tetrabutylammonium iodide (0.02 g, 0.05 mmol). Ethylamine (0.05 g, 0.98 mmol) in tetrahydrofuran (5 mL) was added dropwise, causing the evolution of a little gas. The

mixture was heated under a nitrogen atmosphere to 80 °C for 18 h, cooled to room temperature and the solvent evaporated. The residue was taken into dichloromethane (100 mL) and washed with 1 M HCl (50 mL). The aqueous layer was washed with dichloromethane, and the combined organic phases washed with brine and dried over magnesium sulfate. Chromatography over silica eluting with cyclohexane/dichloromethane (7:3) afforded **154** (0.04 g, 34 %) as a yellow solid; δ_{H} (400 MHz, CDCl_3) 5.41 (1 H, d, $J=2.3$ Hz, $\text{sp}^2\text{-CH}$), 5.13 (1 H, d, $J=2.3$ Hz, $\text{sp}^2\text{-CH}$), 2.89 (1 H, d, $J=17.7$ Hz, CH_α), 2.70 (1 H, d, $J=17.9$ Hz, CH_β), 2.58-2.38 (2 H, m, CH_2), 2.24-2.06 (2 H, m, CH_2); δ_{C} (100 MHz, CDCl_3) 213.1 (C=S), 207.6 (C=S), 138.4, 131.2, 128.9, 127.8, 126.8, 123.4, 119.0, 111.9, 48.8, 39.7, 31.2, 29.0; m/z (EI): found 495.9. $\text{C}_{14}\text{H}_8\text{S}_{10}$ requires 495.8 Da.

Bis-ET spiro donor, 155

Spiro compound **154** (0.04 g, 0.08 mmol) was stirred in triethyl phosphite (2 mL) with **22** (0.036g, 0.16 mmol) and heated to 90 °C under a nitrogen atmosphere for 7 h. The reaction was cooled to room temperature, and evaporated. The crude material was purified by chromatography over silica, eluting with cyclohexane/ dichloromethane (5:2) to give a yellow-brown solid (0.03 g) which could not be fully characterised; NMR inconclusive; m/z (EI): found: 617.6 Da.

8.4 References

- ¹ S. Yang, A. C. Brooks, L. Martin, P. Day, H. Li, P. Horton, L. Male and J. D. Wallis, *CrystEngComm*, **2009**, 11, 993.
- ² P. Hudhomme, C. Boule, J. M. Rabreau, M. Cariou, M. Jubault and A. Gorgues, *Synth. Met.*, **1998**, 94, 73.
- ³ D. Kreher, M. Cariou, S. -G. Liu, E. Levillain, J. Veciana, C. Rovira, A. Gorgues and P. Hudhomme, *J. Mater. Chem.*, **2002**, 12, 2137.
- ⁴ N. Gautier, M. Cariou, A. Gorgues and P. Hudhomme, *Tetrahedron Letters*, **2000**, 41, 2091.

Chapter 9

Recommendations for further work

9 Recommendations for further work

The hydroxyl donors detailed in chapter 2 are of great interest in the formation of radical cation salts, as the hydrogen bonding capabilities could create greater ordering of the crystalline state. Further work should continue the preparation of halide salts of these donors.

Another area of research, which has been initiated but not discussed here, is the preparation of radical cation salts in which the anion employed is the tetraalkylammonium salt of a small chiral organic acid, such as L-malic acid. The hydrogen bonding potential of anions such as this are considerable and in conjunction with electron donors such as the tetrol and hydroxyl discussed in chapter 2, could give greatly compacted and/ or controlled crystal structures.

The pyridyl donors detailed in chapter 3, are interesting due to the potential to bind metals through the nitrogen lone pairs of electrons on the pyridyl ring systems. This has particular use in the preparation of multi-functional devices, in which a conducting system can be located close to a magnetic network. In addition, the relative ease with which the donors form crystals in the neutral charge state allows for better electrocrystallisation results due to the greater purity of the homogenous material.

The electrocrystallisation of electron donors with the sulfamate anion should be further investigated, and compared to the results reported in chapter 4. It would be interesting

to see if many other crystallographic phases are formed, and how the conductivity of these phases vary.

Although the synthesis of chirally pure anionic metal salen complexes is reported in chapter 5, so far no X-ray crystal structures have been obtained for radical cation salts using these anions. This is an area that requires further research, which should provide numerous interesting results.

Appendix 1

GC-MS method

Appendix 1

GC-MS method used for analysis of organic molecules in this thesis.
G3174A US51540141

Control Information

Sample Inlet: GC
Injection Source: GC/ALS
Injection Location: ALS
Use MS: Yes

6890 GC METHOD

OVEN

Initial temp: 50 C (On) Maximum temp: 350 C
Initial time: 2.00 min Equilibration time: 0.25 min

Ramps:

Rate Final temp Final time

1 10.00 300 10.00

2 0.0(Off)

Post temp: 0 C
Post time: 0.00 min
Run time: 37.00 min

FRONT INLET (SPLIT/SPLITLESS)

Mode: Splitless
Initial temp: 250 C (On)
Pressure: 19.00 psi (On)
Purge flow: 45.9 mL/min
Purge time: 5.00 min
Total flow: 50.2 mL/min
Gas saver: On
Saver flow: 20.0 mL/min
Saver time: 10.00 min
Gas type: Helium

COLUMN 1

Capillary Column
Model Number: restex zb-5ms
rtx1 equiv
Max temperature: 340 C
Nominal length: 60.0 m
Nominal diameter: 250.00 um
Nominal film thickness: 0.25 um
Mode: constant flow

Initial flow: 1.0 mL/min
 Nominal init pressure: 16.91 psi
 Average velocity: 26 cm/sec
 Inlet: Front Inlet
 Outlet: MSD
 Outlet pressure: vacuum

SIGNAL 1**SIGNAL 2**

Data rate: 20 Hz	Data rate: 20 Hz
Type: test plot	Type: test plot
Save Data: Off	Save Data: Off
Zero: 0.0 (Off)	Zero: 0.0 (Off)
Range: 0	Range: 0
Fast Peaks: Off	Fast Peaks: Off
Attenuation: 0	Attenuation: 0

THERMAL AUX 2

Use: MSD Transfer Line Heater
 Description:
 Initial temp: 250 C (On)
 Initial time: 0.00 min
 # Rate Final temp Final time
 1 0.0(Off)
 POST RUN
 Post Time: 0.00 min

Front Injector:

Sample Washes	2
Sample Pumps	4
Injection Volume	0.20 microliters
Syringe Size	10.0 microliters
PreInj Solvent A Washes	2
PreInj Solvent B Washes	0
PostInj Solvent A Washes	2
PostInj Solvent B Washes	0
Viscosity Delay	0 seconds
Plunger Speed	Fast
PreInjection Dwell	0.00 minutes
PostInjection Dwell	0.00 minutes

Column 1 Inventory Number: zb-5ms

Column 2 Inventory Number:

MS Acquisition Parameters:

Solvent Delay: 5.00 min
EM Absolute: False
EM Offset: 271
Resulting EM Voltage: 3000.0

MS Scan Parameters:

Low Mass: 35.0
High Mass: 500.0
Threshold: 0
Sample #: 3 A/D Samples 8

MS Zones:

MS Quad: 150 C maximum 200 C
MS Source: 230 C maximum 250 C

TUNE PARAMETERS for SN:

EMISSION: 34.610
ENERGY: 69.922
REPELLER: 34.814
IONFOCUS: 90.157
ENTRANCE_LE: 19.000
EMVOLTS: 2729.412
AMUGAIN: 1878.000
AMUOFFSET: 127.188
FILAMENT: 2.000
DCPOLARITY: 1.000
ENTLENSOFFS: 19.075
MASSGAIN: -503.000
MASSOFFSET: -41.000